

**PROPULSION SYSTEM FLOW STABILITY PROGRAM  
(DYNAMIC)**

**PHASE I FINAL TECHNICAL REPORT  
PART XII. UNSTEADY COMBUSTION IN DUCT BURNERS  
AND AFTERBURNERS**

D. M. Dix, P. L. Duffield and J. E. Smith

*Dist. changed to U2  
on 4/12/1972*

This document is subject to special export controls and each transmittal to foreign governments or foreign nationals may be made only with prior approval of the Air Force Aero Propulsion Laboratory (APLA), Air Force Systems Command, Wright-Patterson Air Force Base, Ohio.

## FOREWORD

This report describes work accomplished in Phase I of the two-phase program, "Propulsion System Flow Stability Program (Dynamic)" conducted under USAF Contract F33615-67-C-1848. The work was accomplished in the period from 20 June 1967 to 30 September 1968 by the Los Angeles Division of North American Rockwell Corporation, the prime Contractor, and the Subcontractors, the Allison Division of General Motors Corporation (supported by Northern Research and Engineering Corporation), the Autonetics Division of North American Rockwell Corporation (supported by the Aeronautical Division of Honeywell, Incorporated), and the Pratt & Whitney Aircraft Division of United Aircraft Corporation.

The program was sponsored by the Air Force Aero Propulsion Laboratory, Wright-Patterson Air Force Base, Ohio. Mr. H. J. Gratz, APTA, Turbine Engine Division, was the Project Engineer.

This volume is Part XII of twenty parts and was prepared by the Northern Research and Engineering Corporation.

Publication of this report does not constitute Air Force approval of the report's findings or conclusions. It is published only for the exchange and stimulation of ideas.

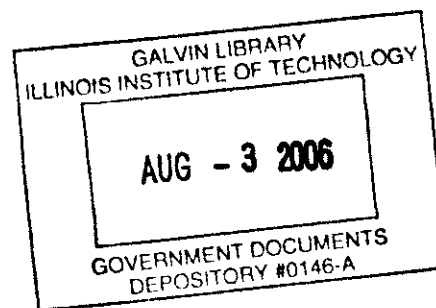


Ernest C. Simpson  
Chief, Turbine Engine Division

# Contrails

## ABSTRACT

An analytical model of combustion instability in afterburners and duct burners has been formulated which incorporates in a readily identifiable way the significant loss and gain processes associated with oscillatory combustion. The dominant loss mechanisms, as revealed by a literature survey and subsequent assessment, are those due to convection and radiation from the nozzle and absorption by acoustic liners. The gain mechanisms have been incorporated in a general way which permits physical interpretation; those mechanisms considered to be of most importance in aircraft burners are those associated with fuel vaporization and turbulent transport processes. The analytical model is also capable of treating approximately the significant nonlinear aspects of combustion instability associated with the dependencies of the major losses and gains on oscillation amplitude. The total mathematical requirements to obtain numerical results are the solution of transcendental algebraic equations and the evaluation of definite integrals. An application of the model to a known experimental situation yielded results which were qualitatively correct and quantitatively of the correct order of magnitude. Finally, a test plan has been formulated to enable the adequacy of the analytical model to be further assessed.



# *Contrails*

## TABLE OF CONTENTS

SECTION		PAGE
I	INTRODUCTION	1
	Problem Definition	1
	Physical Sources and Consequences of Unsteady Combustion	1
	State of the Art	2
	Engineering Difficulties	2
	Program Objectives	3
	Specific Objectives	3
	Ultimate Goals	4
	Method of Approach	5
II	SUMMARY	7
III	RESULTS AND DISCUSSION	9
	Literature Survey	9
	Acoustical Analyses	10
	Assessment of Loss Mechanisms	10
	Assessment of Driving Mechanisms	11
	Elementary Considerations	11
	Model of Driving Process	12
	Appraisal of Driving Mechanisms	13
	Analytical Model	14
	Formulation	14
	Approximate Solution	14
	Nature of Solution	15
	Illustrative Calculation	16
	Formulation of Test Plan	17
IV	CONCLUSIONS AND RECOMMENDATIONS	21
	Conclusions	21
	Recommendations	21
	ILLUSTRATIONS	23
	TABLES	77

# Contrails

APPENDICES		PAGE
A	LITERATURE SURVEY	83
B	ACOUSTIC ANALYSES	127
C	ASSESSMENT OF LOSS MECHANISMS	147
D	LOSS DECREMENTS	167
E	DOWNSTREAM BOUNDARY REPRESENTED BY A COMPLEX ADMITTANCE	173
F	ASSESSMENT OF DRIVING MECHANISMS	175
G	DEVELOPMENT OF THE INSTABILITY MODEL	193
H	ILLUSTRATIVE APPLICATION OF THE INSTABILITY MODEL	205
I	DISCUSSION OF TEST PLAN	215
REFERENCES		223

# Contrails

## LIST OF ILLUSTRATIONS

Figure No.	Title	Page
1	Comparison of Predicted Frequencies with Measured Frequencies for a Large Duct Burner . . . . .	23
2	Gain and Loss Contributions for a 26-Inch-Diameter Burner - First Transverse Mode, Liner Length = 19 Inches . . . . .	24
3	Diagrammatic Representations of Typical Combustor Geometries . . . . .	25
4	Variation of Ratio of Peak Static Pressure (Reed Valve) to Average Static Pressure with Distance Downstream of Flameholder in 26-Inch-Diameter Duct. Airflow, 22.6 pounds per second (from Ref 9) . . . . .	26
5	Amplitude Distribution for Two Flameholder Positions in 6-Inch Burner (from Ref 12) . . . . .	27
6	Variation of Combustion Chamber Inlet Total Pressure with Equivalence Ratio (from Ref 16) . . . . .	28
7(a)	Variation of Screech Limits with Afterburner-Inlet Pressure for 36-Inch-Diameter Afterburner. Afterburner-Inlet Temperature, 1685 deg R (from Ref 12) . . . . .	29
7(b)	Effect of Pressure and Fuel-Air Ratio Upon Screech Boundaries (from Ref 11) . . . . .	30
8	The Effect of Turbulence on Combustion Instability Boundaries (from Ref 15) . . . . .	31
9	Variation of the Lean Screech Limit with Average Mach Number (from Ref 16) . . . . .	32
10	Variation of Lean Screech Limit with Inlet Total Temperature (from Ref 16) . . . . .	33
11	Variation of Screech Frequency with Fuel-Air Ratio (from Ref 14) . . . . .	34
12	Effect of Perforated Liner on Screech Limits in 26-Inch-Diameter Duct (from Ref 12) . . . . .	35
13	Frequency of the Unstable Oscillations in the High Frequency Range as a Function of Chamber Length (from Ref 2) . . . . .	36
14	Effects of Gas Temperature and Velocity on Absorption Coefficients of Cooled Liners (from Ref 25) . . . . .	37
15	Pressure Oscillation Amplitude vs Chamber Length (from Ref 54) . . . . .	38
16	Oscillograph Record Illustrating the Start of the Oscillations (from Ref 52) . . . . .	39
17	Instability Region and Amplitudes (from Ref 54) . . . . .	40
18	Transverse Mode Instability Regions (from Ref 54) . . . . .	41
19	Hydrogen Stability Boundaries (from Ref 54) . . . . .	42
20	Amplitude of Oscillations vs Baffle Length (from Ref 54) . . . . .	43

# Contents

Figure No.	Title	Page
21	Dimensionless Frequency vs Length/Diameter for Several Modes of Oscillation (Annular Cylinder, $a/b = 1.1$ ) . . . . .	44
22	Dimensionless Frequency vs Length/Diameter for Several Modes of Oscillation (Annular Cylinder, $a/b = 1.3$ ) . . . . .	45
23	Dimensionless Frequency vs Length/Diameter for Several Modes of Oscillation . . . . .	46
24	Dimensionless Frequency vs Length/Diameter for Several Modes of Oscillation . . . . .	47
25	Variation of Longitudinal Mode Shapes Upstream and Downstream of a Temperature Discontinuity with Temperature Ratio . . . . .	48
26	Variation of Frequency with Temperature Ratio Across a Temperature Discontinuity . . . . .	49
27	Variation of Longitudinal Mode Shapes Upstream and Downstream of a Temperature Discontinuity with Temperature Ratio . . . . .	50
28	Variation of Frequency with Temperature Ratio Across a Temperature Discontinuity . . . . .	51
29	Variation of Longitudinal Mode Shapes Upstream and Downstream of a Temperature Discontinuity with Temperature Ratio . . . . .	52
30	Variation of Frequency with Temperature Ratio Across a Temperature Discontinuity . . . . .	53
31	Variation of Longitudinal Mode Shapes Upstream and Downstream of a Temperature Discontinuity with Temperature Ratio . . . . .	54
32	Comparison of Predicted Frequencies with Measured Frequencies for the P&W SST Combustor . . . . .	55
33	Comparison of Predicted Frequencies with Measured Frequencies for the P&W SST Combustor . . . . .	56
34	Attenuation in Carbon Dioxide Gas . . . . .	57
35	Attenuation by Water Droplets in Air - Finite Concentration, $C_m$ . . . . .	58
36	Variation of Decrement with Chamber Surface-to-Volume Ratio for First Transverse Mode (Data of Ref 64) . . . . .	59
37	Effect of Nozzle Convergence Angle on Variation of Decrement with Effective Length for First Longitudinal Mode (Data of Ref 64) . . . . .	60
38	Effect of Injector Shape on the Variation of the Decrement with Effective Length for First Longitudinal Mode (Data of Ref 64) . . . . .	61
39	Experimental Inertance and Capacitance of an Acoustic Liner (Data of Ref 65) . . . . .	62
40	Experimental Acoustic Resistance of an Acoustic Liner (Data of Ref 65) . . . . .	63
41	Decrement vs Frequency for an Acoustic Liner (Data of Ref 65) . . . . .	64



# Contrails

Figure No.	Title	Page
42	Acoustic Reactance and Resistance Data vs Sound Pressure Level (Data of Ref 65) . . . . .	65
43	Nonlinear Resistance vs Sound Pressure Level (Data of Ref 67) . . . . .	66
44	Nonlinear Resistance vs Sound Pressure Level (Data of Ref 65) . . . . .	67
45	Effect of Amplitude of Oscillation Upon the Decrement for a Perforated Liner (Data of Ref 67) . . . . .	68
46	Acoustic Impedance as a Function of Velocity through Orifice (Data of Ref 68) . . . . .	69
47	Decrement for Convection Losses - Theoretical Data of Whitehead (Ref 71) . . . . .	70
48	Decrement and Longitudinal Wave Number Calculated as Functions of Imaginary Part of Nozzle Admittance . . . . .	71
49	Decrement and Longitudinal Wave Number Calculated as Functions of Real Part of Nozzle Admittance . . . . .	72
50	Variation of Decrement with Duct Mach Number from Experimental Measurements of Reference 69	73
51	Attenuation of Abrupt Sonic Nozzles (Results of Ref 70) . . . . .	74
52	Gain Contributions for a 27-Inch-Diameter Burner . .	75

# *Contrails*

x

# Contrails

## LIST OF TABLES

Table No.	Title	Page
I	Observed Gas-Turbine Combustion Oscillations . . . .	77
II	Effects of Radial Energy Distribution . . . . .	81

# *Contrails*

## LIST OF ABBREVIATIONS AND SYMBOLS

The practice has been adopted throughout this volume of defining the relevant symbols as they are used in the text. Accordingly, the following nomenclature is confined to the symbols in greatest usage.

A	Acoustic admittance
a	Outer radius of annulus
b	Inner radius of annulus
C	Velocity of sound
$\bar{E}$	Mean value of heat of combustion of fuel per unit mass of mixture at the entrance to the combustion zone
$E'$	Fluctuating value of heat of combustion of fuel per unit mass of mixture at the entrance to the combustion zone
e	Internal energy
f	Oscillation frequency
k	Complex frequency of oscillation
L	Length of burner
M	Mach number
m	Mode number defining tangential oscillation component ( $\cos m\phi$ )
n	Mode number defining longitudinal oscillation component ( $\cos nz$ )
p	Pressure
R	Gas constant, or burner radius
r, $\phi$ , z	Components of cylindrical coordinate system
T	Temperature
t	Time
$\underline{u}$	Gas velocity
$w_c$	Energy release per unit volume

# Contrails

- $z_1$  Axial location of beginning of combustion zone
- $\alpha$  Mode number defining radial oscillation component [ $J_m(\alpha r)$ ]
- $\beta_{m,r}$  Dimensionless radial mode number,  $\pi \beta_{m,r} = \alpha R$
- $\gamma$  Ratio of specific heats
- $\delta$  Oscillation decrement =  $2\pi\lambda/\omega$
- $\lambda$  Damping constant
- $\nu$  Dimensionless longitudinal mode number,  $nL/\pi$
- $\eta$  Dimensionless perturbation pressure,  $p'/p_0$
- $\rho$  Gas density
- $\tau$  Characteristic time of combustion process
- $\tau'$  Fluctuation in characteristic time of combustion process
- $\omega$  Angular frequency of oscillation

In addition, primes have been used to denote fluctuating quantities, and the subscript 0 refers to mean flow conditions.

## Section I

### INTRODUCTION

#### PROBLEM DEFINITION

This investigation is directed toward an assessment of the problems presented by unsteady combustion in duct burners and afterburners. The specific problems of interest are those related directly to the stability of integrated propulsion systems. These problems are best appreciated by a brief discussion of the physical sources and practical consequences of the problems, the present state-of-the-art in the treatment of these problems, and the salient engineering difficulties which remain in the treatment of these problems.

#### PHYSICAL SOURCES AND CONSEQUENCES OF UNSTEADY COMBUSTION

Unsteady combustion phenomena in turbojet and turbofan engines are of two basic types: combustion instability (screech) and the transient process associated with burner light-off.

#### Combustion Instability

This problem is manifested by high frequency pressure oscillations ( $\geq 150$  cps) in the burner, and is commonly referred to as screech due to the noise associated with the process. The frequencies of these oscillations and the spatial distributions of the pressure amplitudes are determined by the resonant acoustical modes of the burner (e.g., longitudinal or "organ pipe" modes and transverse or "sloshing" modes) which are in turn governed by the geometry of the burner and the temperature distribution in the burner. There are two other features of combustion instability which are particularly significant with regard to propulsion system integration problems. First, the occurrence of instability is quite sensitive to relatively small changes in gross operating conditions; hence, its occurrence sometimes appears to be virtually random. Second, it is known that combustion systems which are stable to small disturbances sometimes become unstable when subjected to large disturbances; this character of combustion instability is referred to here as nonlinearity.

The consequences of combustion instability depend upon the amplitude of the pressure oscillations; at large amplitudes (of the order of 50 per cent of the mean static pressure level, say) destruction of the burner results due to either increased heat transfer rates and/or increased pressure loading on the internal structure. At low amplitudes (less than 10 per cent of the mean static level, say) in the case of turbofans, the oscillations may tend to aggravate substantially fan stall problems due to the fact that they expose the fan to a variable back pressure.

## Light-Off

When ignition of a burner occurs, a pressure pulse propagates upstream much in the manner of a blast wave. In a turbojet afterburner, the incidence of this pressure pulse on the turbine leads to an immediate reduction of turbine power and a consequent tendency to stall the compressor. In a turbofan, the incidence of this pulse on the fan has a direct tendency to stall the fan. The possibility also exists that the magnitude of the pressure pulse is sufficient to trigger instability in an otherwise stable burner.

## STATE OF THE ART

### Combustion Instability

At present, combustion instability in burners is treated primarily as a component development problem. That is, when combustion instability has been observed within the normal operating regime of an engine, the usual procedure has been to destroy as much as possible the resonant acoustic properties of the burner by the addition of suitable liners or baffles. This process is largely a trial and error one which is continued until the instabilities disappear. As a result of this historical treatment in which analytical representations of the process, although useful, are not essential, very little analytical effort has been devoted to this problem.

### Light-Off

As in the case of combustion instabilities, the light-off transient has also been treated primarily as a component development problem. The procedure here has been to control the fuel flow rate and the exhaust nozzle setting so as to produce the smallest possible disturbance at light-off within the constraints of a given design. Once again, very little analytical effort has been devoted to this problem.

## ENGINEERING DIFFICULTIES

### Combustion Instability

The most outstanding practical difficulties associated with combustion instability in burners are directly attributable to problems encountered in the integration of an engine and an airframe. As mentioned previously, two notable characteristics of combustion instability are its sensitivity to small changes in gross operating conditions and its non-linearity (i.e., large transient disturbances may produce instability, even though small disturbances do not). It follows that the demonstrated stability of a burner under selected engine test rig conditions does not ensure stability under actual flight conditions; the problem here is not



# Contrails

so much that instability is likely to occur at normal flight conditions, but rather that severe flight conditions resulting in either flow distortion or transient disturbances of appreciable magnitude may trigger instability. It is therefore distinctly possible that some portion of an aircraft's flight envelope may be limited by combustion instability in a burner which was in fact stable under test rig conditions; due to the historically empirical treatment of instability in aircraft burners and the resultant lack of analytical effort, there exists at present no way to predict and/or modify the stability properties of a burner short of an exhaustive program of ground and flight testing and development, which is neither feasible nor desirable. This is the central problem considered in this task.

Another engineering difficulty which is becoming apparent is the increasing amount of development effort which must be devoted to overcoming instability problems in large, high-volumetric-energy-release combustors. Although this difficulty is not directly related to engine-airframe integration problems and the present task is accordingly not directed specifically at this difficulty, the results of this task will obviously be relevant to this problem.

## Light-Off

The major difficulties associated with light-off are also related to the integrated propulsion system, in that here again demonstration of satisfactory performance under engine test rig conditions does not ensure satisfactory performance under actual flight conditions. This is due to the fact that the stall characteristics of the compressor or fan may be significantly altered in extreme flight conditions and hence the effect of the transient pressure pulse on compressor or fan performance will not be the same as at normal operation. A basic requirement for an appreciation of the difference is the form of the pressure pulse produced by light-off; unfortunately, there exists at present no method to predict the magnitude and form of this pulse.

## PROGRAM OBJECTIVES

### SPECIFIC OBJECTIVES

Due to the complexity of any analytical work relevant to unsteady combustion processes in aircraft burners, it was presumptuous to presume that a completely satisfactory dynamic model of these processes could be formulated and tested within the scope of the present task. Accordingly, this task had more limited, but nevertheless ambitious, specific objectives. These objectives were:

1. To formulate and analyze a model or models of unsteady combustion processes in aircraft burners suitable for use in extrapolating the results of rig tests to obtain the permissible operating envelope of a burner under actual flight

# Contrails

conditions. Thus, the model should incorporate important physical mechanisms in a readily identifiable way even though the analytical descriptions of these mechanisms may require the introduction of empirical parameters requiring experimental determination.

2. To formulate a test plan for the verification of the models developed.

It was recognized at the outset that the major question was in fact whether or not these objectives were feasible; the attitude adopted in this task was that the feasibility of these objectives could be best assessed by endeavoring to accomplish them.

## ULTIMATE GOALS

The restricted nature of the specific objectives above tends to mask the practical significance of this task. Accordingly, a set of ultimate goals was also established in order to provide over-all guidance for the effort, in which the present task could be construed as a first step. These ultimate goals were:

1. To determine the practical conditions, if any, at which burners which are stable under test rig conditions can become unstable at actual flight conditions due to the effects of either flow distortion or large transient disturbances.
2. To formulate general test criteria so that satisfactory burner test-rig performance will ensure satisfactory performance at actual flight conditions.
3. To determine those operating parameters which would be effective in controlling the onset of combustion instability at actual flight conditions, and thereby provide a means for extending the flight envelope by an appropriate control system without requiring design modifications of the burner.
4. To determine those design variables which were most effective in enlarging the range of stable operation of a burner and thereby provide a means for minimizing the amount of control necessary in an integrated system.

## METHOD OF APPROACH

The method of approach employed in this task was based on the following rather elementary view of combustion instability. A combustor may be characterized simply as a roughly cylindrical or annular cavity containing an active acoustic medium (i.e., a gas which will both support wave propagation and which may by means of the combustion process also supply energy

# Contrails

to or absorb energy from any wave motion) and bounded by surfaces which may also supply energy to or absorb energy from any wave motion. Two conditions are necessary for instability to occur and they can be described quite simply. First, the system must be capable of supporting oscillations; this capability is in a large measure determined by the physical and geometrical properties of the acoustical media involved and the conditions at the bounding surfaces. Second, at any frequency for which oscillations exist it is necessary for some range of amplitudes below the steady-state amplitude that the energy supplied to the oscillation from either the combustion process and/or from an upstream source such as a fan exceed the energy dissipated by the oscillatory motion either at the boundaries or within the bulk of the gas. At the steady-state amplitude the energy supplied to the oscillation is of course equal to the energy dissipated by it.

Based on the preceding simplified view of instability, the requirements for a satisfactory analytical model are that it must portray the resonance properties of the burner, it must incorporate the significant loss (dissipative) mechanisms, it must incorporate the significant driving (energy addition) mechanisms, and it must be capable of predicting the amplitude of steady-state oscillations. The method of approach employed in this task was formulated accordingly, and consisted of:

1. A survey of the literature related to instability in both gas-turbine burners and rocket-engine combustors. The latter area was anticipated to be quite productive in providing analytical descriptions of the various phenomena inasmuch as considerable effort has been devoted to this area in the past decade.
2. Appropriate acoustical analyses to provide an assessment of the resonant modes which are most likely to be encountered in burners.
3. An assessment of the relative importance of the various losses which can contribute to the damping of wave motion in burners.
4. An appraisal of the relative importance of the various driving mechanisms which can supply energy to wave motion in burners.
5. The formulation of analytical models (consisting of a set of equations and boundary conditions which attempt to define adequately either transient processes and/or steady-state oscillations) incorporating those loss and driving mechanisms found to be significant.
6. A parametric analysis of the models aimed at evaluating the adequacy of the models and at identifying those parameters which most significantly influence the transient response and/or instability characteristics of a given burner.

# *Contrails*

7. The formulation of a test plan suitable for evaluating experimentally the adequacy of the models.

# Contrails

## Section II

### SUMMARY

The major results of this investigation can be summarized as follows:

1. An analytical model of combustion instability has been formulated which incorporates in a readily identifiable way the significant loss and gain processes associated with oscillatory combustion. The dominant loss mechanisms, as revealed by literature survey and subsequent assessment, are those due to convection and radiation from the nozzle and absorption by acoustic liners. The gain mechanisms have been incorporated in a general way which permits physical interpretation; those mechanisms considered to be of most importance in aircraft burners are those associated with fuel vaporization and turbulent transport processes.
2. The analytical model is capable of incorporating significant non-linear aspects of combustion instability. Specifically, the dependencies of the major losses and gains on oscillation amplitude are treated by the model.
3. The analytical model is amenable to relatively simple solution procedures. In all cases, solutions of transcendental algebraic equations and the evaluation of definite integrals constitute the total mathematical requirement.
4. An application of the model to a known experimental situation has produced results which are qualitatively correct and quantitatively of the correct order of magnitude.
5. A test plan has been formulated which will enable the adequacy of the analytical models to be assessed, as well as provide information previously lacking concerning the nature of instability in aircraft burners. The test plan will enable the loss and gain mechanisms to be determined more accurately than in the past, particularly with regard to their dependence upon oscillation amplitude.

These observations support the conclusion that it is indeed feasible to represent unsteady combustion processes by analytical models, and to obtain practically useful results from these models.

# *Contrails*

## Section III

### RESULTS AND DISCUSSION

#### LITERATURE SURVEY

The results of this survey are reported in detail in Appendix A; a synopsis of these results is presented here.

From a survey of over sixty documents pertaining to combustion instability in both gas-turbine and rocket-engine combustors, it was concluded that although the experimental evidence of acoustical instability in gas-turbine burners was abundant, virtually no analytical effort has been devoted to the problem.

Analytical effort devoted to instability in rocket-engine combustors has been substantial. The analytical description of combustion instability based on linearized, acoustical treatments of the Navier-Stokes equations has been reasonably well-developed (Refs 1 and 2, for example); the difficulties in the existing treatments are that they generally incorporate inadequate models of the driving mechanisms and that they are incapable of providing information relevant to the amplitude of an oscillation. Non-linear treatments aimed at determining oscillation amplitudes (e.g., Refs 3 and 4) are both quite complicated and very restrictive.

The various loss mechanisms by which an oscillation can dissipate energy have all been examined analytically in the existing literature. The most serious deficiencies in analytical representations of these loss mechanisms are those associated with liner losses and nozzle losses and in the dependence of the losses upon the amplitude of oscillation.

Although much effort has been devoted to analysis of possible driving mechanisms in rocket-engine combustors, no satisfactory analytical representations were found. The two most popular models are those of Crocco (Refs 2 and 5) and Priem (Ref 6). The Crocco model relates fluctuations in the energy release rate to fluctuations in pressure (or other physical properties) by means of two parameters which cannot be interpreted physically and which can only be determined experimentally for a given burner at specific operating conditions. Priem uses somewhat more realistic models but they too are difficult to interpret physically and also require very complicated nonlinear mathematical treatment.

Possibly the most significant physical result obtained from the rocket literature which is relevant to gas-turbine burners was the observation that the energy involved in a combustion oscillation is very small compared to the energy being released by the steady-state combustion process (typically less than 1 per cent) and further that the energy supplied to or dissipated by a combustion oscillation per oscillation cycle tended to be smaller than the acoustical energy involved in the oscillation (see Ref 7). These observations indicate that the frequencies and mode shapes obtained

# Contrails

from a purely acoustical analysis (that is, an analysis which ignores the energy gains and losses) are in most cases reasonable approximations to the actual situation.

## ACOUSTICAL ANALYSES

Resonant mode shapes and frequencies were determined for cylinders and annuli based on the standard linearized acoustical treatment of the Navier-Stokes equations for various combinations of "closed-end" and "open-end" boundary conditions. Based on these results, it was concluded that the range of frequencies of instability likely to be encountered in aircraft burners was approximately from 150 cps (for a first transverse mode in a large burner) to 7500 cps (for a combined third transverse-first radial mode in a small burner). In the majority of cases of practical interest, the frequencies will be less than 2000 cps.

In an effort to assess the more important aspects of the temperature distribution encountered in burners, solutions were also obtained for cylinders and annuli in which the beginning of the combustion zone was represented by a temperature discontinuity. It was found that the temperature discontinuity produced substantial frequency changes in some cases. For example, Figure 1 indicates the calculated frequencies of the first transverse mode both with and without a temperature discontinuity and the experimentally-observed frequencies for a large duct burner (Ref 8). Another significant effect of the temperature gradient was to increase generally the amount of longitudinal coupling associated with any transverse mode.

A detailed presentation of the acoustical analyses is included as Appendix B.

## ASSESSMENT OF LOSS MECHANISMS

Loss mechanisms in burners can be categorized as either bulk losses or boundary losses depending upon whether they occur within the gas or at the bounding surfaces of the burner. An appropriate measure of these losses is the loss decrement which is defined here by the energy loss per oscillation cycle expressed as a fraction of the total acoustical energy associated with the oscillation. Roughly speaking, for example, if the loss decrement is  $10^{-2}$  then an initial oscillation would "ring" for approximately 100 cycles before being completely damped.

Estimates were made of the maximum decrements expected from the bulk losses due to viscous dissipation, heat conduction, relaxation of the molecular internal energy modes, and the presence of dispersed phases (liquid droplets or smoke particles), with the following results:



# Contrails

<u>Mechanism</u>	<u>Loss Decrement</u>
Viscous Dissipation	$\sim 10^{-4}$
Heat Conduction	$< 10^{-4}$
Relaxation	$< 10^{-1}$
Dispersed Phases	$\sim 10^{-3}$ (droplets) $< 10^{-2}$ (smoke)

Similar estimates were made for the maximum loss decrements to be expected from boundary losses due to viscous dissipation, heat conduction, acoustical absorption by liners, and nozzle losses due to both radiation and convection, with the following results:

<u>Mechanism</u>	<u>Loss Decrement</u>
Viscous Dissipation	$\sim 10^{-2}$
Heat Conduction	$< 10^{-2}$
Acoustic Absorption by Liners	$\sim 1$
Nozzle Losses	$\sim 1$

No satisfactory way was found to estimate the losses due to acoustical radiation from the upstream end of a burner. More detailed discussions of all of the loss mechanisms are presented in Appendices C, D, and E.

From these results, it was concluded that acoustic absorption by liners and radiation and convective losses through nozzles were the most dominant loss mechanisms, and those which must be incorporated into an analytical model.

## ASSESSMENT OF DRIVING MECHANISMS

The assessment of driving mechanisms was troublesome due to the lack of an acceptable analytical representation. It was accordingly necessary to develop such a representation. A complete discussion of the assessment of such mechanisms is presented in Appendix F; only the major results are summarized here.

## ELEMENTARY CONSIDERATIONS

From consideration of a simple spring-mass system acting on a gas in which the energy release rate varies with the pressure level, and extrapolating these results to conditions in an actual burner, it was shown that the energy increment attributable to a fluctuating energy release rate was given by

$$2\delta = \frac{2(\gamma-1)}{P_0 f} \left( \frac{Q_0}{V} \right) N \quad (1)$$

where  $P_0$  = mean static pressure  
 $f$  = oscillation frequency  
 $Q_0$  = mean energy release rate in burner  
 $V$  = total volume of burner  
 $N$  = constant of proportionality between fluctuating energy release rate and fluctuating pressure defined roughly by  $Q'/Q_0 = N(p'/P_0)$  where the primes denote fluctuating quantities.

Here, the energy increment is defined in a manner similar to the loss decrement; it is the energy added per oscillation cycle expressed as a fraction of the total acoustical energy in the burner. It can be immediately concluded from this relation that low pressure levels, low frequencies (large sizes) and high volumetric energy release rates all contribute to greater driving of the oscillation by the combustion process. A typical value for the energy increment for a large duct burner (Ref 8) is approximately  $5N$ . As indicated subsequently, typical maximum values of  $N$  are of order of unity; hence it is quite apparent from the fact that loss decrements are typically of order unity that ample energy is available for driving oscillations depending upon the sensitivity of the energy release rate to pressure fluctuations.

## MODEL OF DRIVING PROCESS

A model of the driving process was constructed based upon the assumption that the steady combustion process could be characterized by a single characteristic time  $\bar{\tau}$ , with the usual physical interpretation that it is the residence time of a fluid element required for the combustion process to proceed within  $e^{-1}$  of completion, and an energy per unit mass  $\bar{E}$  which corresponds to the heat of combustion of the fuel in the fluid element at entry to the combustion zone. The unsteady combustion process was correspondingly characterized by  $\bar{E}'$ ,  $\bar{\tau}'$ , and the fluctuations of these quantities  $E'$ ,  $\tau'$ , in response to fluctuations in gas properties due to oscillations. The primary advantage of this model, and a significant one, is that the characteristic quantities  $\bar{E}$ ,  $\bar{\tau}$ ,  $E'$ , and  $\tau'$  are capable of physical interpretation and hence can be estimated from basic physical considerations.

# Conclusions

The resulting analytical expression for the fluctuating energy release rate was evaluated for typical longitudinal and transverse acoustic modes. Three significant results were noted. First, substantial driving can be achieved in modes with longitudinal components even in the absence of any sensitivity of the characteristic time of the combustion process to pressure fluctuations (i.e.,  $\tau' = 0$ ), indicating the importance of correctly evaluating the longitudinal components associated with transverse waves. Second, maximum driving can be expected at oscillation frequencies such that  $\omega \bar{\tau} \approx 1$  where  $\omega$  is the angular frequency of the oscillation. This provides the necessary criterion for evaluating the potential importance of a driving mechanism (characterized by  $\bar{\tau}$ ) in a specified frequency range. Third, typical maximum values of the rates of the fractional change in energy release to the fractional change in pressure associated with an oscillation are such that  $N$  in Equation 1 is approximately unity. Hence the maximum potential driving available in a burner can be quickly estimated from a knowledge of gross quantities.

## APPRAISAL OF DRIVING MECHANISMS

The physical processes of most potential importance as driving mechanisms are those associated with vaporization of the fuel, chemical reaction of the fuel and air, and turbulent transport processes involved in providing a fuel-air mixture and temperature level appropriate for efficient combustion. An assessment of the relative importance of these mechanisms was made on the basis that a necessary condition for appreciable driving was that  $\omega \bar{\tau} \approx 1$ . Based on estimates of droplet sizes and vaporization times, it was concluded that vaporization was an important mechanism in the frequency range of 100-2000 cps with a relatively larger contribution in the lower part of this range. From estimates of chemical reaction times based on available experimental data, it was concluded that chemical kinetics were unlikely to be an important driving mechanism in aircraft burners. Although only very crude estimates of turbulent transport processes could be performed, it was concluded that they are likely to be of equal importance to vaporization as a driving mechanism in aircraft burners.

Based on the preceding assessment, possible analytical relationships between the characteristic time fluctuation  $\tau'$  and either pressure or velocity fluctuations associated with oscillatory modes were developed for vaporization and transport mechanisms. In the case of vaporization, for low amplitudes of oscillation,  $\tau'$  was related to  $p'$  through a single constant whose value can be estimated from basic physical considerations. For larger amplitudes,  $\tau'$  was related to  $p'$  by the introduction of two additional parameters whose values can best be determined by experiment. In the case of turbulent transport processes, similar relations were developed between  $\tau'$  and the velocity fluctuation  $u'$  since it appeared that the transport processes would be quite sensitive to velocity fluctuations but rather insensitive to pressure fluctuations.

## ANALYTICAL MODEL

The development of the model equations and their solution is presented completely in Appendix G; the major features of the model and its solution are discussed below.

## FORMULATION

The basic analytical model of combustion instability was formulated in a manner similar to that developed by Culick (Ref 1). Acoustical properties of the burner are determined by assuming the burner to be divided into two uniform regions-- hot and cold-- with the interface represented by an acoustical impedance  $A_f$  (due to the physical structure of the flameholder). The governing equations are those of continuity, momentum, and energy linearized for small perturbations for a mean flow in the axial direction only. The boundary conditions are represented by equivalent acoustical impedances,  $\bar{A}_i$ , such that

$$\frac{1}{p'} \frac{\partial p'}{\partial n_i} = \bar{A}_i \quad (2)$$

where  $n_i$  is the normal to the bounding surface. The resulting formulation portrays the effects of acoustical energy losses or gains at the bounding surfaces through the impedances  $\bar{A}_i$  (in general, there are four such impedances corresponding to the upstream boundary, the nozzle, and two liner surfaces) and the effects of driving by the fluctuating energy release rate which appears as an inhomogeneous term in the usual wave equation. The general form of solution to these equations is the usual damped wave solution  $p' \sim e^{-\lambda t} (\cos \omega t + \phi)$  where  $\lambda$  is the damping constant indicative of whether an oscillation will grow or decay and  $\phi$  is an arbitrary phase angle.

The basic physical parameters of this model are in general the five equivalent acoustical impedances (corresponding to four bounding surfaces and the interface between the cold upstream region and the combustion zone), and the four parameters ( $\bar{C}$ ,  $\bar{E}$ ,  $\bar{r}'$ ,  $\bar{E}'$ ) which relate the unsteady combustion process to other fluctuating quantities. Although the model is basically a linearized one, nonlinear effects due to the dependence of these nine parameters on either oscillation amplitude or distortion of mean flow conditions can be treated in an approximate way.

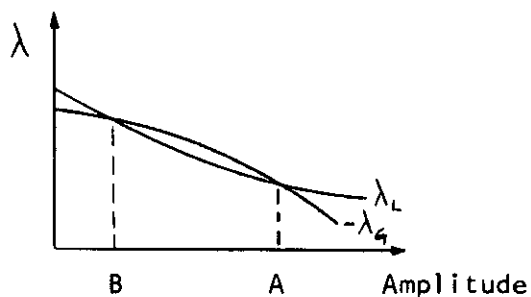
## APPROXIMATE SOLUTION

Two approximate forms of the general solution to the instability model have been obtained. The first form, and the more accurate one, is basically an extended form of that previously presented by Culick (Ref 1) based on an iterative solution where the zero-order solution is in the absence of driving due to fluctuating energy release. No further effort was devoted to this form of the solution due to the fact that numerical answers could be obtained efficiently only through the use of a computer. The second form of the

solution was obtained by a straightforward perturbation procedure in which the zero-order solution was the pure acoustic solution in the absence of any energy losses or gains. The second order solution for the damping constant  $\lambda$  and the frequency  $\omega$  then explicitly portrayed the effects of fluctuating energy release, convection, wall losses, upstream boundary losses or gains, and nozzle losses.

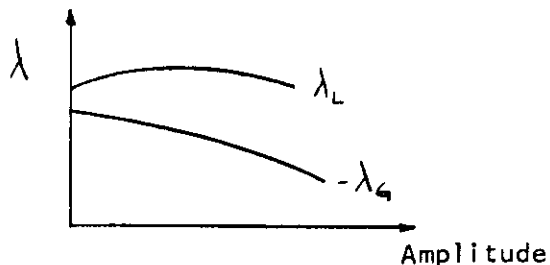
## NATURE OF SOLUTION

The significant features of the solution can best be illustrated by considering the effect of the oscillation amplitude on the damping constant  $\lambda$ . The contributions to  $\lambda$  due to the losses and gains can be separated, and are denoted here by  $\lambda_L$  and  $\lambda_G$ , respectively. By definition  $\lambda_L > 0$  and  $\lambda_G < 0$ ; the solutions of interest are steady-state oscillations, for which  $\lambda_L + \lambda_G = 0$ . The general solution obtained permits the calculation of these quantities as a function of oscillation amplitude and mean flow conditions. A typical case of interest is illustrated below:



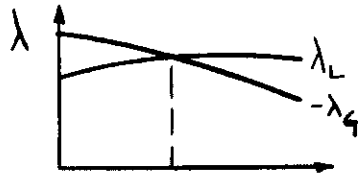
In this case the burner would be stable to disturbance amplitudes less than B but would be unstable to disturbance amplitudes greater than B with a resulting steady-state amplitude of A. This is an illustration of nonlinear instability.

A second case of particular interest is the possible effect of flow distortion on stability characteristics. For example, uniform inlet flow conditions may yield the following forms of  $\lambda_G$  and  $\lambda_L$ :



which is of course a stable situation. Distorted flow conditions may produce the following forms:

# Contrails



which is now an unstable situation resulting in an oscillation of amplitude  $A$ .

The precise forms of the  $\lambda_q - \lambda_L$  curves depend upon the gross geometry and operating conditions of the burner as well as the nine parameters of the model (i.e., the five equivalent acoustical impedances associated with the four bounding surfaces and the interface between the cold upstream region and the combustion zone, and the four parameters ( $\bar{C}, \bar{E}, \bar{C}', E'$ ) which relate the unsteady combustion process to other fluctuating quantities). Accordingly, the stability problem of a burner is readily analyzed with this model provided that these nine parameters can be specified, including their dependencies on oscillation amplitude, frequency, mode shape, and mean flow conditions. Conversely, the model can be used to obtain the relevant dependencies of some of these parameters from experimental results; this important feature forms the basis for the test plan discussed subsequently.

## ILLUSTRATIVE CALCULATION

The stability model was applied to an afterburner for which a limited amount of experimental data was available (Ref 9). The basic nature of this data was that in the absence of an acoustical liner combustion instability occurred in the burner, in the first transverse mode of oscillation with an amplitude of 310 psf. In the presence of an acoustical liner at the same operating conditions, instability did not occur (the detection threshold of instability was an amplitude of approximately 50 psf; i.e., an oscillation below this amplitude would not be recorded as instability).

For this burner, both with and without the acoustic liner, the values of the nine parameters required by the instability model were estimated from available analytical results, and the  $\lambda_L$  and  $\lambda_q$  curves were constructed from the solution of the model. These curves are shown as the solid lines in Figure 2 (the ordinates in this figure are  $\text{Im}(k_q^2)$  and  $\text{Im}(k_L^2)$  where  $k^2 \equiv (\omega + i\lambda)^2 \equiv k_o^2 + k_q^2 + k_L^2$ , and hence are not precisely equivalent to  $\lambda_L$  and  $\lambda_q$ ; however it is true that  $\lambda_L + \lambda_q = 0$  when  $\text{Im}(k_o^2) + \text{Im}(k_q^2) = 0$ ). These curves are in agreement with the experimental results to the extent that unstable operation is predicted in the absence of the liner, and stable operation is predicted with the liner present. Detailed results of these calculations are presented in Appendix H.

A better appreciation of the accuracy of the theoretical results is obtained by considering, for example, the form of the  $\lambda_q$  curve necessary

to match the experimental results based on the assumption that the theoretical losses are equal to the actual losses. The form of this  $\lambda_G$  curve is indicated by the dashed line in Figure 2, and is determined by the requirements that, in the absence of the liner,  $-\lambda_G$  must equal  $\lambda_L$  at the observed oscillation amplitude and that, in the presence of the liner,  $-\lambda_G$  must equal  $\lambda_L$  at some amplitude below the detection threshold of 50 psf. The correct form of the  $\lambda_G$  curve is thus not too considerably different from the theoretically computed one; further, it has been shown from purely analytical considerations that the nonlinear effects of amplitude on  $\lambda_G$  are such to reduce  $\lambda_G$  at higher amplitudes. In view of this fact and the fact that the solid curves in Figure 2 were based on purely analytical information, the results are considered to be quite satisfactory and to provide a strong indication that the basic analytical framework is sound.

## FORMULATION OF TEST PLAN

The test plan which was formulated is discussed completely in Appendix I; the major features of this plan are presented here. The purposes of the test plan are:

1. To obtain simultaneously stability data and loss data under controlled conditions in order that the nine parameters required by the model can be determined more precisely.
2. To compare the analytical results of the model and the experimental results at conditions other than those from which the parameters were evaluated, and thereby assess the adequacy of the model.
3. To demonstrate the occurrence of nonlinear instability in a model burner by subjecting a stable configuration to successively larger disturbances.
4. To obtain, in one instance, an indication of the effects of flow distortion on the stability properties of a model burner.

The test plan consists of the following tests to be conducted on a model burner:

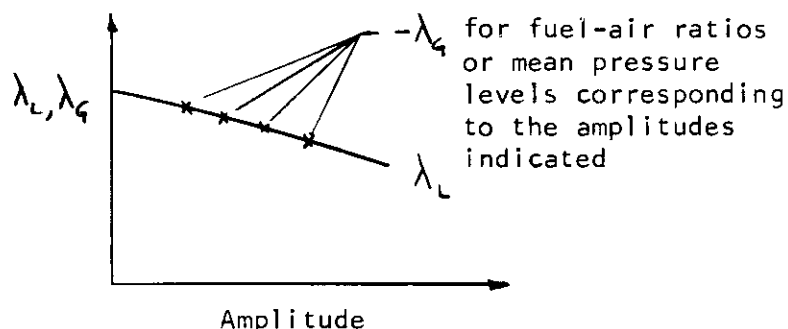
1. The determination of the acoustical losses associated with the nozzle and the upstream boundary of the burner under cold flow conditions. This can be accomplished by observing the decay rate of resonant oscillations induced by an appropriate oscillator. The amplitude dependence of these losses is of particular interest.
2. The determination of the acoustical losses associated with a liner, under cold flow conditions. This can be accomplished by adding different lengths of liner to the basic burner configuration and observing the decay rate of oscillations as in 1 above.

# Conclusions

3. The determination of oscillation amplitudes as a function of fuel-air ratio and mean static pressure level in the burner, with combustion. This is a straightforward procedure provided that instability can be induced in the burner. It is anticipated that appropriate modifications of the fuel injection system will be necessary to induce instability. Data should be obtained for various lengths of liner in the burner.
4. The determination of oscillation amplitudes as a function of fuel-air ratio and mean static pressure level in the burner, with combustion and when subjected to external oscillatory disturbances of appreciable magnitude. Emphasis here will be placed upon investigating operating conditions which yield stable performance in the absence of external disturbances.
5. A repeat of step 4, but with various inlet flow distortion patterns imposed upon the burner rather than external oscillatory disturbances.

The results of steps 1 and 2 will enable the  $\lambda_L$  curves to be computed analytically to an acceptable degree of accuracy for all test conditions. For each given combination of geometrical configuration and resonant mode this will result in basically one experimentally based curve of  $\lambda_L$  versus oscillation amplitude.

The results of step 3 for any given combination of geometrical configuration and resonant mode will permit the parameters of the driving mechanism which determine its amplitude dependence to be determined. That is, a plot of the following form can be constructed to determine  $\lambda_G$  as a function of amplitude:



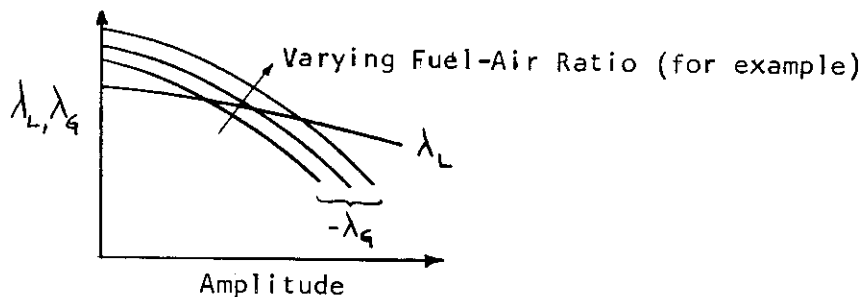
Here, the  $\lambda_L$  curve is the experimentally based one obtained from the results of step 2, and the intersection points for  $-\lambda_G$  are determined from the requirement that  $-\lambda_G = \lambda_L$  for any oscillation of steady amplitude. Inasmuch as the dependence of  $\lambda_G$  on fuel-air ratio and mean pressure level has already been incorporated into the analytical model, then the results for a single geometrical configuration can be used to



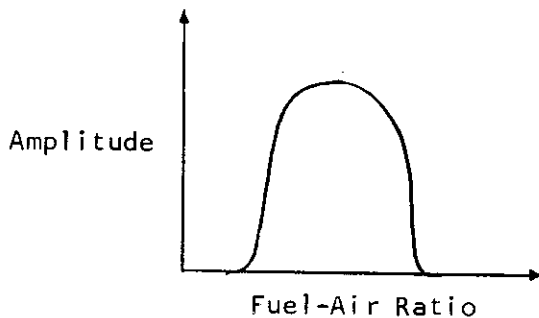
# Contrails

determine the parameters of the driving mechanism. These parameters should then be applicable to all geometrical configurations (i.e., those with different liner lengths) for the prediction of  $\lambda_G$ .

The results of step 3 for the geometrical configurations other than the one used to determine the parameters of the driving mechanism will permit the adequacy of the model to be assessed. This can be accomplished by first constructing the  $\lambda_G - \lambda_L$  curves for a particular configuration:



The intersections of the theoretical  $\lambda_G$  curves with the experimentally based  $\lambda_L$  curve will then enable the oscillation amplitude to be determined as a function of fuel-air ratio (or mean pressure level):



This theoretical curve can then be compared directly with the experimental observations.

# *Contrails*

## Section IV

### CONCLUSIONS AND RECOMMENDATIONS

#### CONCLUSIONS

The most significant conclusions resulting from this task are as follows:

1. An analytical model of combustion instability has been formulated which incorporates in a readily identifiable way the significant loss and gain processes associated with oscillatory combustion.
2. The analytical model is capable of incorporating significant non-linear aspects of combustion instability.
3. The analytical model is amenable to relatively simple solution procedures.
4. An application of the model to a known experimental situation produced results which were qualitatively correct and quantitatively of the correct order of magnitude.
5. A test plan has been formulated which will enable the adequacy of the analytical models to be assessed, as well as provide information previously lacking concerning the nature of instability in aircraft burners.

Based on these conclusions, it is further concluded that it is indeed feasible to represent unsteady combustion processes by analytical models, and to obtain practically useful results from these models.

#### RECOMMENDATIONS

It is recommended that the proposed test plan be implemented. In addition, it is recommended that a complementary analytical program be conducted in order to improve both the utility and physical appreciation of the present analytical model. This program would consist of:

1. The development of a computer program based on the analytical model developed in this task to enable the natural frequencies, mode shapes, and acoustical energy transfers to be rapidly evaluated. For the purposes of the present program these calculations were performed by hand, and were quite tedious and time-consuming. Existence of a computer program would render the evaluation of the results of the test plan considerably more efficient, and would also make possible rather complete parametric analyses in order that the features of the model can be better appreciated.

# Contrails

2. The analysis of the results of the proposed test plan in the manner previously described.
3. Parametric analyses of typical situations in order to obtain a better description of the driving mechanisms, and to isolate those parameters of most significance in potential methods for the control and/or elimination of combustion instability in propulsion systems.

In addition to the results related specifically to a complete assessment of the analytical model, the combined test plan and analytical program recommended above is expected to yield the following analytical results related to the ultimate goals of the over-all effort described on page 4:

1. For two typical burners which are stable under test rig conditions, the determination of the practical conditions at which they can become unstable at actual flight conditions due to the effects of flow distortion or large transient disturbances.
2. For two typical burners, the formulation of specific rig-test criteria such that satisfactory rig tests will ensure satisfactory performance at actual flight conditions.
3. For two typical burners, the determination of the operating parameters which would be effective in controlling the onset of combustion instability at actual flight conditions.

In addition to providing useful results for the typical burners examined, these results will also serve to illustrate the general technique to be employed.

Finally, it is recommended that a simple one-dimensional unsteady flow model of light-off transients on both compressor/fan and burner stability can be assessed.

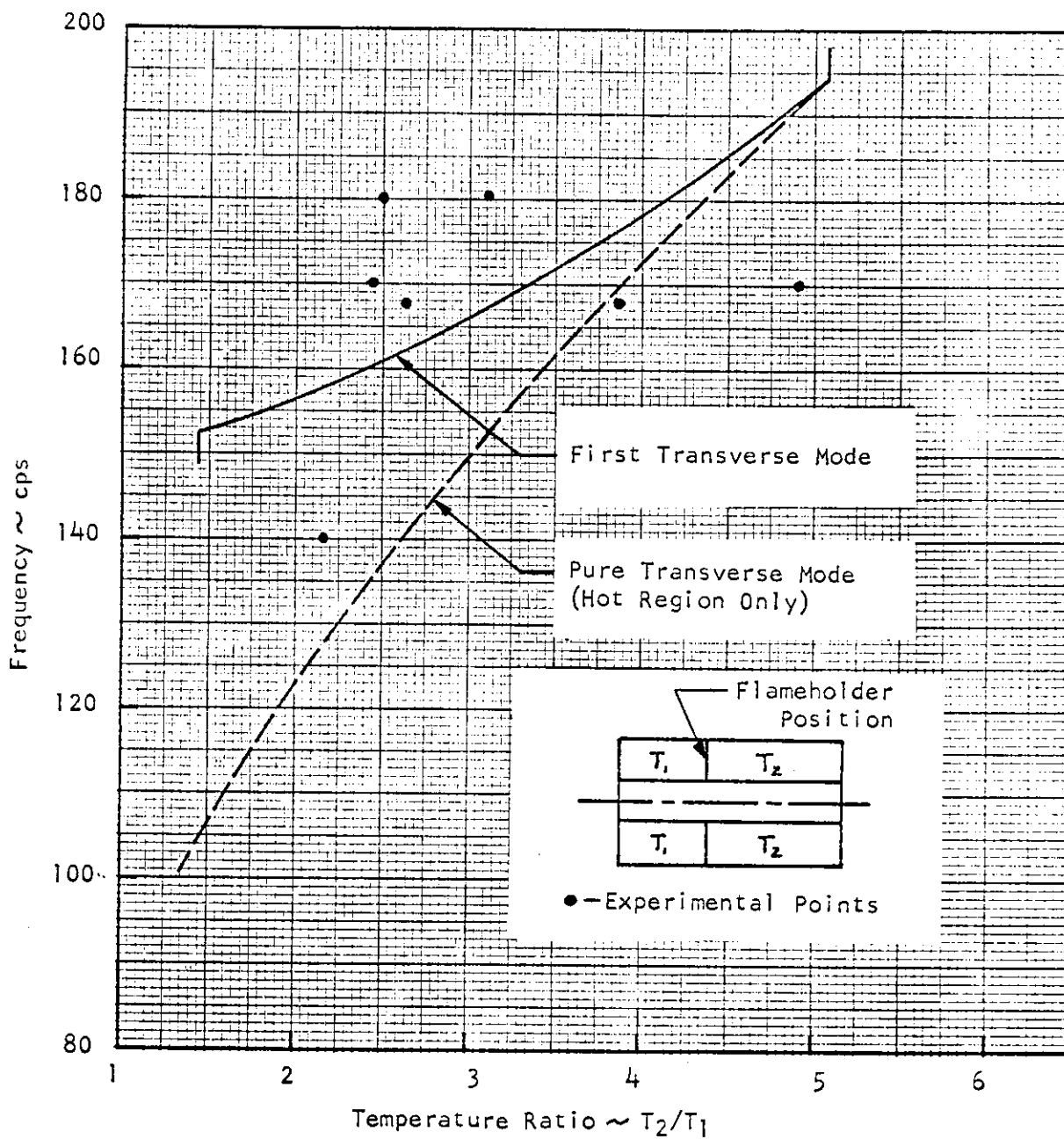


FIGURE 1 - COMPARISON OF PREDICTED FREQUENCIES WITH MEASURED FREQUENCIES FOR A LARGE DUCT BURNER

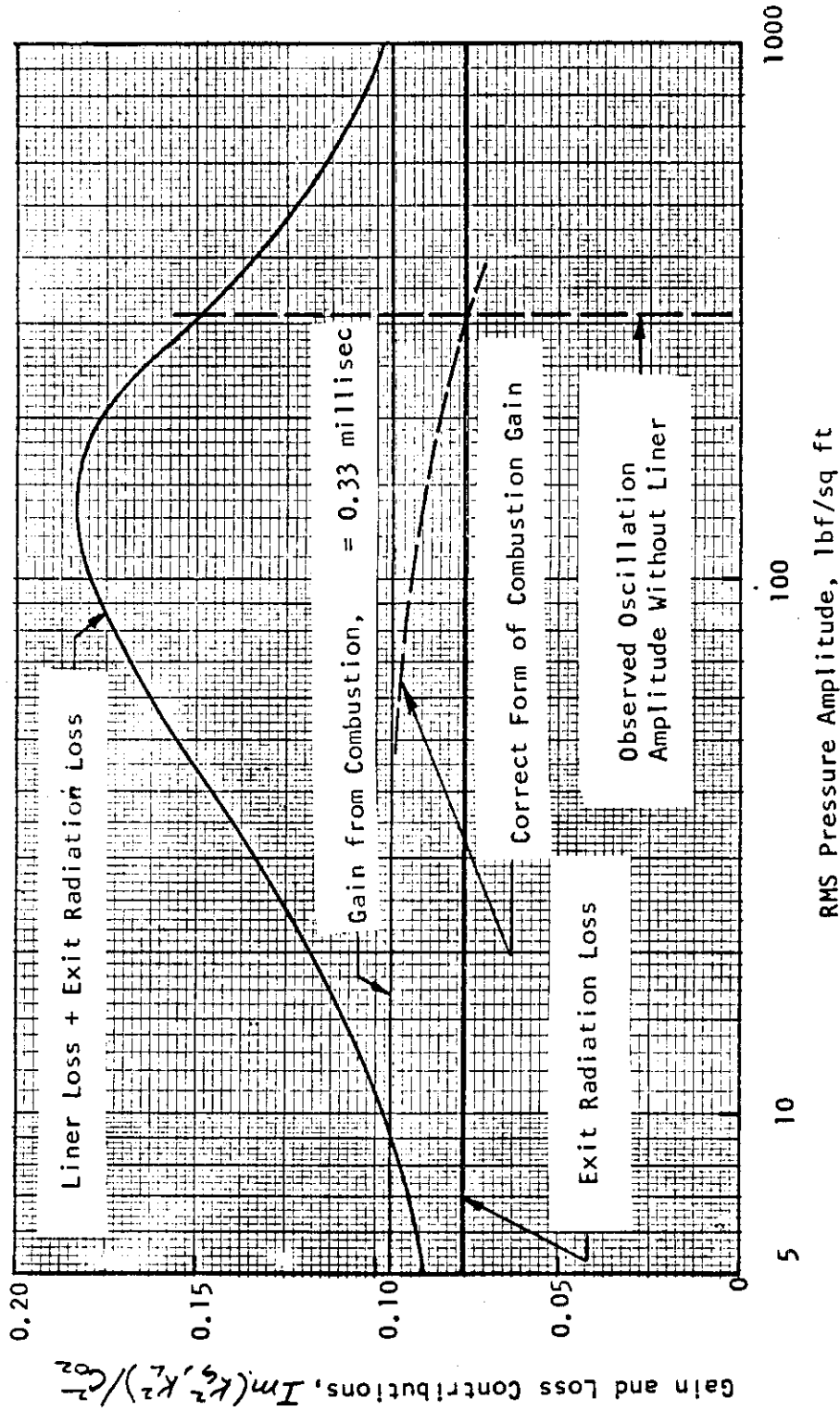
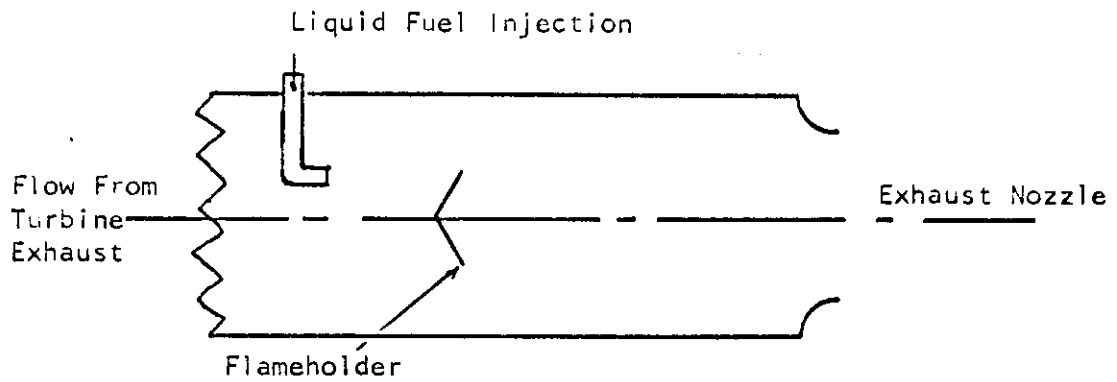
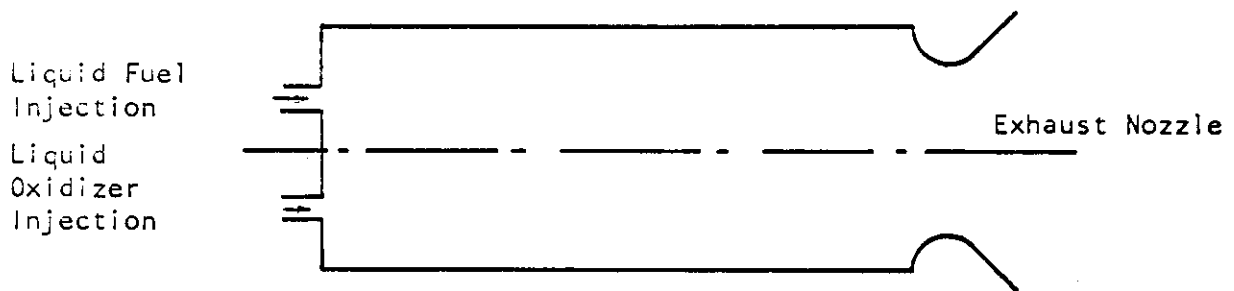


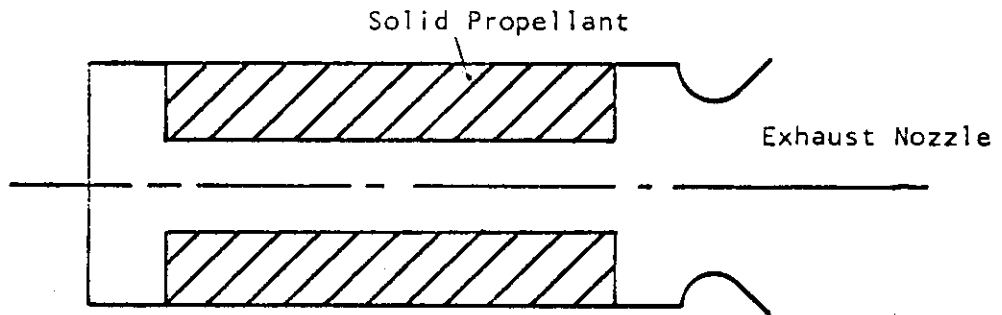
FIGURE 2 - GAIN AND LOSS CONTRIBUTIONS FOR A 26-INCH-DIAMETER BURNER - FIRST TRANSVERSE MODE, LINER LENGTH = 19 INCHES



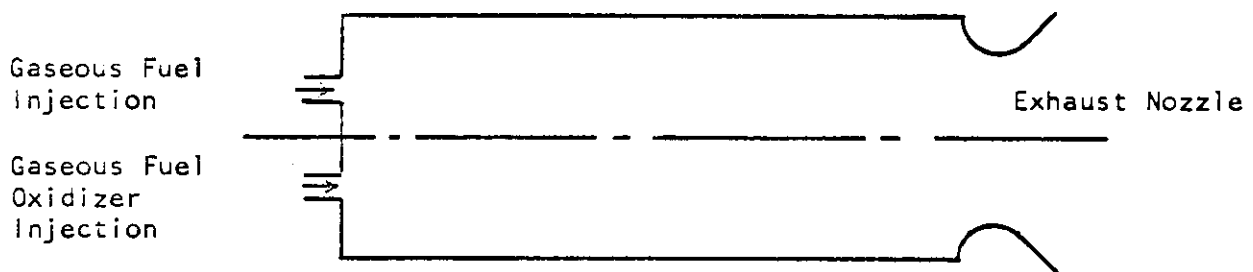
a. Afterburner Schematic



b. Liquid-Rocket Combustor



c. Solid-Rocket Combustor



d. Gaseous-Rocket Combustor

FIGURE 3 - DIAGRAMMATIC REPRESENTATIONS OF TYPICAL COMBUSTOR GEOMETRIES

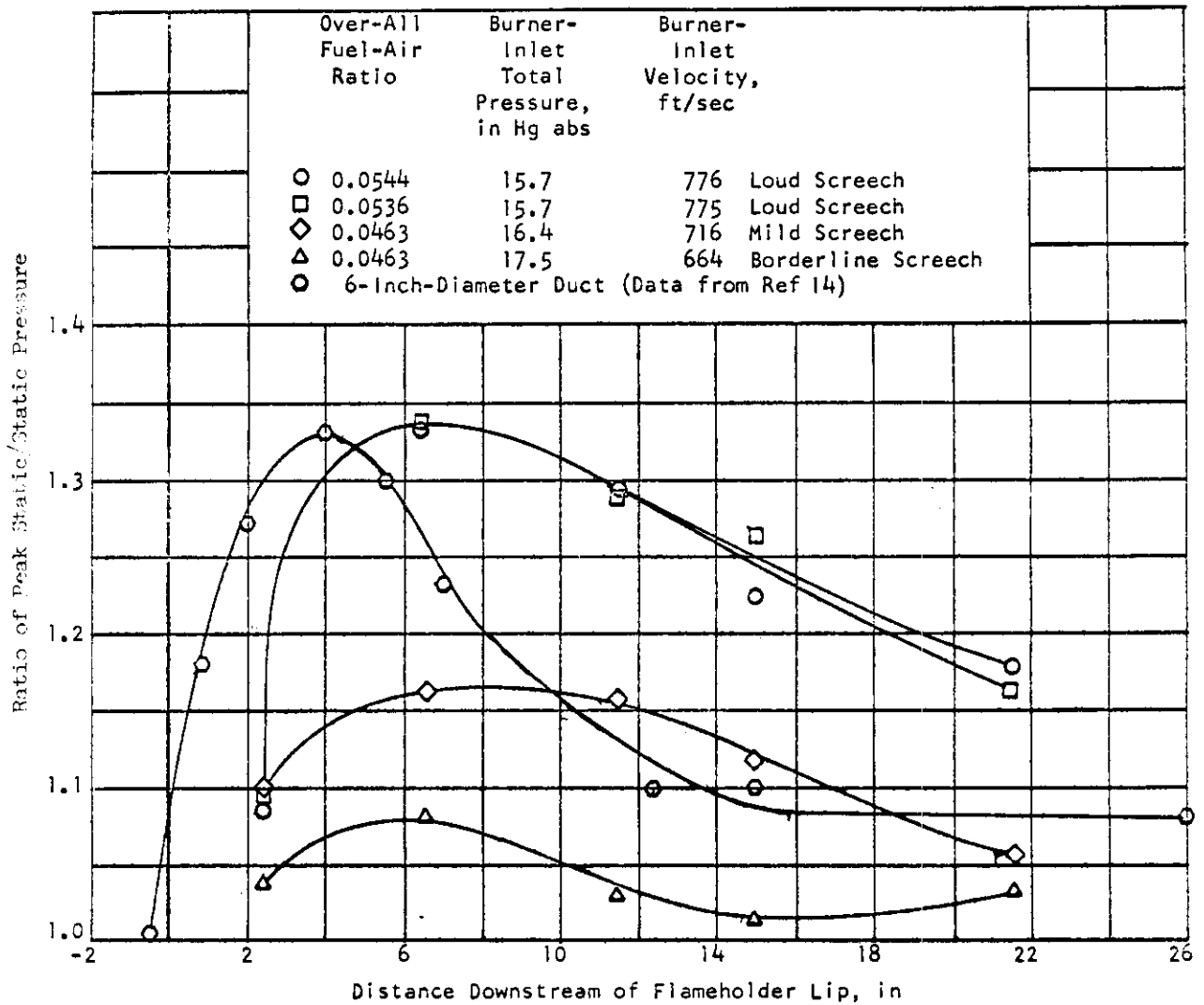
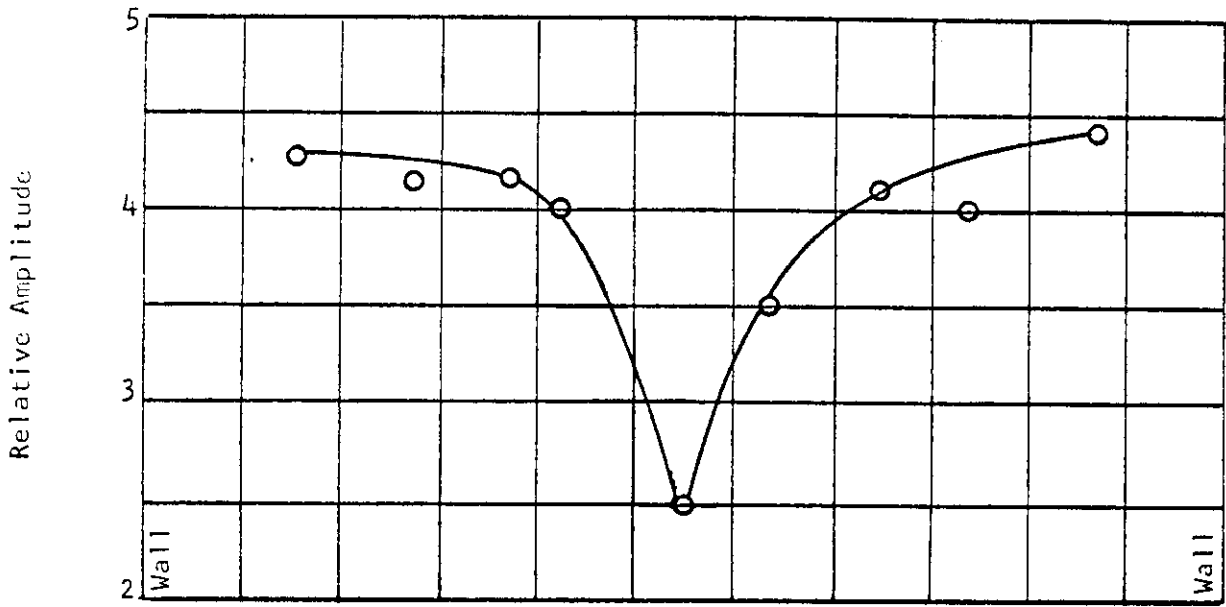


FIGURE 4 - VARIATION OF RATIO OF PEAK STATIC PRESSURE (REED VALVE) TO AVERAGE STATIC PRESSURE WITH DISTANCE DOWNSTREAM OF FLAMEHOLDER IN 26-INCH-DIAMETER DUCT, AIRFLOW, 22.6 POUNDS PER SECOND (FROM REF 9)



# Contrails



Amplitude Profile Across 6-Inch Burner

Flameholder Position    A □    B ○

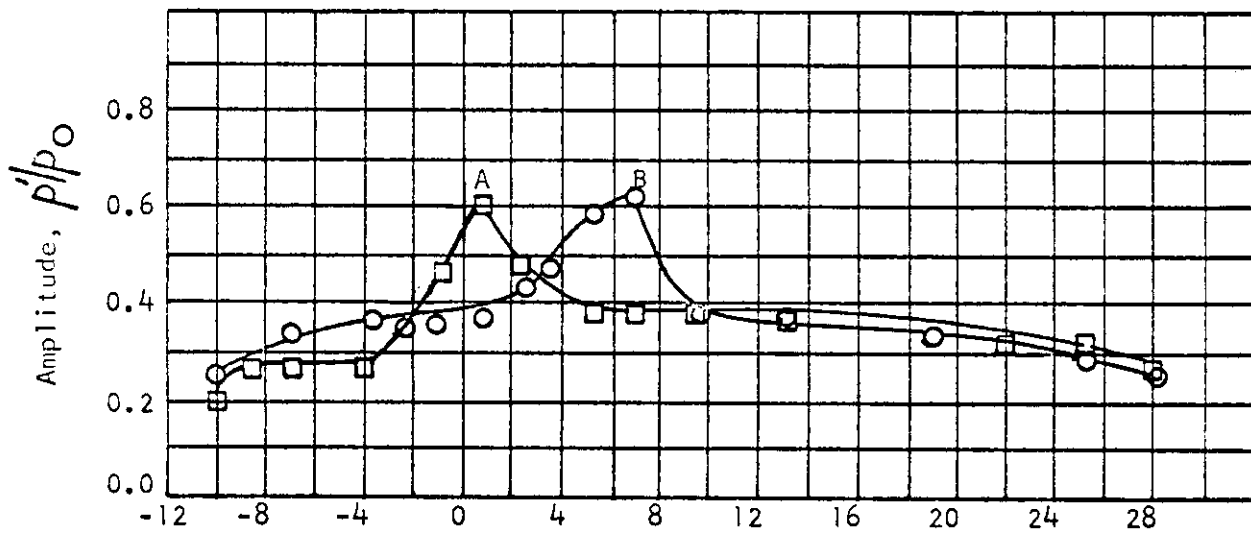


FIGURE 5 - AMPLITUDE DISTRIBUTION FOR TWO FLAMEHOLDER POSITIONS IN 6-INCH BURNER (FROM REF 12)

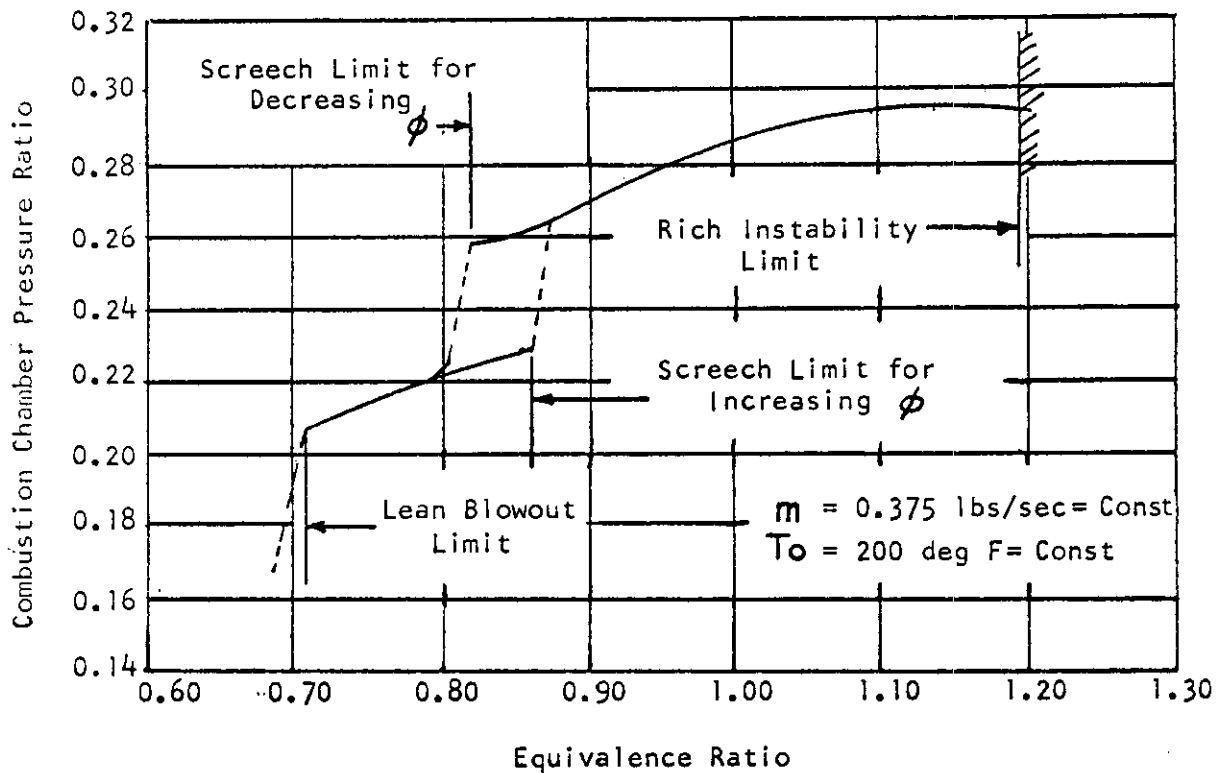


FIGURE 6 - VARIATION OF COMBUSTION CHAMBER INLET TOTAL PRESSURE WITH EQUIVALENCE RATIO (FROM REF 16)

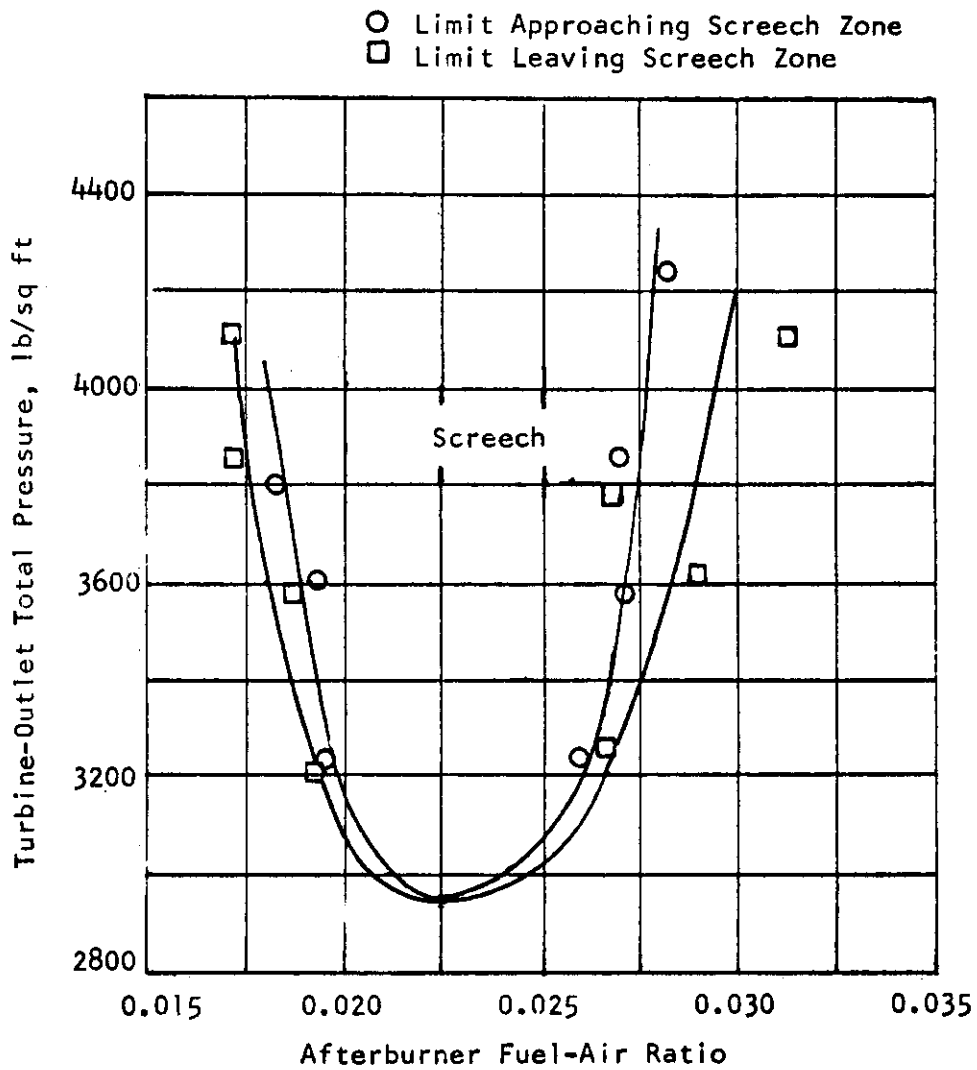


FIGURE 7(a) - VARIATION OF SCREECH LIMITS WITH AFTERBURNER-INLET PRESSURE FOR 36-INCH-DIAMETER AFTERBURNER. AFTERBURNER-INLET TEMPERATURE, 1685 DEG R (FROM REF 12)

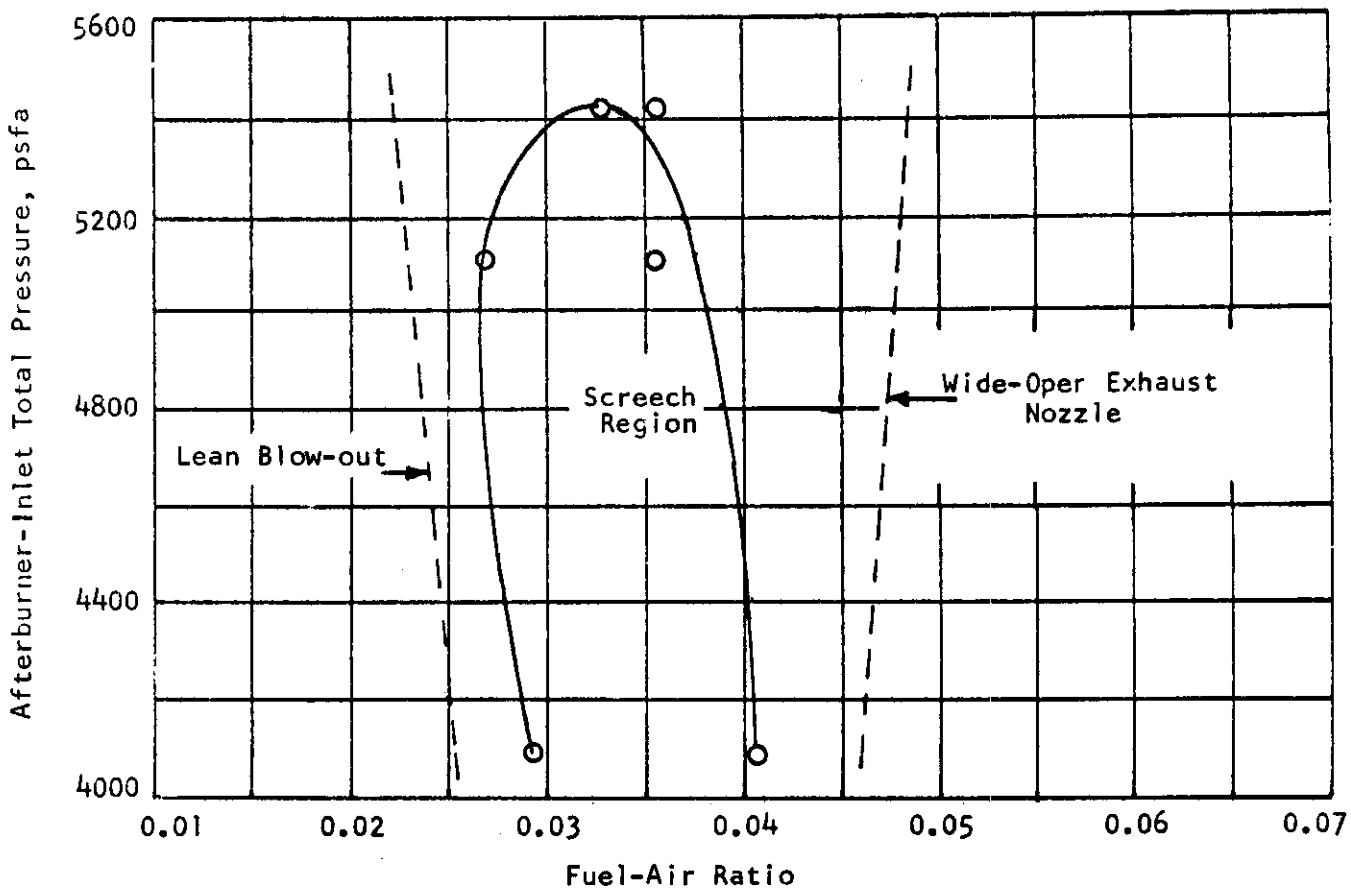


FIGURE 7(b) - EFFECT OF PRESSURE AND FUEL-AIR RATIO UPON SCREECH BOUNDARIES (FROM REF 11)

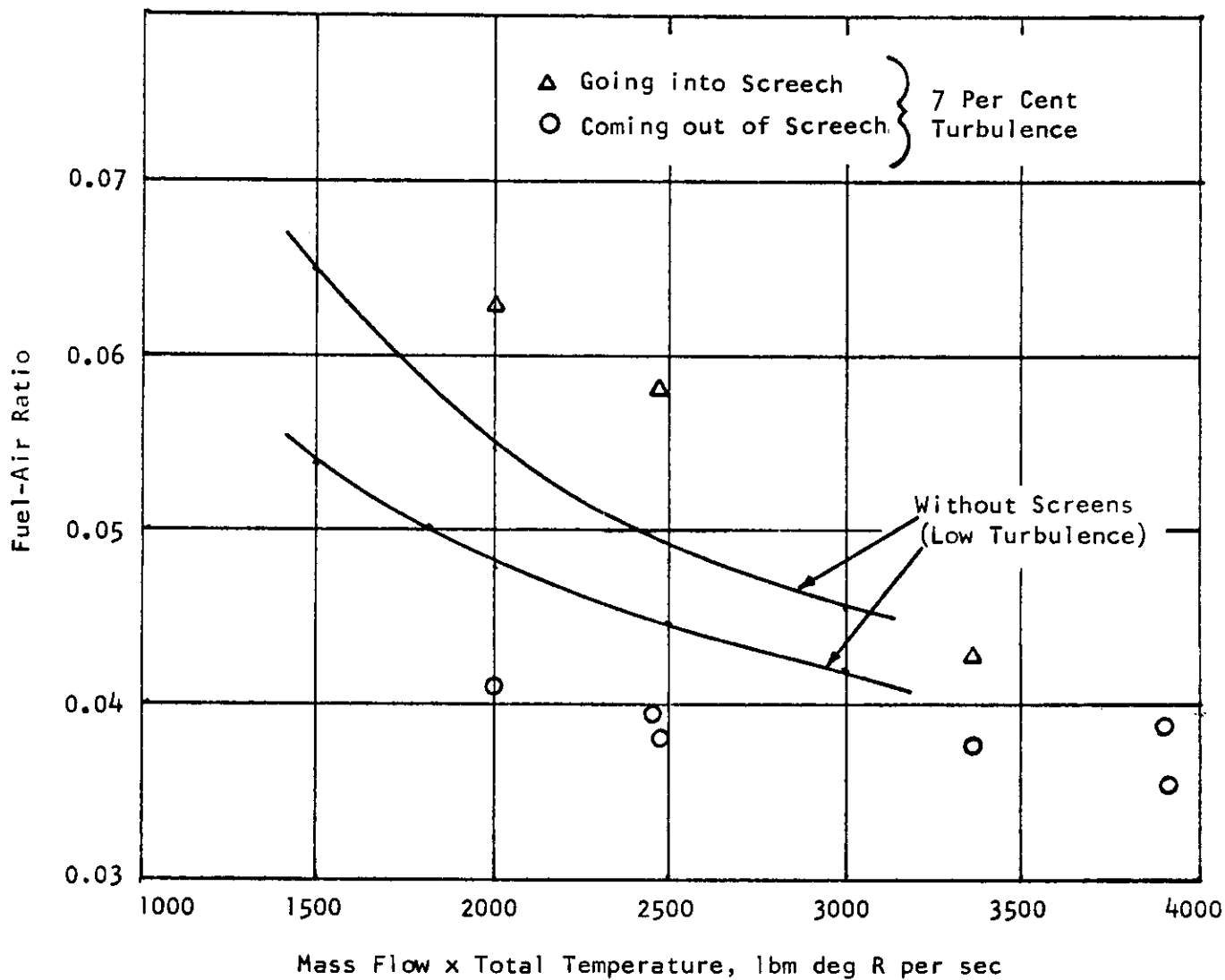


FIGURE 8 - THE EFFECT OF TURBULENCE ON COMBUSTION INSTABILITY BOUNDARIES (FROM REF 15)

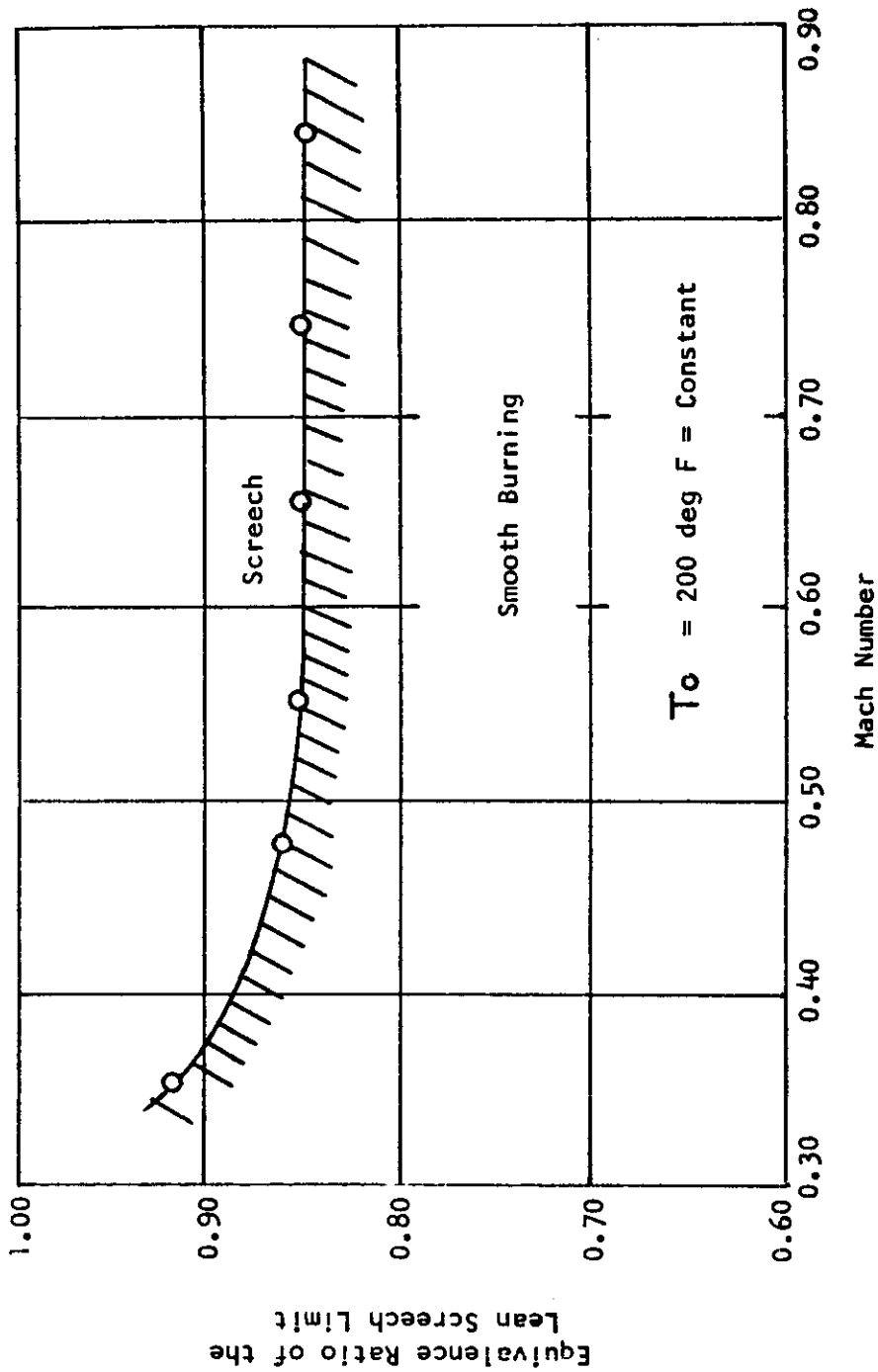


FIGURE 9 - VARIATION OF THE LEAN SCREECH LIMIT WITH AVERAGE MACH NUMBER (FROM REF 16)

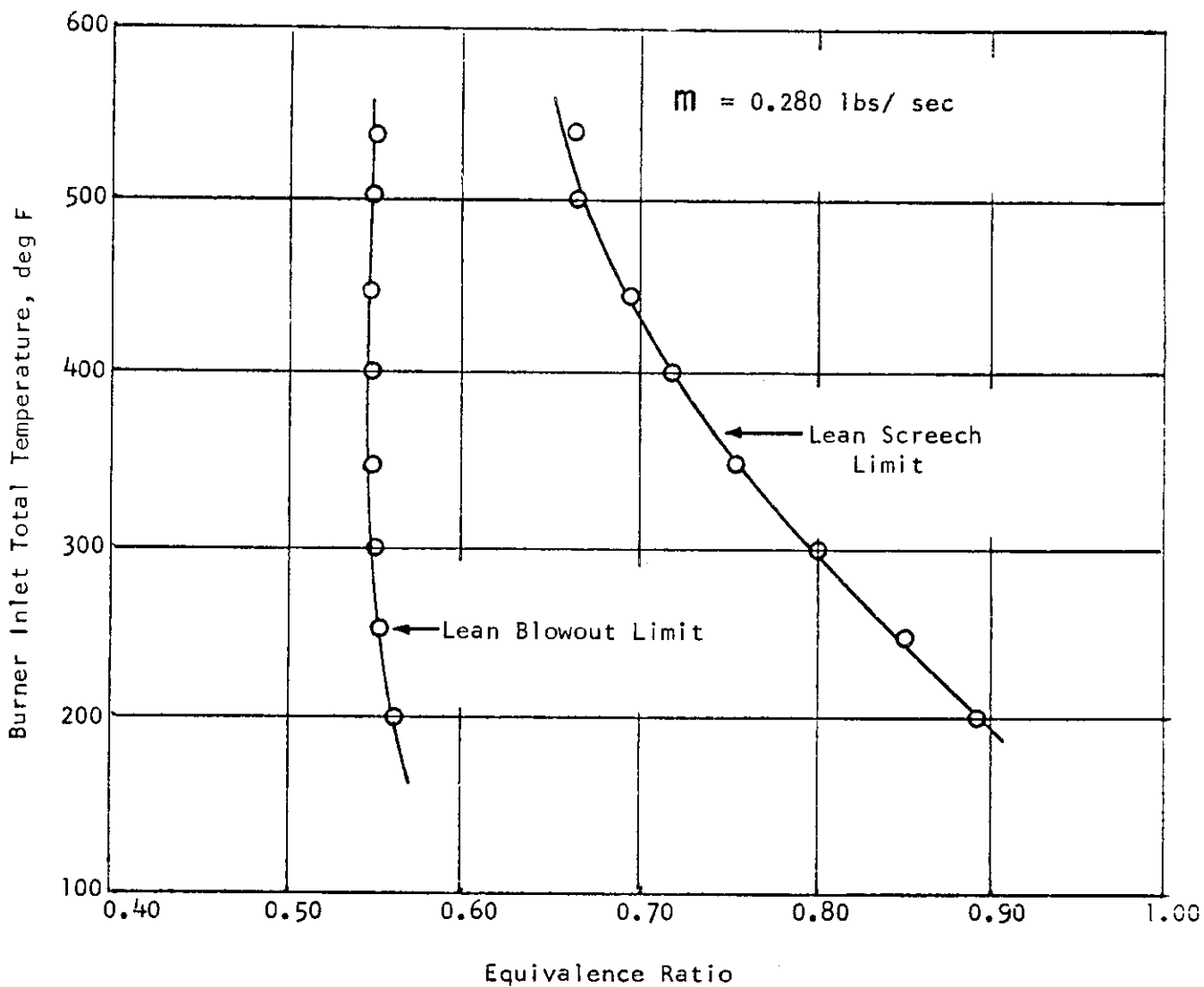


FIGURE 10 - VARIATION OF LEAN SCREECH LIMIT WITH INLET TOTAL TEMPERATURE (FROM REF 16)

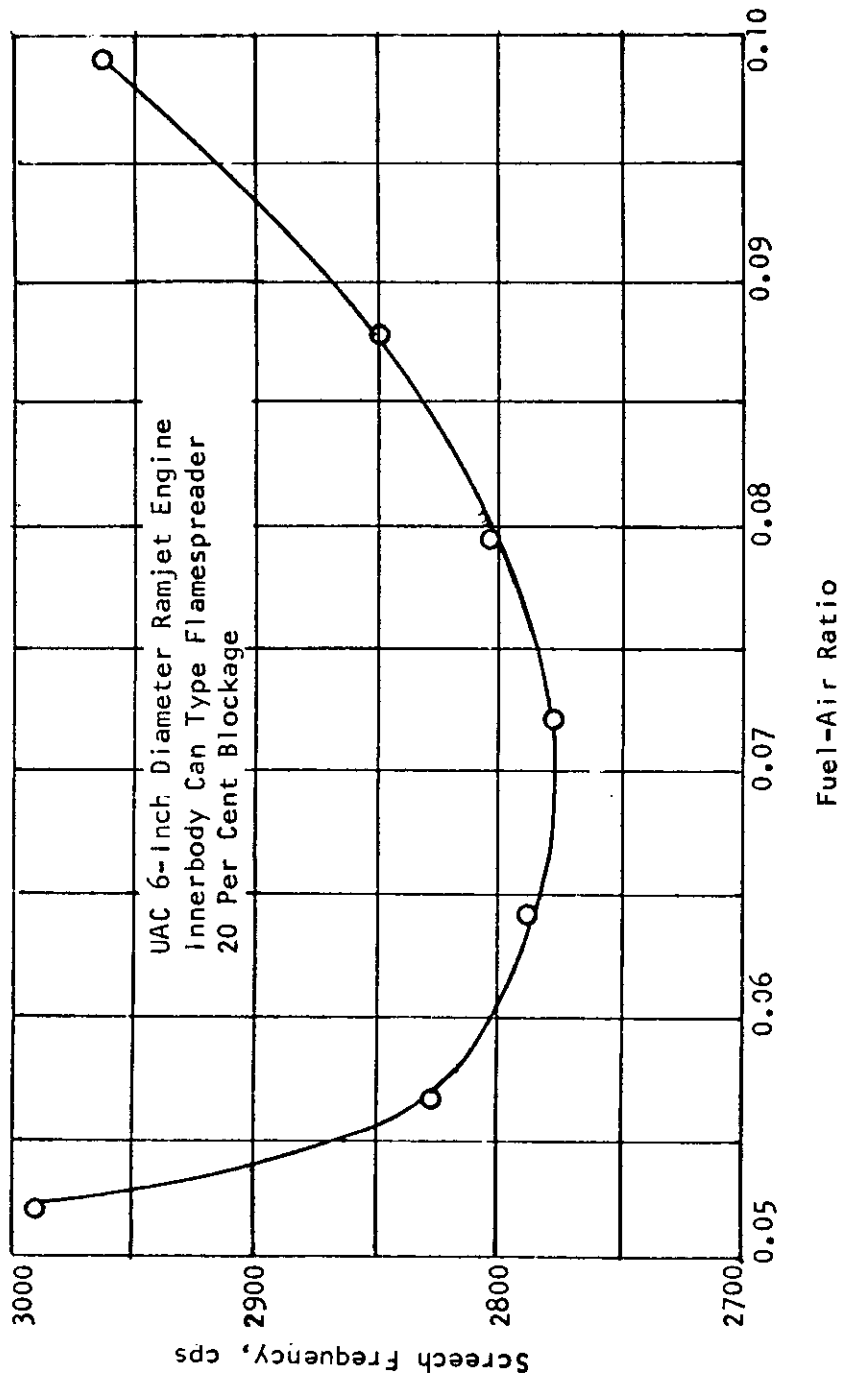
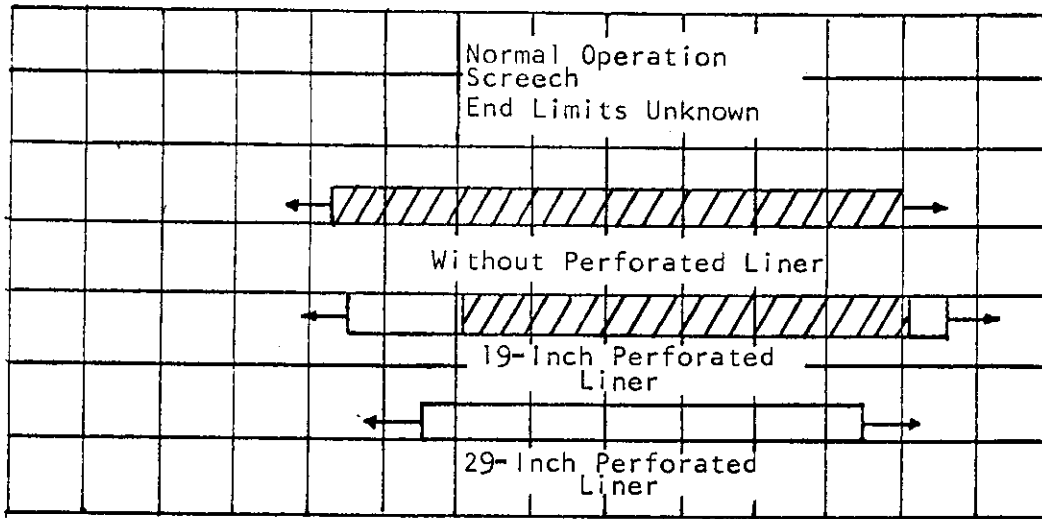


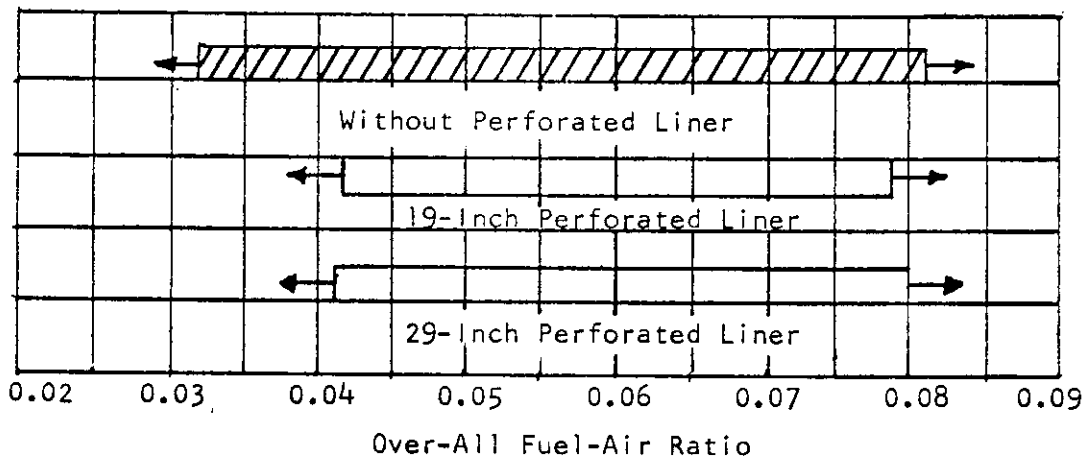
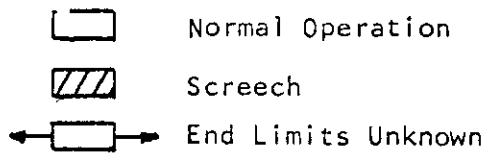
FIGURE 11 - VARIATION OF SCREECH-FREQUENCY WITH FUEL-AIR RATIO (FROM REF 14)



Liner starts at the same axial location as flameholder exit



a. Burner-Inlet Total Pressure, 1750 lbs per sq ft



b. Burner-Inlet Total Pressure, 1400 lbs per sq ft

FIGURE 12 - EFFECT OF PERFORATED LINER ON SCREECH LIMITS IN 26-INCH-DIAMETER DUCT (FROM REF 12)

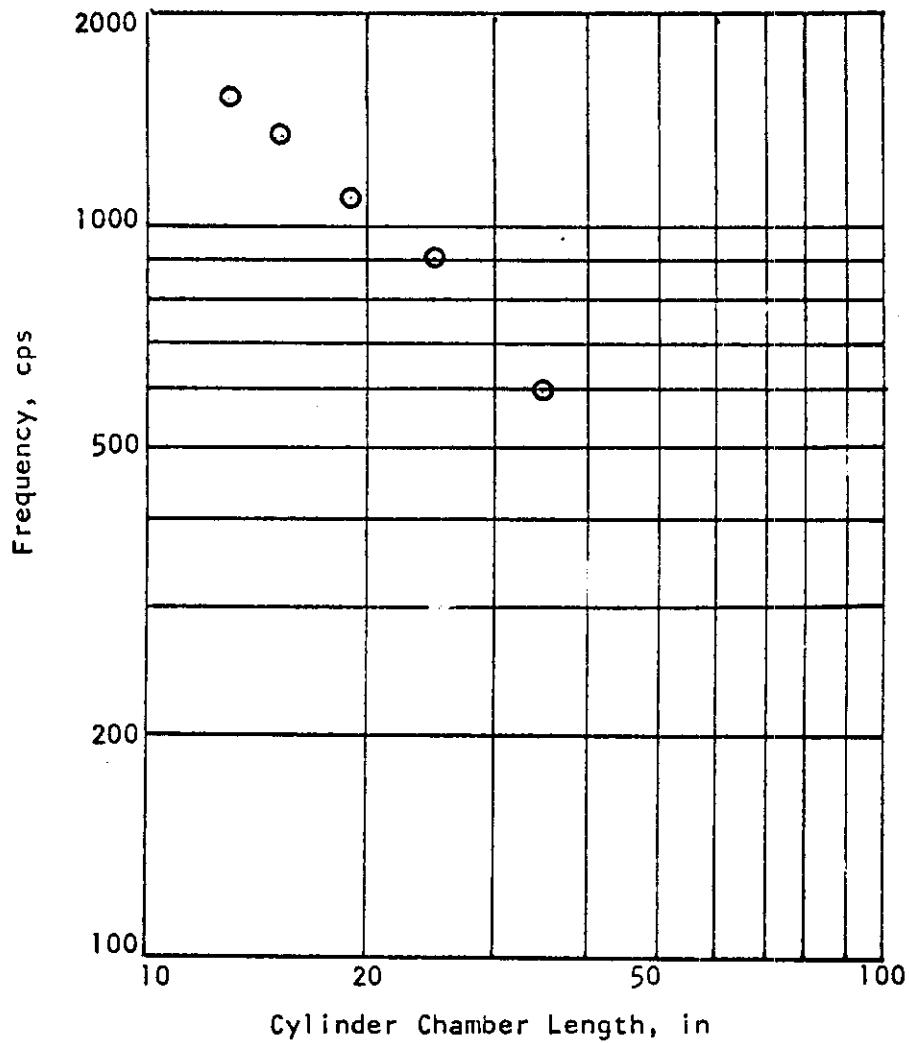


FIGURE 13 - FREQUENCY OF THE UNSTABLE OSCILLATIONS IN THE HIGH FREQUENCY RANGE AS A FUNCTION OF CHAMBER LENGTH (FROM REF 2)

Frequency, 7200 cps  
Backing Cavity, 0.169 in

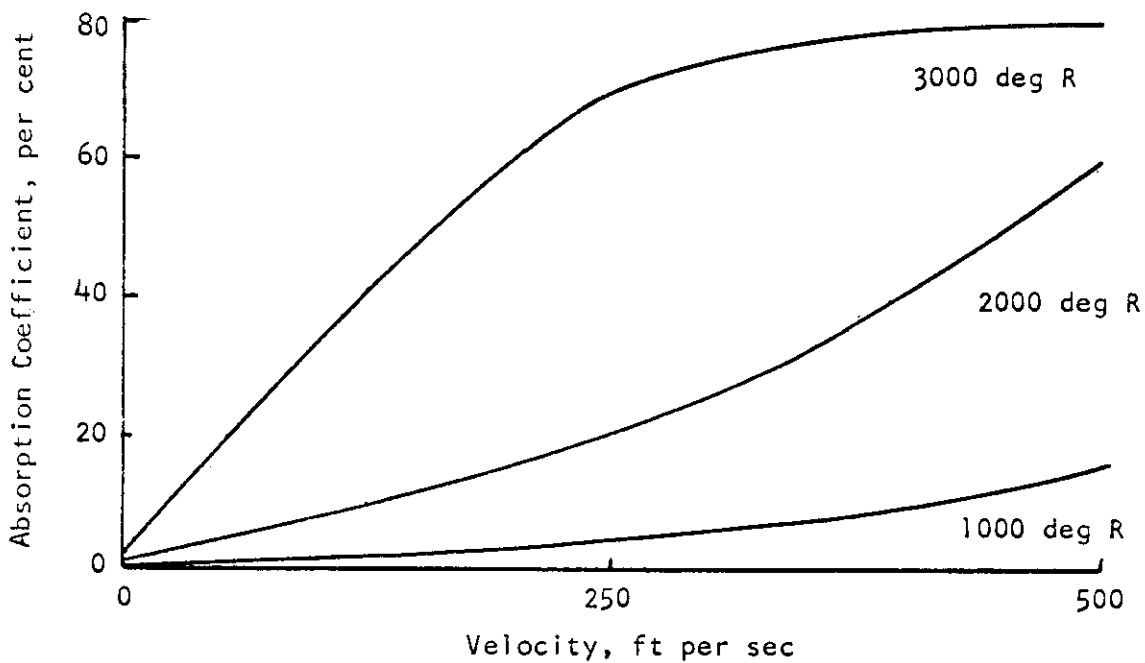


FIGURE 14 - EFFECTS OF GAS TEMPERATURE AND VELOCITY ON ABSORPTION COEFFICIENTS OF COOLED LINERS (FROM REF 25)

# Contrails

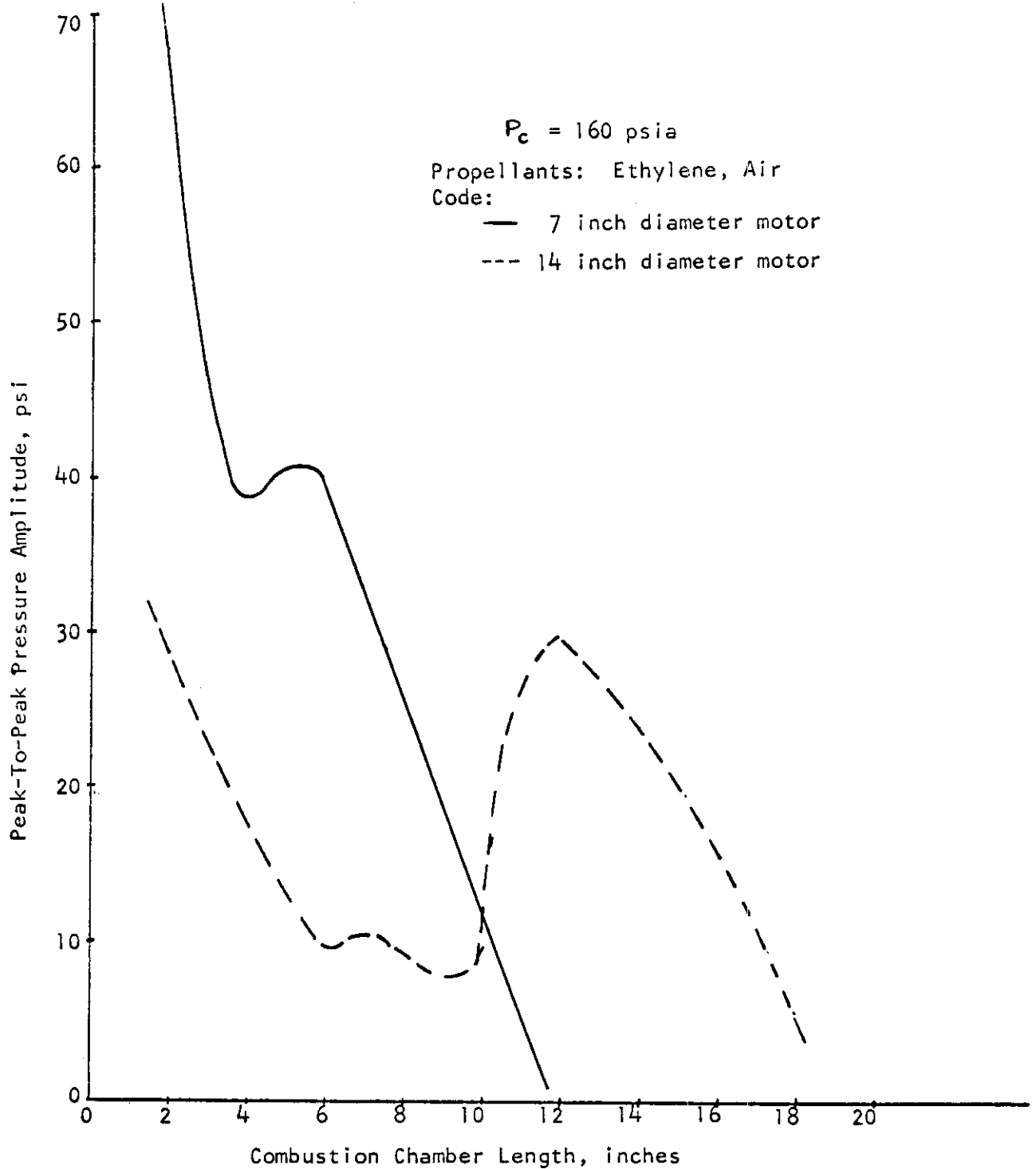


FIGURE 15 - PRESSURE OSCILLATION AMPLITUDE  
VS CHAMBER LENGTH (FROM REF 54)

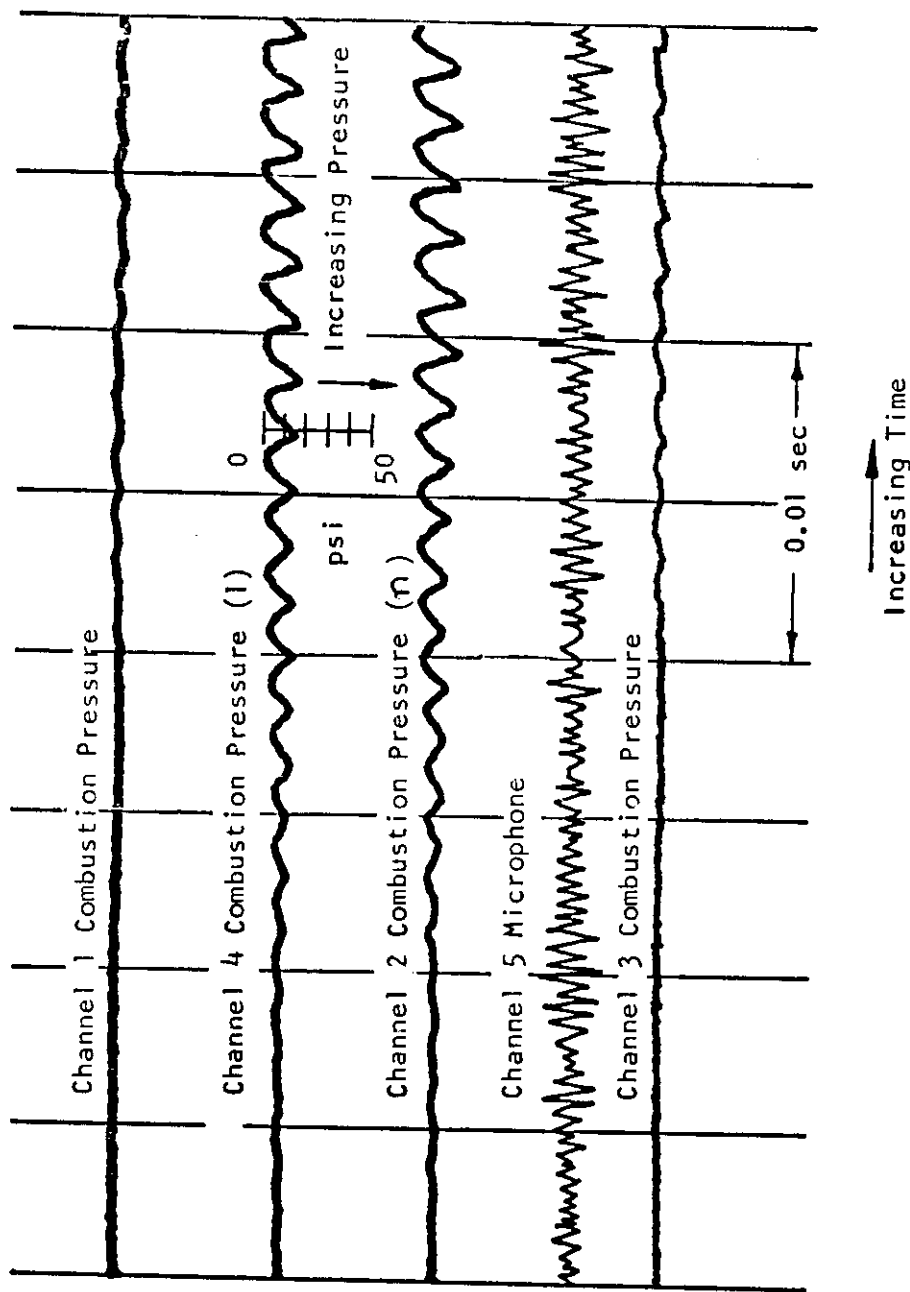


FIGURE 16 - OSCILLOGRAPH RECORD ILLUSTRATING THE START OF THE OSCILLATIONS (FROM REF 52)

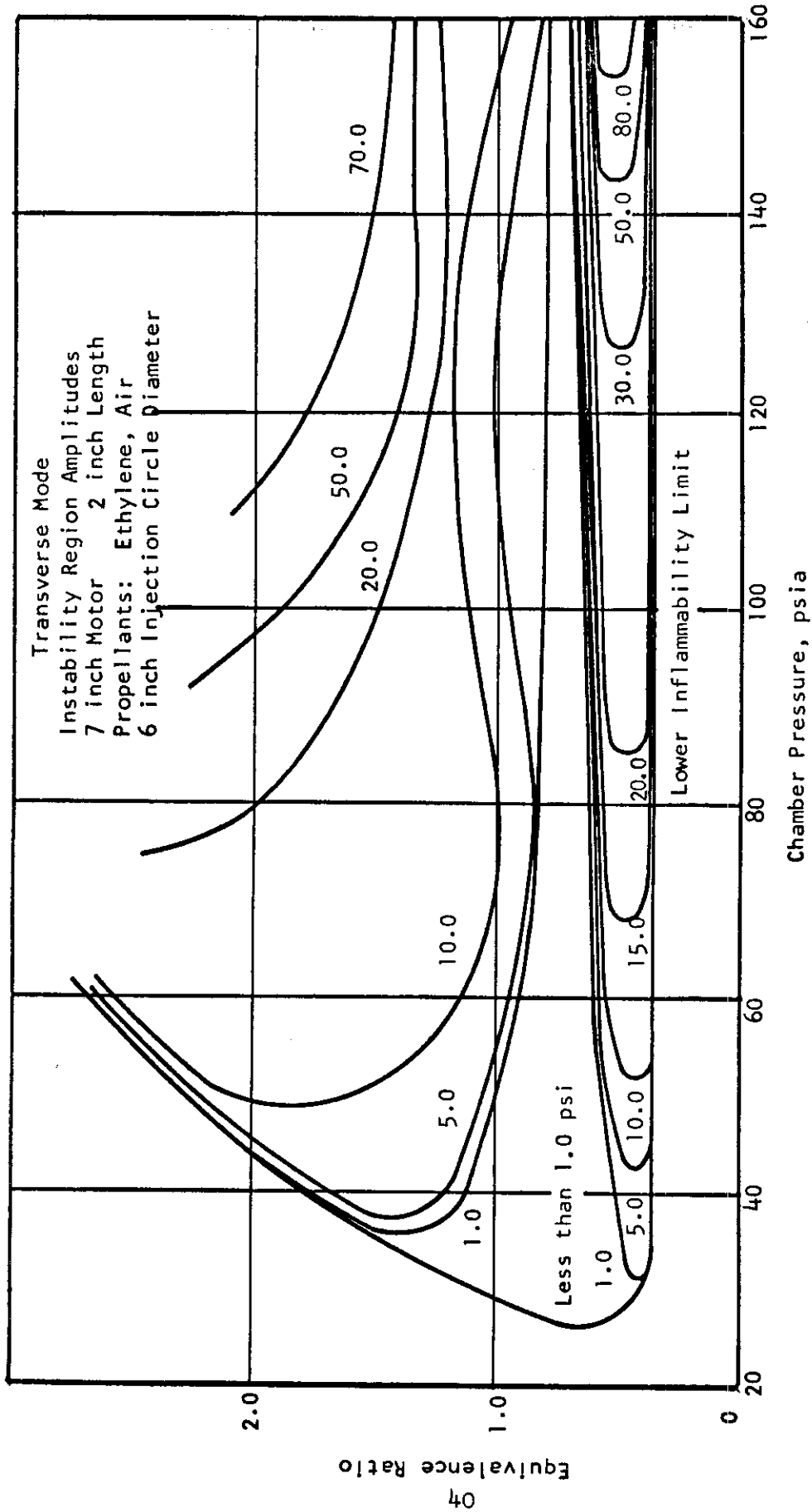


FIGURE 17 - INSTABILITY REGION AND AMPLITUDES (FROM REF 54)

Transverse Mode Instability Regions  
7 inch Dia Motor 2 inch-12 inch Length  
Propellants: Ethylene, Air

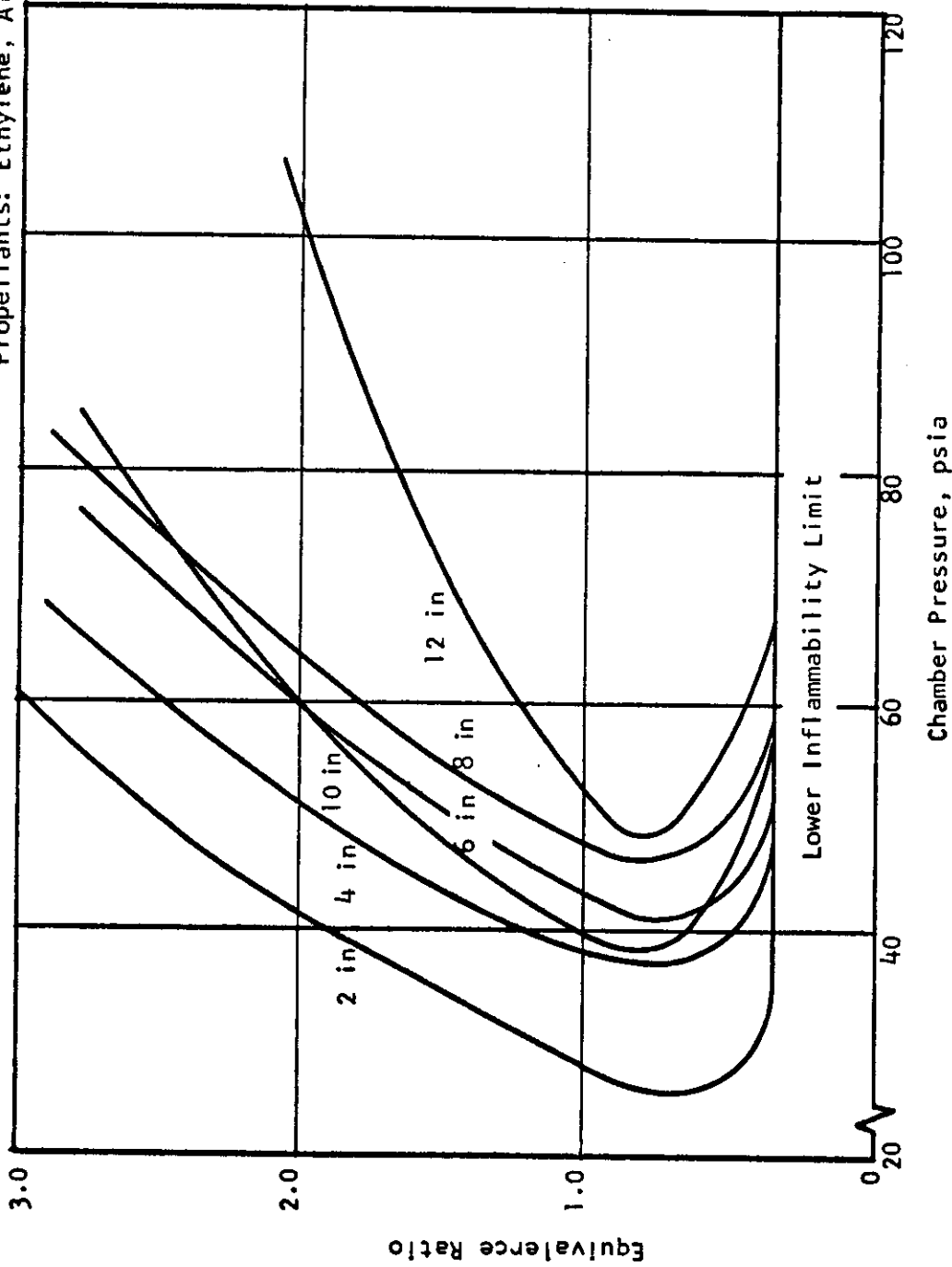


FIGURE 18 - TRANSVERSE MODE INSTABILITY REGIONS (FROM REF 54)

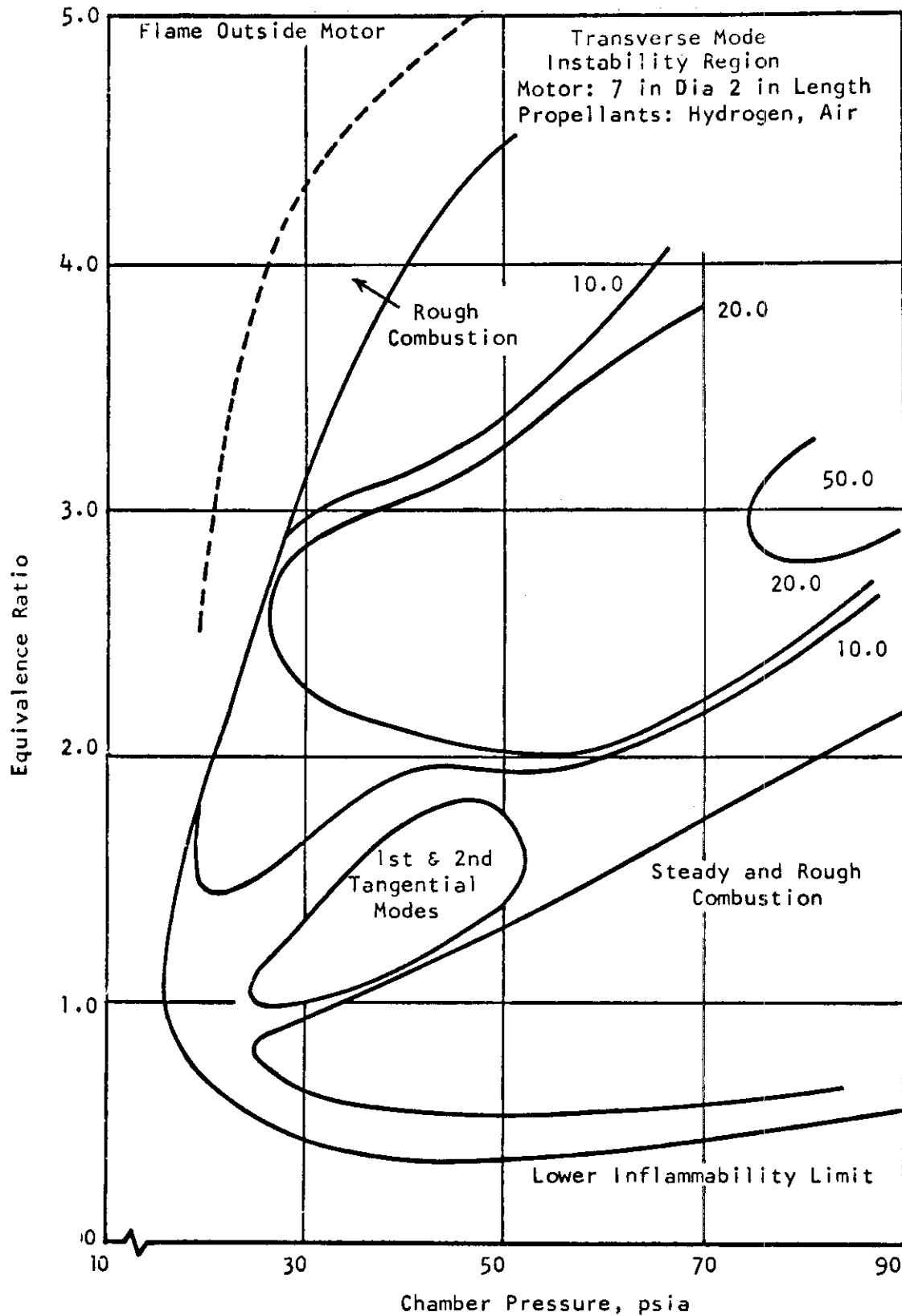


FIGURE 19 - HYDROGEN STABILITY BOUNDARIES (FROM REF 54)



# Contrails

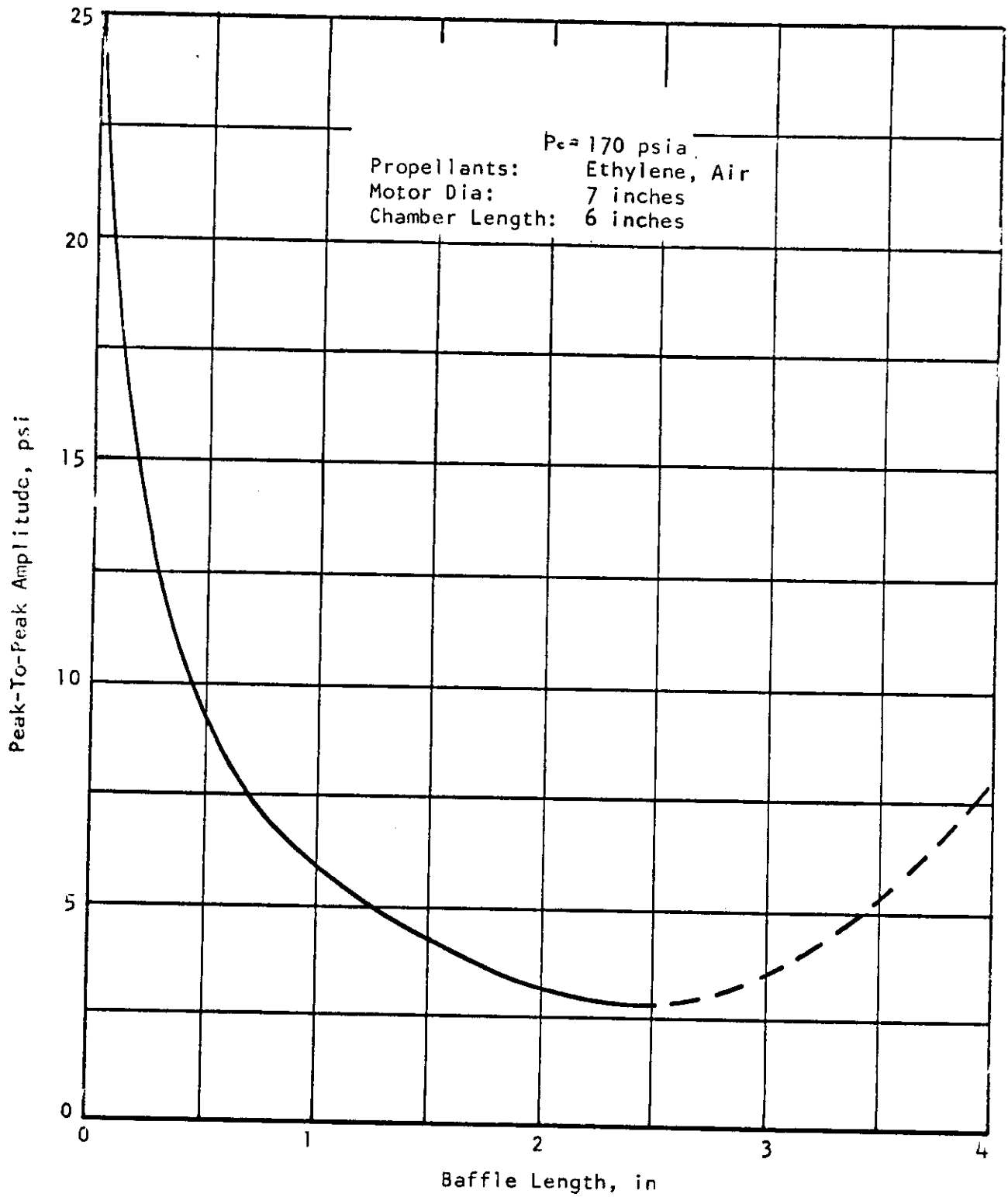


FIGURE 20 - AMPLITUDE OF OSCILLATIONS  
VS BAFFLE LENGTH (FROM REF 54)

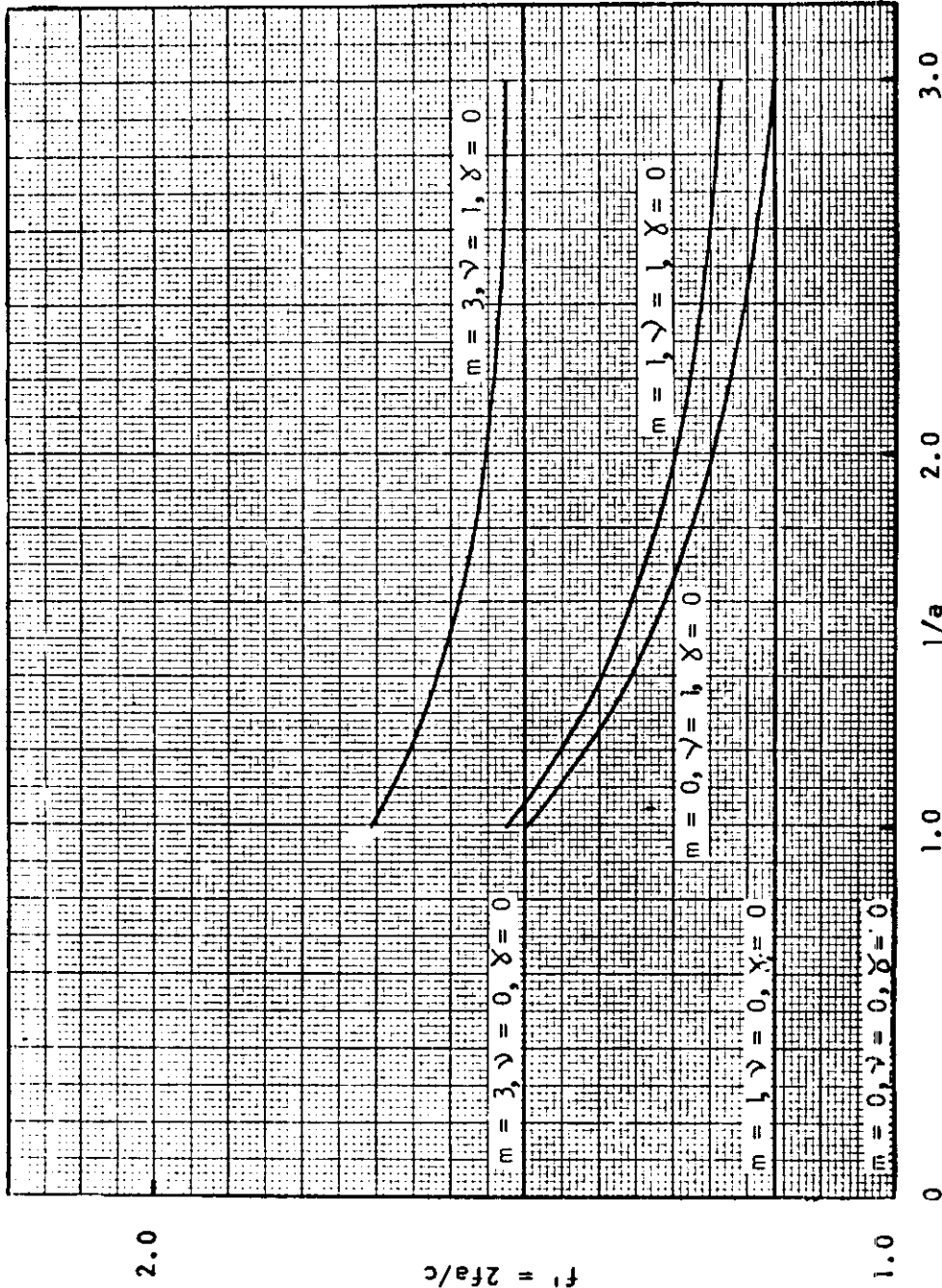


FIGURE 21 - DIMENSIONLESS FREQUENCY VS LENGTH/DIAMETER FOR SEVERAL MODES OF OSCILLATION (ANNULAR CYLINDER,  $a/b = 1.1$ )

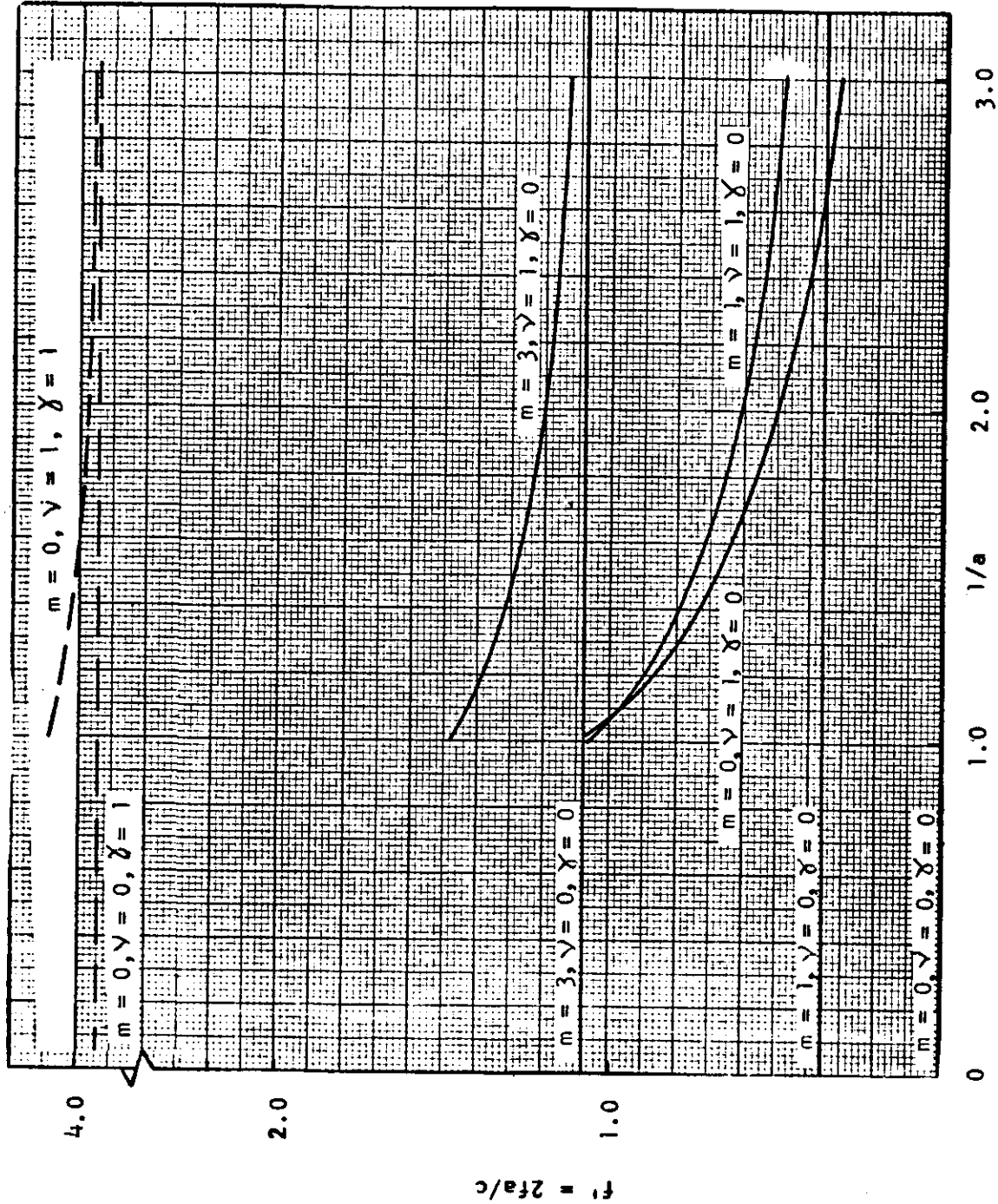


FIGURE 22 - DIMENSIONLESS FREQUENCY VS LENGTH/DIAMETER FOR SEVERAL MODES OF OSCILLATION (ANNULAR CYLINDER,  $a/b = 1.3$ )

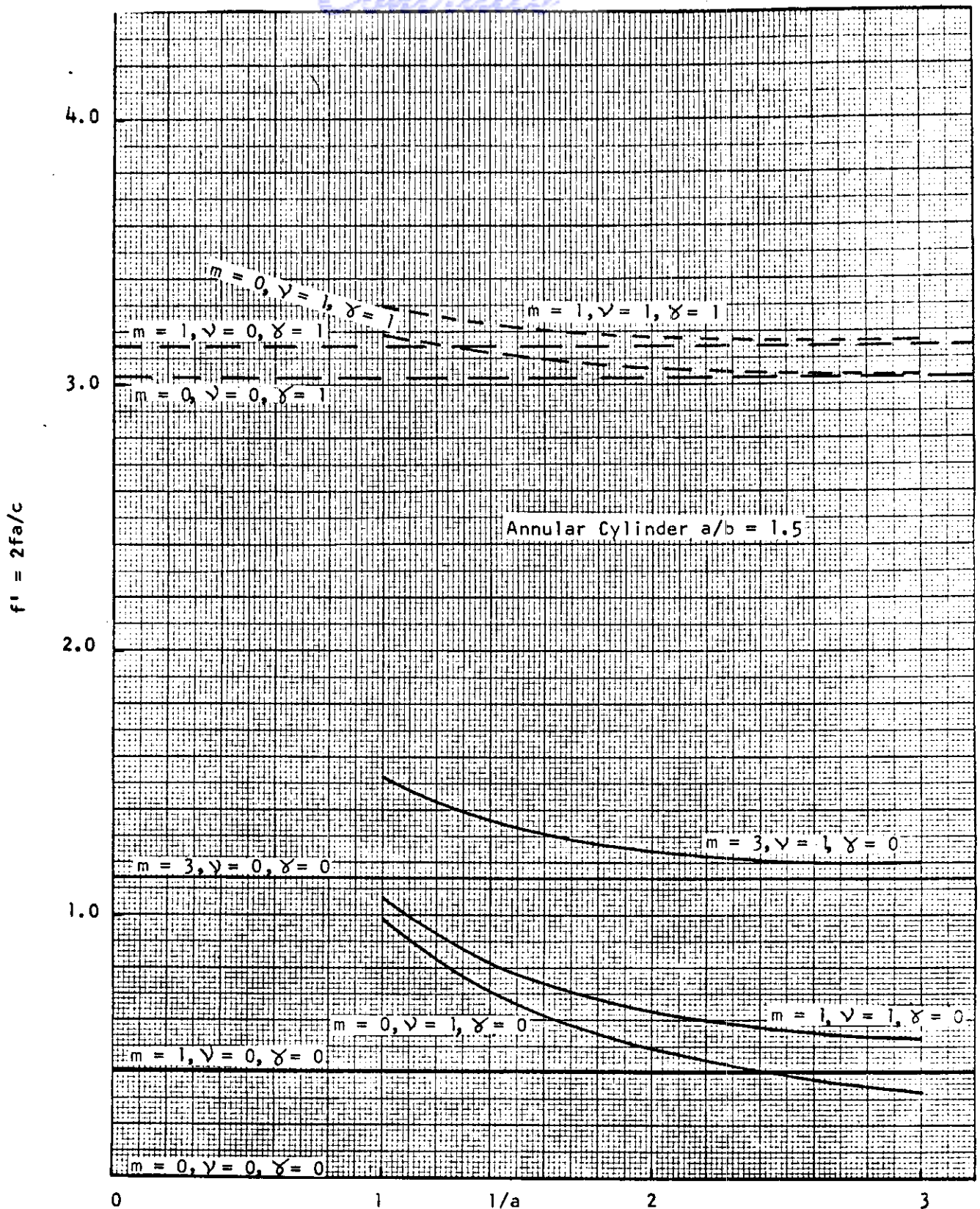


FIGURE 23 - DIMENSIONLESS FREQUENCY VS LENGTH/DIAMETER FOR SEVERAL MODES OF OSCILLATION

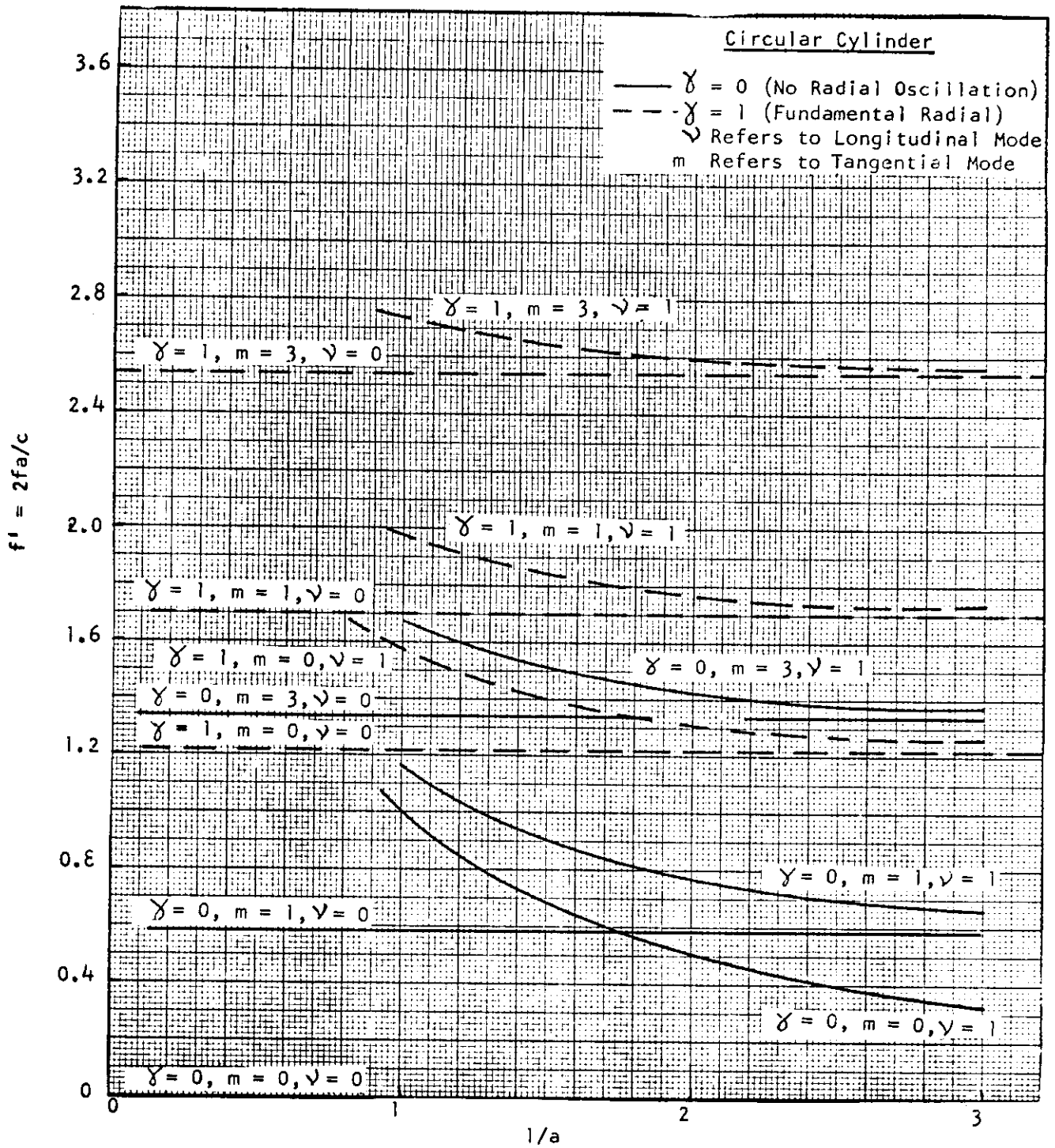


FIGURE 24 - DIMENSIONLESS FREQUENCY VS LENGTH/DIAMETER  
FOR SEVERAL MODES OF OSCILLATION

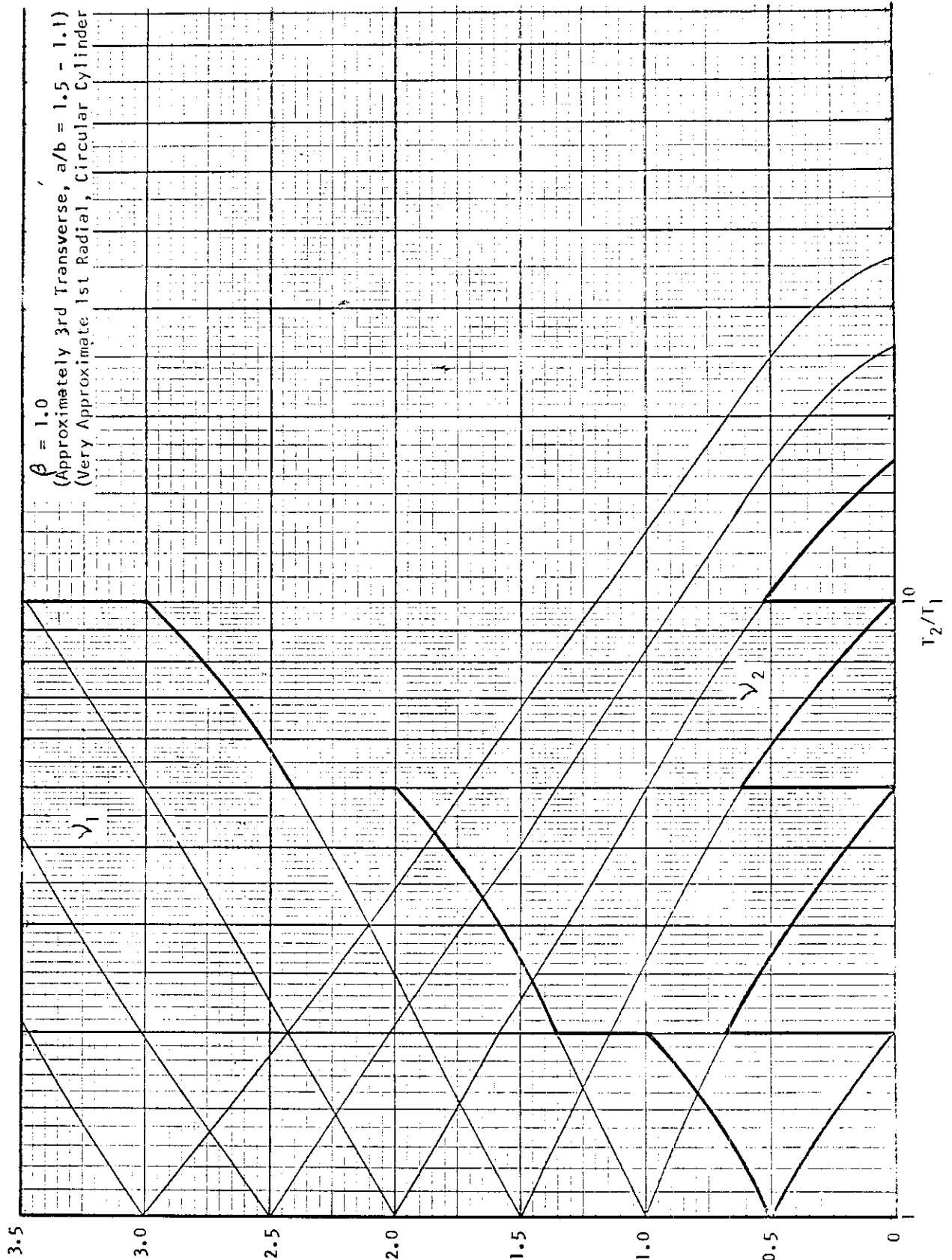


FIGURE 25 - VARIATION OF LONGITUDINAL MODE SHAPES UPSTREAM AND DOWNSTREAM OF A TEMPERATURE DISCONTINUITY WITH TEMPERATURE RATIO

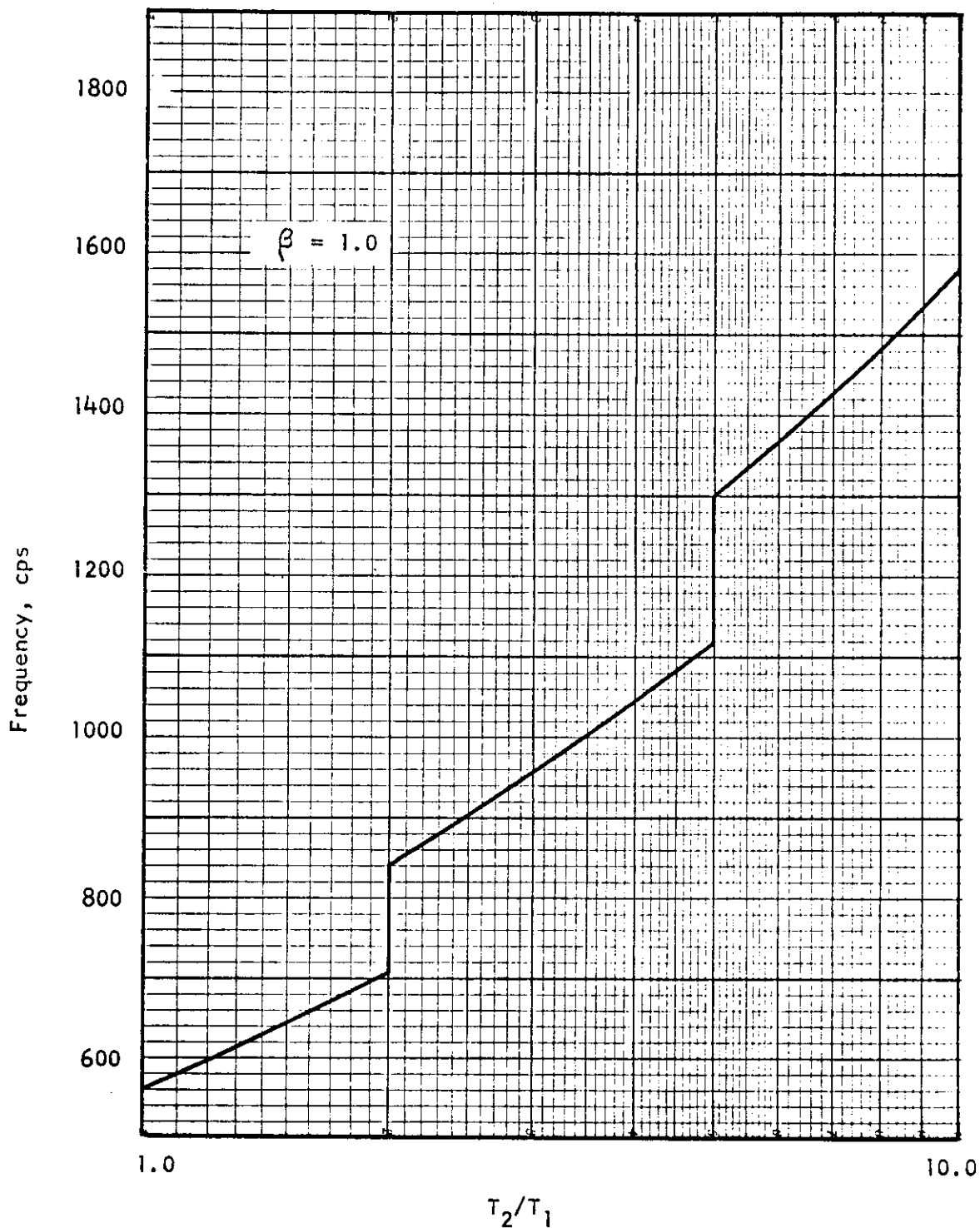


FIGURE 26 - VARIATION OF FREQUENCY WITH TEMPERATURE RATIO  
ACROSS A TEMPERATURE DISCONTINUITY

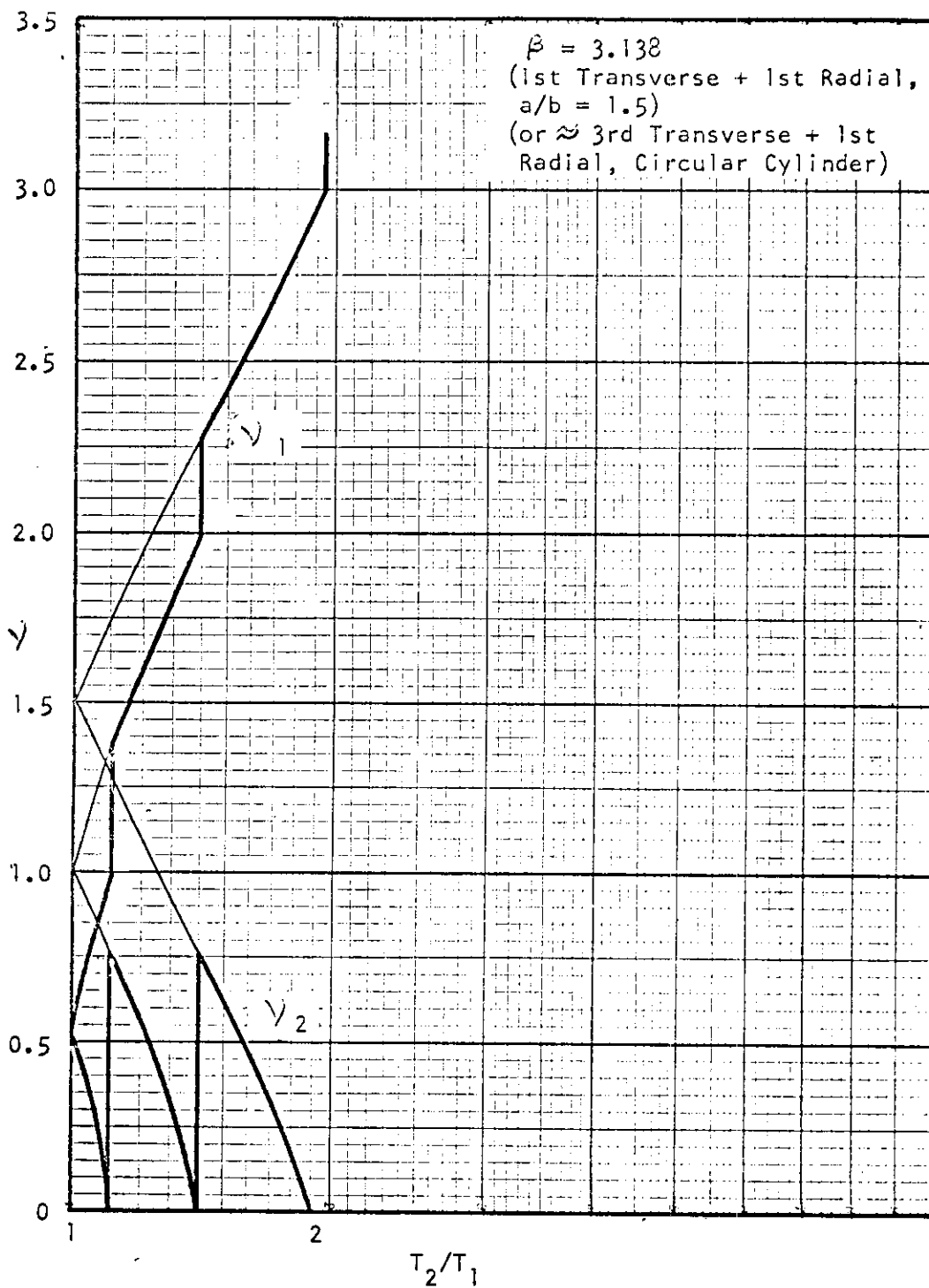


FIGURE 27 - VARIATION OF LONGITUDINAL MODE SHAPES UPSTREAM AND DOWNSTREAM OF A TEMPERATURE DISCONTINUITY WITH TEMPERATURE RATIO



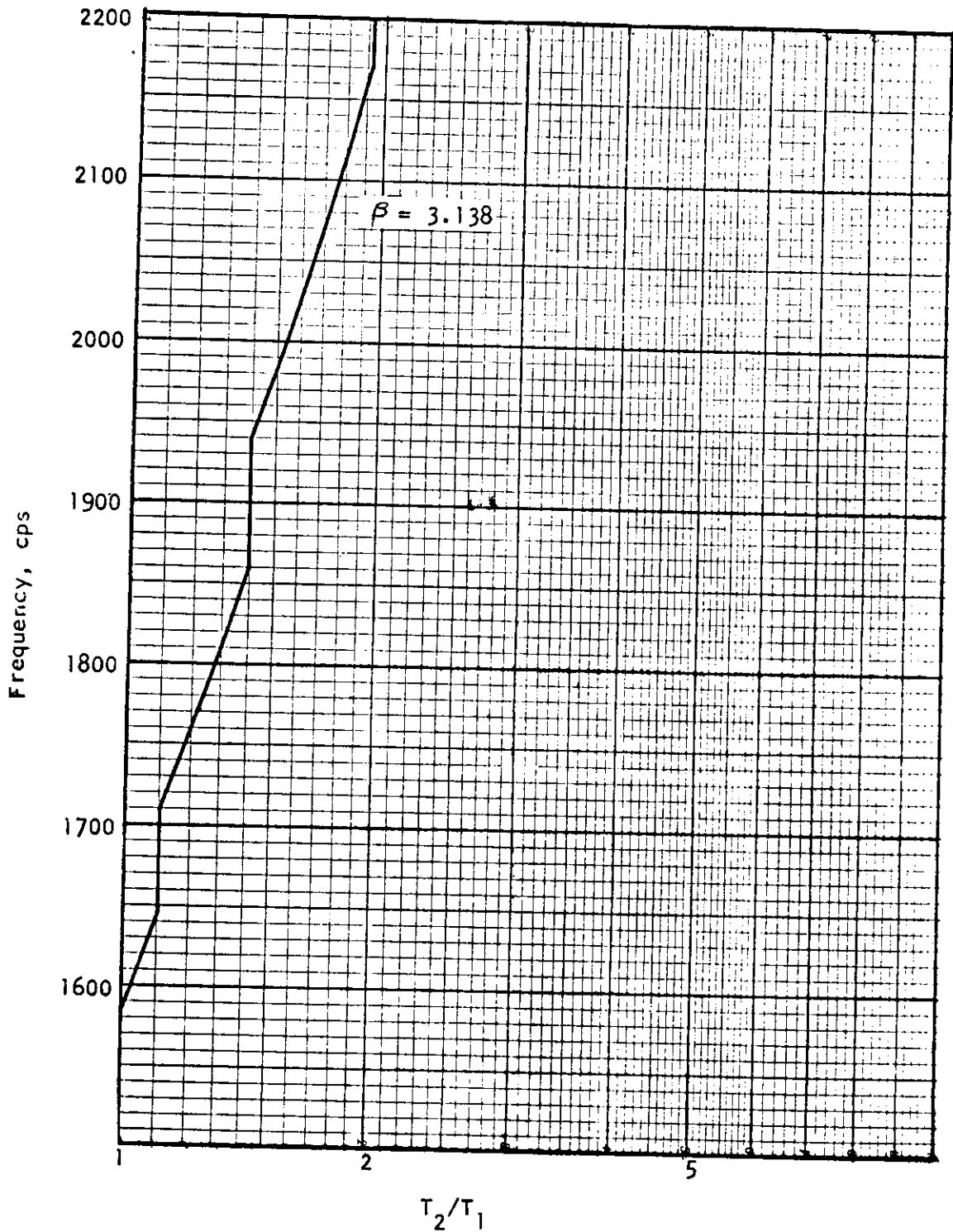


FIGURE 28 - VARIATION OF FREQUENCY WITH TEMPERATURE RATIO  
ACROSS A TEMPERATURE DISCONTINUITY

# Contrails

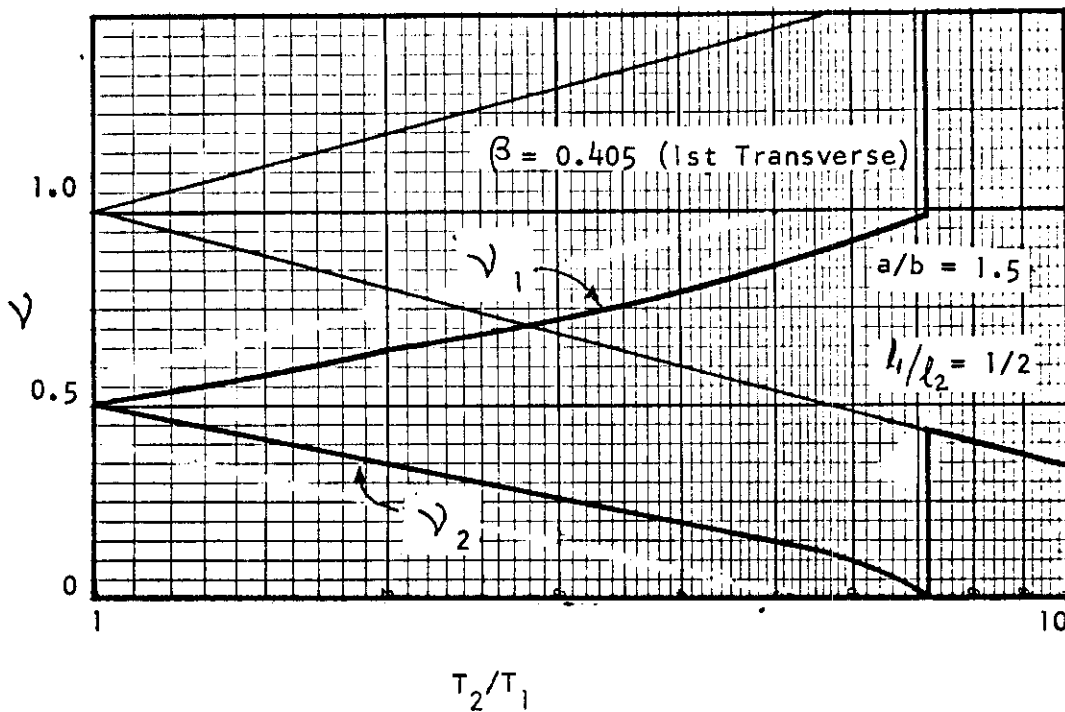


FIGURE 29 - VARIATION OF LONGITUDINAL MODE SHAPES UPSTREAM AND DOWNSTREAM OF A TEMPERATURE DISCONTINUITY WITH TEMPERATURE RATIO

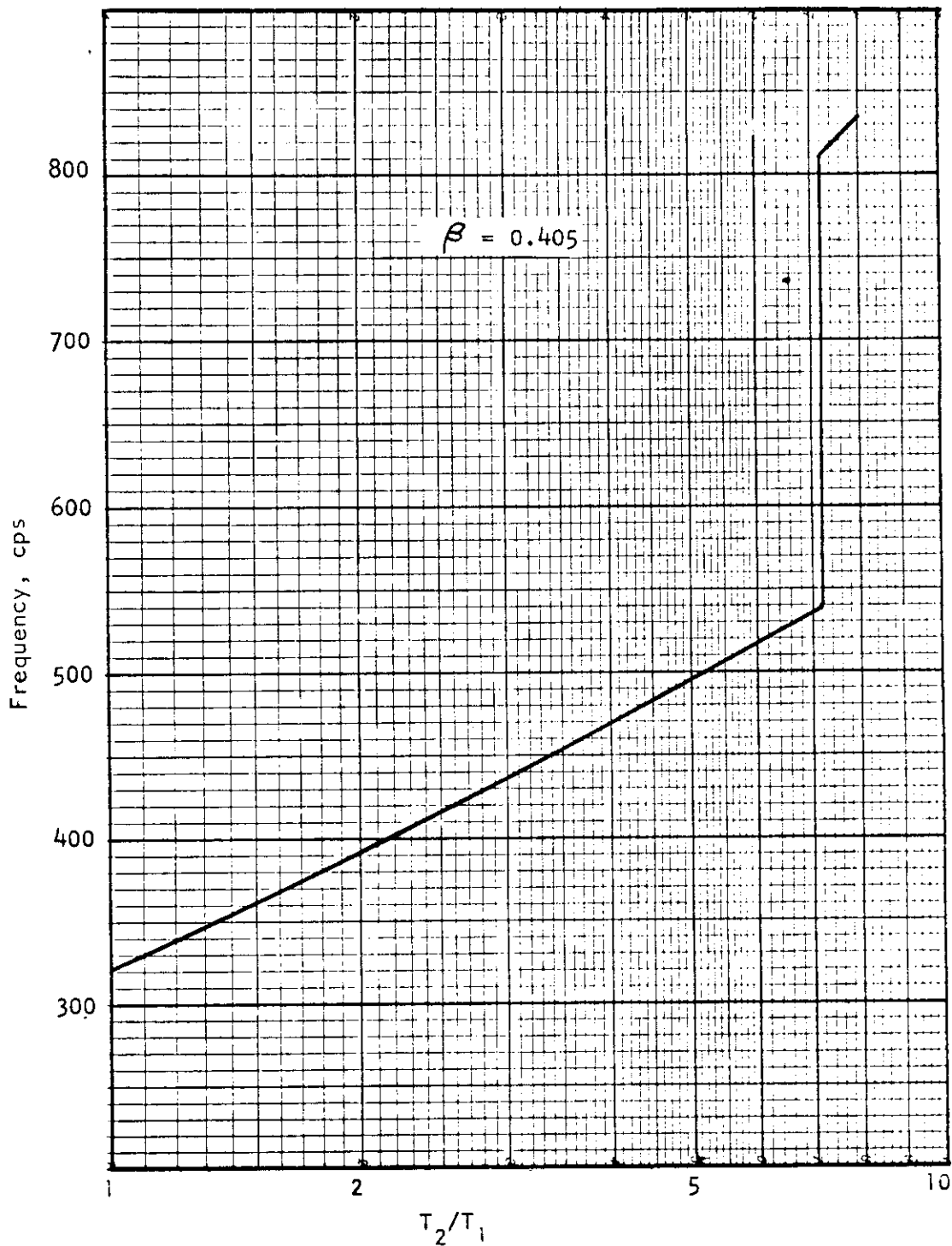


FIGURE 30 - VARIATION OF FREQUENCY WITH TEMPERATURE RATIO  
ACROSS A TEMPERATURE DISCONTINUITY

# Contrails

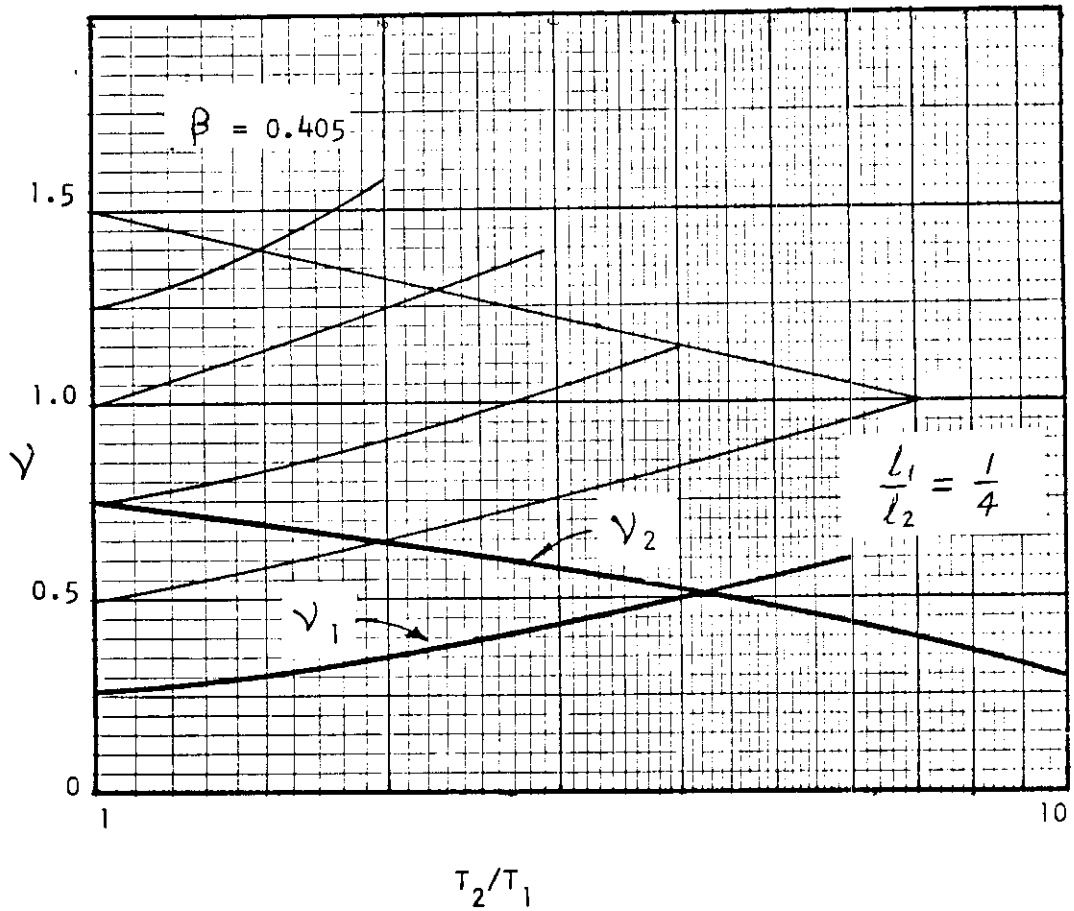


FIGURE 31 - VARIATION OF LONGITUDINAL MODE SHAPES UPSTREAM AND DOWNSTREAM OF A TEMPERATURE DISCONTINUITY WITH TEMPERATURE RATIO

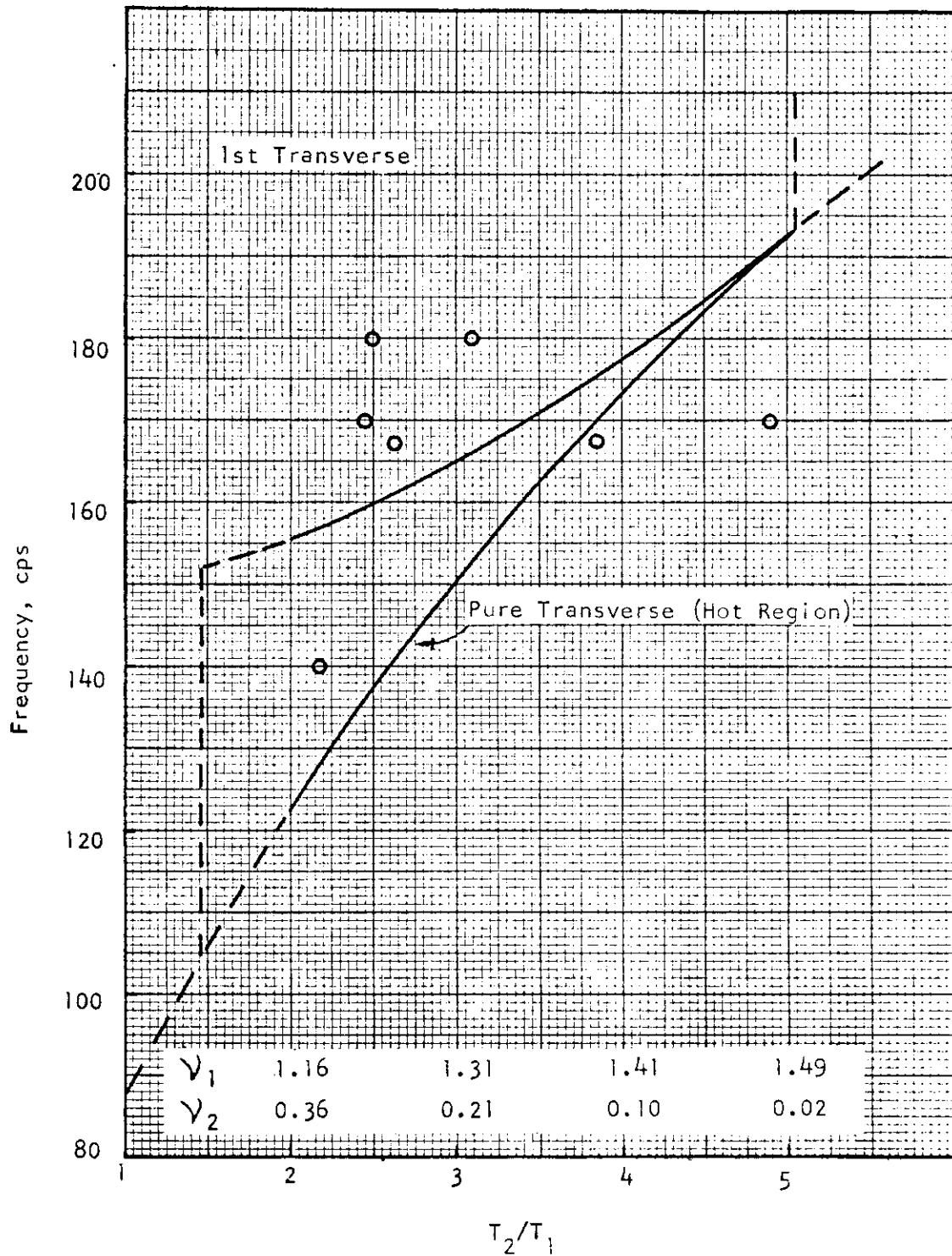


FIGURE 32 - COMPARISON OF PREDICTED FREQUENCIES WITH MEASURED FREQUENCIES FOR THE P&W SST COMBUSTOR

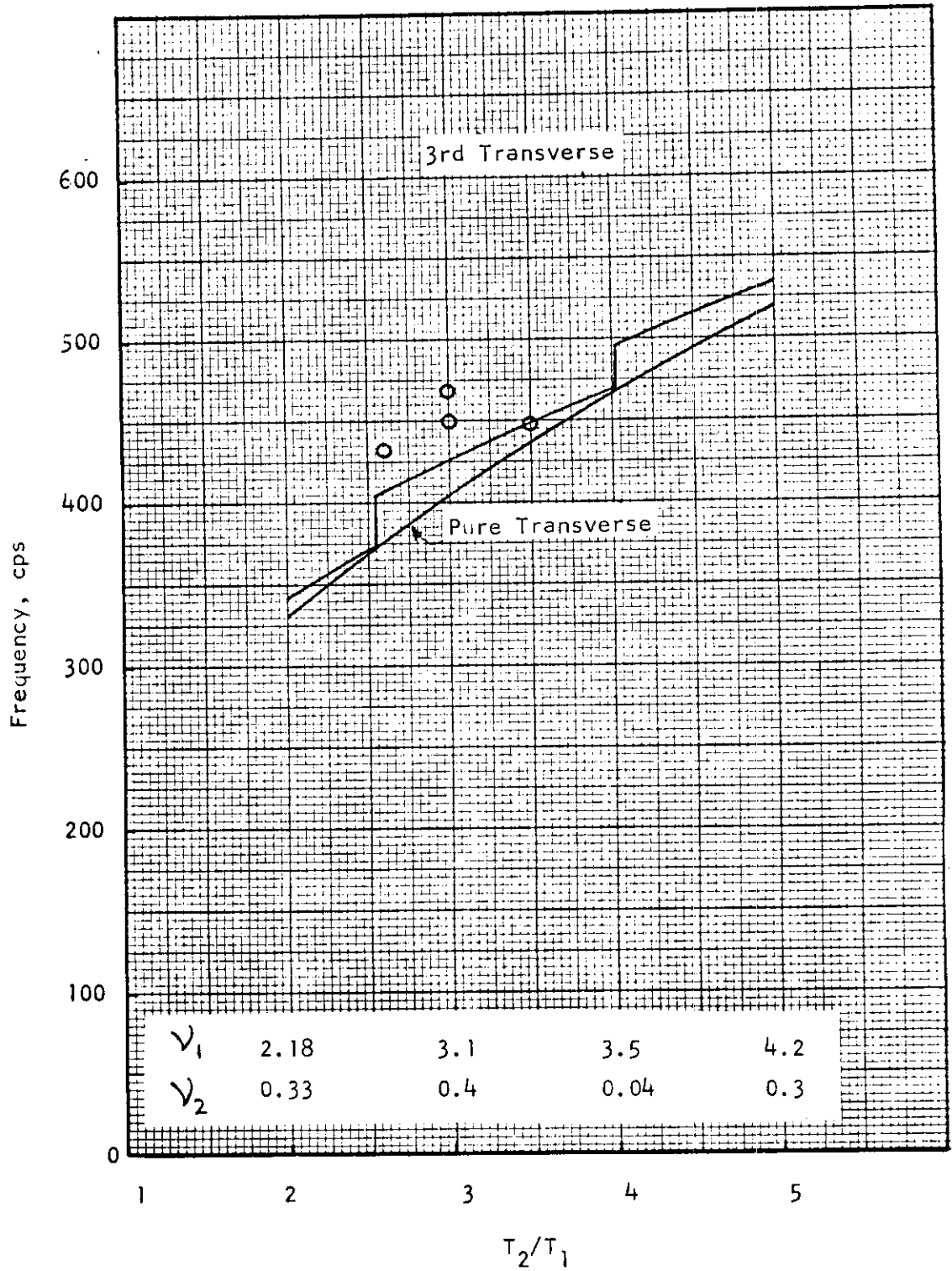


FIGURE 33 - COMPARISON OF PREDICTED FREQUENCIES WITH MEASURED FREQUENCIES FOR THE P&W SST COMBUSTOR

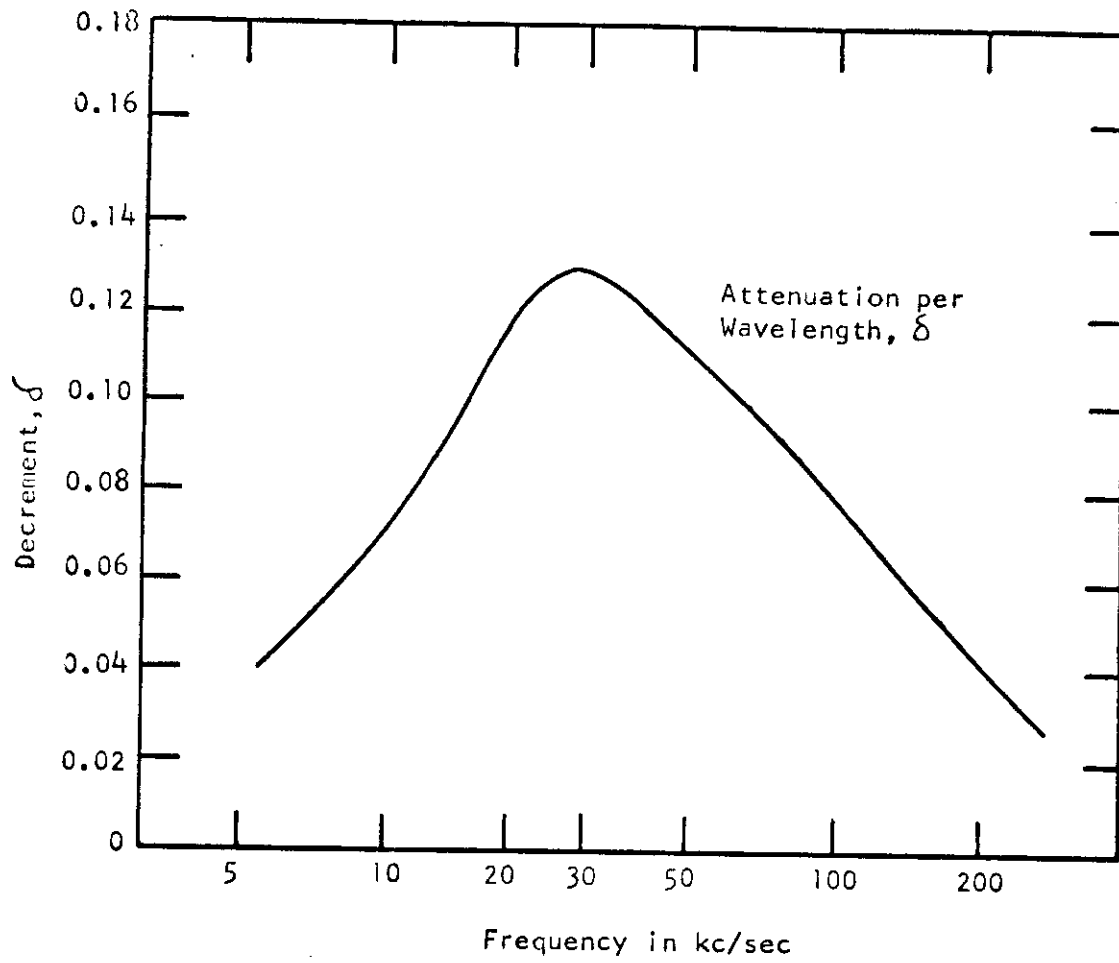


FIGURE 34 - ATTENUATION IN CARBON DIOXIDE GAS

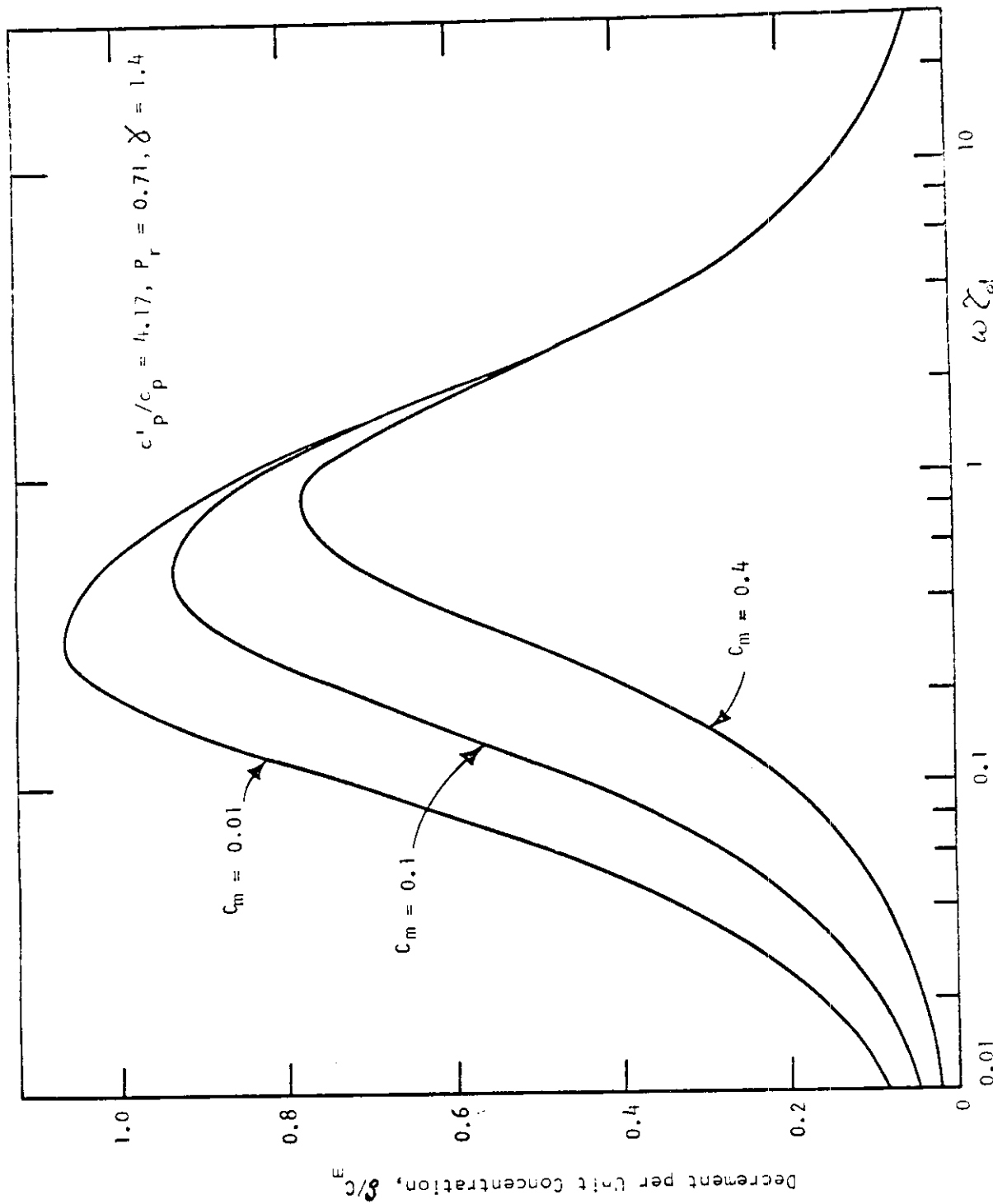


FIGURE 35 - ATTENUATION BY WATER DROPLETS IN AIR - FINITE CONCENTRATION,  $c_m$



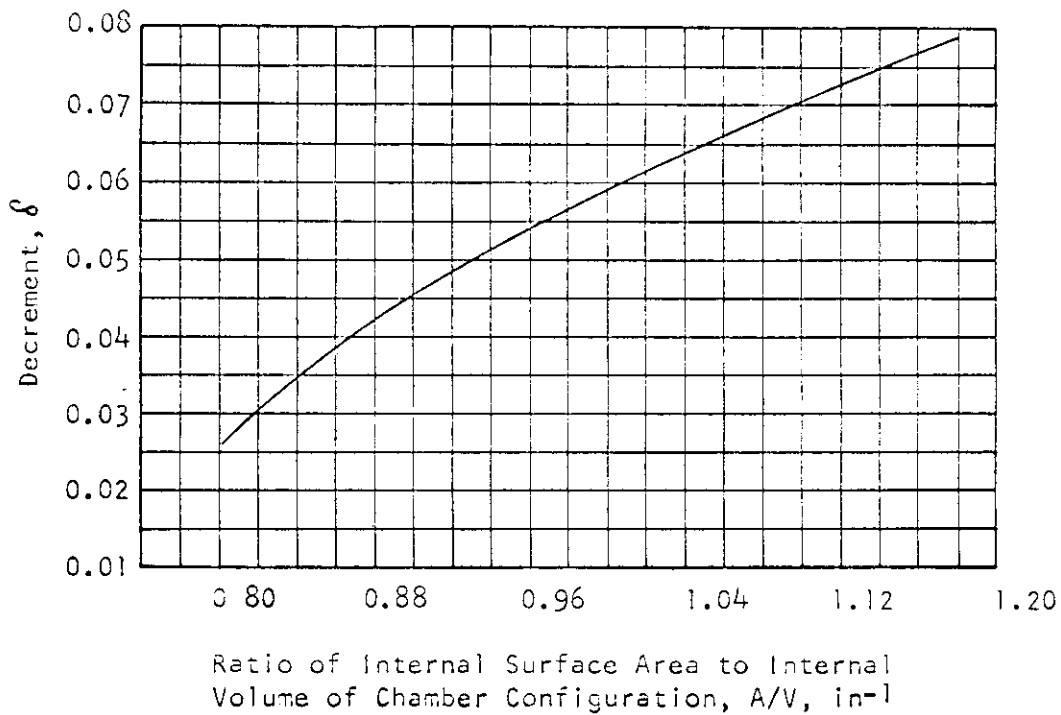


FIGURE 36 - VARIATION OF DECREMENT WITH CHAMBER SURFACE-TO-VOLUME RATIO FOR FIRST TRANSVERSE MODE (DATA OF REF 64)

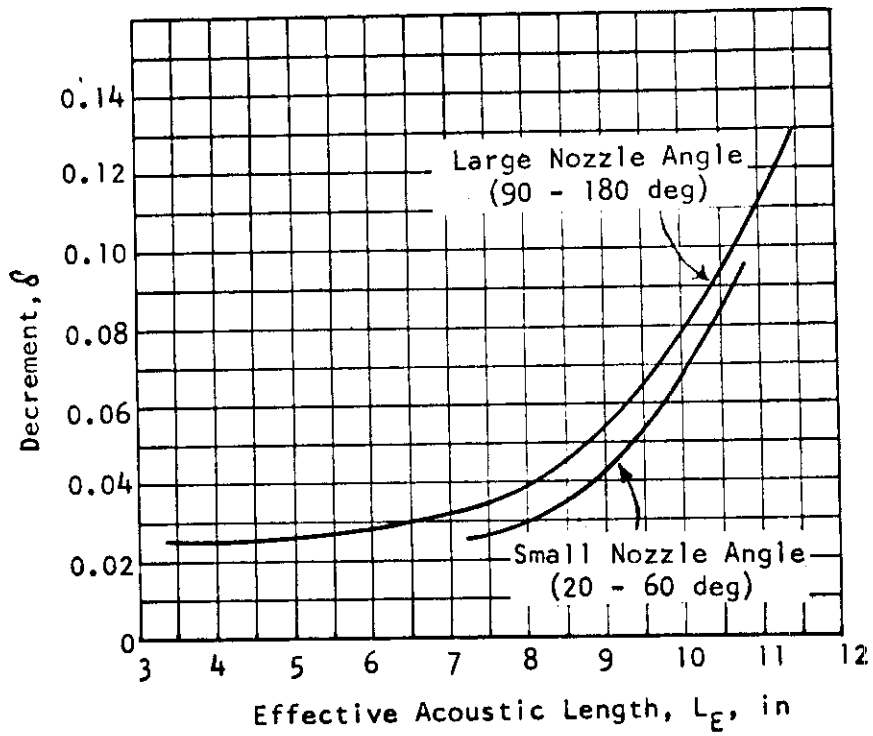
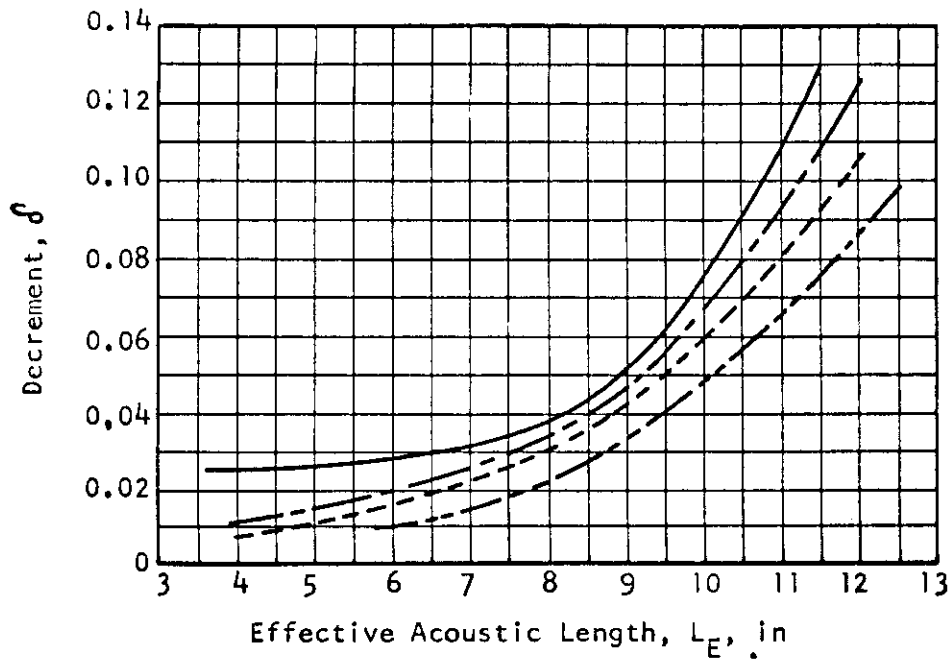


FIGURE 37 - EFFECT OF NOZZLE CONVERGENCE ANGLE ON VARIATION OF DECREMENT WITH EFFECTIVE LENGTH FOR FIRST LONGITUDINAL MODE (DATA OF REF 64)



Key for Injector Type

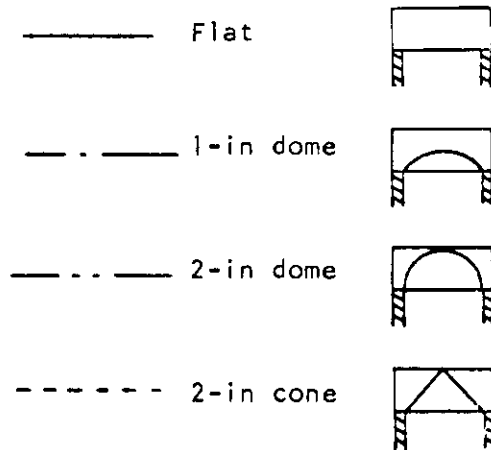


FIGURE 38 - EFFECT OF INJECTOR SHAPE ON THE VARIATION OF THE DECREMENT WITH EFFECTIVE LENGTH FOR FIRST LONGITUDINAL MODE (DATA OF REF 64)

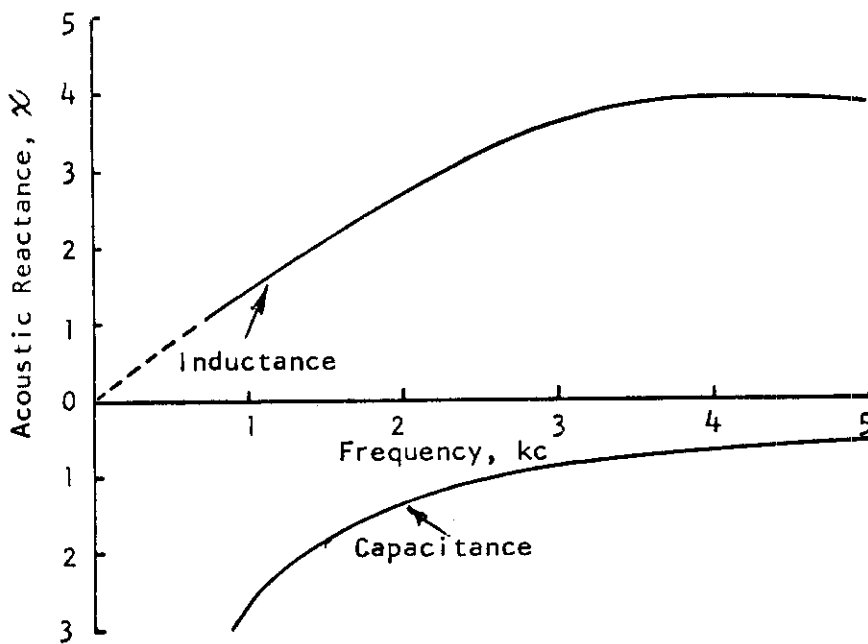


FIGURE 39 - EXPERIMENTAL INERTANCE AND CAPACITANCE OF AN ACOUSTIC LINER (DATA OF REF 65)

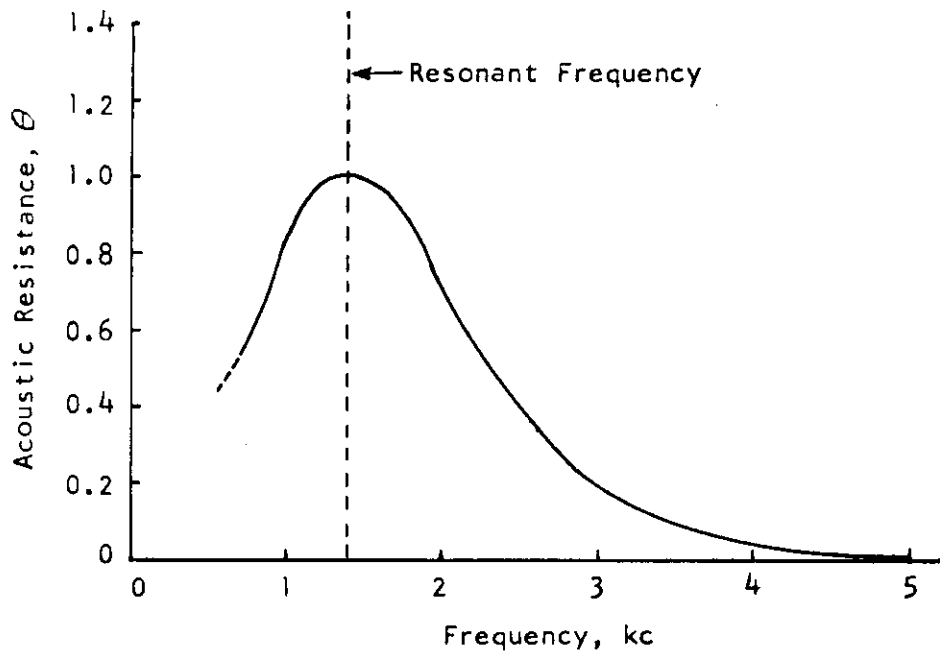


FIGURE 40 - EXPERIMENTAL ACOUSTIC RESISTANCE  
OF AN ACOUSTIC LINER (DATA OF REF 65)

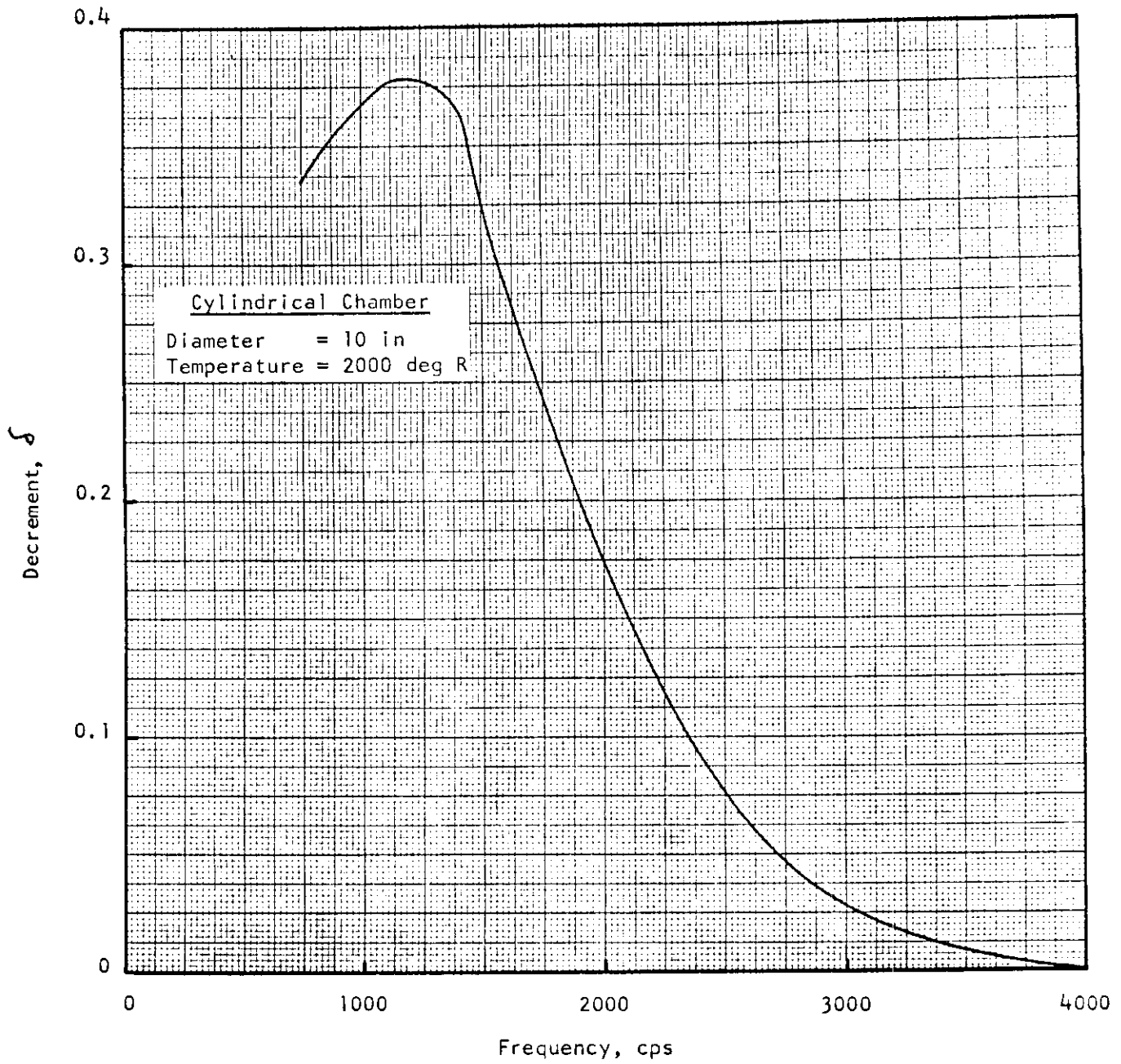


FIGURE 41 - DECREMENT VS FREQUENCY FOR AN ACOUSTIC LINER (DATA OF REF 65)

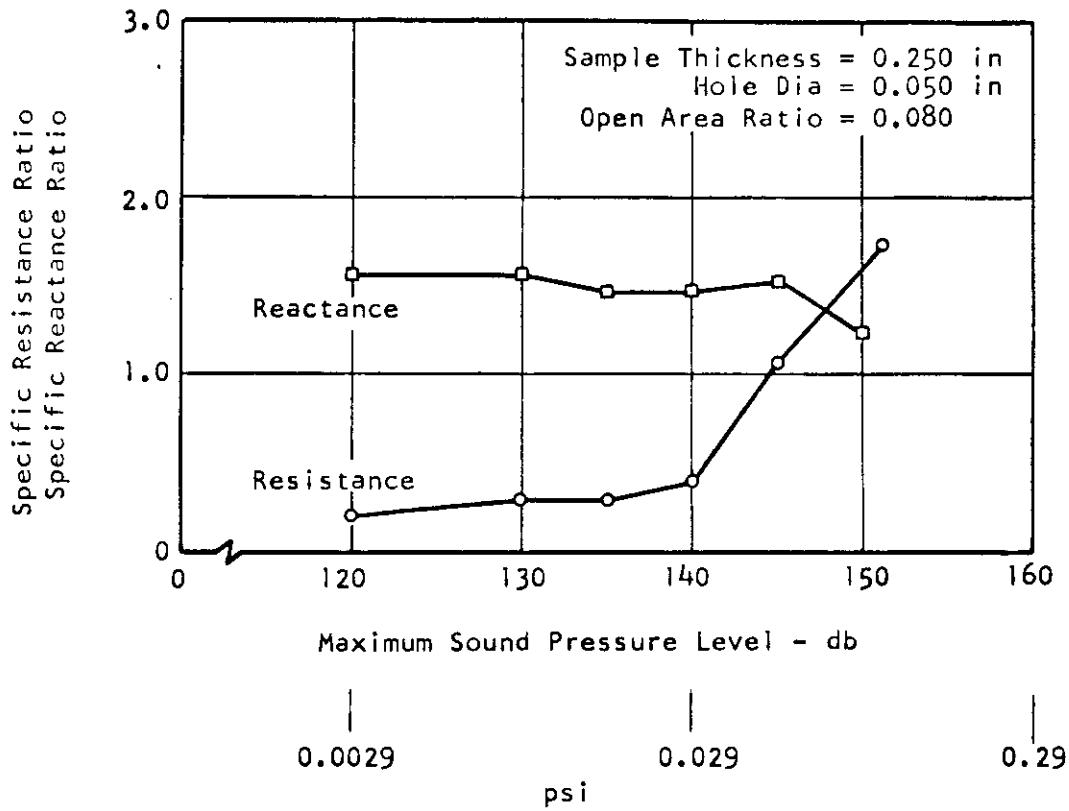


FIGURE 42 - ACOUSTIC REACTANCE AND RESISTANCE DATA  
VS SOUND PRESSURE LEVEL (DATA OF REF 65)

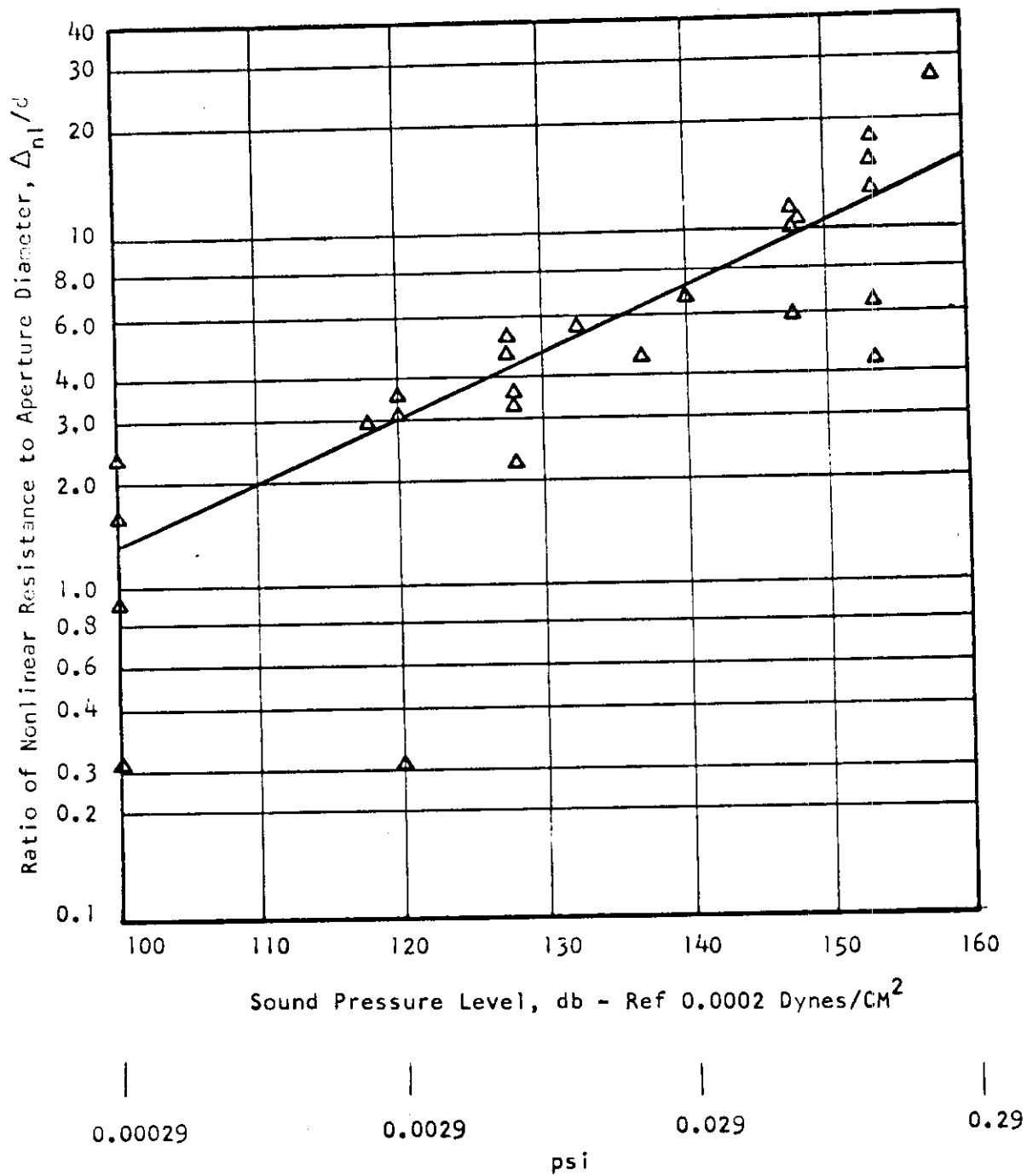


FIGURE 43 - NONLINEAR RESISTANCE VS SOUND PRESSURE LEVEL (DATA OF REF 67)



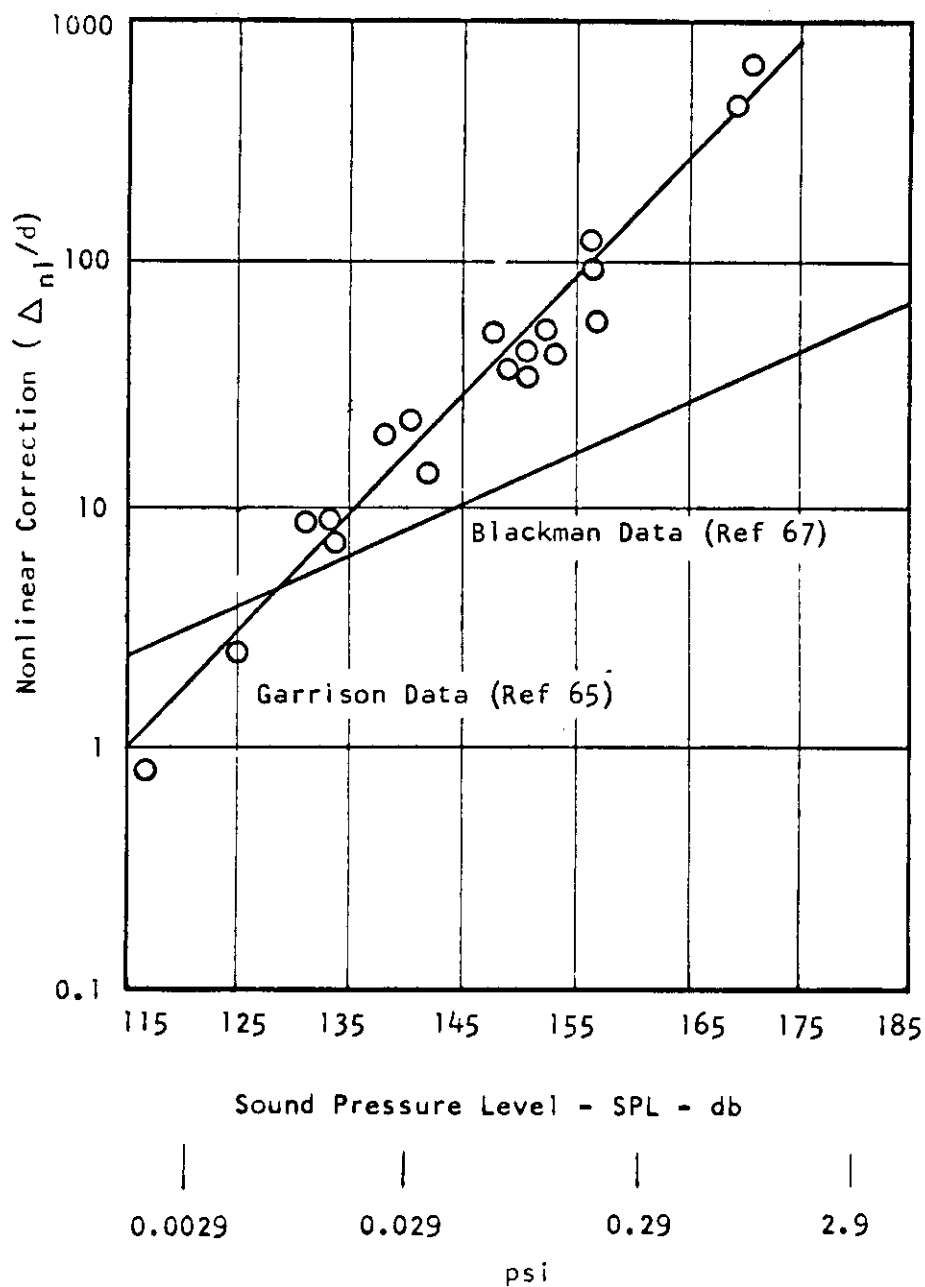


FIGURE 44 - NONLINEAR RESISTANCE VS SOUND PRESSURE LEVEL (DATA OF REF 65)

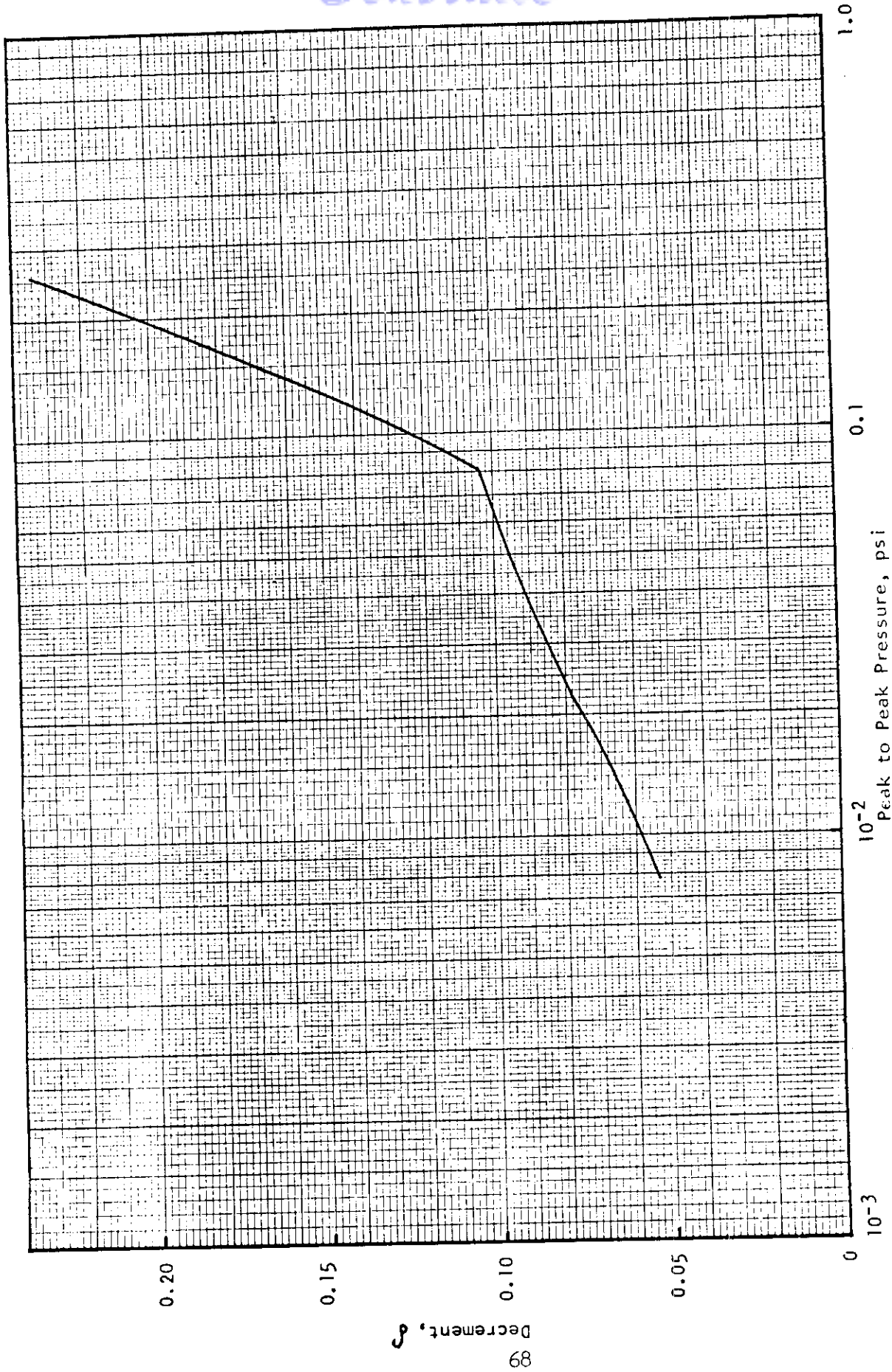


FIGURE 45 - EFFECT OF AMPLITUDE OF OSCILLATION UPON THE DECREMENT FOR A PERFORATED LINER (DATA OF REF 67)

# Contrails

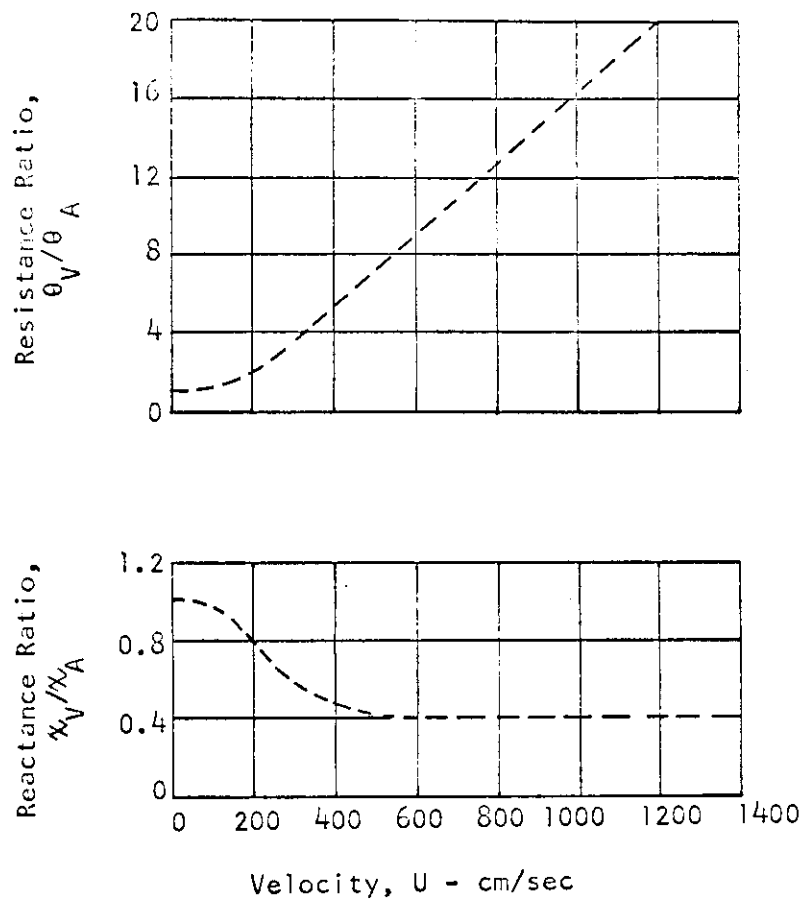


FIGURE 46 - ACOUSTIC IMPEDANCE AS A FUNCTION OF VELOCITY THROUGH ORIFICE (DATA OF REF 68)

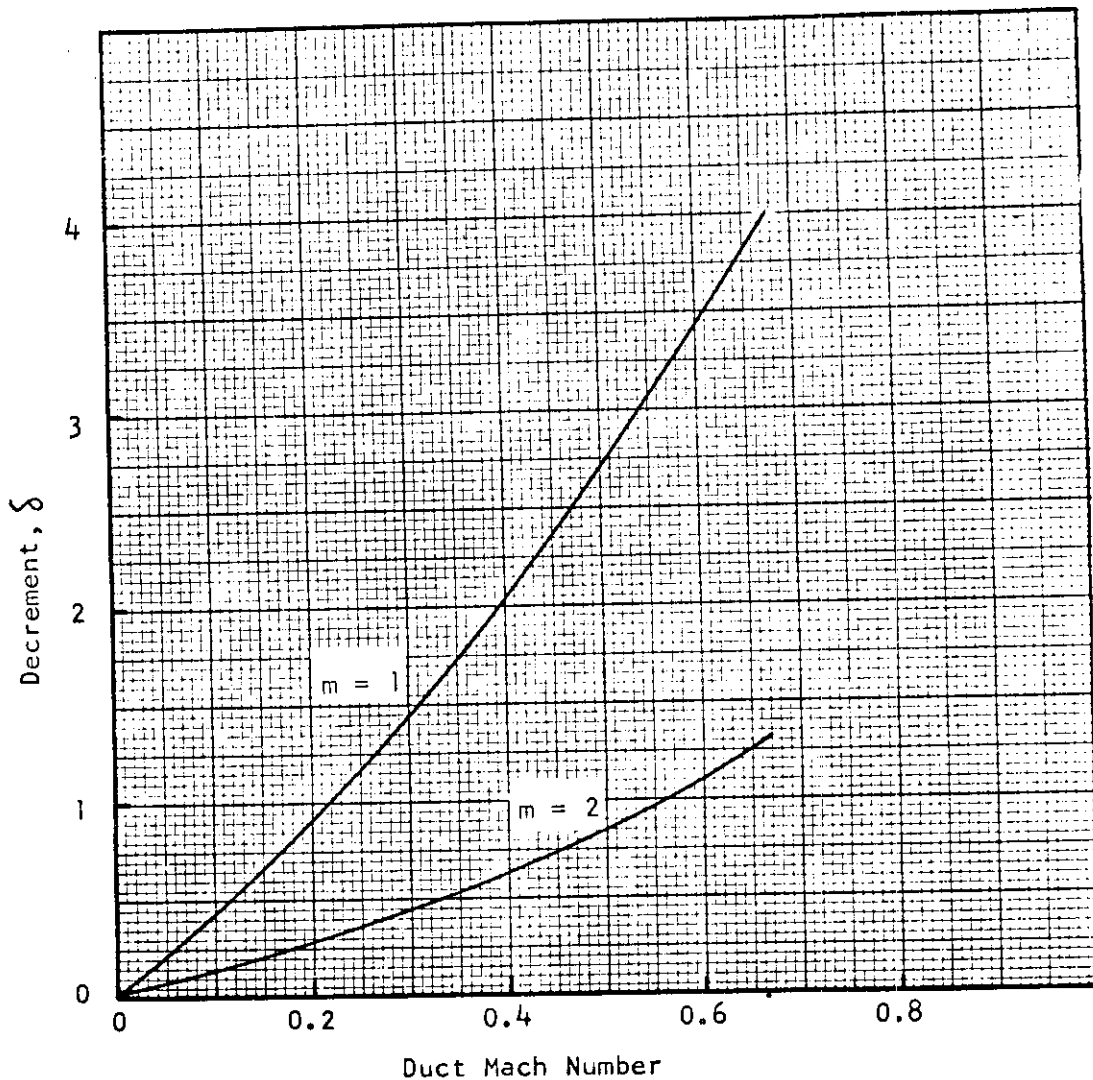


FIGURE 47 - DECREMENT FOR CONVECTION LOSSES -  
THEORETICAL DATA OF WHITEHEAD (REF 71)

Contract

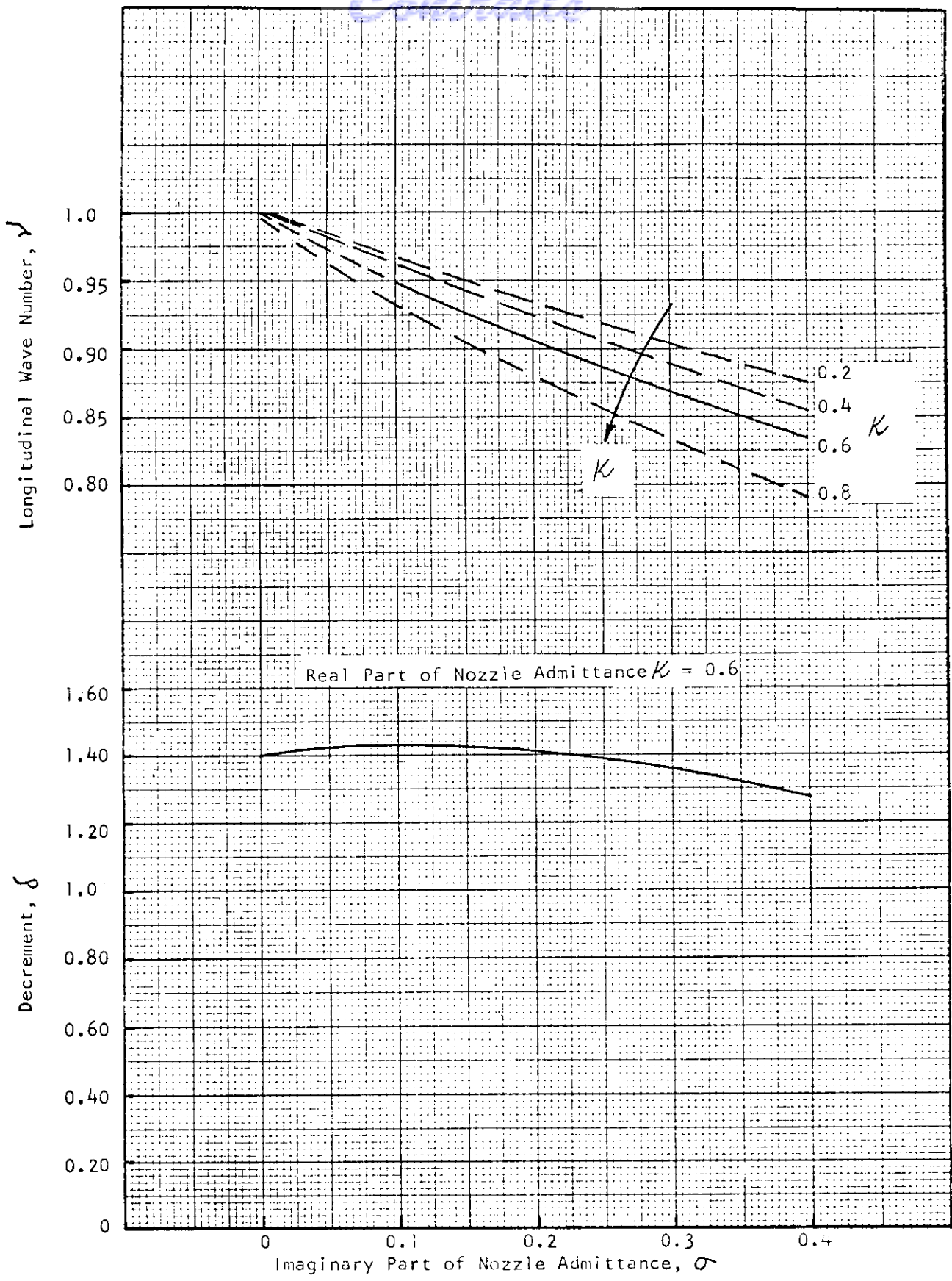


FIGURE 48 - DECREMENT AND LONGITUDINAL WAVE NUMBER CALCULATED AS FUNCTIONS OF IMAGINARY PART OF NOZZLE ADMITTANCE

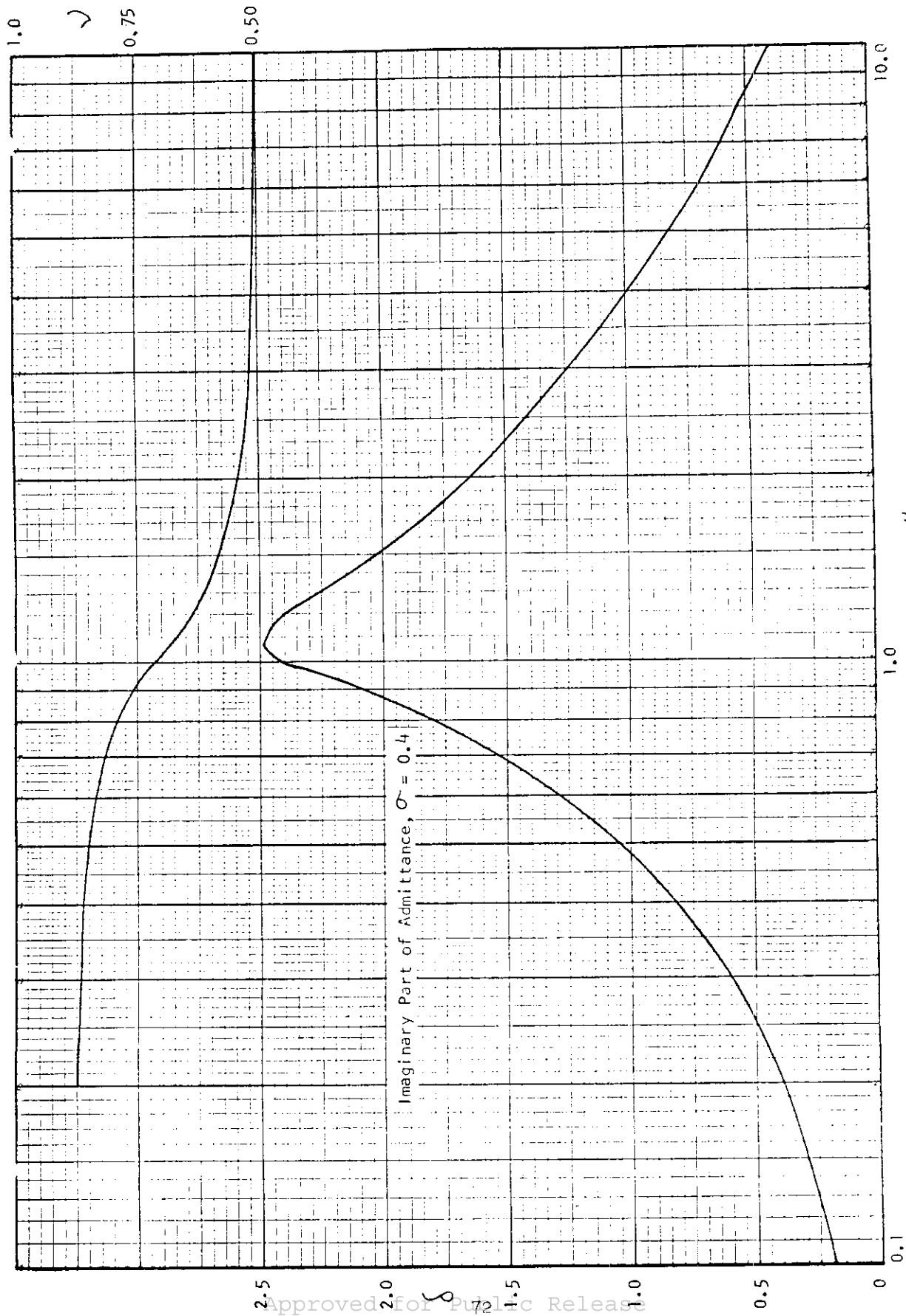
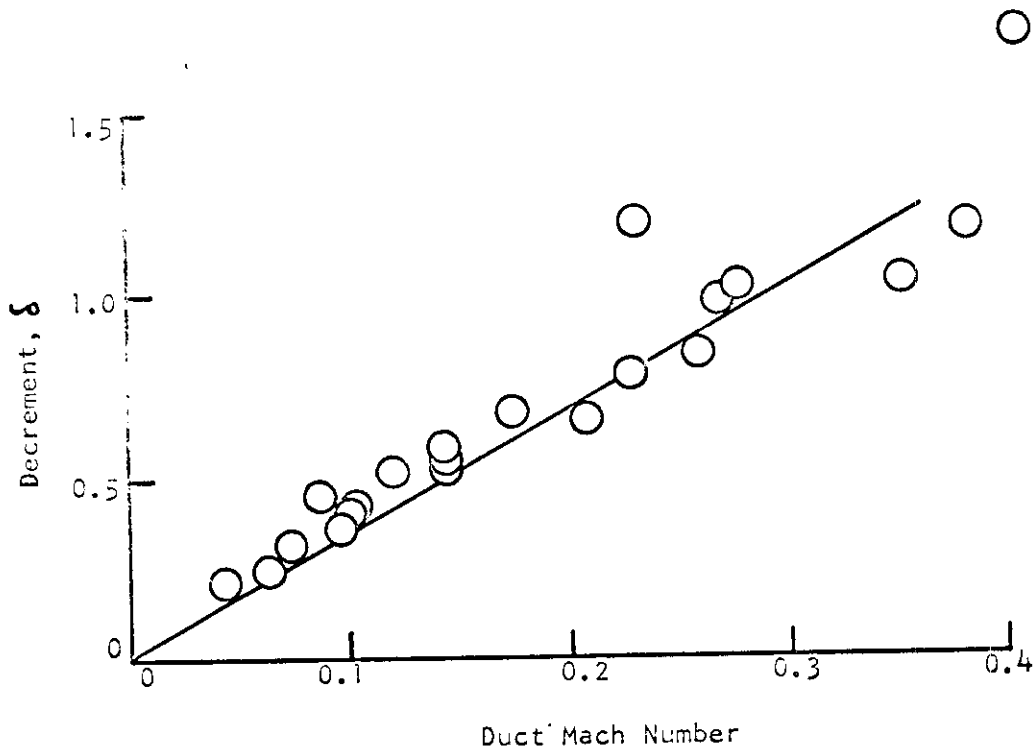


FIGURE 49 - DECREMENT AND LONGITUDINAL WAVE NUMBER CALCULATED AS FUNCTIONS OF REAL PART OF NOZZLE ADMITTANCE



# Contrails



Mach number varied by changing ratio of nozzle throat area to duct area

FIGURE 51 - ATTENUATION OF ABRUPT SONIC NOZZLES (RESULTS OF REF 70)



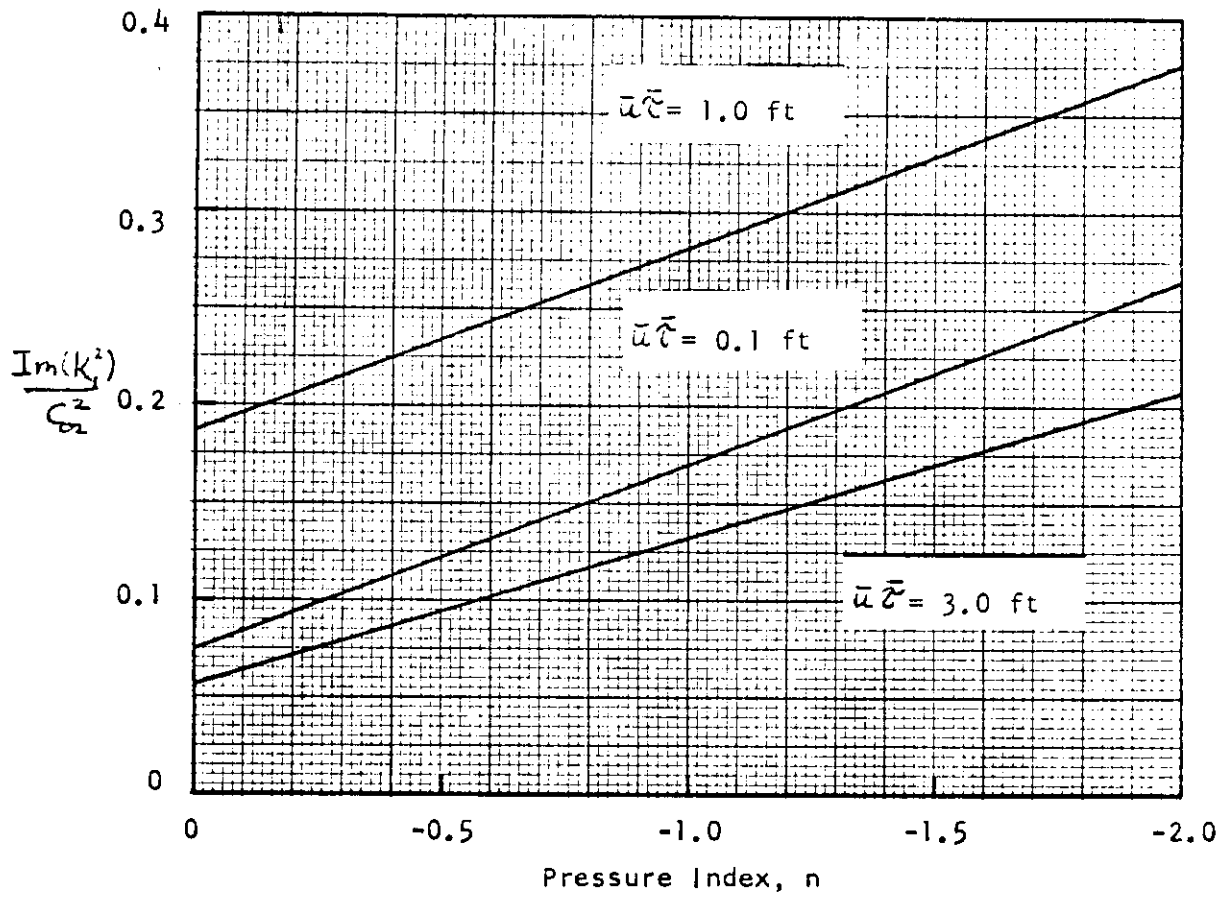


FIGURE 52 - GAIN CONTRIBUTIONS FOR A 26-INCH-DIAMETER BURNER

# *Contrails*

TABLE I - OBSERVED GAS-TURBINE COMBUSTION OSCILLATIONS

Source of Information	Type of Combustor	Size of Combustor in	Mode of Oscillation	Frequency of Oscillation cps	$\frac{fL}{c}$ { 0.92 1T 1.54 2T 2.06 3T
NACA (Ref 9)	Afterburner	32 dia	2nd T	780	1.28
			3rd T	1160-1240	1.9-2.04
			4th T	1320-1600	2.16-2.6
	Experimental	26 dia	1st T	550-730	0.73-0.97
			2nd T	960-1140	1.3-1.54
			3rd T	1360-1600	1.84-2.16
			4th T	1600-1950	2.16-2.64
			5th T	1950-2060	2.64-2.79
	Experimental	20 dia	1st T	760-930	0.77-0.95
	Experimental	14 dia	1st T	1090-1340	0.78-0.94
	Experimental	8 dia	1st T	1680-2170	0.69-0.89
NACA (Ref 11)	Afterburner	32.6 dia	1st T	510-560	0.85-0.93
			3rd T	1190-1260	2.02-2.13
			1st R	1150-1300	0.61-0.69
NACA (Ref 12)	Experimental	7 dia	1st T	2530	0.9

TABLE I - OBSERVED GAS-TURBINE COMBUSTION OSCILLATIONS (CONT.)

Source of Information	Type of Combustor	Size of Combustor in	Mode of Oscillation	Frequency of Oscillation cps	$\frac{fL}{c}$
	Experimental	6 dia	1st T	3280	1.0
NACA (Ref 13)	Experimental	26 dia	not stated	800-3000	---
United Aircraft (Ref 14)	Ramjet	6 dia	not stated, not longl.	2450-3350	0.75-1.02
General Electric (Ref 18)	Experimental	6 dia	1st T	2900	0.89
		8 dia	1st T	2200	0.9
		12 dia	1st T	1500	0.92
			2nd T	2400	1.5
			3rd T	3250	2.03
		18 dia	1st T	1050-1200	0.96-1.1
		32 dia	3rd T	1250	2.04
		28 dia	1st T	660	0.94
Marquardt (Ref 15)	Ramjet				
			2nd T	1100	1.57
			3rd T	1350	1.93

TABLE I - OBSERVED GAS-TURBINE COMBUSTION OSCILLATIONS (CONT.)

Source of Information	Type of Combustor	Size of Combustor in in	Mode of Oscillation	Frequency of Oscillation cps	$\frac{fL}{c}$
California Inst. of Technology (Ref 16)	Experimental 2-D	10 x 2½ in	1st T	1800	0.59
			2nd T	3700	1.2
			3rd T	5300	1.73
			1st T	3800	0.50

# *Contrails*

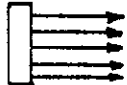
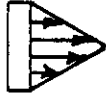

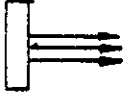

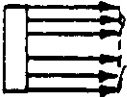
TABLE II - EFFECTS OF RADIAL ENERGY DISTRIBUTION

(Head End Injection)

Propellants: Premixed Ethylene-Air

Chamber Pressure: 150 psia

Chamber Dimensions: 7-inch diameter, 6-inch length

Distribution	Mode	Amplitude	E
I 	First Tangential	7 psi	1.00
II 	Stable	0	0.60
III 	First Tangential	11	1.20
IV 	First Radial	13	0.16
V 	Stable	0	0.65
VI 	First Tangential	40	1.47

(From Ref 53)

# *Contrails*



## Appendix A

### LITERATURE SURVEY

#### INTRODUCTION

Consistent with the objectives of the program, the present literature review is intended for the general purpose of assessing the state-of-the-art of analytical descriptions of combustion instability phenomena in duct burners and/or afterburners (hereafter referred to as merely "burners") of gas-turbine engines and in combustors of liquid-, solid-, and gaseous-propellant rocket engines. The more specific purpose is to assess these analytical descriptions with respect to their potential utility in describing combustion instability in gas-turbine burners, with the ultimate hope of establishing, if possible, appropriate forms of analytical models for these burners.

It should be pointed out that it was felt at the outset that sufficient similarities in combustion instability existed between gas-turbine burners and liquid-rocket combustors to justify a review of the liquid-rocket literature, which is considerably more abundant than the gas-turbine literature. During the course of the review, it became apparent that many similarities in combustion instability processes also existed between gas-turbine burners and both solid-propellant and gaseous-propellant rockets. Hence, the scope of the literature review was extended to include some of the literature pertinent to the latter engines. In the context of the scope of the review, it is also emphasized that the present review can in no sense be considered exhaustive; this is a slight departure from the original intent, but it is unavoidable in view of the overwhelming numerical superiority of the number of articles available compared to the available human and financial resources. Notwithstanding this limitation, the present review is considered both representative of the available literature and satisfactory for the purpose of assessing analytical approaches.

As in any other rational attempt to describe analytically the behavior of physical systems, a knowledge of the observed physical behavior of typical systems is an invaluable guide for the direction of analytical effort. This is particularly true for studies of combustion instability-- a phenomenon which can involve the interaction of several complex physical processes. Accordingly the first section of this review, which deals with the available gas-turbine burner literature, contains descriptions of the observed experimental behavior of combustion instability in burners. It must also be confessed that little choice is available to the reviewer with regard to this emphasis on experimental results, since virtually no analytical descriptions of combustion instability in these burners exists.

The subsequent sections of the review deal with, in order, the literature on combustion instability in liquid rockets, solid rockets, and gaseous rockets. In these sections, the primary emphasis is placed on analytical developments, and references to experimental results are made only to assess

the validity of these developments. This relative emphasis is deemed consistent with the primary objective of the review, which is an assessment of potentially useful analytical descriptions; although experimental results for rockets are unquestionably of value in assessing the validity of corresponding analytical approaches, the physical conditions encountered in rockets are sufficiently different from those encountered in gas-turbine burners to make a detailed description of experimental results in the former engines a relatively unrewarding effort.

As a prelude to reviewing the specific literature, the following subsections are devoted to a general discussion of the high frequency combustion instability problem which is intended to provide a framework for the succeeding literature review. The nature of the physical processes which can be of significance are described, and their physical consequences are indicated. The points of similarity and difference between the processes occurring in the various combustors are emphasized, in order that the analytical developments can be properly assessed.

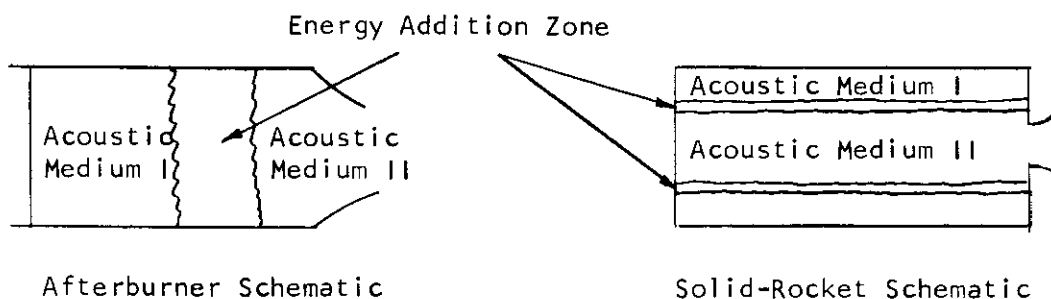
## GENERAL PROBLEM OF HIGH FREQUENCY COMBUSTION INSTABILITY

Typical schematic arrangements of a gas-turbine burner and various rocket combustors are shown in Figure 3. As can be seen, all of these arrangements are quite similar; all but the solid-rocket combustor provide for the functions of mixing of the fuel and oxidizer (and vaporization, if required), burning, and subsequent exhaust of the combustion products into a thrust-producing nozzle. The nature of solid propellants is such that only the latter two functions are required. The geometry in all cases is basically an uncluttered cylindrical cavity (in a ductburner, the shape is, of course, annular); in solid rockets, a portion of the cavity is occupied by the solid propellant which changes dimensions as burning continues.

The physical manifestations of high frequency combustion instability in any of these configurations is basically the occurrence of low to extremely high amplitude pressure oscillations within the chamber. In all types of chambers these oscillations cause an increase in heat transfer rates to the walls; other more specialized problems include the aggravation of fan stall problems in duct burners and an increase in mean burning rate in solid-propellant rockets. Usually, these oscillations result in the eventual destruction of the chamber. The most significant features of these oscillations with regard to their origin are the amplitude and wavelength of the pressure distribution in the chamber at any instant of time (which generally will be slowly varying in either the axial or circumferential direction and possess a roughly sinusoidal form in the other direction) and the frequency of the oscillation at any given point. Of particular interest is the location of the peak amplitude, since this will generally correspond to the location of energy addition to the oscillation, and the spatial decay of the amplitude from the peak value, since this yields an indication of the magnitude of the energy loss from the oscillation. A final characteristic of these oscillations which is quite important is their so-called nonlinear behavior; that is, the presence or absence of these

oscillations in any given system may depend upon the amplitude of an applied initial disturbance. It is often found that a system will behave in a stable manner (i.e., no oscillations) when subjected to only small disturbances, but will become unstable (i.e., sustain oscillations of appreciable amplitude) when subjected to larger disturbances.

For the purposes of describing combustion instability in analytical terms, it is convenient to characterize the combustor as consisting of three rather distinct regions: two regions which are described as being occupied by passive acoustical media (i.e., media which will support wave propagation and in which energy addition to oscillations from within the volume is negligible), and separated by a third region which can be described as an energy addition zone. This characterization is indicated schematically below:



As will be described, this characterization represents an oversimplified view of the combustor, but it is nevertheless one which, with suitably liberal interpretations, can be used to describe all of the analytical developments to date relevant to combustion instability. In terms of this model, two requirements for instability exist, and they can be described quite simply. First, it is necessary that the system as a whole be capable of supporting oscillations; this capability is in large measure determined by the physical and geometrical properties of the acoustical media involved and the boundary conditions appropriate to the various interfaces. Second, it is necessary that at any unstable frequency of oscillation the energy being supplied to the oscillation (primarily in the energy addition zone, but possibly also at the boundaries) exceed the energy being dissipated by the oscillatory motion. The more important considerations involved in quantitatively evaluating these requirements in terms of the idealized analytical characterization are described in the following paragraphs.

## Description of Acoustical Media

A rigorous description of the behavior of the acoustical media in our idealized model would involve the solution of the full time dependent conservation equations of mass, chemical species, momentum, and energy subject to the appropriate boundary conditions. Such an approach (in addition to being completely intractable) tends to obscure the important facets of the physical behavior of these media. The latter behavior is best appreciated

# Contrails

by considering the various effects in a linear fashion, since it can be assumed that the resultant behavior will in at least some qualitative way resemble a superposition of the individual effects.

The basic resonant characteristics of a gaseous medium are illustrated by the well-known acoustical solutions for a uniform, stationary gas, enclosed in a rigid cylindrical container of radius  $a$  and length  $L$  and subjected to small sinusoidal perturbations. The time-dependent pressure and velocity perturbation fields can be expressed as

$$\begin{aligned} p_i &= \text{real part of } p' e^{i\omega t} \\ \underline{v}_i &= \text{real part of } \underline{v}' e^{i\omega t} \end{aligned} \quad (\text{A-1})$$

with

$$p' = A p_0 \cos\left(\frac{\ell\pi z}{L}\right) J_m\left(\beta_{mn} \frac{r}{a}\right) \cos(m\phi) e^{i\omega t} \quad (\text{A-2a})$$

for standing waves, or

$$p' = A p_0 \cos\left(\frac{\ell\pi z}{L}\right) J_m\left(\beta_{mn} \frac{r}{a}\right) e^{i(m\phi + \omega t)} \quad (\text{A-2b})$$

for spinning waves, and

$$\underline{v}' = \frac{c}{\rho_0 \omega} \nabla p' \quad (\text{A-3})$$

where the integers  $\ell$ ,  $m$ ,  $n$  define the modes, and  $\beta_{mn}$  is determined from

$$\left. \frac{d}{dr} \left( J_m\left(\beta_{mn} \frac{r}{a}\right) \right) \right|_{r=a} = 0 \quad (\text{A-4})$$

The characteristic oscillation frequencies are obtained from

$$\frac{\omega}{c_0} = \left[ \left(\frac{\ell\pi}{L}\right)^2 + \left(\frac{\beta_{mn}}{a}\right)^2 \right]^{\frac{1}{2}} \quad (\text{A-5})$$

In the above relations the subscript 0 refers to conditions in the uniform unperturbed state. Similar solutions can be obtained if the ends of the cylinder are assumed open.

The relevance of solutions of the preceding type to the behavior in appropriate parts of a combustor depends upon several factors. First, the effects of the volume losses in the medium are not included in the above solutions. These losses can arise from the effects of viscosity and thermal conductivity, the presence of solid particles in the medium, gas-phase chemical reactions, and "sound absorption" (the excitation of molecular vibrational states by the oscillating motion); all of these losses result in a conversion of the energy of the ordered oscillating motion to random thermal energy and can be rigorously represented by appropriate terms in the governing conservation equations. As these effects are analogous to any other form of vibrational damping, they can appreciably affect the characteristic frequencies and mode shapes if their magnitudes are sufficiently

# Contrails

large. If the magnitudes of these losses are relatively small, the characteristic frequencies and mode shapes will be virtually unaffected; even in this case, however, the amplitude of the oscillations can be expected to be strongly influenced by these losses. Since the magnitudes of these losses depend upon the thermodynamic state of the medium, it can be expected that their relative importance will not be the same for, for example, gas-turbine burners and solid-rocket combustors. Nevertheless, the analytical treatment of these losses can be expected to be quite similar for all types of combustors.

A second factor affecting the utility of the simple acoustic solutions is the derivation of the actual boundary conditions for a given media from those of either a solid wall or a constant pressure surface. In acoustic parlance, these boundary conditions are represented by normal admittances, defined as

$$A = \frac{\rho' \cdot \underline{n}}{p'}$$

where  $\underline{n}$  is the unit normal vector of the surface. In physical terms, these boundary conditions determine the amount of energy which is extracted from or added to the oscillatory motion at the bounding surfaces. If the energy transfer at these surfaces is large compared with the acoustic energy intensity within the volume, then the characteristic mode shapes and frequencies will deviate substantially from their simple acoustical forms. Conversely, if the surface energy transfer is relatively small, the characteristic frequencies and modes will be virtually unaffected; the amplitude of any oscillation can, however, be expected to be strongly influenced by this energy transfer in any case. The energy transfer at the boundaries arises due to several mechanisms: viscous and thermal losses in the acoustic boundary layer, the imposition of a sinusoidal disturbance at a boundary by means of an external energy source (such as the disturbance created by wakes from fan blades in duct burners), the generation of oscillations in an adjacent medium, acoustic radiation from the nozzle, and, of course, the vital energy transfer which results from the response of the energy addition zone to a pressure disturbance. Again, it may be anticipated that the relative importance of the various energy transfer mechanisms will be different for each type of combustor, but that the analytical treatment of each mechanism will be similar.

Other factors which affect the relevance of the simple acoustic solutions are the inhomogeneity of the medium (i.e., the variation of unperturbed flow field parameters over a wave length), the importance of the unperturbed flow field (measured by the Mach number), and the magnitude of the oscillation amplitude. All of these factors can influence the characteristic modes and frequencies significantly, and a rigorous analysis of their effects considerably complicates the governing equations (so much so as to render them intractable).

## The Energy Addition Zone

The energy addition zone of course plays a vital role in the process of combustion instability, since it represents the source of energy for the oscillation. The major feature of interest in this zone is its response to fluctuations in flow field properties. This is in accord with the so-called Rayleigh principle, which is merely the statement that the maximum energy input to the oscillation will occur when the fluctuating energy release rate (in response to a pressure fluctuation) is in phase with the pressure fluctuation.

Several factors must be considered when contemplating the physical behavior and the associated analytical description of this region. First, the spatial extent of the region greatly influences both the conceptual and analytical difficulty involved in describing its behavior. If, for example, the extent of this region in at least one dimension is small compared with the relevant acoustic wave length, its acoustic properties may be conveniently represented by the appropriate admittances it presents to the adjacent regions, and a substantial simplification in the analysis can be achieved. On the other hand, if the spatial extent of the region is large compared with the acoustical wave length, the internal acoustical properties of the region must be considered (in addition to the vital energy release mechanisms), with the result that any description of the behavior of this region becomes more complex. At this point, it should be obvious that the line of demarcation between the energy addition zone and the more passive acoustic regions in a chamber is anything but sharp, and varies widely depending upon the type of chamber being considered. The solid-rocket chamber is perhaps blessed with the most well-defined burning zone-- a narrow region at the surface of the solid propellant; on the other hand, the energy addition zone in a liquid rocket can be expected to be rather diffuse due to the simultaneous occurrence of mixing, vaporization, and combustion.

The spatial orientation of the energy addition zone is also of importance in determining the case with which instabilities may be generated. If, as depicted in the left-hand sketch on page 80, the zone is oriented generally transverse to the axis of the chamber, it may be expected that the energy transfer to an axial mode may be substantially greater than to a transverse mode. On the other hand, if the energy addition zone is oriented generally concentric to the axis of the chamber (as shown in the right-hand sketch on page 80, it may be expected that the energy transfer to tangential or radial modes would be favored.

Several physical processes can influence the time-dependent behavior of the energy addition zone (in addition to its spatial extent) and vary widely depending upon the type of chamber. In all chambers, turbulent heat and mass transfer (or more generally, "mixing") processes and gas-phase chemical kinetics can be important in influencing the energy release rate. In liquid rockets and possibly in gas-turbine burners, the processes of liquid vaporization and mixing can also play a role, while in solid rockets heat conduction within the solid propellant, erosion, and solid-phase chemical reactions may be important. In any given chamber, the

# Contrails

time-dependent energy release rate will be controlled by the particular process or processes with the longest response times, and the identification of these processes is an important part of the description. Once again, it cannot be expected that the various processes will be of the same relative importance in all types of chambers, but their analytical representations may be of more general utility.

Finally, the nature of the interaction between the energy addition zone and the adjacent regions must be considered. First, a steady oscillation will be maintained only when the energy supplied to the oscillation (presumably at the interfaces between the energy addition zone and the adjacent media) is exactly balanced by the energy lost throughout the chamber. The magnitude of the rate of energy supplied to the oscillation is obviously a quantity of interest, as well as the way in which any analytical description of the energy addition process accomplishes the necessary relationship to the properties of the system as a whole. The technique by which the latter is accomplished is an important assessment to be made of any previous work. Second, the frequency response characteristics (both experimentally observed and analytically predicted) is an important quantity. This response will in general indicate whether instability is inherent in the burning process (typified by a very high amplitude response in a narrow frequency range) or whether, as believed more likely, it is basically determined by acoustical resonance. In the latter case, a relatively flat frequency response would be indicated.

## GAS TURBINE DUCT BURNER AND AFTERBURNER LITERATURE

### INTRODUCTION

This portion of the literature review has been restricted to instabilities in the afterburner and ramjet type of combustion chamber. Rocket engine instabilities are reviewed separately in subsequent sections of this report.

Both low frequency longitudinal oscillations and high frequency transverse modes are encountered in practice. However, for the purposes of this study attention is restricted to the latter modes of oscillation because the instabilities associated with longitudinal modes are, in general, less harmful in practice and can be tolerated. Further, even when these lower frequency oscillations become intolerable their elimination or suppression is generally achieved by simple design changes, often in the fuel-control system. However, problems associated with coupled modes (transverse modes with longitudinal components) are more difficult, and are therefore included in the present investigation.

### OBSERVED COMBUSTION OSCILLATIONS

Combustion oscillations for which any detailed information is available have been reported to occur in three types of combustion chambers:

# Contrails

1. Gas-turbine afterburners
2. Ramjet combustors
3. Experimental burners designed specifically for the investigation of combustion instabilities. The cross-sectional form of these burners is either circular or thin rectangular (pseudo two-dimensional).

The significant differences between these three types of burners lies only in their ranges of operating conditions, for example, pressure, inlet temperature, and composition of the inlet gases (the afterburner always receives vitiated air, the ramjet pure air, and the experimental burner either). These changes in operating conditions will significantly affect the physical properties of the fuel-air mixture; e.g., higher temperatures will speed up the fuel droplet evaporation processes thereby reducing the liquid droplet density and size in the combustion zone.

In almost all of the reported combustor instabilities, the mode of oscillation was tangential ranging from the fundamental mode to the fifth overtone. Other basic modes of oscillation, radial and longitudinal, have not been experienced in the types of combustors considered here, with one exception. The exception is the observation of a radial oscillation in a NACA afterburner (Ref 11), in which the fuel was injected predominantly near the combustor centerline; under conditions of more uniform fuel injection, the same burner exhibited a tangential mode of instability. Possible variations on the three basic modes of oscillation include nonstationary modes in which the nodal points of the oscillation move, and combinations of the three basic modes either stationary or nonstationary. However, in only one instance has a reported oscillation fallen into any of these categories; this was a spinning transverse mode experienced in a NACA experimental burner (Ref 12).

A summary of some of the observed instabilities that have been reported in the literature is presented in Table 1. The table shows, for each oscillation observed, the frequency and mode of the oscillation, the type, shape, and size of the combustor and the source of the information. In several cases a range of frequencies is shown; this arises for one of two reasons: (a) Several tests were performed with the same basic combustor exhibiting the same mode of oscillation, and the range of frequencies resulted from minor differences between tests affecting perhaps the local flame temperature distribution. (b) Unsteady behavior of the combustion causing the frequency to wander.

Also shown in the table is a dimensionless frequency  $fL/c$ , evaluated for each of the observed instabilities, where  $f$  is the measured frequency,  $c$  is the sonic velocity evaluated at a typical average burner temperature of 3000 deg R and  $L$  is a burner dimension which is taken to be half the circumference for the tangential mode, the radius for the radial mode and the breadth for the transverse mode of the 2-D combustor. It can be seen that the dimensionless frequency is reasonably constant for each mode of



oscillation having a value of approximately 0.85 for the fundamental oscillation, 1.4 for the second overtone, 2.0 for the third overtone and so forth. An acoustic analysis of cylindrical ducts (see Ref 12) gives corresponding values of 0.92, 1.54, and 2.06, respectively. These discrepancies can be attributed to the uncertainties in the temperature of the combustion products. In Reference 9 the temperatures are between 2100 deg R and 3500 deg R, and can be considered to be typical of the variations from the temperature 3000 deg R which was assumed when evaluating the non-dimensionalized frequencies in Table I. These uncertainties in temperature can account for discrepancies of approximately 10 per cent.

The combustion oscillations observed in these three types of burners are essentially similar and, therefore, no distinction is made between instabilities associated with each burner type.

The magnitudes of the reported pressure oscillations are large fractions of the mean pressure level. Rogers and Marble (Ref 16) show peak to peak amplitudes of 24 per cent of the inlet total pressure at stoichiometric conditions. Bragdon and Lewis (Ref 14), and Harp, et al (Ref 9) show fluctuations in excess of 50 per cent of the mean level.

All of the waveforms reported in the cited references are predominantly sinusoidal and do not exhibit steep pressure variations that are associated with traveling shock waves.

The variation in pressure amplitudes with axial distance downstream of a flameholder are shown in Figures 4 and 5. The peak amplitudes occur approximately one duct radius downstream of the flameholder. The variation in pressure amplitude with axial position is very small ( $< 10$  per cent) except in the region of the flame front itself.

The modes of instability have been identified in different ways by different groups of workers. In Reference 12, pressure measurements were made at several points on the duct periphery; by comparing the phasing of the pressure oscillations the mode can be readily identified. In Reference 14, similar pressure measurements were confirmed using photographic and luminosity measurements. Newton and Truman (Ref 18) used remote microphones and compared their results with analytically computed frequencies. In all cases the identification of the transverse modes has been clearly substantiated.

## THE OBSERVED EFFECTS OF COMBUSTOR PARAMETERS UPON STABILITY BOUNDARIES

The effects of burner operating parameters on screech differ widely for different burner designs. However, the occurrence of screech has been shown to be consistently related to fuel-air ratio. It has been found that a lower limit for fuel-air ratio exists for given operating conditions, below which combustion is stable. A similar upper limit also exists above which combustion is stable. In practice these upper limits cannot always be attained due to excessive operating pressures and temperatures.

It has also been observed that there is some hysteresis associated with the lower stability limit, an example of which is illustrated in Figure 6. The stability limit occurs at a higher equivalence ratio when this ratio is increasing, compared with the limiting equivalence ratio when it is decreasing. This can be explained in terms of the nonlinearity of combustion instability, that is, a combustion system can be stable to small oscillations (which corresponds to entering an instability region) but unstable to larger amplitude disturbances. This situation can be regarded as analogous to leaving an unstable region.

In the following sections, some observed effects reported in the literature of various operating parameters on the stability boundaries and on the frequency of oscillation are presented.

## Effect of Pressure

At pressure levels generally encountered in afterburners (2-3 atmospheres), the effect of increasing the total pressure at the combustor inlet has been found (Refs 12, 13, and 15) to extend the range of unstable fuel-air ratios. This effect is shown in Figure 7(a). At higher pressures the instability disappears (3 atmospheres). This is shown in Figure 7(b).

Reference 12 reports only small changes in frequency with variation in afterburner pressure level, although no quantitative information is given. An increase in frequency was observed in Reference 9 (633 to 718 cps) when the combustor pressure increased from 12.6 to 17.5 inches of mercury. However, this was attributed to lower through-flow velocity and higher combustion efficiency.

## Effect of Inlet Temperature

The effects of inlet temperature upon stability boundaries have been studied by several workers. The lean screech limiting equivalence ratio has been found to increase as the inlet temperature decreases. This is shown in Figure 8 (from Ref 15), and in Figure 10 (from Ref 16). In the latter figure the limiting equivalence ratio increases from 0.66 to 0.9 as the inlet temperature decreases from 500 deg F to 180 deg F. This variation is similar to that obtained when decreasing the pressure level. Reduction in pressure level and temperature both increase the reaction times which therefore suggests that the reaction rates have an important bearing upon the onset of combustion instability.

In Reference 14, it was reported that the instability frequency varied as the square root of the combustion temperature. Therefore, when everything is held constant except the inlet air temperature, the frequency will increase as the inlet temperature increases. This is consistent with an acoustical mode of oscillation.

## Effect of Inlet Velocity

Evidence of the effects of combustor inlet velocity on a 26-inch diameter duct is reported in Reference 9, where it is shown that with a constant mass flow and fuel-air ratio, the frequency increases from 633 cps to 718 cps when the burner inlet velocity decreases from 1000 ft per sec to 670 ft per sec. However, in Reference 16, where tests are described of a pseudo two-dimensional burner, no variation in screech frequency or lean instability boundary occurred when the Mach number at the lip of the flameholder varied between 0.4 and 0.6. This is shown in Figure 10.

## Effect of Fuel-Air Ratio on Frequency

If the postulate that screech is an acoustic oscillation is correct, then the frequency of oscillation should be dependent upon the temperature in the combustor which, in turn, is dependent upon the fuel-air ratio. Measurements of frequencies at different fuel-air ratios for various burners support this reasoning as shown by the results of Reference 12 for a 36-inch diameter afterburner and a 6-inch experimental burner, Reference 9 for a 26-inch experimental burner, and Reference 14 for a 6-inch ramjet. In all cases, the frequency increased with fuel-air ratio up to a certain value (presumably corresponding to stoichiometric conditions) and then decreased. Typical results from Reference 14 are shown in Figure 11 where the frequency varies from 2750 cps to 2925 cps when the equivalence ratio varies from approximately 0.6 to 1.0.

## Effects of Geometrical Parameters

Geometrical parameters which have been investigated are: burner length, burner diameter, gutter width, and flameholder blockage. The effect of increasing the burner length has been found in one investigation (Ref 14) to have no effect on the range of unstable operation and in another investigation (Ref 13) to extend the unstable operating range. Increasing the burner diameter was shown in Reference 14 to extend the range of fuel-air ratios for which screech occurred. Screech tendency was found to be less severe for narrow flameholder gutters than for wide ones (Ref 11) with the same flameholder blockage; reducing the blockage by removing some of the gutters did not have the same effect. In Reference 15, however, it was found that increasing the flameholder blockage extended the unstable range of fuel-air ratios.

The acoustical theory for screech instability is again borne out by the dependence of frequency on the diameter of combustor. This effect is best illustrated by Table I which shows the frequency to be inversely proportional to the burner diameter for a given mode of oscillation. It is to be expected that the frequency of oscillation for the transverse modes is independent of the length of the burner. This conjecture is supported by the observations of References 12, 14, and 16.

## Effect of Burner Enclosure Surface

The effects of changing the surface conditions of the inside of the burner enclosure were investigated by NACA (Refs 9 and 11) in an attempt to find a means of suppressing screech. A first attempt was made in Reference 9 by attaching longitudinal pins 2 inches high to the inside wall of a 32-inch diameter afterburner with the object of interfering with the tangential motion of the oscillating gases. A slight reduction on the unstable operating range of fuel-air ratios was obtained and the frequency of the screech increased indicating that the oscillations were occurring in a 28-inch diameter cylinder of gas, that is, just inside the pins.

Subsequent attempts by NACA to suppress screech were made using perforated and corrugated liners in the 32-inch afterburner and a 26-inch experimental burner. The corrugated liners also had small circumferential louvers to provide cooling. With both types of liner, screech was completely eliminated under all operating conditions tested provided the liner was of sufficient length. Liners of various length were tested and it was found that below a critical length of liner, screech was encountered as shown in Figure 12 (from Ref 12), the severity of which depended upon various factors including flameholder design, liner length, and operating conditions.

## Effect of Other Parameters

Other parameters which have been investigated, primarily by NACA (Refs 9, 11, 12, 13, and 17) include such quantities as inlet air velocity profile, amount of swirl in the inlet air, distribution of fuel at injection, location of fuel injection relative to flameholders and flameholder design. The results of these investigations, however, did not provide any systematic correlation between the variables and the stability boundaries.

One further parameter investigated (Ref 14) which did provide a useful result was the inlet turbulence level. It was found that reducing the level of turbulence of the inlet air by adding screens increased the hysteresis effect experienced at the lean fuel-air ratio boundary. This means that the unstable operating range is reduced for increasing fuel-air ratios but extended for decreasing fuel-air ratios. Quantitative estimates are not possible, as the data shown in Figure 8 does not give the relative turbulence level without screens. This phenomenon can be attributed in part to nonlinearity. However, it should be noted that turbulence delays the onset of screech which is contradictory. The reasons for this contradiction are unclear due mainly to the lack of understanding of the effects of turbulence upon the driving forces.

## PHYSICO-CHEMICAL MECHANISMS ASSOCIATED WITH OSCILLATING COMBUSTION

### The Role of Acoustics in Unsteady Combustion

It is generally accepted in most of the published literature, that high-frequency instabilities in the afterburner ramjet combustor are acoustical in nature. A United Aircraft publication (Ref 14), claims that screech in a ramjet is definitely not an acoustic oscillation; this claim, however, is based on measurements which indicate that screech is not a longitudinal, organ-pipe type oscillation. The possibility of a transverse acoustic oscillation did not seem to occur to the authors of this paper which was, in fact, one of the earliest (1951) published papers on the subject of screech.

Evidence to support the acoustic theory is abundant. Table I, for example, shows that the frequency of oscillation is approximately inversely proportional to the burner diameter for a given mode, the relation to be expected from an acoustic-type oscillation. Further evidence is provided by the dependence of frequency on the temperature of the gases, through the sonic velocity, as shown by the results of tests made at various fuel-air ratios. Finally, the fact that screech can be suppressed or eliminated by introducing an acoustic liner into the combustor is a good indication that the oscillations are acoustic.

If indeed screech is an acoustic oscillation then the analytical approach to the problem should indicate an acoustic analysis of the combustion chamber. A difficulty which arises, however, is the representation of the various boundary conditions which provide the driving force and the damping forces for the oscillation. Several driving mechanisms have been proposed in the literature and are reviewed in the following section.

### Driving Mechanisms

All of the proposed driving mechanisms for high-frequency combustor instabilities involve a varying heat release rate. According to the Rayleigh Principle, if energy is released into the system when the oscillating pressure is near its maximum value, then the driving is a maximum. In References 9 and 12 the varying heat release rate is postulated to be a result of the dependence of the chemical kinetics on the temperature and pressure, and in References 17 and 18 wrinkling of the flame front is suggested as being the cause. A more complex mechanism is suggested by Rogers and Marble (Ref 16); the following is a description: Vortices shed from the flameholder mix with the hot gases in the wake of the flame and, after a time lag, ignite releasing heat away from the centerline of the combustor, driving the gases into a sloshing motion. The transverse motion of the gases induces the shedding of a further vortex and so forth.

Another mechanism involving vortex shedding was proposed in the United Aircraft report (Ref 14). Here the vortex formation increases the burning

# Contrails

rate through increased turbulence and flame front area. The sudden expansion of gases due to the increased heat release rate momentarily stops further induction of fresh reactants which in turn results in a decrease in heat release rate. The resulting drop in pressure causes a surge of fresh charge and further vortex formation.

In the development of an analytical model for the analysis of high frequency oscillations it may not be necessary to be specific as to the exact mechanism involved. This approach, however, introduces empirical constants which have to be determined experimentally.

## Dissipation Mechanisms

In order that the stability boundaries and pressure amplitudes can be predicted analytically, the total acoustic energy which is absorbed or dissipated must be included in the analysis. The following list of possible dissipative mechanisms includes those most commonly encountered in the literature.

1. Radiation of energy upstream.
2. Radiation of energy downstream (including nozzle losses).
3. Energy losses due to viscous forces and absorption at the walls.
4. Viscous forces in the fluid.
5. Acceleration of the steady incoming gas into the oscillating mode.

It is usual in practice to compute separately each of these contributions to the dissipation of acoustic energy, and the total is then the sum of each of the contributions. Within the context of gas-turbine engine burners virtually no analytical work has been published directed towards determining the losses associated with the above mechanisms. However, some of these contributions have been studied in rocket combustors, and will be reviewed in the later sections of this report.

It has been found experimentally (shown in Fig 12) that acoustic liners can be used to control and even eliminate screech due to transverse oscillations. In this situation it can be reasonably deduced that the acoustic energy loss at the walls is the dominant loss term. Therefore, it should be possible to use experimental results showing oscillating amplitudes as a function of acoustic liner length to deduce the magnitude of the driving energy as a function of amplitude. A prerequisite for this exercise will be the absorbing characteristics of the liner. Methods of computing these characteristics have been developed for rocket combustors, and will be presented later.

## Ranges of Combustor Sizes and Operating Conditions

A knowledge of the range of sizes of burners and the ranges of conditions under which they operate will be essential in the proposed study. It will be of particular value when evaluating the worth of experimental results for use in aiding the development of an analytical model.

The following is the result of a very brief survey of the ranges of parameters which are currently encountered in afterburners and bypass burners:

Size of Burners	20 inches to 60 inches diameter
Mass Flow per Area of Burner	approximately 0.2 lbm per sec sq inch
Burner Inlet Temperature (Afterburner)	1400 deg R to 2600 deg R
Burner Inlet Temperature (Bypass)	500 deg R to 850 deg R
Burner Pressure	5 psia to 45 psia

## CONCLUDING REMARKS

1. The high frequency combustor instabilities, commonly termed screech, have been identified in most cases reported in the literature as transverse modes of oscillation, ranging from the fundamental to the fifth overtone.
2. Screech is generally accepted as being an acoustic type of oscillation; evidence for this is provided by the dependence of the frequency of oscillation on burner diameter and gas temperature.
3. A time varying heat release rate is thought to be the driving mechanism behind the oscillations possibly as a result of the dependence of the chemical kinetics on temperature and pressure.
4. Various damping or energy dissipative mechanisms have been observed in the literature. Indeed acoustic damping of perforated liner surfaces can be used to completely eliminate serious transverse combustion instabilities.
5. Many similarities exist between screech and the instabilities encountered in rocket engines. For this reason, it would appear to be reasonable to use experience gained from the work done on rockets as a guide to the approaches to be taken in the analysis of screech in the present context.
6. The analyses and models to be developed in this study must be applicable

to the ranges of conditions presented in the previous section of this report.

## LIQUID ROCKET LITERATURE

### INTRODUCTION

The review of the literature on high frequency instabilities in gas-turbine burners presented in the foregoing sections indicates quite clearly that analytical approaches to the problem are conspicuously lacking. It is for this reason that consideration has been given to the results of the vast analytical effort in the field of liquid rocket instabilities which share many of the characteristics of the instabilities encountered in gas-turbine burners as will be demonstrated in the following sections. It is hoped that by studying the problem areas in liquid rockets that are common to gas-turbine burners, some useful guidance in the analytical approach to the problem of screech will be provided. Specific areas in which it is thought that the liquid-rocket instability analyses will contribute useful ideas and information are:

1. The formulation of a burning zone model relating the periodic energy release rate to the fluctuating flow-field properties.
2. The derivation of the equations describing the acoustical aspects of the problem; these equations include the time dependent conservation equations of mass, chemical species, momentum, and energy. The knowledge to be gained from this type of information is an appraisal of what is considered to be the relative importance of the various terms in the equations and in particular how the various acoustical losses associated with the flow field are treated.
3. The specification of conditions at the boundaries of the acoustic chamber. One of the chamber boundaries, namely the nozzle, is of particular interest since the treatment of this rather complex (acoustically) component has received considerable attention by several investigators in the liquid rocket field. The treatment of acoustic liners, which may in some cases form the circumferential boundary, has received some attention though the usefulness of information gleaned from this work is limited due to the extreme sensitivity of the absorptive effectiveness of the liners to flow field and acoustic parameters.
4. Finally, the linking of the burning zone or energy release model with the acoustic problem and in particular how the acoustic losses are made to balance the energy released.

So far no reference has been made to the liquid rocket experimental results reported in the literature. The view that has been adopted in this literature review is that experimental results will provide useful



information if they serve to substantiate an assumption, a model, or a result in the liquid rocket analyses that is of interest in the present investigation of gas-turbine burners. In addition, experimental results are of interest which shed light on the nature or form of high frequency instability in liquid rockets thus providing an indication of the similarities with gas-turbine screech. The review of the literature which covers experimental work has been conducted accordingly.

## Organization of the Review

The review of the literature on instability in liquid rockets is presented in the following manner. In the first section, the similarities of the liquid rocket engine to the gas-turbine burner are discussed, first in general terms with regard to geometry and operating conditions and then more specifically in connection with features which affect, or might affect, the unstable operation of the engine. In the next section, a survey is presented of some of the published results of experimental investigation which provide information regarding the nature of high-frequency instabilities in liquid rocket engines. The main section of the review follows; this concerns the analytical approaches to the problem of liquid rocket instability which have appeared in the literature. The section is subdivided into a description of the general approaches to the problem, driving mechanisms, loss mechanisms, boundary conditions, and finally descriptions of the Priem (Ref 3) and Crocco (Ref 2) analyses. The review is completed by a section of concluding remarks.

## SIMILARITIES AND DISSIMILARITIES OF LIQUID ROCKETS TO GAS-TURBINE BURNERS

This section has been included in the review because it is important to be aware, at the outset, of the similarities and, perhaps more important, the difference between the liquid rockets and the gas-turbine burner. It is important because the interpretation and possible subsequent utilization of results or methods of approach associated with various aspects of the liquid-rocket effort is dependent upon these similarities and differences.

Basically, the liquid rocket engine and the gas-turbine burner perform a similar task in a similar manner inasmuch as they both react a fuel with an oxidant in a constant pressure chamber and utilize the energy produced to provide a thrust by discharging the products of combustion through a nozzle. Similarity also lies in the geometric form of the combustors which generally fit the description of a circular cylinder (though annular geometries may be encountered in ducted-fan burners); this geometric similarity is important from acoustic considerations.

Unlike the gas-turbine burner which exhibits a constant gas mass flow downstream of the flameholder, the mass flow of gas through the liquid rocket engine varies from zero at the injector face to a maximum at the

# Contrails

nozzle entrance. However, the flow Mach numbers at the nozzle entrance are typically the same as those encountered in afterburners, namely about 0.3; in both cases the nozzles operate with sonic throats. Thus both the side-wall and nozzle (downstream) boundary conditions in a liquid rocket may be similar to those existing in gas-turbine burners; however, the use of cooling liners or acoustic damping liners in either case will in general considerably modify the wall damping characteristics.

The ranges of operating parameters of liquid rocket engines are shown in the table below. Included in the table for comparison are equivalent values for the gas-turbine burner.

<u>Parameter</u>	<u>Liquid Rocket</u>	<u>Gas-Turbine Burner</u>
Chamber Pressure, psi	300-500	5-45
Chamber Temperature, deg R	1800-8000 average value 5500	4500
Nozzle Entrance Mach Number	0.3	0.4
Diameter of Burner, inches	60	20 to 60

It is evident from this summary of operating conditions that the liquid rocket operates at pressures more than an order of magnitude greater and considerably higher temperatures than the gas-turbine burner. This difference is clearly a very significant factor when considering the combustion process since all of the stages making up the combustion phenomenon are in some respect pressure and/or temperature dependent. The acoustic aspects of the problem will also be influenced to some extent (for example through the acoustic velocity) by the pressure and temperature levels.

Viewing the combustion chamber, as in the introduction to this report, as consisting of a combustion zone and passive acoustic zones, the liquid rocket presents quite a different picture to that of the gas-turbine burner. In the gas-turbine burner, two acoustic zones may possibly be defined separated by a thin combustion or energy addition region (the flame front). One zone comprises the region between the compressor discharge and the flameholder which includes a diffuser, and may also include a fuel injection system and a fuel vaporization and mixing region; the vaporization can be interpreted as a distributed mass addition process. The second acoustic zone is the region between the flameholder and the nozzle entrance; it is anticipated that the acoustic losses associated with this zone will be much greater than with the upstream zone. The liquid rocket engine on the other hand has only one acoustic zone which is shared spatially with the combustion and mass-addition zone.

The solid wall upstream is quite different from the boundary presented by the upstream acoustic zone in the gas-turbine burner. This difference of upstream boundary will have greater relevance when longitudinal modes of oscillation are encountered, but even in the tangential

# Contrails

mode, some influence may be exerted for example by the circumferential property variations produced by the turbine or fan.

If the fuel is sprayed into the airstream upstream of the flame stabilizers in a gas-turbine burner, the fuel vaporizes and mixes with the air before reaching the combustion zone. Combustion takes place in a relatively short distance after the gases pass through the flame front and the rate of combustion is controlled either by the time taken to heat (by conduction and eddy diffusion) the fresh charge to a temperature where reaction begins or by the reaction time. In the liquid rocket, the propellants are sprayed directly into the combustion zone and therefore jet breakup, atomization, vaporization, and turbulent mixing are added to the stages involved in the combustion process within the combustion zone. If any one of these additional stages controls the over-all rate of the combustion process then an extremely relevant difference arises between the liquid rocket and the afterburner. Evidence presented later in the report suggests that the rate-controlling step is indeed different in the two cases.

Finally, the difference in location of the mass generation process between the rocket and the gas-turbine burner is important when considering mass and momentum conservation. The need to consider a spatial burning rate distribution in the liquid rocket is avoided in the treatment of the gas-turbine burner problem in which the energy release region may be represented one dimensionally.

## OBSERVED LIQUID-ROCKET INSTABILITY

In this section of the report, details are given of some of the high frequency instabilities which have been reported in the literature. The object of this section is to gain an insight into the types of high-frequency instabilities which are normally experienced in liquid rockets and how they are affected by various combustor parameters, thus providing some indications of the similarities or dissimilarities with afterburner/duct burner instabilities.

### General Observations on the Nature of Instabilities

Some of the earlier experimental work on liquid rocket instabilities was directed towards an understanding of the nature of high frequency instabilities, with particular regard to determining which quantities were involved in the oscillations. Using a cylindrical chamber with a slit window and pressure measuring devices, Berman and Cheney (Ref 19) observed that high-frequency longitudinal instability (the different modes of high frequency instability are discussed in the next section) is characterized by the presence of pressure waves traveling back and forth in the combustion chamber. The pressure oscillations may be continuous waves or may be complicated by the presence of shock waves, in which cases the amplitude of the oscillations are generally greater. Visual observation of dark

regions in the oscillating flow were interpreted as regions of low temperatures which moved downstream with the speed of the gas stream. These oscillations of temperature and entropy occurred only during large amplitude pressure oscillations. Ellis, et al (Ref 20) using a similar burner to Berman measured pressure and velocity fluctuations at the same axial location and found them to be consistent in both phase and frequency.

Such basic investigations of the nature of oscillations in the transverse mode of instability do not appear to have been reported though it is fairly evident that fluctuations of all flow parameters accompany these oscillations. Reardon (Ref 21), however, reported no evidence of shock waves in his experimental investigations of the tangential mode of instability.

## Modes of Instability

The flow of gases in the liquid rocket motor are capable of oscillating in the same modes as the gas-turbine burner; these are longitudinal, tangential, radial, and many combinations of these basic modes. The particular mode in which an engine oscillates appears to be determined to a great extent by the geometry of the chamber rather than the operating conditions or the form of the initial disturbance. Thus, Reardon (Ref 21) claims that the purely longitudinal mode appears for burner length to diameter ratios ( $L/D$ ) much greater than unity, the purely transverse modes appear for  $L/D \ll 1$  and mixed longitudinal and transverse modes appear for  $L/D \sim 1$ . This claim is partially substantiated by some of the reported observed liquid rocket instabilities. Berman and Cheney (Ref 19), observed longitudinal instability for  $L/D$  ratios greater than 3.3; below this value they found difficulty in obtaining instability (presumably of any mode). Hammer and Agosta (Ref 22) experienced a longitudinal mode in a rocket 21 inches long and 2 inches in diameter; the amplitude of these pressure oscillations was approximately one third of the mean static pressure in the chamber. The longitudinal mode of instability has been experienced by Crocco, et al (Ref 23) for  $L/D$  ratios as low as two; here the amplitude of the oscillations was quite small having an RMS value of about 6 per cent of the mean static pressure.

Tangential modes of instability have been observed by Ross and Datner (ref 24) for  $L/D$  ratios less than three and by Bailey (Ref 25) for an  $L/D$  ratio of 3.2. In this latter work, the peak to peak amplitude of the first tangential mode observed was 160 per cent of the nominal burner pressure. The higher amplitude of the tangential mode over the longitudinal mode is further indicated by observations of Reardon (Ref 21) showing peak to peak amplitudes of up to 300 per cent for the first tangential.

The earlier statement that the mode of instability in a liquid rocket is independent of the characteristics of the initial "triggering" disturbance is supported by the results of Combs, et al (Ref 26) who in their stability rating experiments using bombs and a pulse gun found that although the first few cycles of the oscillations followed the forced mode of the disturbance, the eventual mode of instability was generally a third tangential accompanied by the first radial. The foregoing observations

are strongly indicative of acoustic oscillations; further evidence in this direction is provided when the observed frequencies of the instability are treated in a later section.

As in the case of gas-turbine burners, the radial mode of instability is rarely encountered (the above quoted Reference 26 is an exception); Reardon (Ref 21) observes that the frequency of appearance of the different transverse modes of instability, in descending order are: first tangential, second tangential, first radial, and first combined radial and tangential. The experiments of Reardon also indicate that the spinning tangential mode appears in preference to the standing mode. Tests performed with specially designed barriers in the combustion zone to constrain any instability to a standing oscillation showed that under certain conditions the combustor could be stable in the standing mode (barrier in place) but unstable in the spinning mode (barrier absent).

The conclusions to be drawn from these observations of the modes of instability in liquid rockets are that for  $L/D$  ratios less than about 3, which include most afterburner and duct burner combustion chambers, the predominant mode of instability is tangential. For this mode, the amplitude of oscillation is quite large, certainly too large to be treated with confidence by a linear analysis; this was found to be often the case for screech in afterburners.

## Observed Frequencies of Instability

The relation which the characteristics of observed instability oscillations bear to the purely acoustic characteristics of the rocket chamber can provide valuable information regarding the nature and location of losses in the oscillating system.

A good indication of the acoustic tendencies of the oscillations is provided by frequency measurements. Berman and Cheney (Ref 19) reported that observed frequencies of self-maintained longitudinal mode oscillations in the high-frequency range were closely associated with the fundamental acoustic mode in the combustion chamber with both ends closed. These observations were made with combustors of various length; the results are shown in Figure 13 which indicates the expected inverse linear dependency of frequency upon length. Similar results were obtained by Ellis, et al (Ref 20). In the tangential mode of oscillation, Ross and Datner (Ref 24) observed that the frequency of oscillation in the "sloshing mode" agrees with calculations from acoustic theory. In support of this, Reardon (Ref 21) observes that the frequency of fully developed pure transverse modes fall within a few per cent of the acoustic frequency of the corresponding mode.

It is perhaps worth considering a specific case of an observed instability in which the frequency, mode, and other relevant parameters were measured. Bailey (Ref 25) measured a first-tangential mode instability in a liquid rocket under the following conditions:

# Contrails

Diameter of Rocket, 2R	3.7 inches
Nominal Pressure	1000 psi
Frequency of Oscillation, $f$	7200 cps
Estimated Sonic Velocity, $C$ (Based on a Flame Temperature of 5000 deg R)	3500 ft per sec

Thus, the dimensionless frequency,  $\alpha = 2fR/c$  evaluated for this particular instability has a value  $\alpha = 0.606$ . The value of  $\alpha$  calculated from pure acoustic theory for the first-tangential mode is 0.586, indicating surprisingly close agreement with the measured value.

It is fairly evident from the foregoing observations that the oscillations associated with high frequency instabilities in liquid rocket engines closely resemble, in some respects, the pure acoustic modes of oscillation in a circular cylinder. This was found to be the case also with the gas-turbine burner.

## ANALYTICAL TECHNIQUES

In this section the analytical approaches to the various aspects of high-frequency instabilities are reviewed. Where an assumption or method of approach is supported by experimental evidence, reference will be made to that experimental work. The section is presented in the following manner: First, a general over-all view is taken of the problem of analyzing the instabilities. Subsequent sections deal with particular aspects of the problem including driving mechanisms, loss mechanisms, and boundary conditions. Finally, specific analyses of the instability problem performed by Priem (Ref 3) and by Crocco (Ref 2) are examined. Throughout the review, emphasis will be placed on the usefulness of the various proposed mechanisms and techniques to the development of an analysis for gas-turbine burners.

### General Approach

The complete solution of the equations governing instabilities in combustion chambers is beyond feasibility at the present time due to their extreme complexity. However, several attempts have been made to obtain approximate solutions to the equations for liquid rockets in special limiting cases by making simplifying assumptions. The most common and also most simplifying assumption made is to assume that the amplitudes of the oscillations associated with the instability are small compared with steady-state values. This "small perturbation" technique reduces the equations to a linear form and with the addition of various other simplifications, the equations are made more amenable to solution. A serious drawback with the linearization method is that the results of the analysis were limited to the determination of stability boundaries. Analyses of

# Contrails

this type have been carried out for both longitudinal and transverse modes of instability by Crocco (Refs 2, 27, and 28), Culick (Ref 1) and Dynamic Science Division (Ref 29); some of these will be considered in more detail later in the report.

More useful information can be derived from a nonlinear analysis of the problem for the following reasons: (a) There are likely to be operating regions where the system is stable to small perturbations but unstable to large disturbances; the sort of information that would be most desirable in such a situation would be plots of the stability boundaries for different magnitudes of initial disturbance. (b) The subsequent variations of pressure and velocity following a disturbance, whether leading to stability or instability, can be estimated. The need for a nonlinear analysis is particularly important in the case of the afterburner/duct burner problem where instability may be triggered by transient effects resulting from light-off or aircraft maneuvers. Nonlinear analyses have been carried out by Priem (Ref 3), Beltran (Ref 30), and Zinn (Ref 31) for the tangential mode and by Sirignano (Ref 4) for the longitudinal mode. However, in order to make the analysis tractable, drastic simplifications have been made. The major simplifications in the "Priem" type of analysis is the limitation of the equations to oscillatory flow in one dimension, namely in the tangential direction. With the addition of several other assumptions described later, the equations of motion are solved using a numerical technique and a high speed computer. The approach taken by Zinn (Ref 31) and by Sirignano (Ref 4) in their nonlinear analyses was to use a perturbation technique in which the dependent variables are expressed as power series of an amplitude parameter. In the solution of the rather vast array of resulting equations, it was found impractical to retain terms higher than the second order in Zinn's analysis of the first tangential mode and the third order in Sirignano's analysis of the longitudinal mode. Apart from any other considerations, it can be stated that the sheer complexity of the techniques applied to the analysis of nonlinear instabilities in liquid rockets render them unsuitable for our purposes in the study of gas-turbine burner instabilities. This does not mean, however, that these approaches to the problem should be rejected, since many of the mechanisms and assumptions employed in the models may provide useful information.

Regardless of the over-all approach to the problem, each analysis has as its starting point the time-dependent conservation equations for mass, momentum, and energy for the oscillatory motion of the gas. The mass and momentum equations include terms accounting for the mass generation of gas as the liquid propellants vaporize. The problem of mass addition in the gas-turbine burner is somewhat different because the vaporization zone can be upstream of the combustion zone.

In its complete form, the momentum equation should include terms for pressure gradients, viscous losses within the flow field and friction at the walls; the latter term is generally neglected in the liquid rocket work. The energy equation should satisfy one basic requirement namely that the acoustical energy generated by the combustion process plus the energy entering the system from, for example, the compressor should be balanced by

# Contrails

the total acoustical losses from the system. That this requirement is satisfied is not always clear in some of the analyses presented in the literature, particularly the analysis of Priem (Ref 10). The losses which should appear in the energy balance and those that do appear in the various analyses are discussed in detail in a later section.

## Instability Driving Mechanisms

In this section, the various proposed ways in which it is possible for energy to be added to the oscillating system are considered. Most of the proposed driving mechanisms rely on the Rayleigh Principle which states that the maximum addition of energy into an acoustically oscillating system is obtained when the energy release occurs at or near the maximum of the pressure disturbance. The possibility of such a situation can arise if any of the rate controlling stages in the heterogeneous combustion process is pressure dependent. Generally, in liquid rocket combustion, vaporization of the fuel or oxidant is considered to be the controlling step (Refs 36, 30, 32, and 33). Priem (Ref 3) has related the propellant vaporization rate to the unsteady component of tangential velocity for the case in which the relative velocity between liquid droplet and gas is large; the relation is

$$\omega' = (\rho')^{1/2} \left[ 1 + \left( \frac{v_{\theta}'}{\Delta v'} \right)^2 \right]^{1/4}$$

where  $\omega'$  is a dimensionless instantaneous burning rate  
 $\rho'$  is dimensionless gas density  
 $v_{\theta}'$  is the dimensionless tangential component of gas velocity  
 $\Delta v'$  is the dimensionless relative velocity between gas and liquid droplets.

Bletran (Ref 30) extended Priem's analysis to include all values of the relative velocity between gas and liquid phase. More extensive work on the dynamic response characteristics of propellant vaporization has been carried out by Heidmann and Wieber (Refs 32 and 33).

Other stages in the combustion process which have been considered as possible sources of energy for supporting instability are: propellant atomization (Ref 6), effects of the oscillations on the spatial distribution of the fuel spray (Ref 29), mixing of the vaporized propellant with the hot flame by diffusion (Ref 34), or recirculation (Ref 35) and finally, the actual chemical reaction stage (Refs 3, 4, and 6). The chemical reaction stage of the combustion process in liquid rocket engines is, however, considered to be too short to provide any control in the over-all rate (Refs 35 and 36); indeed Sirignano (Ref 36) who performs an analysis for rocket combustor instability based on chemical kinetic control, suggests that the analysis is more applicable to gas rockets where chemical reaction rates are more likely to control the combustion process.

In the gas-turbine burner, as previously indicated, the combustion zone in some cases may be regarded as being quite distinct from the region



# Contrails

in which atomization, vaporization, and fuel/air mixing occur; in these cases, it is therefore very unlikely that fluctuations in the rates of these latter mentioned processes could influence the energy release rate into the system. More likely to be the rate-controlling stages in the gas-turbine burner are either the actual chemical kinetics or the heating of the fresh charge of reactants by heat conduction and eddy diffusion from the products of combustion. In the treatment of the chemical kinetic stage of the combustion process the Arrhenius equation is exclusively employed. The energy release relation developed by Priem (Ref 3) is the following:

$$\omega' = \left(\frac{c}{c_0}\right)^\eta (p')^\eta \exp \left[ \frac{E}{RT_0} \left(1 - \frac{1}{T'}\right) \right]$$

where  $C$  is the mole fraction of unburned gas

$E$  is the energy of activation

$R$  is the gas constant

$T$  is the gas temperature

$\eta$  is the order of the reaction; values between 1.5 and 2.5 were employed by Priem. The suffix zero refers to mean conditions.

Crocco's approach to combustion instability (Ref 2) is radically different in that the generating and dissipating mechanisms are not used explicitly. According to this theory, the time taken between the injection of a propellant into the combustion chamber and the point of conversion into products of combustion may be divided into two parts. The first part of the time lag is supposed to be insensitive to chamber conditions whereas the second part, the so-called sensitive time lag  $\tau$ , is sensitive to the gas state and, therefore, to fluctuations in the gas state. During the sensitive time lag, the propellant conversion rate is proportional to the instantaneous fractional pressure perturbation (small perturbations only are considered) where the constant of proportionality is a factor  $\eta$ , termed the interaction index. The burning rate can be written in terms of  $\eta$  and  $\tau$  in the following manner from Reference 2.

$$\frac{m_b - \bar{m}_b}{\bar{m}_b} = -\eta \frac{p(t) - p(t-\tau)}{\bar{p}}$$

where  $t$  = time

$m_b$  = instantaneous burning rate

$p$  = pressure

$(\bar{\quad})$  = time averaged quantities.

The two factors  $\eta$  and  $\tau$  must be determined from actual tests as they have no physical interpretation. According to Sirignano (Ref 36), the sensitive time lag concept is only applicable to liquid propellant rockets. If this is indeed the case then it would seem that such a concept is unsuitable for the analysis of the duct/afterburner combustor.

It is important to note that in liquid rocket analyses, associated with the fluctuating energy release rate is a fluctuating mass generation rate

# Contrails

due to the conversion of liquid phase propellant to the gas phase. In afterburners and duct burners, the mass addition due to fuel vaporization is quite small. Thus in an analysis of the combustion zone of such burners, the mass and momentum conservation equations should not include terms accounting for mass generation, as is the case in most liquid rocket analyses.

In the next section the various energy losses are considered which arise from the oscillations in the gas and thus exert a damping influence on the system.

## Loss Mechanisms

The loss mechanisms considered in two of the more notable liquid rocket instability analyses by Priem and by Crocco are summarized by Priem in Reference 37. The principal loss in both cases is what Priem terms nozzle radiation; perhaps convection would be a more accurate description of the loss which arises because of the acceleration of the gases as they move downstream. Some of this loss may be recovered at the nozzle where reflection from the convergent portion of the nozzle occurs. This partial recovery is accounted for in the Crocco analysis when the downstream boundary condition (i.e., at the nozzle entrance) is applied; this will be discussed further in the next section which deals with boundary conditions. Priem, on the other hand, ignores the nozzle reflection. The only other losses considered in either analysis are the viscous and thermal losses in the gas stream which are considered by Priem. However, Priem shows that the viscous dissipation terms in his analysis have a negligible effect on the results (Ref 3). In support of this, Culick (Ref 1) developed the following expression for the ratio of viscous dissipation to dissipation by mean flow convection out of the combustion zone:

$$(\text{Viscous Dissipation})/\text{Convective Losses} = \frac{4 \omega^2 L \nu}{36 M_e C}$$

where  $\omega$  is the frequency

$L$  is combustor length

$\nu$  is kinematic viscosity

$b$  is a constant (function of mode shape) usually between 2.0 and 4.0

$M_e$  is mean flow Mach number

$C$  is the speed of sound.

Taking typical values for these variables ( $C = 3000$  ft per sec,  $\nu = 10^{-4}$  ft<sup>2</sup> per sec,  $L = 1$  ft,  $M_e = 0.1$ ) this ratio equals about  $10^{-5}$ .

Losses which were not considered by either Crocco or Priem and which may be very important, particularly in the case of afterburners and duct burners fitted with acoustic liners, are wall losses. Acoustic absorption at the walls may be due to wave attenuation due to the porosity of the surface, or alternatively thermal losses which accompany viscous dissipation along the surface.

Theoretical acoustical energy absorption coefficients have been computed by Bailey (Ref 25). Typical results for a transverse mode are shown

in Figure 14, which shows the sensitivity of the absorption coefficient to temperature and gas velocity. Indeed this sensitivity is such that when coupled with the added effects of backing cavity size and pressure, it was not possible to design an experiment to confirm the computed coefficients satisfactorily. It should be noted that in this work the effects of nonlinearity upon the absorption coefficients were included. Losses resulting from the inclusion of baffles may be considered in the same manner as wall losses. In general, wall losses would enter the analysis in the form of boundary conditions which is the subject of the next section of this report.

## Boundary Conditions

The boundary conditions which would apply at some of the boundaries in the analysis of oscillating flow in a duct burner or afterburner are quite different from those applied in the analyses so far attempted for liquid rocket instabilities. However, one boundary which they do have in common is the propulsion nozzle which has received considerable attention in the liquid rocket investigations particularly by Crocco and his co-workers. The nozzle boundary condition is represented as an admittance coefficient which relates the pressure fluctuations in the flow to velocity or mass flow fluctuations at the nozzle entrance. The original work in this direction was performed by Tsien (Ref 38) who analyzed the case of small disturbances (linear case) in the purely longitudinal mode in a circular-section nozzle. This work was extended by Culick (Ref 39) to include three dimensional oscillations and by Crocco (reviewed in Ref 40) to include, in addition to three dimensional oscillations, rectangular and thin annular cross-sectional nozzles, nonlinear oscillations in the longitudinal mode for short nozzles and in the transverse mode for multi-orifice nozzles.

The wall boundary condition when acoustic liners are present, though not appearing in any of the analyses to date, is treated by Sirignano (Ref 41) in a similar manner to the nozzle, insofar as the boundary condition is represented as a complex admittance coefficient. Sirignano's treatment of the acoustic wall problem is nonlinear. An empirical treatment of the acoustic liner has been pursued at Pratt and Whitney Aircraft (Ref 42); here the losses are represented by an energy absorption coefficient. This latter treatment, however, ignores compressibility effects which, according to Sirignano, are of great importance.

Undoubtedly the greatest difference between the boundary conditions of the liquid rocket and of the afterburner duct burner lies in the upstream boundary condition which for a liquid rocket engine is a rigid wall perpendicular to the gross flow direction and for a duct burner or afterburner is a fan or turbine exit separated from the burner by a diffusing passage in which fuel may be evaporated and mixed with the gas flow. This type of boundary has not, of course, been treated in the liquid rocket analyses. A treatment involving the determination of an admittance coefficient as in the case of the nozzle suggests itself.

## Methods of Solution of Equations

Some of the more noteworthy methods of solving the conservation equations are considered in this section with a view to incorporating some of the techniques employed into the analysis of afterburner and duct burner screech. As previously mentioned, the analyses may be divided into linear analyses and nonlinear analyses and, although the approach to the afterburner problem should be strictly nonlinear, some integration of linear and nonlinear aspects of the problem may be possible. For this reason it is considered worthwhile to examine some of the linear analyses which have been carried out. By the same token, analyses of longitudinal as well as tangential modes of instability will be examined even though afterburner screech has been shown to be predominantly a tangential oscillation.

A solution to the simple case of longitudinal, linear oscillations was obtained by Crocco (Ref 2) by considering conditions to vary only with time and axial distance. The square of the Mach number at the nozzle entrance was assumed to be small compared with unity. With Crocco's time lag concept and a nozzle boundary condition, a Bessel-function solution to the equations was obtained. This type of analysis, however, can yield only stability boundaries and in this case the boundaries are expressed in terms of the  $n$  and  $\tau$  factors. These two factors, which for a given propellant injection system are functions of pressure and mixture ratio, have to be determined experimentally. In Reference 27, tests were performed with a combustor of variable length; stability boundaries were determined by varying the chamber length for each mixture ratio. It was observed from both experiment and theory that a lower and upper stability boundary existed for each mixture ratio. This fact was employed to provide a check on the results of the theoretical analysis by estimating values of  $n$  and  $\tau$  from the lower stability boundary and using the results to predict the upper stability boundary. The comparison between measured and predicted upper boundaries was found to be surprisingly good.

Crocco adapted his time lag theory to the transverse mode of instability (Ref 28) but again to the linear case. To obtain a solution to the equations in this case, an order of magnitude analysis was performed to eliminate several of the terms. The nozzle boundary condition in this case was more complex than in the longitudinal mode as velocity components in both the axial and tangential directions were involved. Again, the solution of the equations yielded only stability limits in terms of  $n$  and  $\tau$ . Tests were performed by Crocco (Ref 28) with a variable sector rocket motor oscillating in the tangential mode and stability boundaries were constructed in the sector angle/mixture ratio plane. Using the results of the analysis for transverse oscillations, the experimentally determined stability boundaries were transposed into  $n$ /mixture ratio and  $\tau$ /mixture ratio planes. These results were then compared with the experimentally determined values of  $n$  and  $\tau$  as functions of mixture ratio for the longitudinal instabilities described earlier (Ref 27). The agreement was fairly good particularly in view of the fact that the injectors were not identical in the two cases; the conclusion drawn by Crocco from this result is that the time lag concept is as well suited to the transverse mode of oscillation as to the longitudinal mode for which it was originally developed.

# Contrails

Turning now to the nonlinear treatments of liquid rocket instability, the method of Priem (Ref 3) is perhaps the most notable. Priem derived the conservation equations in cylindrical coordinates for a one-dimensional annular geometry. In deriving these equations, it was assumed that the radial velocity component and all derivatives in the radial direction are zero, the axial velocity does not vary with angular position and all second derivatives in the axial direction are zero. To determine the derivatives in the axial direction, a condition for conservation of energy, momentum, and mass for the entire system was applied. Since it is assumed that none of the terms vary in the axial or radial direction (presumably this statement refers only to the one-dimensional annular ring considered), the equations have only to be integrated in the tangential direction. Priem further assumes that mass, momentum, and energy in the complete annulus do not vary with time and that the axial derivatives do not vary with angular position. A further implicit assumption that disturbances propagated both upstream and downstream directions do not reflect back again (even partially) and interact with the streamwise element of the combustion zone being considered. After all these assumptions, four equations involving four unknown axial derivatives of pressure, density, temperature, and velocity are obtained.

Included in the conservation equations are a term  $\dot{m}$  which represents the mass generation rate and another term  $\dot{V}$  representative of the viscous damping losses. The factor  $\dot{V}$  is supplied as an input to the problem but the mass generation factor  $\dot{m}$  is formulated from the consideration of various mass addition models. In Reference 6, Priem employs three different mass addition models in his analysis based on liquid atomization, vaporization, and chemical kinetics. The results of the analysis showed that the chemical reaction step is only important at low conversion rates which are generally not encountered in full-scale liquid rockets.

The solution of the conservation equations together with the four simultaneous equations for the axial derivatives are solved numerically. An initial disturbance imposed on either the instantaneous pressure or the velocity component in the tangential direction provides the starting conditions for zero time. The results of the analysis are in the form of time histories of the angular distributions of the pressure and the tangential velocity. Clearly different values for the initial disturbance may be specified thus enabling complete stability maps to be constructed for all values of the initial disturbance.

This method of analysis because of its nonlinearity and because it treats the tangential mode of oscillation, would appear to be well suited to the problem of afterburner and duct burner screech. However, some of the assumptions made in the analysis are of an extremely doubtful nature and will require further investigation to establish a better understanding of their consequences. Furthermore, the actual numerical solution of the equations, even with a computer, is an extremely tedious and costly procedure and its application in the present investigation does not seem very feasible in its present form.

## SOLID-ROCKET LITERATURE

### GENERAL

It must be confessed at the outset that this review of solid-rocket literature is basically concerned with the efforts at analytical representation of the combustion instability process by a single group of workers (Refs 7, and 43-39) with but a single exception (Ref 50). The justification of this procedure rests upon two factors: first, the cited references form perhaps the most complete and coherent account of the analytical description of the solid-rocket combustion instability problem to be found in the literature; and second, the nature of the agreement between analysis and experiment can be described at best as only qualitative, so that little can be gained by a detailed review of experimental results.

The analytical developments can be conveniently described in terms of the characterization depicted by the right-hand sketch on page 80. That is, the product gases and the solid propellant are treated as dissipative acoustic media, separated by a thin (compared to wave length) zone at the solid surface where most of the energy addition occurs.

### DESCRIPTION OF ACOUSTICAL MEDIA

The most general representation of the acoustical behavior of the gaseous combustion products employed to date is that presented by McClure, Hart, and Bird (Ref 43). The governing equations are taken as those governing small perturbations in a stationary, homogeneous medium which is slightly dissipative:

$$(\nabla^2 + k^2)p_1 = 0$$
$$\dot{v}_1 = \left[ \frac{c}{\omega \rho} - \frac{2\alpha' c}{\omega^2 \rho} \right] \nabla p_1$$

where  $\rho$  is the mean gas density,  $\omega$  is the angular frequency, and

$$k = \omega/c = (\omega/c_0) - i\alpha'$$

where  $c_0 = (\gamma p_0/\rho_0)^{1/2}$ . The index  $\alpha'$  is the usual acoustical decay coefficient and provides an approximate representation of volume losses in the gas. Even in this case, however, the authors choose to treat the losses as a perturbation so that, in fact, the representation is the pure acoustic one, and reduces to the mode shapes and frequencies given previously for a rigid cylindrical container.

Reference 43 also includes the treatment of the wave propagation characteristics of the solid medium, but as this is irrelevant to

# Contrails

gas-turbine burners, the analysis merits no description here. It is of interest to note that the result of the analysis, for typical conditions encountered in solid rockets, showed that the characteristic frequencies and mode shapes were in general closely described by those which would be encountered in the gas phase or solid phase alone (in the absence of any interaction between gas and solid). As will be discussed, however, the participation of the solid has a significant influence on stability.

The most significant feature of the analytical treatment of acoustical properties presented in Reference 43 (and used subsequently in References 7 and 44-47) is that the modes and frequencies of oscillation are obtained by neglecting the effects of energy losses and gains.

## LOSS MECHANISMS

The various loss mechanisms which may be active in the gaseous combustion products have been treated in increasing degree in References 7 and 43-47. These losses are summarized most completely in Reference 7, and are best assessed in terms of the acoustic decay coefficient,  $\alpha$ , divided by the oscillation frequency,  $f$ , where by definition

$$\frac{\alpha}{f} = \frac{\langle dE/dt \rangle}{f \langle E \rangle}$$

where  $\langle \rangle$  denotes the time average, and  $E$  is the acoustical energy per unit volume. Thus,  $\alpha/f$  is a quantitative measure of the fraction of acoustical energy dissipated per cycle of oscillation.

The volume losses which have been treated (to a point where analytical expressions exist for their evaluation) are listed in the following table, with their typical magnitudes for solid rockets:

<u>Loss</u>	<u>Typical <math>\alpha/f</math></u>
Viscothermal	negligible
Solid Particle	$\leq 0.03$
Molecular Relaxation (Absorption)	0.001
Solid Viscosity	0.001

The viscothermal loss is the usual one attributable to molecular viscosity and thermal conductivity; the solid particle damping loss is due to the damping action (via drag) of small particles interspersed in the gas; the molecular relaxation loss is that due to increased transfer of energy to molecular vibration states as a result of the oscillatory motion; the solid viscosity loss is due to viscous dissipation in the solid. The losses are evaluated on the basis that the mode shape and

# Contrails

frequency are themselves unaffected by the losses, and this is obviously a good assumption here.

The surface losses must be evaluated to include the effects of mean velocity (Ref 47). The resulting acoustic decay coefficient is then determined from (Ref 7):

$$\alpha = \frac{\frac{1}{2} \left\langle \int_S dS \cdot \left\{ \rho_0 \underline{v}_1 + \frac{\rho_0^2 v_0}{\rho_0 c_0^2} + \rho_0 (v_0 \cdot \underline{v}_1) \underline{v}_1 \right\} \right\rangle}{\left\langle \rho_0 \int_V v_1^2 dV \right\rangle}$$

where the numerator represents the acoustical energy flux across a bounding surface and the denominator is the acoustical energy within the bounded volumes ( $v_0$  is the mean velocity). The surface losses which have been treated are listed in the following table, with typical values for solid rockets:

<u>Loss</u>	<u><math>\alpha/f</math></u>
Viscous	0.002
Thermal	0.001
Nozzle	$\leq 0.1$

The viscous and thermal losses are due to dissipation in the acoustic boundary layer; the nozzle losses are due to both acoustical energy transport and radiation from the nozzle. The latter losses have not been fully treated (Ref 7) and are difficult to estimate for transverse modes. The value of  $\alpha/f$  given above is typical of axial modes, for which the loss is large enough to affect appreciably the characteristic frequencies and mode shapes; the losses for transverse modes are expected to be considerably smaller in the general case.

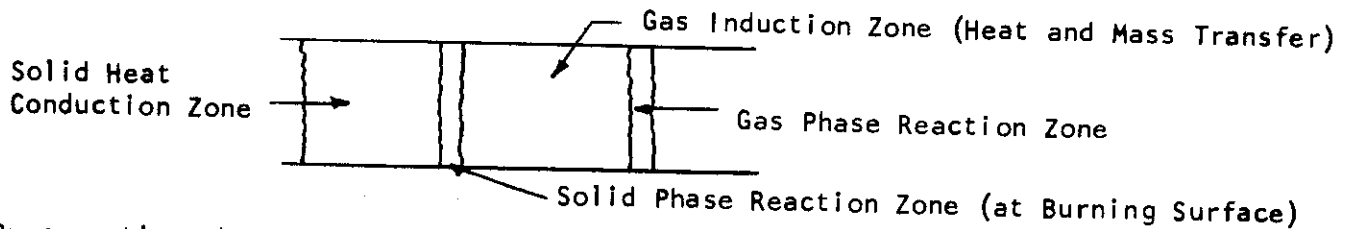
All of the losses above are treated on the basis of small amplitudes; little work appears to have been done regarding the potentially nonlinear behavior of the losses (Ref 7). The most remarkable feature of the losses is their small magnitude, again indicating that instability results from a delicate balance between small energy input and small energy loss.

## THE ENERGY ADDITION ZONE

The response of the energy addition zone to pressure fluctuations has been analyzed in References 48 and 49. The model proposed considers the energy addition zone as composed of four regions, illustrated on the following page.



# Contrails



By computing characteristic response times for chemical reaction, heat conduction in the unburned gas, heat conduction in the solid, convection effects in the induction zone, and solid phase reaction, Hart and McClure (Ref 48) conclude that only the processes of heat transfer and convective effects in the gas induction zone, and heat conduction in the solid are sufficiently slow to be considered on a transient basis. Hence, the model consists of a region in which the transient heat conduction into the solid propellant is dominant, a region in which a nongaseous fuel is vaporized through endothermic reactions (described by steady-state relations), an induction region where the vapor is heated to some ignition temperature (in which transient heat transfer and convection processes dominate), and a flame front characterized by an ignition temperature and a flame speed. The spatial extent of the entire energy addition zone is much smaller than an acoustic wave length, permitting the assumption that the pressure is spatially uniform. The resulting analysis is quite lengthy and is aimed at determining the acoustic admittance of the burning surface:

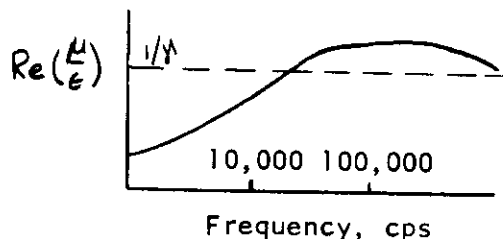
$$A_p = - \frac{v_0}{p_0} \left[ \frac{\mu}{\epsilon} - \frac{1}{\gamma} \right]$$

where

$$\epsilon = \frac{p_1 - p_0}{p_0}$$

$$\mu = \frac{p_1 v_1 - p_0 v_0}{p_0 v_0}$$

Although the model described above obviously has little relationship to the gas-turbine burner problem, two observations are pertinent. First, even a model of this simplicity yields seventeen parameters which may be combined into eleven dimensionless groups which can be varied independently; this makes the establishment of general trends virtually impossible. Second, a characteristic which emerged from the calculation of several numerical results was that the frequency response of the burning surface was rather flat, as illustrated below.



When  $Re(\nu/\epsilon) > 1/\gamma$ , energy is supplied to the oscillation; the nature of the preceding sketch indicates that the resonant frequency of an instability is determined almost entirely by the acoustical properties of the chamber. It is pointed out in Reference 48 that this type of frequency response is not characteristic of time-lag behavior (such as that employed by Crocco (Ref 2) in liquid rocket work).

A more recent analysis (Ref 50) of the burning surface has included a nonlinear treatment based on the technique put forward by Priem (Ref 3) in conjunction with liquid rocket work. These results again indicate the nonlinear nature of the problem in that some specific examples indicate that an initial pressure disturbance of the order of 5 per cent of the mean level will lead to instability in a system which is stable to smaller disturbances. The analysis suffers from the same limitations as Priem's original one, particularly with regard to the fact that the magnitude of the acoustical losses is not related to conditions outside the energy addition zone.

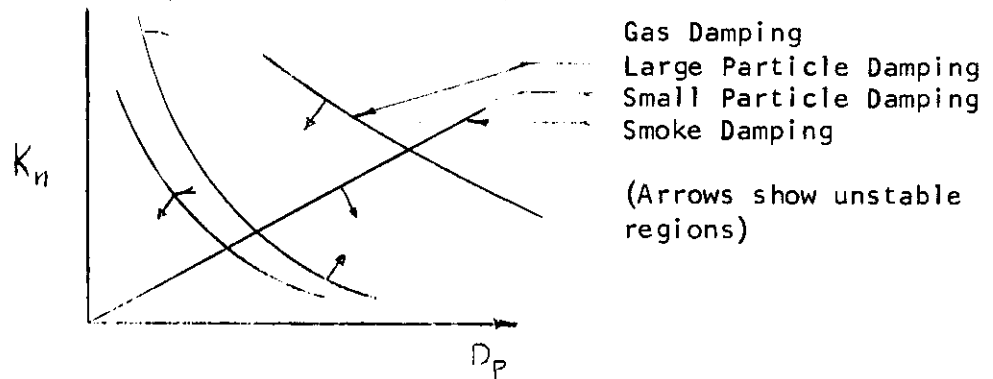
The work quoted above relating to the energy addition zone has included also some consideration of the mechanism of erosive burning, wherein the mean burning rate of the solid is sensitive to the velocity component tangential to its surface. This is not particularly pertinent to gas-turbine burners, and hence is not discussed here.

## SOME OVER-ALL RESULTS

On the basis of the analytical descriptions described previously, McClure, Hart, and Bird (Ref 43) qualitatively explained the observed intermittent unstable behavior with burning time in solid-propellant rockets (see, for example, Ref 51). Specifically, they showed that the combination of gas-phase damping and viscous damping in the solid was sufficient to produce stability in regions where the solid was participating in the wave motion (which, in turn, only occurred during certain intervals during burning). These results serve to emphasize that any analysis of instability requires consideration of both the energy gains and energy losses, and that at least a qualitative assessment of these quantities can be made on the basis of loss-free solutions for acoustic modes and frequencies.

A second qualitative agreement with experimental observations was obtained by Bird, McClure, and Hart in Reference 44. Here they showed that the observed stability behavior of a given propellant in terms of the boundary in the " $K_n$ - $D_p$ " plane could be theoretically explained ( $K_n$  is ratio of burning surface area to nozzle throat area and  $D_p$  is the diameter of the inner surface of the annular solid-propellant segment). The linear stability was evaluated on the basis of determining the energy gain by their previous analysis of the burning surface (Ref 48), and evaluating the energy losses on the basis of the rigid cylinder acoustic modes and frequencies. The stability boundaries obtained by considering various loss mechanisms are shown schematically on the following page.

# Contrails



Here the smoke damping curve was adjusted (by suitable selection of particle size and concentration) to correspond to the observed behavior. The authors also noted in References 44 and 46 that scaling results from a small chamber to a large chamber would be somewhat less than straightforward since the various loss mechanisms scale differently.

In summary, the analytical descriptions of combustion instability in solid-propellant rockets are capable of providing qualitative agreement with the observed physical behavior. Unfortunately, quantitative predictions cannot yet be made. The major difficulty as could be expected appears to lie in an appropriate quantitative model of the response of the energy addition process to either infinitesimal or, particularly, finite disturbances. The descriptions of acoustical behavior and loss mechanisms utilized in solid-propellant work do, however, appear to have application to gas-turbine burners.

## GAS-ROCKET LITERATURE

### INTRODUCTION

Although gas-fueled rockets are not in themselves of major practical interest for propulsion purposes, they have received considerable attention by combustion instability workers for the following very good reasons.

1. They exhibit many of the unsteady combustion phenomena found in rocket combustors that are of great practical interest.
2. Gas rockets eliminate those phenomena peculiar to liquid and solid propellant combustors, and therefore any transient combustion phenomena can be attributed entirely to the gas phase alone.

It has already been stated that there are many similarities between the unsteady combustion phenomena observed in liquid rocket combustors and those observed in duct burners and afterburners. It therefore follows from the first reason given above that these similarities should also exist between

gas rockets and duct burners and afterburners. Further, in the gas-turbine combustion literature review it was concluded that the combustion processes in duct and afterburners may occur essentially entirely in the gaseous phase, thereby enhancing the relevance of gas rockets within the context of the current study.

In this section the results of the literature review that are presented have been restricted to those that are deemed relevant to the problem under consideration; namely, high frequency transverse combustion oscillations. Further, to provide the information that will be applicable to the development of afterburner and duct burner combustion models, the presentation is in the following order:

1. Assessment of the observed characteristic frequencies.
2. Evaluation of instability mechanisms that have been proposed.
3. A description of the formulation and analysis of existing transient combustion models.

## OBSERVED CHARACTERISTIC FREQUENCIES OF GAS-ROCKET COMBUSTION INSTABILITIES

As in the other types of rocket combustor, the majority of attention given to gas-rocket combustion instabilities has been directed towards the low-frequency longitudinal modes. More recently, however, transverse modes have been observed and reported in References 52 through 56. Bowman (Ref 56) was primarily interested in the lower modes but observed that the first tangential mode (7500 cps) occurred simultaneously with the fundamental longitudinal mode ( $\sim 630$  cps) for premixed hydrogen-air and methane-air mixtures. Unfortunately, insufficient information is given to permit any conclusions to be drawn concerning the nature of this transverse mode, that is, whether it was a true acoustic-type oscillation.

A large body of experimental data has been reported by Zucrow, Osborn, and their co-workers at Purdue University (Refs 52 through 55). These reports present the results of a systematic series of experiments aimed at investigating the influence of each of the following variables on combustion pressure oscillations:

1. The geometry of a cylindrical combustion chamber.
2. The chemical properties of different propellant combinations.
3. The location of the injector and injected mass velocities.

These experiments were repeated for premixed and unmixed propellants. Unfortunately only the stability boundaries and pressure amplitudes are reported together with a description of the type of oscillatory mode. The oscillatory frequencies are not presented which make it difficult to determine whether the oscillations can be related to the acoustical

properties of the chamber. However, it is possible to draw the following conclusions from the reported observations:

1. The aspect ratio (length/diameter) of the chamber has a significant influence upon the amplitudes of the transverse modes of pressure oscillations (see Fig 15).
2. At an aspect ratio of 1.0, there is a tendency for coupling to occur between the tangential and longitudinal modes of oscillation.
3. The injection pattern exerts a predominant influence upon the mode of oscillation (see Table II).

All of these characteristics are consistent with acoustical resonance phenomena in cylindrical combustors.

The acoustical nature of the pressure fluctuations associated with oscillatory combustion has been questioned by Sirignano and Crocco (Ref 4) in view of the waveforms observed in certain situations in longitudinal modes. These oscillatory pressure waveforms consist of shock-type discontinuities followed by exponential decays, examples of which may be seen in Figure 16 (from Ref 52). It may be argued that these waveforms are also typical for transverse modes, thereby introducing uncertainties into any analytical model which postulates sinusoidal variations in the unsteady pressures, velocities, etc. However, closer examination of Figure 16 shows that even when such "shock" type instabilities develop, they are initially sinusoidal and remain so even when their amplitudes are 50 per cent or more of the final amplitude. Further, the frequency of oscillation does not appear to be significantly dependent upon the wave shape. It seems, therefore, reasonable to conclude that analytical modes can justifiably postulate sinusoidal fluctuations in the dependent flow variables in order to establish stability boundaries using frequencies computed from an acoustic analysis of the combustor.

## EVALUATION OF INSTABILITY MECHANISMS

The analytical models and experiments described in the literature for studying gas-rocket combustion instability have been specifically designed so that the number of mechanisms that influence stability are kept to a minimum. The supporting mechanisms have been reduced to:

1. The reaction rates of the combustion process.
2. The mixing rate of the propellant (in unmixed experiments only).

The dissipative mechanisms remain the same as in liquid-rocket combustors. It should be noted that all of these mechanisms will be present in gas-turbine duct burners and afterburners.

An initial attempt was made to evaluate the significance of each of the supporting and dissipative mechanisms by reviewing existing such

# Contrails

evaluations in the published literature. However, analytical evaluations are dependent upon the validity of the postulates made when defining a combustion model together with the accuracy of the subsequent analysis. Deficiencies in both respects suggested that it was better to base the evaluations of the mechanisms which contribute to combustion instabilities upon experimental observations.

Zucrow, et al (Ref 54) present comprehensive experimental data for premixed fuel-air mixtures oscillating in transverse modes. The stability boundaries obtained in these experiments are shown in Figures 17, 18, and 19. In Figure 17, the ethylene-air boundaries are shown in plots of equivalence ratio against chamber pressures together with contours of pressure amplitude. It may be seen that pressure amplitudes of 70 psi may be obtained at chamber pressures of 110 psia. The influence of chamber length upon the stability boundaries are shown in Figure 18 where it can be seen that the heel of the stability boundaries occur at higher chamber pressures as the chamber length increases. A similar stability plot for hydrogen-air is shown in Figure 19.

Zucrow, et al, conclude that increasing the heat release rates of fuels produce the following effects:

1. A broadening of the range of equivalence ratios sustaining combustion pressure oscillations.
2. An increase in the maximum amplitude of the pressure oscillations.
3. When the activation energy of a fuel increases, two resonant peaks become more pronounced. These amplitude peaks occur at conditions corresponding to fuel-lean and fuel-rich mixtures. An explanation for this phenomena can be given using the critical combustion temperature model postulated in Reference 57. This will be dealt with in more detail later in this chapter.

The injector location influences the instability mode shape in the manner illustrated in Table II for ethylene. Injection on the combustor centerline produces radial modes. Injection near the combustor surface produces tangential modes, while intermediate locations may produce stable operation.

The amplitudes of oscillation may be greatly reduced by introducing baffles into the chamber. Zucrow, et al, measured reductions in amplitude of up to an order of magnitude when the baffle length occupied half of the total combustor length. These results are shown in Figure 20.

When the additional complexity of fuel-air mixing was added, Zucrow, et al, found that the following conclusions could be drawn from their experimental results. In combustors employing "impinging jet" injectors when rapid mixing occurs the combustion oscillations are reaction controlled, and the intensity of oscillations are directly related to the heat release rates. Further, when fuel-air mixing occurs only through turbulent mixing

processes, chemical effects are relatively unimportant.

In all of the preceding experimental data the ratio of nozzle exit area to combustor cross-sectional area was approximately 1/200, so that nozzle losses were negligible.

Bowman (Ref 56) reviews the available published information on the effects of the injector thermal conductivity and combustion gas heat-transfer coefficients upon stability boundaries. He concludes that there is no observable effect of heat-transfer coefficient; further experiments where the injector was covered with a thermal insulator exhibited the same stability limits as when it was left uninsulated.

## ANALYTICAL MODELS DESCRIBING UNSTEADY COMBUSTION

At this time no models of tangential oscillatory combustion phenomena in gas-fueled rockets have been postulated that are amenable to precise analysis, and which provide adequate predictions of stability boundaries and oscillatory amplitudes. In these respects gas rockets, although simpler, are not understood significantly better than solid- and liquid-rocket combustion instabilities. However, several authors have postulated models which when analyzed and compared with experimental data have provided some insight into the nature of gaseous combustion instability. Most of these efforts have been directed at the longitudinal modes of instability, the latest of which is by Sirignano and Crocco (Ref 4).

The Sirignano-Crocco analysis attempts to find solutions to the non-linear equations of motion. The principal assumptions are:

1. The response time of the combustion process is small compared to the period of oscillation.
2. A plane shock wave propagates with constant period between the injector face and the nozzle reflecting alternatively from each of them.
3. The combustion chamber is long, so that the nozzle and combustion zone have zero length.

In order to determine some explicit information about the combustion instability, three parameters are defined:

1. A simplified Arrhenius combustion law which is a measure of the energy release in the air-fuel mixture

$$r = B \exp\left(-\frac{E}{RT}\right)$$

# Contrails

where  $T$  = combustion temperature  
 $R$  = universal gas constant  
 $E$  = activation energy  
 $B$  = pre-exponential factor (independent of  $T$ )  
 $r$  = energy release parameter.

2. A pressure amplitude parameter,  $\epsilon$ , defined as

$$\epsilon = \bar{M} \left\{ (\gamma-1) \frac{E}{RT} - \left( \frac{3\gamma-1}{2} \right) \right\}$$

where  $\gamma$  = ratio of specific heats  
 $\bar{M}$  = mean Mach number.

It should be noted that at a stability boundary  $\epsilon = 0$ .

3. A wave shape parameter,  $\lambda$ , defined as

$$\lambda = \frac{16\bar{M} \left\{ \left( \frac{\gamma-1}{2} \right) \frac{1}{1-\nu} \right\}^2 \left\{ 2 \left( \frac{E}{RT} \right)^2 - 3 \left( \frac{E}{RT} \right) - \frac{\gamma(3\gamma-1)}{(\gamma-1)^2} \right\}}{(\gamma+1)(1+\nu) \left\{ \frac{1-\bar{M}}{1+\bar{M}} \left( \frac{1+\nu}{1-\nu} \right) + \frac{1+\bar{M}}{1-\bar{M}} \right\}}$$

where  $\nu = (\gamma-1)\bar{M}/2$ . This parameter is a measure of the exponential decay in pressure behind the shock front.

It follows from the definition of  $\epsilon$  that at a stability boundary

$$\left( \frac{E}{RT} \right)_{\text{Limit}} = \frac{3\gamma-1}{2(\gamma-1)}$$

It should be noted that instability can occur when  $\epsilon > 0$ , therefore for a given propellant combination, instability can occur when  $T < T_{\text{crit}}$ , where  $T_{\text{crit}}$  is defined by the last equation. From this requirement it can be seen that there may be two instability limits, one on either side of the maximum combustion temperature (at stoichiometric conditions). When the maximum combustion temperature is less than  $T_{\text{crit}}$  only one combustion instability will occur. This explains why ethane and methane fuels only exhibit one region of instability, whereas the more reactive fuels such as ethylene and hydrogen exhibit two regions, as shown in Figures 17 and 19.

Bowman, et al (Ref 57) have used this approach to show that when a diluent inert gas is progressively added to hydrogen-air mixtures, the two stability limits converge, until finally only an instability region exists.

It should be noted that assumption 1 in the Sirignano-Crocco model is of doubtful validity in transverse modes, particularly at low combustor temperatures. In addition, the second assumption is doubtful as the wave thickness may be a significant fraction of the wave length.



# Contrails

Culick (Ref 1) has carried out a theoretical investigation of high frequency gaseous fuel combustion instability for a general three-dimensional case with distributed combustion. Stability limits are obtained when the equations can be linearized. These limits are presented such that the effects of combustion, nozzle, and mean flow can be separated. Inasmuch as the approach adopted in this report is based on this work, no discussion is included in this appendix; the development is presented in Appendix G.

Zucrow, et al (Ref 55) completed a theoretical study aimed at deriving the important similarity parameters that influence the oscillatory behavior of the combustion process. The analysis was based on an idealized rocket motor consisting of four sections:

1. A mixing region.
2. An induction region.
3. A narrow combustion zone.
4. A region containing only combustion products up to the nozzle entrance.

The perturbation equations, expressing momentum in the axial and tangential directions, continuity, energy, and state of the mixture, were developed by making the following assumptions:

1. The mean flow was in the axial direction.
2. There were no components of fluctuating velocity in the axial direction.
3. Terms of order (Mach number)<sup>2</sup> were neglected.
4. The fluctuating quantities were expressed as

$$\phi' = \phi_+ e^{i(\omega t - \theta)}$$

where  $\omega$  = frequency  
 $t$  = time  
 $\theta$  = phase angle  
 $\phi_+$  = amplitude of disturbance.

The relevant equations that were derived are

$$\frac{d}{dt} \left( \frac{v_+}{P_+} \right) + \frac{v_+}{P_+} \left( i \frac{\omega}{v_+} + \frac{4}{3} \frac{M}{\rho v_+ r^2} \right) - i \frac{1}{r \rho v_+} = 0$$

# Contrails

and

$$\frac{V_+}{P_+} = -\frac{1}{\bar{\rho} C} \left[ 1 - i \frac{k}{\omega} \bar{v}_z \frac{d}{dz} (\ln \bar{T}) + i \frac{(\gamma-1)}{\omega} \left( \frac{q_R^+}{P_+} + \frac{q_L^+}{P_+} \right) - i \frac{P_+}{P_+} \left( \frac{C^2 \bar{v}_z^2}{\omega} \right) \frac{d \bar{v}_z}{dz} \right]$$

where  $\mu$  = viscosity  
 $\rho$  = density  
 $v$  = velocity  
 $P$  = pressure  
 $z$  = axial coordinate  
 $r$  = radius  
 $T$  = temperature  
 $(\bar{\quad})$  = mean value  
 $C$  = speed of sound  
 $q_R^+$  = rate of volumetric energy release  
 $q_L^+$  = rate of energy loss to walls.

The above equations were integrated by assuming that the variables were constant within each of the four sections of the model combustor. Then using the following definitions:

$$\frac{V_+}{P_+} = \gamma C = \gamma^* / \bar{\rho} C$$

$$\frac{P_+}{P_+} = \epsilon$$

$$\frac{q_R^+}{P_+} = q_R^*$$

$$\frac{q_L^+}{P_+} = q_L^*$$

$$\gamma_{injection}^* - \gamma_{nozzle}^* = f \left[ (N_{RE})_M, (N_{RE})_S, \left( \frac{q_R^*}{\bar{v}_z} \right)_r, \left( \frac{q_L^*}{\bar{v}_z} \right)_s, \right. \\ \left. \frac{L_M}{R}, \frac{L_R}{R}, \frac{L_S}{R}, \frac{T_{ad}}{T_0}, \frac{T_c}{T_0}, \gamma \right]$$

where  $L_M$ ,  $L_R$ ,  $L_S$  are characteristic lengths of the mixing, reaction, and residence regions,

$T_{ad}$  = adiabatic flame temperature  
 $T_c$  = temperature at nozzle

$T_b$  = inlet temperature  
 $N_{Re}$  = Reynolds number.

These functional relationships were then used to correlate experimental data because the admittance  $\gamma$  is a fundamental quantity which has an important effect upon the oscillatory combustion processes. These correlations were only moderately successful, due possibly to some of the unnecessarily restrictive assumptions in the analysis.

One additional reason for the limited success of the correlations of Zucrow, et al, are that the change in acoustic admittance between the injector and nozzle, while without doubt greatly influencing the unsteady combustion processes, does not in itself completely characterize the problem. The nozzle and acoustic absorption at the walls will also be important and should be adequately represented in analytical and experimental models. Further, the driving mechanism for instability is not related in the analytical model to the local flow conditions. In reaction rate controlled instabilities, this feature is of primary importance.

## CONCLUDING REMARKS

Gas-rocket combustion instabilities exhibit most of the characteristics exhibited by liquid-fueled rockets. The dominating driving mechanism is associated with chemical reaction, except when combustion occurs in poorly mixed propellants.

The relative influence of the nozzle, baffles, and other dissipating mechanisms cannot be ascertained directly from the gas-rocket literature as experiments have not included these effects systematically. From the analytical point of view, Culick's approach (Ref 1) is quite attractive. Zucrow, et al, (Ref 55) have developed an approach which may be useful, if developed further, in deciding what the important variables are that should be simulated and controlled in experiments on duct burners and afterburners.

Finally, it should be noted that no analytical work has been done within the context of gas rockets which will enable the amplitudes of nonlinear instabilities to be computed.

# *Contrails*

## Appendix B

### ACOUSTIC ANALYSES

#### INTRODUCTION

Experimental observations of high-frequency instabilities in gas-turbine burners have led to the conclusion (see Appendix A) that the pressure oscillations associated with the instabilities are acoustic in nature. The term acoustic oscillation is here meant to imply regular oscillations resulting from successive reflections at the chamber boundaries of waves (disturbances) traveling at the local sonic velocity. Acoustic oscillations in combustion chambers, unlike those of an organ pipe for example, are complex; the complexity can be attributed to the following:

1. The chamber geometry is often complicated.
2. The temperature and, therefore, the sonic velocity of the gases in the chamber are not uniform.
3. The chamber boundaries are not simple, that is, they are not pure reflectors or pure absorbers.
4. Energy is added to the acoustic oscillation, probably in the heat addition zone of the chamber.
5. Energy is removed from the acoustic oscillation by various loss mechanisms.

Despite the complexity of the real problem, some useful information can be gained from an analysis of a much simplified problem in which only the geometry and an idealized temperature distribution are retained as complicating factors. The most valuable information to be gained from this simple acoustic analysis is the prediction of natural acoustic frequencies of combustion chambers, which is surprisingly insensitive to the gross simplifications employed. The prediction of frequencies of oscillation is an important first step in the investigation of combustor instabilities because the relative influence of many of the possible loss and driving mechanisms in the acoustic system are frequently dependent. Thus, the assessment of mechanisms which might provide acoustic energy gains and losses in the system requires a prior knowledge of the frequencies of oscillation. In addition to providing useful frequency information, the simple acoustic analysis is by way of a simple introduction into the real problem to be tackled subsequently.

The objectives of this appendix are to establish the natural

# Contrails

frequencies and modes\* of oscillation of enclosures representative of gas-turbine burners, in the absence of energy gains and losses. The analysis will be extended to include the effects of a temperature discontinuity in the enclosure, an idealization of the presence of a flame front.

The approach to the problem will be to set up the equations of motion for a particle of oscillating gas, make use of the small perturbation assumption, neglecting second order and higher terms, and to solve the equations with simple boundary conditions. In the general case, the boundaries of an acoustic chamber would be represented by an admittance coefficient,  $A$  defined by

$$A = \frac{u_n'}{p'}$$

where  $u_n'$  is the normal component of the velocity perturbation at the boundary  
 $p'$  is the perturbed or acoustic pressure at the boundary.

In general, the admittance coefficient is a complex quantity. The simple boundary conditions employed in the present chapter are those corresponding to a closed, rigid boundary when  $A = 0$  and to an open boundary when  $1/A = 0$ . The more general boundary condition and its associated energy losses are dealt with in Appendix C.

## EQUATIONS OF MOTION

The motion of a particle of gas oscillating in an acoustic field can be represented by the usual conservation equations of mass and momentum which, in vector notation are:

$$\text{Conservation of Mass} \quad \nabla \cdot \rho \underline{u} = -\frac{\partial \rho}{\partial t} \quad (\text{B-1})$$

$$\text{Conservation of Momentum} \quad \nabla p = -\rho \frac{\partial \underline{u}}{\partial t} \quad (\text{B-2})$$

where  $p$  is the instantaneous local pressure  
 $\rho$  is the instantaneous local density  
 $\underline{u}$  is the instantaneous local velocity

Assuming that perturbations from the equilibrium values of the above quantities are small, the notation on the following page is employed:

---

\* The term "mode" or "mode shape" is used to describe the manner (but not including amplitude) in which the acoustic pressure (or any other quantity) varies in space, and is generally represented by components in the coordinate directions.

# Contrails

$$\begin{aligned}p &= p_0 + p' \\ \rho &= \rho_0 + \rho' \\ u &= u'\end{aligned}$$

where the subscript 0 denotes equilibrium values; the case of zero mean velocity is being considered. Consistent with the small perturbation assumption, the waves are taken to be adiabatic, then:

$$\frac{p'}{p_0} = \left(\frac{\rho'}{\rho_0}\right)^\gamma \quad (\text{B-3})$$

where  $\gamma$  is the ratio of specific heats. The sonic velocity in the fluid is given by:

$$c_0^2 = \frac{\gamma p_0}{\rho_0} \quad (\text{B-4})$$

Equations B-1 through B-4 can be manipulated (see Refs 58 and 59 for example) to give the wave equation:

$$\nabla^2 p' = \frac{1}{c_0^2} \frac{\partial^2 p'}{\partial t^2}$$

In cylindrical polar coordinates, which is the coordinate system employed in the following analyses, the wave equation is:

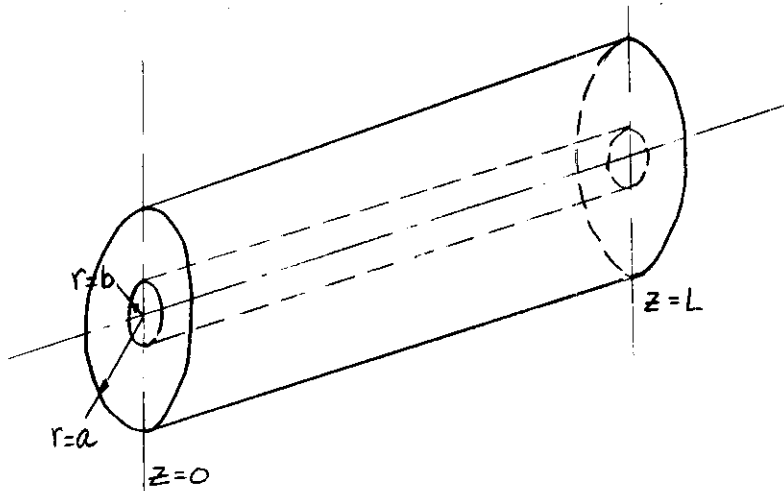
$$\frac{1}{r} \frac{\partial}{\partial r} \left( r \frac{\partial p'}{\partial r} \right) + \frac{1}{r^2} \frac{\partial^2 p'}{\partial \phi^2} + \frac{\partial^2 p'}{\partial z^2} = \frac{1}{c_0^2} \frac{\partial^2 p'}{\partial t^2} \quad (\text{B-5})$$

Solutions to the wave equation can be obtained for given boundary conditions yielding the perturbed pressure as a function of time and position. From these solutions the frequencies of the various modes of oscillation are derived, where each mode of oscillation corresponds to a different eigenvalue of the solution.

## FREQUENCIES OF NORMAL MODES OF ANNULAR CYLINDERS

The geometrical configuration which is of greatest interest in the study of gas-turbine burners is the annular cylinder which has as a limiting case, the circular cylinder. In the following analysis, the annular space between two perfectly rigid parallel walls at radii  $r = a$  (outer wall) and  $r = b$  will be considered. The end boundary conditions at  $z = 0$  and  $z = L$  will be taken as either perfectly rigid walls or open ends.

# Contrails



Methods for solving the wave equation are well known (see Ref 60 for example) and need not be presented here. The most general form of the solution to Equation B-5 can be written as:

$$p' = (K_1 e^{i\alpha z} + K_2 e^{-i\alpha z}) (K_3 e^{im\phi} + K_4 e^{-im\phi}) [K_5 J_m(\alpha r) + K_6 Y_m(\alpha r)] e^{-i\omega t} \quad (B-6)$$

where  $K_1$  to  $K_6$  are constant coefficients which, in general, are complex  
 $n, m$  and  $\omega$  are constants

$$\alpha \text{ is given by } \alpha^2 = (\omega/c_0)^2 - n^2 \quad (B-7)$$

$J_m$  is the Bessel function of the first kind

$Y_m$  is the Bessel function of the second kind.

The two terms in each of the brackets of Equation B-6 represent forward and backward propagating waves in each of the three coordinate directions. The time dependence of the perturbed pressure is simple harmonic and the constant  $\omega$ , appearing in the exponent of the last term of Equation B-6 is the angular frequency of the oscillation.

## BOUNDARY CONDITIONS AT THE CYLINDER ENDS

When considering the end boundary conditions, Equation B-6 is more conveniently written:

$$p' = f(r, \phi) (K_1 e^{i\alpha z} + K_2 e^{-i\alpha z}) e^{-i\omega t} \quad (B-8)$$

where  $f(r, \phi)$  is some function of  $r$  and  $\phi$  only.

Two limiting cases of the cylinder-end boundary conditions are considered:

1. Closed rigid end, when  $w' = 0$  at the boundary.



# Contrails

2. Open end, when  $p' = 0$  at the boundary.

The expression for the perturbed velocity,  $u'$  can be obtained from the momentum equation in the  $z$  direction and Equation B-8. The momentum equation in  $z$  direction is

$$\frac{\partial u'_z}{\partial t} = -\frac{1}{\rho_0} \frac{\partial p'}{\partial z} \quad (\text{B-9})$$

From Equations B-8 and B-9,

$$u'_z = -\frac{n}{i\omega\rho_0} f_1(r,\phi) (K_1 e^{in z} - K_2 e^{-in z}) e^{-i\omega t} \quad (\text{B-10})$$

First consider the case in which the cylinder is closed at both ends, that is,  $u'_z = 0$  at  $z = 0$  and  $z = L$ . The first condition yields, from Equation B-10,  $K_1 = K_2$ , and Equation B-10 becomes

$$u'_z = -\frac{n}{i\omega\rho_0} f_1(r,\phi) K_1 \sin n z e^{-i\omega t} \quad (\text{B-11})$$

Applying the second condition to Equation B-11:

$$\sin nL = 0$$

$$n = 0, \frac{\pi}{L}, \frac{2\pi}{L}, \dots$$

The various values of  $n$  correspond to the various possible modes of the longitudinal component of oscillation. Thus,  $n = 0$  corresponds to no longitudinal component,  $n = \pi/L$  is the fundamental mode,  $n = 2\pi/L$  is the second longitudinal and so forth. For simplicity, a new quantity  $\nu$  is defined by  $\nu = nL/\pi$ ; then  $\nu$  has values 0, 1, 2, etc., for the various longitudinal harmonics, and can be defined as the number of half wavelengths in the longitudinal pressure variation over the length of the chamber. The expression for the perturbed pressure for a cylinder with closed ends can now be written as:

$$p' = f(r,\phi) \cos(\nu\pi z/L) e^{-i\omega t} \quad (\text{B-12})$$

Following a similar procedure to that above, for the case of a cylinder with both ends open, the resulting expression for the perturbed pressure becomes:

$$p' = f(r,\phi) \sin(\nu\pi z/L) e^{-i\omega t} \quad (\text{B-13})$$

# Contrails

where again,  $\nu = 0, 1, 2, 3, \text{etc.}$ , for the various modes of the longitudinal component of oscillation.

It is a fairly simple extension to show that for the case of one end open and the other end closed,  $\nu$  takes values of  $1/2, 3/2, 5/2, \text{etc.}$

## BOUNDARY CONDITIONS AT THE CYLINDER WALLS

Equation B-6 is again, for convenience, written in an abbreviated form:

$$p' = f(z, \phi) [K_5 J_m(\alpha r) + K_6 Y_m(\alpha r)] e^{-i\omega t} \quad (\text{B-14})$$

At the wall boundaries, since the walls are assumed to be impervious and rigid, the velocity normal to the walls must be zero. The momentum equation applied in the radial direction yields:

$$\frac{\partial w_r'}{\partial t} = -\frac{1}{\rho_0} \frac{\partial p'}{\partial r} \quad (\text{B-15})$$

Equations B-14, B-15, and the boundary conditions lead to the condition:

$$\frac{\partial}{\partial r} [K_5 J_m(\alpha r) + K_6 Y_m(\alpha r)]_{r=a} = 0$$

and

$$\frac{\partial}{\partial r} [K_5 J_m(\alpha r) + K_6 Y_m(\alpha r)]_{r=b} = 0$$

therefore,

$$\frac{K_5}{K_6} \left[ \frac{\frac{\partial J_m(\alpha r)}{\partial r}}{\frac{\partial Y_m(\alpha r)}{\partial r}} \right]_{r=a} + 1 = 0$$

and

$$\frac{K_5}{K_6} \left[ \frac{\frac{\partial J_m(\alpha r)}{\partial r}}{\frac{\partial Y_m(\alpha r)}{\partial r}} \right]_{r=b} + 1 = 0$$

thus,

$$\left[ \frac{\frac{\partial J_m(\alpha r)}{\partial r}}{\frac{\partial Y_m(\alpha r)}{\partial r}} \right]_{r=a} = \left[ \frac{\frac{\partial J_m(\alpha r)}{\partial r}}{\frac{\partial Y_m(\alpha r)}{\partial r}} \right]_{r=b} \quad (\text{B-16})$$

# Contrails

For each value of  $m$  there will be an infinite number of solutions to the preceding equation. Let the values of  $\alpha r$  which satisfy Equation B-16 be  $\pi \beta_{m,\delta}$  (a function of the ratio  $a/b$ ), where  $\delta$  is an index signifying the number of the solution.  $\delta$  is taken to run from 0, that is, it has values 0, 1, 2, 3, etc., where  $\delta = 0$  corresponds to no radial component of oscillation,  $\delta = 1$  corresponds to the fundamental radial component, and so forth.

## SOLUTION OF THE BOUNDARY CONDITION (EQUATION B-16)

By expansion of the Bessel functions  $J_m$  and  $Y_m$ , it can easily be shown that:

$$\frac{dJ_m(\alpha r)}{dr} = \frac{\alpha}{2} [J_{m-1}(\alpha r) - J_{m+1}(\alpha r)]$$

and

$$\frac{dY_m(\alpha r)}{dr} = \frac{\alpha}{2} [Y_{m-1}(\alpha r) - Y_{m+1}(\alpha r)]$$

The boundary equation, therefore, becomes:

$$\left[ \frac{J_{m-1}(\alpha r) - J_{m+1}(\alpha r)}{Y_{m-1}(\alpha r) - Y_{m+1}(\alpha r)} \right]_{r=a} = \left[ \frac{J_{m-1}(\alpha r) - J_{m+1}(\alpha r)}{Y_{m-1}(\alpha r) - Y_{m+1}(\alpha r)} \right]_{r=b} \quad (\text{B-17})$$

A graphical method of solution of the above equation to determine  $\beta_{m,\delta}$  is indicated and this has been carried out for several values of  $m$  and of  $a/b$  ratio. The results will be presented later in the appendix.

For the limiting case of a circular cylinder ( $b = 0$ ), the boundary equation becomes:

$$J_{m-1}(\alpha a) = J_{m+1}(\alpha a)$$

## CONDITIONS IN THE TANGENTIAL DIRECTION

Although there are no fixed boundaries in the tangential direction of motion, an examination of the oscillations in this direction reveals two special cases which are worthy of note. The expression for perturbed pressure, Equation B-6, can be abbreviated to:

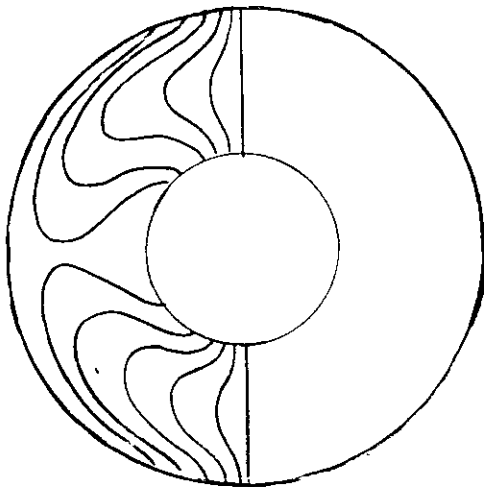
# Contrails

$$p' = f(r, z) (K_3 e^{im\phi} + K_4 e^{-im\phi}) e^{-i\omega t} \quad (\text{B-18})$$

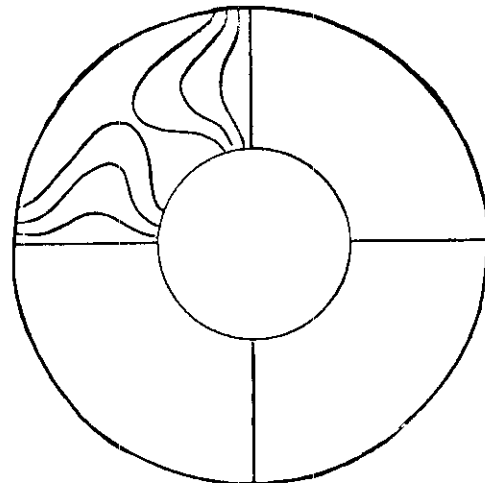
Two special cases of the above equation may be considered. The first is when  $K_3 = K_4$ , which gives:

$$p' = f(r, z) 2K_3 \cos m\phi e^{-i\omega t}$$

This corresponds to standing waves in the tangential plane, that is, waves in which the modes (positions of maximum pressure) are at fixed locations at all times. The value of the constant  $m$  determines the mode of the tangential component of oscillation; thus,  $m = 0$  represents no tangential component,  $m = 1$  represents the first transverse and so forth. The sketches below illustrate the wave patterns (in terms of lines of constant pressure) for  $m = 1$  and 2.



$m=1$



$m=2$

It should be noted that the tangential component of the acoustic velocity,  $u'_\phi$  is out of phase with the pressure perturbations. This can be seen from the momentum equation applied to motion in the tangential direction:

$$\frac{\partial u'_\phi}{\partial t} = -\frac{1}{\rho r} \frac{\partial p'}{\partial \phi}$$

Thus

$$u'_\phi = \frac{f(r, z)}{i\omega \rho r} 2K_3 m \sin(m\phi) e^{-i\omega t}$$

# Contrails

The second special case of Equation B-18 arises when  $K_3$  or  $K_4$  vanishes; then:

$$p' = f(r, z) K_3 e^{i(m\phi - \omega t)}$$

The real part of the above expression for the perturbed pressure will have the form:

$$p' = f(r, z) A \left\{ \begin{array}{l} \cos(m\phi - \omega t) \\ \sin(m\phi - \omega t) \end{array} \right\}$$

where  $A$  is real. Thus, it can be seen that there is no value of  $\phi$  for which the pressure is always a maximum, but that the nodal points rotate with an angular frequency of  $1/m$  times the frequency of oscillation. This type of oscillation is termed a rotating or spinning mode. In this mode, unlike the standing mode, the tangential component of the acoustic velocity is in phase with the pressure perturbations as may be seen from the momentum equation which yields:

$$u'_\phi = \frac{m}{\omega r} f(r, z) K_3 e^{i(m\phi - \omega t)}$$

## FREQUENCY OF OSCILLATION

It has been shown in the preceding sections that the mode of an oscillation can be represented by the three parameters  $m, \nu, \delta$  which correspond respectively to the tangential, longitudinal and radial components of oscillation. It is desirable to relate the frequency of oscillation to these parameters and to the geometry of the chamber.

The frequency of oscillation is given by:

$$f = \frac{\omega}{2\pi}$$

The angular frequency,  $\omega$ , is related to the mode shape by Equation B-7 which, rewritten, is

$$\omega^2 = c_0^2 (\alpha^2 - n^2)$$

Therefore,

$$f = \frac{c_0}{2\pi} (\alpha^2 - n^2)^{1/2}$$

Defining a dimensionless frequency,  $f'$  by:

$$f' = \frac{2fa}{c_0} = \frac{a}{\pi} (\alpha^2 - n^2)^{1/2}$$

# Contrails

and introducing the quantities  $\beta_{m,y}$  (solutions to Equation B-16) and  $\nu$ , then

$$f' = \left[ \beta_{m,y}^2 + \left( \frac{a\nu}{L} \right)^2 \right]^{1/2} \quad (B-19)$$

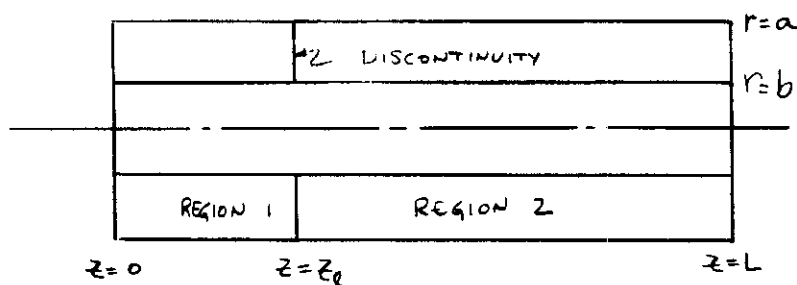
Values for the dimensionless frequency have been computed for various modes of oscillation and for various  $L/a$  and  $a/b$  ratios. The results are plotted in Figures 21 through 24 against  $L/a$  ratio where each figure represents one of the following  $a/b$  ratios: 1.1, 1.3, 1.5, and  $\infty$  (circular cylinder). Only the lower modes of oscillation have been computed as these are generally the only ones of interest in gas-turbine burners.

The most striking effect shown by the results is the large increase in the frequency when a radial component of oscillation is introduced into the mode for the annular cylinders. This result is to be expected since the radial distances in an annulus are much smaller than the circumferential and longitudinal distances. The effect of  $L/a$  ratio is most significant for low values of  $L/a$  ( $\approx 1$ ) and for the lower transverse modes of oscillation; for the combined modes considered the effect of  $L/a$  ratio is practically non-existent for  $L/a$  greater than three.

The evaluation of actual frequencies (in cycles per sec) for practical combustion chamber configurations and conditions will be left until after the effect of a temperature discontinuity in the chamber has been included in the analysis. The inclusion of this effect will be the subject of the following section.

## INCLUSION OF A TEMPERATURE DISCONTINUITY

One of the effects of the combustion process in a combustion chamber is to divide the chamber roughly into two zones of substantially different temperatures and, therefore, sonic velocities. It is the purpose of this section to estimate the effects on the mode and frequency of oscillation of the presence of a temperature discontinuity. The temperature distribution in the chamber is idealized to a step change in temperature in the axial direction with no mean temperature variations in the radial and tangential directions. For the purpose of this analysis, the ends of the annular cylinder will be taken to be closed and rigid. The sketch below illustrates the nomenclature employed in the following analysis:



# Contrails

Suffix 1 refers to the enclosure between  $z = 0$  and the discontinuity at  $z = z_l$  and Suffix 2 applies between  $z = z_l$  and  $z = L$ .

The solutions to the wave equation for the two regions 1 and 2 can be written in the following form:

$$P_1' = f_1(\phi, r)(A_1 \cos n_1 z + B_1 \sin n_1 z) e^{-i\omega_1 t} \quad (\text{B-20})$$

$$P_2' = f_2(\phi, r)(A_2 \cos n_2 z + B_2 \sin n_2 z) e^{-i\omega_2 t} \quad (\text{B-21})$$

## BOUNDARY CONDITIONS

At the closed ends, the boundary conditions are:

$$\left(\frac{\partial P_1'}{\partial z}\right)_{z=0} = 0 \quad (\text{B-22})$$

$$\left(\frac{\partial P_2'}{\partial z}\right)_{z=L} = 0 \quad (\text{B-23})$$

At the temperature discontinuity, the following conditions must apply:

$$(P_1')_{z=z_l} = (P_2')_{z=z_l} \quad (\text{B-24})$$

This condition is necessary because there cannot be a pressure discontinuity with zero through-flow velocity in the chamber.

$$(u_{z,1}')_{z=z_l} = (u_{z,2}')_{z=z_l} \quad (\text{B-25})$$

This merely states that particles of gas in each region immediately adjacent to the boundary formed by the temperature discontinuity must oscillate with the same axial component of velocity as that of the boundary. It is assumed that the variations (oscillations) in the position of the temperature discontinuity, given by  $z_l$ , can be neglected and  $z_l$  is taken to be constant. Since the boundary Equation B-25 is true for all  $t$ , it follows that:

$$\left(\frac{\partial u_{z,1}'}{\partial t}\right)_{z=z_l} = \left(\frac{\partial u_{z,2}'}{\partial t}\right)_{z=z_l} \quad (\text{B-26})$$

It should be pointed out that the interface conditions expressed by Equations B-24 and B-25 do not account for the effect of a flameholder in

# Contrails

stabilizing the position of a flame front. That is, in the presence of a flameholder, the interface (flame front) is not free to oscillate completely unconstrained. A more realistic boundary condition can be expressed as

$$(p')_{z=z_f} = (p')_{z=z_2} \quad (\text{B-27})$$

and

$$\left(\frac{u'_{z,1}}{p'}\right)_{z=z_f} = A_f \quad (\text{B-28})$$

where  $A_f$  is the acoustic impedance of the flame front. Equivalently, the following can be used in place of Equation B-25:

$$(u'_{z,1})_{z=z_f} = K(u'_{z,2})_{z=z_2} \quad (\text{B-29})$$

where  $p_2/p_1 \leq K \leq 1$ . Although these conditions could be incorporated into the final instability model, they are not necessary for the considerations of this appendix.

The perturbation momentum equation in the  $z$  direction for an element in the chamber is

$$\rho_0 \frac{\partial u'_z}{\partial t} = - \frac{\partial p'}{\partial z}$$

Therefore, Equation B-26 becomes:

$$\left(\frac{1}{\rho_{0,1}} \frac{\partial p'_1}{\partial z}\right)_{z=z_1} = \left(\frac{1}{\rho_{0,2}} \frac{\partial p'_2}{\partial z}\right)_{z=z_2}$$

or, neglecting second order effects,

$$\left(\frac{\frac{\partial p'_1}{\partial z}}{\frac{\partial p'_2}{\partial z}}\right)_{z=z_2} = \frac{T_{0,2}}{T_{0,1}} \quad (\text{B-30})$$

Substitution of Equation B-22 into Equation B-20 yields  $\beta_1 = 0$ , and at  $z = z_2$

$$p'_1 = A_1 f_1(\phi, r) \cos n_1 z_2 e^{-i\omega_1 t} \quad (\text{B-31})$$



# Contrails

and

$$\frac{\partial P_1'}{\partial z} = -n_1 A_1 f_1(\phi, r) \sin n_1 z_L e^{-i\omega t} \quad (\text{B-32})$$

Equation B-23 substituted into Equation B-21 yields

$$B_2 = A_2 \tan n_2 L$$

$$(P_2')_{z=z_L} = A_2 f_2(\phi, r) (\cos n_2 z_L + \tan n_2 L \sin n_2 z_L) e^{-i\omega t} \quad (\text{B-33})$$

and

$$\left(\frac{\partial P_2'}{\partial z}\right)_{z=z_L} = -n_2 A_2 f_2(\phi, r) (\sin n_2 z_L - \tan n_2 L \cos n_2 z_L) e^{-i\omega t} \quad (\text{B-34})$$

Insertion of Equations B-32 and B-34 into Equation B-30 gives:

$$\frac{n_1 A_1 f_1(\phi, r) \sin n_1 z_L}{n_2 A_2 f_2(\phi, r) (\sin n_2 z_L - \tan n_2 L \cos n_2 z_L)} = \frac{T_{0,2}}{T_{0,1}} \quad (\text{B-35})$$

and insertion of Equations B-31 and B-33 into Equation B-24 gives:

$$\frac{A_1 f_1(\phi, r)}{A_2 f_2(\phi, r)} = \frac{\cos n_2 z_L + \tan n_2 L \sin n_2 z_L}{\cos n_1 z_L} \quad (\text{B-36})$$

Combination of Equations B-35 and B-36, after some manipulation leads to:

$$\frac{n_1 \tan n_1 z_L}{n_2 \tan n_2 (z_L - L)} = \frac{T_{0,2}}{T_{0,1}} \quad (\text{B-37})$$

Defining two parameters  $\nu_1$  and  $\nu_2$  as follows:

$$\nu_1 = \frac{n_1 z_L}{\pi}$$

$$\nu_2 = \frac{n_2 (L - z_L)}{\pi}$$

# Contrails

then Equation B-37 becomes:

$$\left( \frac{L - z_2}{z_2} \right) \frac{z_1 \tan z_1 \pi}{z_1 \tan z_2 \pi} = - \frac{T_{0,2}}{T_{0,1}} \quad (\text{B-38})$$

In the above equation, the unknown quantities are  $z_1$  and  $z_2$ ; another relation between them is required in order to solve the problem. This relation is provided by the requirement that the frequency of oscillation in region 1 is equal to the frequency in region 2, that is,  $\omega_1 = \omega_2$ . It is a further requirement, that the transverse component mode shapes be the same in the two regions, that is,  $m_1 = m_2$ ,  $\beta_1 = \beta_2$  and, therefore,  $\beta_{m,\beta,1} = \beta_{m,\beta,2}$ .

Equating the frequency in the two regions yields

$$\frac{C_{0,1}}{2\pi} \sqrt{\alpha_1^2 + \beta_1^2} = \frac{C_{0,2}}{2\pi} \sqrt{\alpha_2^2 + \beta_2^2}$$

Substituting  $\beta_{m,\beta}$  and  $z$  into the above relation and neglecting the differences in specific heat ratio between the two regions, the relation becomes

$$\frac{\beta_{m,\beta}^2 + \left( \frac{z_1 a}{z_2} \right)^2}{\beta_{m,\beta}^2 + \left( \frac{z_2 a}{L - z_2} \right)^2} = \frac{T_{0,2}}{T_{0,1}} \quad (\text{B-39})$$

For given combustor geometry, temperature ratio, and transverse mode shape, Equations B-38 and B-39 can be solved simultaneously to determine the longitudinal components of oscillation  $z_1$  and  $z_2$  in the two temperature regions. From these results the frequency of oscillation can be computed from:

$$f = \frac{C_{0,1}}{2} \left[ \left( \frac{\beta_{m,\beta}}{a} \right)^2 + \left( \frac{z_1}{z_2} \right)^2 \right]^{1/2}$$

and the dimensionless frequencies from:

$$f_1' = \left[ \beta_{m,\beta}^2 + \left( \frac{z_1 a}{z_2} \right)^2 \right]^{1/2}$$

$$f_2' = f_1' \left( \frac{T_{0,1}}{T_{0,2}} \right)^{1/2}$$

# Contrails

Using a graphical method to solve Equations B-38 and B-39,  $\alpha_1$  and  $\alpha_2$  have been evaluated for the following conditions:

$$\begin{aligned}L/a &= 2.0 \\z_2/L &= 1/2 \text{ and } 1/4 \\T_{0,2}/T_{0,1} &= 1 \text{ to } 7 \\B_{m,y} &= 0.405 \text{ (first transverse mode with } a/b = 1.5) \\B_{m,y} &= 1.0 \text{ (approximately third transverse with } a/b = \\& \quad 1.1 \text{ to } 1.5) \\B_{m,y} &= 3.14 \text{ (first transverse and first radial with } \\& \quad a/b = 1.5 \text{ or third transverse and first radial } \\& \quad \text{circular cylinder).}\end{aligned}$$

Figure 25 shows the results for  $B_{m,y} = 1.0$  and  $z_2/L = 1/2$ . Only the first few solutions to the equations are presented; these show that for a given solution, the longitudinal mode number of region 1 (the cold side of the flame front) increases and the mode number of region 2 decreases, as the temperature ratio is increased. A point is reached, however, where the wave number of region 2 becomes zero and any further increase in the temperature ratio must lead to a jump to the next higher mode number. Accompanying the jump in  $\alpha_2$ , the mode number of region 1,  $\alpha_1$ , must also jump to the next higher mode. The heavy line in Figure 25 traces the path of the lowest mode of oscillation as the temperature ratio is varied and shows the mode number of region 2 to vary between 0 and approximately 0.5 and that of region 1 to increase continuously. The frequencies of oscillation corresponding to the lowest mode are presented in Figure 26 and are seen to increase steadily with a superimposed series of jumps. (The arbitrarily chosen conditions for which the frequencies were evaluated are: sonic velocity of the gases in region 1 = 1000 ft per sec, diameter of chamber = 2 ft.)

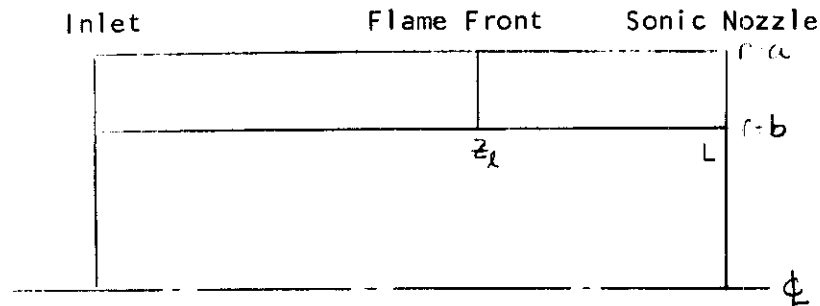
The effect of increasing the transverse mode parameter,  $B_{m,y}$ , is to compress the temperature scale of the figures as shown by the results plotted in Figures 27 and 28 for  $B_{m,y} = 3.14$  and also in Figures 29 and 30 for  $B_{m,y} = 0.405$  which, of course, shows the reverse effect. Figure 31 shows how the position of the discontinuity in the chamber influences the longitudinal mode shapes; here the effect is merely to displace the values of  $\alpha_1$  and  $\alpha_2$  roughly in proportion to the change in length of the respective zones.

## PREDICTION OF FREQUENCIES OF OSCILLATION IN ACTUAL BURNERS

The purpose of this section is to establish the range of frequencies of oscillation which are likely to be encountered in actual gas-turbine burners. In addition, a comparison is made between frequencies measured in a full scale duct burner and frequencies estimated for conditions approximating those of the burner. This will provide an indication of the acceptability of the simplifications made in the analysis. The data for the comparison are provided by tests on the duct burner of the Pratt and Whitney SST engine which are reported in Reference 9. The geometry of the

# Contrails

Pratt and Whitney duct burner has been simplified for the purpose of the analysis to that of an annular duct of the dimensions shown in the sketch below:



The values of the dimensions are given by:

$$\text{Annulus Radius Ratio, } a/b = 1.3$$

$$\text{Flame Front Position, } z_f/L = 0.6$$

$$\text{Length of Radius Ratio, } L/a = 2.0$$

$$\text{Outer Radius, } a = 3 \text{ ft}$$

Other simplifying assumptions made are:

1. The temperature rise due to combustion takes place at the flame front in a single step change.
2. The inlet to the annulus has the admittance of an open end.
3. The sonic nozzle at exit from the annulus has the admittance of a closed end.
4. The through-flow velocity has no effect upon the acoustics of the chamber.

The range of fuel-air ratios over which instability was experienced during the testing of the burner is 0.015 to 0.05 which, with a range of inlet temperature of 650 deg R to 1100 deg R and an average combustion efficiency of 90 per cent, corresponds to a range of temperature ratios across the flame front of 2 to 5. Up to the third transverse mode of oscillation was observed in the tests but no experience of radial components was reported. In the present estimates, therefore, only the first and third transverse modes will be analyzed. For these two cases, the values of the transverse mode number,  $\beta_{m,\gamma}$  (obtained from the first solutions of Equation B-17 for  $a/b = 1.3$  and  $m = 1$  and  $3$ ) are  $\beta_{1,0} = 0.37$  and  $\beta_{3,0} = 1.08$ , respectively.

The frequency of oscillation for the natural modes is given by the equation

# Contrails

$$f = \frac{C_{0,1}}{2} \left[ \left( \frac{\beta_{m,1}}{a} \right)^2 + \left( \frac{\nu_1}{z_2} \right)^2 \right]^{1/2}$$

where the longitudinal mode number,  $\nu_1$ , is determined from the analysis procedure presented in the previous section for various temperature ratios and for the two values of  $\beta_{m,1}$ .

The results of the analyses are shown in the following table which also includes, for interest, the values of the longitudinal mode number,  $\nu_2$ , downstream of the flame front. A mean value of the sonic velocity upstream of the flame front,  $C_{0,1}$ , was taken to be 1400 ft per sec.

First Transverse Mode,  $\beta_{1,0} = 0.37$

$T_2/T_1$	$\nu_2$	$\nu_1$	f (cps)
2	0.36	1.16	155
3	0.21	1.31	165
4	0.10	1.41	177
5	0.02	1.49	193

Third Transverse Mode,  $\beta_{3,0} = 1.08$

$T_2/T_1$	$\nu_2$	$\nu_1$	f (cps)
2	0.33	2.18	342
3	0.40	3.1	426
4	0.04	3.5	466
5	0.30	4.2	535

The above results are shown plotted in Figures 32 and 33 as frequency against temperature ratio together with a representative sample of the measured frequencies reported in Reference 9. Also included in the figures are the frequencies that would arise downstream of the flame front for the pure transverse mode oscillation; these are included to show the importance, or otherwise, of the longitudinal component introduced by the temperature discontinuity.

A comparison between the predicted and the measured frequencies indicates that the magnitude of the frequency is predicted quite well but that the trend of increasing frequency with temperature ratio cannot be discerned from the experimental measurements. The effect of the longitudinal coupling resulting from the temperature discontinuity is

# Contrails

seen to be quite significant for the lower transverse mode where the frequency is increased by as much as 25 per cent. For the third transverse mode, however, the effect of the longitudinal coupling is fairly insignificant, producing percentage increases in the frequency of the same order as the scatter in the experimental measurements (about 6 per cent).

With regard to establishing the range of acoustic frequencies which are likely to be encountered in gas-turbine burners, the frequencies in the preceding example represent the lower end of the frequency scale. This is true for the following reasons: (a) The size of the combustor considered is probably as large as any currently employed. (b) The lowest possible frequency for a given chamber generally arises in the first transverse mode. A lower limit for the frequency range sought is therefore estimated as 150 cycles per sec.

The upper limit of the frequency range is more difficult to assess because: (a) It is not easy to put a limit on the highest mode of oscillation to be expected in practice. (b) The smallest size of combustion chamber of interest is not well defined. However, the following conditions typical of a small afterburner are considered to be, at least, representative of those yielding the highest frequencies encountered in practice:

Mode of Oscillation - Third Transverse + First Radial

Chamber Geometry - Circular Duct

Diameter of Chamber - 1.0 ft

Temperature of Gas Stream - 4000 deg R

The frequency of oscillation for the above conditions can be obtained from the results presented in Figure 24, which yields  $f \approx 7500$  cps. The above estimates indicate that the plausible range of natural acoustic frequencies of gas-turbine combustors covers almost two orders of magnitude ranging from 150 cps to 7500 cps.

## CONCLUSIONS

Frequencies of natural modes of oscillation have been evaluated for a duct of annular cross-section and with either closed or open ends. The results indicate that the frequency of oscillation is the lowest for either the first transverse mode or the first longitudinal mode depending upon the annulus radius ratio and the length to diameter ratio of the chamber. The highest frequencies arise when a radial component of oscillation appears in the mode; this is particularly the case when the annulus height is small compared with the diameter.

When a temperature discontinuity in the axial direction is introduced into the analysis of the chamber, the longitudinal mode shape is modified

# Contrails

from that of a chamber with uniform temperature. As the temperature ratio across the discontinuity increases from unity, the lowest longitudinal mode shape downstream of the temperature step varies between approximately a quarter wavelength variation and no axial variation ( $\lambda$  between 0.5 and 0). Upstream of the temperature step where the temperature remains constant, the longitudinal mode factor increases continuously with temperature ratio. Comparisons of the estimated natural acoustic frequencies of a duct burner with actual measured frequencies indicate that the simplifications made in the simple acoustic analyses do not greatly affect the frequency predictions.

Also important in the evaluations of the various loss and gain mechanisms is the range of frequencies of oscillation to be expected in practice. Use has been made of the analyses presented in this appendix to evaluate this range of frequencies; the values for limits of the range are estimated to be 150 and 7500 cycles per sec.

# *Contrails*



### ASSESSMENT OF LOSS MECHANISMS

#### INTRODUCTION

The term loss mechanisms refers to the manner in which acoustic energy, that is energy existing as a result of the oscillations in the gases, is dissipated from the system considered, either as a direct loss by convection and radiation or by conversion into thermal energy. Loss mechanisms play an extremely important role in the oscillatory behavior of a combustion chamber. Clearly, if the acoustic energy dissipated is less than that supplied to an oscillation by the driving mechanism, then the oscillation will be unstable. Generally, however, the damping increases as the amplitude of the oscillation increases and a stable (though often harmful) oscillation develops. Thus, the loss mechanisms not only determine whether an initial disturbance (augmented by a driving mechanism) will lead to a divergent or convergent oscillation but also at what amplitude a divergent oscillation will stabilize.

The main purpose of the work reported in this chapter is to identify all of the loss mechanisms which could arise in a combustion chamber and then to obtain an order of magnitude estimate of each one for conditions which might be encountered in afterburners. This procedure permits several of the loss mechanisms to be rejected as being insignificant in the present study. A considerable simplification of the subsequent instability model formulation is thus achieved and further, an appreciation of the important losses is acquired.

A measure of the contribution to acoustic damping of the various loss mechanisms is most conveniently provided by the decrement of the oscillation which can be deduced as follows. For a damped oscillation, the expression for perturbed pressure may be written in the form:

$$p' = (\text{some function of position and mode shape}) \times e^{i(\omega + i\lambda)t}$$

The exponential time dependence term comprises an oscillatory part,  $e^{i\omega t}$ , where  $\omega$  is the angular frequency (which, for a damped oscillation, is a weak function of time) and a damping part,  $e^{-\lambda t}$ , where  $\lambda$  is the reciprocal of the modulus of decay. Thus, the fractional decrease in pressure amplitude over one period of oscillation (period =  $2\pi/\omega$ ) is  $e^{-2\pi\lambda/\omega}$ , where  $\omega$  is assumed to be constant over the period of oscillation. The exponent  $2\pi\lambda/\omega$  ( $= \lambda/f$  where  $f$  is the frequency of oscillation) is termed the decrement  $\delta$  of the damped oscillation and is a measure of the damping per cycle of oscillation. The decrement may also be related to the energy loss per cycle by noting that the energy in an acoustic oscillation is proportional to  $(p')^2$ ; thus, the fractional loss in energy during one cycle of oscillation is  $1 - e^{-2\delta}$ . When the rate of energy dissipation is small compared with the total energy of oscillation ( $\delta \ll 1$ ), the fractional energy loss per cycle is approximately  $2\delta$ . Therefore the decrement is a direct measure of the energy loss per cycle, provided the

# Contrails

losses are small. In the present work it is convenient to think of a separate decrement for each loss mechanism where the total decrement is the sum of the decrements of the separate losses.

Identification of the various loss mechanisms and estimates of the decrements associated with them is aided by the literature published on rocket engines where both experimental measurements and theoretical analyses of several of the losses appear. In many cases, where losses by acoustic radiation are involved, the decrement must be estimated for particular modes of oscillation from admittance functions. The relation between the decrement and the admittance coefficient of an acoustic liner, for example, is given by the following relation, which is derived in Appendix D:

$$\delta = \frac{1}{2} \ln \left( \frac{1}{1 - E_w} \right)$$

where

$$E_w = \frac{2 \rho_0 c_0 \operatorname{Re}[A]}{g_0 \left[ 1 - \left( \frac{m}{\pi \beta_{m,\nu}} \right)^2 \right] \left[ \beta_{m,\nu}^2 + \left( \frac{\nu a}{L} \right)^2 \right]^{1/2}}$$

$\operatorname{Re}[A]$  is the real part of the admittance

$\rho_0$  is the unperturbed density

$c_0$  is the sonic velocity

$a$  is the chamber diameter

$L$  is the chamber length

$m$ ,  $\nu$ , and  $\beta_{m,\nu}$  define the mode of oscillation and are defined in Appendix A.

For a nozzle, the corresponding expression for the decrement is (also derived in Appendix D):

$$\delta = \frac{1}{2} \ln \left( \frac{1}{1 - E_N} \right)$$

where, for the case of a closed-end upstream boundary,

$$E_N = \frac{\pi \nu \rho_0 c_0 a \cot(\nu \pi) \operatorname{Re}[A]}{g_0 L \left[ \beta_{m,\nu}^2 + \left( \frac{\nu a}{L} \right)^2 \right]^{1/2}}$$

A similar expression applies for the upstream radiation losses.

In the following section the various loss mechanisms are listed and described. This is followed by sections in which the decrements of the losses are estimated and then compared for relative importance. Finally,

areas are outlined in which further effort, particularly experimental effort, could be beneficially applied to the study of loss mechanisms.

## IDENTIFICATION OF THE VARIOUS LOSSES

Loss mechanisms in a combustion chamber, may be divided into two groups according to the location of the acoustic energy loss from the system. Thus, there are bulk losses which arise as a result of energy conversion within the main gas stream and there are losses at the boundaries of the chamber. The nature of the boundary losses depends upon the definition of the system boundaries; for example, losses to a chamber wall may be considered as radiation losses if the boundary is taken to be just inside the chamber wall but must be considered as energy conversion losses if the boundary is the wall itself.

Consider first the loss mechanisms in the bulk gas stream. These losses are all a result of the conversion of acoustic energy, which is represented by the amplitude of the oscillation, to internal energy of the gas stream. Four possible loss mechanisms exist:

1. Viscous Bulk Losses - These losses arise from the action of viscous stresses associated with relative fluid particle velocities, the viscous stresses tending to equalize the velocities and thereby reduce the acoustic energy.
2. Heat Conduction Losses - Acoustic waves are generally accepted as being approximately adiabatic waves and, as such, involve gradients in temperature as well as pressure and density. There is thus a tendency for heat to flow from regions of high temperature to regions of low temperature resulting in a reduction in the amplitude of the oscillation and, therefore, in a loss of acoustic energy.
3. Relaxation Bulk Losses - The pressure fluctuations of an acoustic oscillation are accompanied by fluctuations in temperature (assuming approximately adiabatic compressions and rarefactions) and therefore in internal energy of the gas stream. However, a finite length of time (relaxation time) is required for the internal energy modes (e.g., molecular vibration) of polyatomic gases to adjust themselves to changes in temperature; the delay arises in imparting the additional energy, by molecular collision, to the various internal energy modes of the molecules. This time lag between the increase or decrease in pressure and the corresponding increase or decrease in internal energy means that during some portion of the compression part of the cycle, the internal energy will be decreasing and therefore tending to oppose the pressure increase. Conversely, during some portion of the expansion part of the pressure wave, the internal energy will increase in opposition to the pressure decrease; the net result will be an attenuation of the pressure wave and a consequent decrease in acoustic energy. Clearly the damping effect will be a maximum when the pressure and internal

# Contrails

energy oscillations are 180 degrees out of phase, that is, when the time lag is equal to one-half of the period of oscillation.

4. Losses Due to Dispersed Phases in the Fluid - Dispersed phases in the gas stream can be in the form of spray droplets both upstream of the flame front and in the combustion zone or carbon particles downstream of the flame front. The losses arise from additional viscous and heat transfer losses due to the relative motion and temperature difference between the particles and the gas and also from dispersion of the acoustic waves. In the case of the fuel spray, additional attenuation of the acoustic waves is created by the influence of acoustic waves on the fuel evaporation rate resulting in temperature fluctuations which, because of a time lag, will be out of phase with the temperature oscillations in the acoustic wave.

In all cases except particle dispersion, the damping of acoustic waves in the bulk gas stream results from a phase lag between the pressure and density oscillations. Thus, the degree of damping in these cases is a strong function of frequency oscillation, being greatest when the relaxation times are of the same order as the cycle times.

Of the losses at the boundaries of the combustion chamber, consideration is given to six loss mechanisms:

1. Viscous Wall Losses - Little need be said concerning this mechanism which is similar to the viscous bulk loss mechanism with the exception that the viscous forces occur in the boundary layer of the combustion chamber wall.
2. Heat Conduction Wall Losses - Here again, little description is needed. Heat is conducted away from the temperature peaks at a higher rate than from the temperature troughs resulting in a damping of the acoustic oscillation.
3. Radiation Losses to Walls and Liners - Acoustic energy incident upon a solid combustor wall is almost entirely reflected back into the chamber. However, a small proportion of the energy is absorbed by the wall due to the flexing of the wall under the varying local pressure distribution, the energy being lost in heating the wall due to flexure and as external acoustic radiation. The absorbing properties of a wall are conveniently expressed in terms of an acoustic admittance which relates the normal component of velocity fluctuations to the pressure fluctuations and is a function of the frequency of oscillation. The wall absorption coefficient frequently encountered in acoustic work is generally based on "white" radiation (radiation of many wavelengths and incident from all directions) in which case it is not applicable to the oscillations encountered in combustion chambers which are of a single wavelength and incident from a single direction. In cases where the absorption coefficient is measured from a single-frequency, plane-wave oscillation, the

# Contrails

acoustic admittance is related to the absorption coefficient by the following relation:

$$\alpha = 1 - \left| \frac{1 - A}{1 + A} \right|^2$$

where  $\alpha$  is the absorption coefficient of the wall  
A is the complex admittance.

Acoustic damping at the circumferential boundary is often increased by the introduction of an acoustic liner located in such a manner that a small space exists between the liner and the outer wall. Perforations in the liner, together with the space behind the liner, form an array of cavities which at certain frequencies have excellent absorbing properties. The mechanisms of dispersion of acoustic energy in the cavities is the conversion of the acoustic energy to turbulent kinetic energy as the gases oscillate back and forth through the orifices (Ref 41). A disadvantage in the use of acoustic liners is that the cavities must be designed to resonant at the frequency of the acoustic oscillation, and therefore are effective only over a limited frequency range.

4. Radiation Losses from the Nozzle - Longitudinal components of oscillation in the combustion chamber experience a direct radiation loss through the open propulsion nozzle. The radiation through the nozzle is influenced by the sloping walls of the convergent portion of the nozzle from which the acoustic radiation is reflected back and forth across the nozzle eventually either leaving the nozzle exit or returning back into the chamber. The treatment of nozzle losses is very complex and is approached in terms of an admittance coefficient which depends upon nozzle geometry and frequency of oscillation.
5. Convection Losses from the Nozzle - Convection losses arise because of the through-flow velocity of gas. The acoustic energy of the oscillation exists entirely as a state or condition of the gases in the chamber. Thus, as the gases are ejected from the chamber through the nozzle, the acoustic energy "content" of the gases must be ejected with the gases. In general, the only acoustic energy carried into the chamber by the incoming gases is all or part of the energy radiated upstream from the oscillations generated within the chamber. An exception to this might arise when the oscillation under consideration is fed by fluctuating flow conditions resulting from turbomachinery blade rows upstream; this, however, would be classed as a driving mechanism and is, therefore, not considered in this appendix.
6. Radiation Losses Upstream - Acoustic energy is also lost by radiation to the upstream boundary which in general will comprise a diffuser (which, traveling in the upstream direction, will appear

# Contrails

to be a nozzle) terminating in a turbomachinery blade row. Due to a complete absence of information on the geometric properties of such a boundary, the treatment of this loss will clearly present considerable difficulty. A useful assumption which can be made, however, is that all of the energy radiated upstream is carried back into the chamber by convection.

## ESTIMATION OF THE VARIOUS LOSSES

Having established where the possible losses can arise in a combustion chamber, it is now necessary to estimate order-of-magnitude values for these losses so that unimportant loss mechanisms may be rejected from further consideration. Most of the losses are dependent upon the mode and frequency of oscillation and also upon the gross geometry of the combustor. It will, therefore, be necessary to consider all conditions which are likely to be encountered in duct burners and afterburners, before rejecting any of the mechanisms. As mentioned earlier in the chapter, the basis upon which the loss mechanisms will be assessed is the value of the decrement  $\delta$ . Estimates of the decrement for each loss mechanism will be based upon available experimental and analytical results appearing in the literature.

### BULK LOSSES

#### Viscous Bulk Losses

Viscous bulk losses may be estimated from theory presented in fundamental acoustics textbooks, for example, Reference 59. Some manipulation of the equations presented in Reference 59 leads to the following expression for the decrement,  $\delta_v$ :

$$\delta_v = \frac{8\pi^2 f \mu}{3\rho_0 c_0^2} \quad (C-1)$$

where  $f$  is frequency of oscillation cycles per sec  
 $\mu$  is viscosity of gas lbm per ft sec  
 $\rho_0$  is density of gas lbm per ft<sup>3</sup>  
 $c_0$  is acoustic velocity ft per sec.

An assumption made in the derivation of the above expression is that the time taken for the velocity to reach  $e^{-1}$  of its final value following a step change in pressure (relaxation time) is very much smaller than a period of oscillation. This assumption is seen to be valid for combustion chamber conditions from the following expression for the relaxation time (Ref 59):

$$\tau = \frac{4\mu}{3\rho_0 c_0^2}$$

# Contrails

For typical combustor conditions,  $\tau$  is of the order of  $10^{-9}$  seconds compared with  $10^{-3}$  seconds for a period of oscillation. It will be seen later that the contribution from viscous bulk damping is negligible compared with damping by other mechanisms; only the maximum possible value of the decrement is, therefore, computed for this mechanism.

Equation C-1 shows the decrement to be proportional to the frequency  $f$ ; also since  $\rho_0 c_0^2$  is almost independent of temperature and  $\mu$  increases with temperature, the maximum value of  $\delta$  will occur at high frequency of oscillation, high gas temperature and low pressure. Representative of such requirements in a gas-turbine burner might be:

Frequency = 5000 cps, maximum

Temperature = 4000 deg R, maximum

Pressure = 1 atmosphere, minimum

$$\therefore \delta_v = \frac{8\pi^2 \times 5000 \times 0.157}{3 \times 0.0066 \times 9 \times 10^6 \times 3600} \approx 10^{-4}$$

## Heat Conduction Bulk Losses

The classical acoustic approach (Ref 59) shows that the heat conduction bulk loss is related to the viscous bulk loss by the relation:

$$\frac{\delta_h}{\delta_v} = \frac{3(\gamma-1)}{4N_{Pr}}$$

where  $\delta_h$  is the decrement of heat conduction loss  
 $\gamma$  is the ratio of specific heats  
 $N_{Pr}$  is the Prandtl number.

Thus, for the combustor conditions considered in the estimate of  $\delta_v$ , the corresponding value of  $\delta_h$  is:

$$\delta_h = \frac{3 \times 0.3}{4 \times 0.85} \times 10^{-4} = 0.25 \times 10^{-4}$$

## Relaxation Bulk Losses

Attenuation of acoustic waves by molecular relaxation is a function of the gas species, the gas temperature and the frequency of oscillation. Figure 34 taken from Reference 59 shows how the decrement,  $\delta$ , varies with frequency for carbon dioxide gas; the results were obtained experimentally. The maximum attenuation occurs when the relaxation time of the molecule equals the period of oscillation. The results shown in Figure 34 suggest that at a frequency of 5000 cps, the decrement for pure carbon dioxide would

# Contrails

be approximately 0.04. However, the presence of water vapor in the gas (the case in gas-turbine burners) greatly reduces (in the manner of a catalyst) the relaxation time of the molecules to such an extent that the presence of only 1 per cent water vapor increases the frequency of maximum attenuation to beyond  $2 \times 10^6$  cps (Ref 59). Under these circumstances, the attenuation from molecular relaxation of carbon dioxide cannot be significant at the frequencies of interest. Of all the gases present in combustors, only nitrogen has a molecular relaxation time of the same order of magnitude as a typical period of oscillation, and the condition only arises in the low temperature region upstream of the flameholder. Thus, at a temperature of 1400 deg R and 2 atmospheres pressure, the relaxation time for the nitrogen molecule lies somewhere between  $0.5 \times 10^{-4}$  and  $10^{-3}$  seconds depending upon the water vapor content of the gases (Ref 61). (Some disagreement arises on this point, since Reference 59 claims that water vapor has no effect on the molecular relaxation time of nitrogen.) Thus, the range of plausible relaxation times,  $\tau$  overlaps the range of possible periods of oscillation,  $1/\omega$  ( $3 \times 10^{-5}$  to  $3 \times 10^{-4}$  seconds) and the condition for maximum attenuation, i.e.,  $\omega\tau = 1$ , could conceivably arise in a combustion chamber. An estimate of the order of magnitude of the maximum attenuation from molecular relaxation can be made from a relation presented in Reference 62 which may be rewritten as:

$$\delta = \frac{\pi R c_i \omega \tau}{c_v^0 (c_v^\infty + R)(1 + \omega^2 \tau^2)}$$

where  $R$  is the gas constant  
 $c_i$  is the specific heat of the first excited vibrational state  
 $c_v^0$  and  $c_v^\infty$  are the specific heats at constant volume for zero acoustic frequency and for infinite acoustic frequency, respectively.

At 1400 deg R,  $c_i = 1.065$  calories per mole deg C  
 $c_v^0 = 6.02$   
 $c_v^\infty = 4.96$  and for maximum attenuation,  $\omega\tau = 1$

$$\therefore \delta_{\text{MAX}} = \frac{\pi \times 1.987 \times 1.065}{6.02 (4.96 + 1.987) \times 2} = 0.08$$

Since nitrogen accounts for approximately 75 per cent of the gases, the actual decrement will be in the order of 0.06.

## Losses Due to Dispersed Phases in the Fluid

Here two separate estimates are made, one for damping due to the fuel spray and the other for carbon particles in the products of combustion. The estimates in this section are based on the work of Temkin and Dobbins at Brown University (Ref 63).



# Contrails

Particle damping is a strong function of frequency of oscillation and for this mechanism to provide a significant contribution to the acoustic damping in a combustion chamber, the period of oscillation must be close to the particle relaxation time. Figure 35 illustrates this requirement for various concentrations of water droplets in air; the quantities plotted are the decrement per unit mass concentration of droplets against the product of particle relaxation time and angular frequency of oscillation.

A theoretical relation between the decrement and the particle relaxation time has been developed by Temkin (Ref 63); the relation is

$$\delta = \frac{C_m \omega \tau_d}{1 + \omega^2 \tau_d^2} + (\gamma - 1) \left( \frac{C_p'}{C_p} \right) \frac{C_m \omega \tau_t}{1 + \omega^2 \tau_t^2} \quad (C-2)$$

where  $C_m$  is the mass concentration of particles  
 $\omega$  is angular frequency of oscillation  
 $C_p'$  is specific heat of particle  
 $C_p$  is specific heat of gas  
 $\tau_d$  is dynamic relaxation time of the particle  
 $\tau_t$  is thermal relaxation time of the particle.

The relaxation times are given by the following relations:

$$\tau_d = \frac{2R^2 \rho'}{9\mu} \quad (C-3)$$

and

$$\tau_t = \frac{R^2 C_p' \rho'}{3k} \quad (C-4)$$

where  $R$  is particle radius  
 $\rho'$  is particle density  
 $\mu$  is gas viscosity  
 $k$  is gas thermal conductivity.

Consider first the damping due to the fuel spray. Typical properties of fuel are:

$$\begin{aligned} \rho' &= 50 \text{ lbm per ft}^3 \\ C_p' &= 0.6 \text{ Btu per lbm deg F} \\ R &= 100 \text{ microns} \\ C_m &= 0.067 \text{ maximum.} \end{aligned}$$

Properties of air at 1000 deg R are:

$$\begin{aligned} \rho &= 0.037 \text{ lbm per ft}^3 \\ C_p &= 0.25 \text{ Btu per lbm deg F} \\ N_{Pr} &= 0.67 \end{aligned}$$

# Contrails

$$\begin{aligned}\delta &= 1.35 \\ \mu &= 0.07 \text{ lbm per ft h}\end{aligned}$$

Then from Equations C-3 and C-4:

$$\begin{aligned}\tau_d &= 0.043 \text{ sec} \\ \tau_t &= 0.1 \text{ sec.}\end{aligned}$$

For the ranges of frequencies of oscillation and droplet sizes experienced in gas-turbine burners, values of  $\omega\tau_d$  are always greater than unity. It therefore follows (see Figure 35 for example) that the maximum attenuation will occur at the lowest frequency of oscillation. The lowest natural frequency in gas-turbine burner chambers is of the order of 100 cps. Thus,  $(\omega\tau_d)_{min} = 27$ , which from Figure 35 is seen to give an attenuation well below the maximum value. Substitution of the above quantities into Equation C-2 yields:

$$\delta = 3.4 \times 10^{-3}$$

The effect of droplet size on the decrement is quite significant and a reduction in size from 100 microns radius (value taken above) to 50 microns results in an increase in the decrement to 0.014. The above estimates of the decrement are extremely crude since both the droplet size and the droplet mass distribution have been taken to be uniform over the chamber volume. In addition, the effects of droplet vaporization have been ignored. However, it is felt that the above calculations serve the intended purpose of obtaining an indication of the order of magnitude of the loss involved. Should the loss mechanism prove to be an important one, a more thorough investigation of the mechanism could be carried out.

The second source of particle attenuation lies in the carbon particles in the products of combustion. Equations C-2, C-3, and C-4 employed in the estimate of fuel-spray attenuation apply also in this case. Typical properties of carbon particles are:

$$\begin{aligned}\rho' &= 100 \text{ lb per ft}^3 \\ C_p' &= 0.4 \\ R &= 1 \text{ micron maximum} \\ C_m &= 0.06 \text{ maximum possible}\end{aligned}$$

The above value for  $C_m$  assumes that all of the carbon in the products of combustion is free carbon; this condition would never, of course, be experienced in practice (a more realistic value of  $C_m$  would be 0.0006). Properties of air at 3000 deg R are:

$$\begin{aligned}\rho &= 0.01 \text{ lb per ft}^3 \\ C_p &= 0.32 \text{ Btu per lbm deg F} \\ \mu &= 0.15 \text{ lbm per ft} \\ N_{Pr} &= 0.8 \\ \delta &= 1.3.\end{aligned}$$

Then from Equations C-3 and C-4:

$$\begin{aligned}\tau_d &= 6 \times 10^{-6} \\ \tau_t &= 9 \times 10^{-6}\end{aligned}$$

In this case the product  $\omega\tau_d$  is less than unity for the range of frequencies of interest and, therefore, maximum attenuation will occur at the highest frequency experienced. For the gas-turbine burner, a typical (high) natural frequency of oscillation is of the order of 5000 cps; the corresponding value of  $\omega\tau_d$  is 0.18. Substitution of the above quantities into Equation C-2 yields  $\delta = 0.016$ .

For the conditions encountered here, the decrement is approximately proportional to frequency of oscillation, particle size and particle concentration. In the above estimate of the decrement, values of the quantities were chosen so as to obtain an upper limit for the decrement. The particle concentration in particular is unlikely to approach anywhere near the value chosen; it may be safely assumed, therefore, that the decrement due to carbon (smoke) particle damping will be much less than the value 0.016 indicated above.

## BOUNDARY LOSSES

Boundary losses are somewhat more complicated than bulk losses because they depend upon the mode shape of the oscillation, that is the direction in which the net wave is propagating, whereas bulk losses depend upon the mode shape only through the frequency of oscillation. In order to make estimates of the decrements for boundary losses, it will be necessary to specify mode shapes. Observations of combustion instabilities in gas-turbine burners suggest that the mode of oscillation is generally tangential; it was seen in the Appendix A, however, that due to the flame front and to the chamber-end boundary conditions, some coupling of the longitudinal components must also be present. The simple approach that is taken in the following estimates of boundary losses is to compute a decrement for each component of oscillation, that is, a tangential decrement,  $\delta_t$ , a radial decrement,  $\delta_r$ , and a longitudinal decrement  $\delta_l$ . It seems reasonable to suppose that the decrement of the resultant oscillation is the sum of the decrements of the components:

$$\delta = \delta_t + \delta_r + \delta_l$$

## Viscous Wall Losses

Reference 59, for example, provides a theoretical analysis of the viscous wall loss for a longitudinal mode oscillation. Slight manipulation of the result presented yields the following relation for the longitudinal decrements:

# Contrails

$$\delta_l = \frac{1}{a} \left[ \frac{\pi \mu}{f \rho_0} \right]^{1/2} \quad (C-5)$$

where  $a$  is the radius of the chamber. This equation shows that the decrement increases with temperature and decreases with pressure, chamber diameter, and frequency (if the above relation is employed to determine the longitudinal decrement of a coupled longitudinal-transverse mode, the frequency employed will be that of the resultant oscillation). The following conditions should provide an upper limit for the longitudinal viscous wall damping:

$$a = 0.5 \text{ ft}$$

Temperature = 200 deg R (near the wall)

Pressure = 1 atmosphere

$$f = 2000 \text{ cps (first longitudinal with } L = 1 \text{ ft)}$$

From Equation C-5, then,  $\delta_l = 3.2 \times 10^{-3}$ .

Reference 7 presents a relation which extends Equation C-5 to include any mode of oscillation; this relation can be written to give the decrement as:

$$\delta = \frac{T_w}{a T_0} \left[ \frac{2 \mu_w}{c_0 \rho_w} \right]^{1/2} \frac{\left[ \left( \frac{2}{L} \right)^2 + \left( \frac{m}{a} \right)^2 \right]}{\left[ 1 - \left( \frac{m}{\pi \beta_m r} \right)^2 \right] \left[ \left( \frac{2}{L} \right)^2 + \left( \frac{\beta_m r}{a} \right)^2 \right]^{5/4}} \quad (C-6)$$

It will be noted that in addition to the effects of complex mode shapes, Equation C-6 also takes account of the effects of a temperature difference between the wall (suffix  $w$ ) and the mean bulk gas stream (suffix  $c$ ). Evaluation of  $\delta$  from Equation C-6 for the first transverse mode produces a value of  $3.7 \times 10^{-3}$  which is almost the same as that for the first longitudinal mode. Other modes of oscillation will merely produce lower values of  $\delta$ .

Experimental measurements have been made of acoustic losses in a model rocket combustion chamber (Ref 64) which are claimed to be predominantly viscous wall losses. The experimental procedure employed was to establish a particular mode of oscillation in the chamber by means of an acoustic driver and then to monitor the pressure decay after switching off the driver. All three principal modes of oscillation were investigated. The evidence leading to the conclusion that the losses were viscous wall losses was as shown on the following page:

# Contrails

1. The chamber was closed, thus eliminating convection losses.
2. The walls were rigid and solid, thus eliminating radiation losses.
3. Losses in the longitudinal mode are correlated by an effective chamber length.
4. Losses in the transverse mode are correlated by the internal surface to volume ratio.

Figure 36 presents the variation of the decrement,  $\delta$  with the internal surface area to volume ratio for the first standing transverse mode. The results shown do not appear to follow the trends predicted by the simple theory which are given by Equation C-6 as  $\delta$  proportional to (diameter)<sup>-1/2</sup>. Extrapolation of the experimental data shows that zero decrement does not occur at zero surface-to-volume ratio but at some quite significant finite value. This may be due in part to the effects of the chamber ends which are not taken into account by the theory. The most significant discrepancy, however, between the experimental results and the theoretical predictions is the value of the decrement, which is underestimated by the theory by more than an order of magnitude. This discrepancy was noted by the authors in Reference C-6 but no explanation was offered.

Similar results were obtained for the first longitudinal mode where the decrement was found to be correlated by an effective chamber length as shown in Figures 37 and 38. This effective acoustic length takes account of the nozzle convergence angle (the nozzle was plugged at the throat). Again, the measured decrements are seen to be much larger than those predicted by the simple theory.

The radial mode of oscillation experienced very little damping no doubt because only the end walls contribute any viscous damping in this mode. The table below shows a comparison of the decrement of each of the three fundamental modes of various chamber lengths.

Total Length,		Mode					
		Longitudinal		Transverse		Radial	
in	cm	Coefficient of Decay per Cycle,	Resonant Frequency, cps	Coefficient of Decay per Cycle,	Resonant Frequency, cps	Coefficient of Decay per Cycle,	Resonant Frequency, cps
12	30.48	0.1295	598	0.0304	1364	0.00564	2368
10	25.40	0.0642	728	0.0389	1360	0.00963	2871
8	20.32	0.0350	921	0.0419	1362	0.01165	2944
6	15.24	0.0383	1241	0.0524	1370	0.00822	2794
4	10.16	0.0252	1905	0.0721	1389	0.00880	2729

# Contrails

## Heat Conduction Wall Losses

From theoretical considerations (Ref 59), the heat conduction wall losses are related to the viscous wall losses by:

$$\delta_{hc} = \delta_v \frac{\gamma^{1/2} - \gamma^{-1/2}}{N_{Pr}^{1/2}}$$

where  $\delta_{hc}$  is the decrement for heat conduction losses  
 $\delta_v$  is the decrement for viscous wall losses  
 $\gamma$  is the ratio of specific heats  
 $N_{Pr}$  is the Prandtl number of the gas.

For typical combustion chamber conditions, the heat-conduction decrement is less than the viscous wall decrement by a factor of approximately 0.3.

## Radiation Losses to Acoustic Liners

Estimates of radiation losses to perforated liners can be made from the rather limited experimental data on acoustic admittance coefficients for liners appearing in the literature (Refs 65 and 66). In Appendix D, a relation is derived between the decrement and the real part of the admittance for the case of a circular cylinder. The relation derived is:

$$\delta = \frac{1}{2} \ln \left( \frac{1}{1 - E_w} \right)$$

where

$$E_w = \frac{2 \rho_0 c_0 \operatorname{Re}[A]}{\rho_0 \left[ 1 - \left( \frac{m}{\pi \beta_{m,y}} \right)^2 \right] \left[ \beta_{m,y}^2 + \left( \frac{2a}{\lambda} \right)^2 \right]^{1/2}} \quad (C-7)$$

and  $\operatorname{Re}[A]$  is the real part of the admittance  $A$ . Acoustic liner data appearing in the literature are presented in terms of the complex acoustic reactance  $\mathcal{F}$  rather than the admittance  $A$ ; the two quantities are related by:

$$\mathcal{F} = \theta + i\chi = \frac{1}{A} = \frac{1}{\kappa + i\sigma}$$

Thus, the real part of the admittance which is required in Equation C-7 is given by:

$$\operatorname{Re}[A] = \kappa = \operatorname{Re} \left[ \frac{1}{\mathcal{F}} \right] = \frac{\theta}{\theta^2 + \chi^2} \quad (C-8)$$

This means that the loss associated with the acoustic liner is dependent upon both the real and imaginary parts of the acoustic impedance of the liner.

The impedance of a liner is a function of the frequency of oscillation, the amplitude of oscillation, the velocity of flow past the liner and also the velocity through the liner. From the evidence that is available, it would appear that  $Re[A]$  increases with amplitude of the disturbance and with velocity both through and past the liner. The effect of frequency, however, is to provide maximum damping at some frequency which is a characteristic of the liner design.

Figures 39 and 40 show variations with frequency of the real and imaginary parts of the acoustic impedance of a liner, measured by Pratt and Whitney (Ref 65). The imaginary part of the impedance, termed the reactance, is presented as a capacitance and an inductance; the reactance is obtained by summing its two components. The decrement, calculated from Equations C-7 and C-8 for a cylindrical chamber of diameter 10 inches and with a gas temperature of 2000 deg R, is plotted against frequency in Figure 41. The result shows how the damping decreases at either side of the resonant frequency. At the resonant frequency of 2200 cycles per sec, the decrement reaches the maximum value of 0.38.

The influence of the amplitude of the oscillation upon the impedance is shown by the data of Reference 65 which are plotted in Figure 42. Both the real and imaginary parts of the impedance remain essentially constant up to an intensity level of about 140 db when the real part (resistance) suddenly increases. This increase in resistance at high amplitudes is attributed to nonlinear effects resulting from flow changes and increased turbulence in the orifices of the liner. The nonlinear region was investigated experimentally by Blackman (Ref 67); the results are shown, in Figure 43, in terms of a nonlinear correction factor  $\Delta_{nl}$  which is incorporated in Blackman's equation for acoustic resistance as follows:

$$\theta = \frac{4}{\sigma \rho_0 c_0} \left( \frac{\pi \mu \rho_0 f}{g_0} \right)^{1/2} \left( 1 + \frac{t}{d} + \frac{\Delta_{nl}}{d} \right)$$

where  $\sigma$  is the fraction of open area of the resonator array and the terms  $1$ ,  $t/d$ , and  $\Delta_{nl}$  represent the facing, neck, and nonlinear losses, respectively. The nonlinear correction factor has also been evaluated by Garrison (Ref 65) and is shown in Figure 44 together with a line representing Blackman's data. Considerable difference between the two sources of data is evident and this is explained by Garrison (Ref 42) to result from differences in the methods of taking results and from an effect due to facing thickness. Figures 43 and 44 should therefore be taken merely as examples of how the amplitude can affect the resistance of an acoustic liner.

The effects of amplitude upon the decrement,  $\delta$ , can be seen by taking the results shown in Figure 42 and reevaluating them in terms of decrement and pressure amplitude for a particular combustion chamber configuration. Figure 45 shows the results plotted in this manner for a circular chamber of 10 inches diameter with a gas temperature of 2000 deg R, and oscillating in the first transverse mode.

# Contrails

Effects of a flow velocity past acoustic liners have not been investigated to the extent where useful information can be extracted. A flow velocity through acoustic liners has been investigated experimentally by McAuliffe (Ref 68) and the effects on resistance ratio and reactance ratio are shown in Figure 46, where the ratios are based upon the values at zero velocity. The effect of the velocity on the decrement depends upon the relative values of resistance,  $\theta$ , and reactance,  $\chi$ , at zero velocity. Thus, for low amplitude oscillations where  $\theta_0^2 \ll \chi_0^2$ , the decrement increases with through-flow velocity. For high amplitude oscillations, however, where  $\theta_0 = O(\chi_0)$ , the decrement decreases with velocity. The following table illustrates the effect:

<u>Sound Pressure Level (db)</u>	<u>Decrement at Velocity</u> <u>Decrement at Zero Velocity</u>	
	<u>Vel. = 7 ft/s</u>	<u>Vel. = 20 ft/s</u>
120	2.9	5.2
150	0.73	0.16

## Convection Losses from the Nozzle

A method of assessing this loss is to include a through-flow velocity in the acoustic analysis of the combustion chamber. Such an analysis has been carried out, for a one-dimensional longitudinal oscillation in a circular duct, by Whitehead (Ref 71). The analysis was performed for both varying duct Mach number and varying exit Mach number; the results for an exit Mach number of unity, which is the case of interest here, have been extracted and replotted in Figure 47 as decrement,  $\delta$ , against duct Mach number. Since the decrement is a measure of the energy lost per cycle, the lowest mode and therefore lowest frequency of oscillation produces the highest decrement. It is probable, therefore, that for a coupled transverse longitudinal mode, the decrement would be substantially less than that shown in Figure 47 for the fundamental longitudinal mode.

## Radiation Losses from the Nozzle

An estimate of the decrement for nozzle radiation losses associated with a longitudinal component of oscillation can be obtained by solving the wave equation with the nozzle boundary condition represented by a complex admittance coefficient. The solution to the wave equation in this case differs from the solution presented in the last chapter which was for the case where energy gains and losses were excluded. The form of the solution for a damped oscillation was given in the introduction to this appendix as:

$$p' = f(r, \phi, z, v, m, \delta) e^{i(\omega + i\lambda)t}$$



# Contrails

The real and imaginary parts of the complex frequency  $(\omega + i\lambda)$  can be evaluated from specified boundary conditions and then the decrement is obtained from:

$$\delta = \frac{2\pi\lambda}{\omega}$$

In Appendix E, the decrement has been evaluated for the case of a closed upstream boundary, zero through flow velocity and pure longitudinal oscillation. The results are plotted in Figures 48 and 49 for constant real part,  $\kappa$ , and constant imaginary part,  $\sigma$ , of the admittance, respectively. Also plotted in the figures is the longitudinal mode number,  $\nu$ , for the lowest mode. For the range of  $\sigma$  considered (which from Ref 1 appears to represent the range to be expected) the decrement is quite insensitive to the imaginary part of the admittance. The real part of the admittance, has a considerable effect on the decrement which is zero at zero  $\kappa$  (solid wall value) and rises to a fairly sharp maximum and then falls back to zero as  $\kappa$  becomes very large (open end value). For the value of  $\sigma$  chosen, the decrement reaches a peak value of 2.5.

Experimental measurements have been made (Refs 69 and 70) from which the decrement can be calculated for longitudinal, damped oscillations in a cylindrical chamber with a nozzle. However, in both of the references cited, the tests were carried out with a through-flow velocity, in order to provide a sonic nozzle condition. Thus, the nozzle radiation losses were accompanied by convection losses through the nozzle. The results of the measurements are shown in Figures 50 and 51 which show the decrement as a function of nozzle entry Mach number. Ideally, it should be possible to subtract the losses due to nozzle convection from the above results and thus obtain the losses due to nozzle radiation. However, if this is attempted using the estimates of nozzle convection from the last section it is seen that the estimated convection loss is greater than the combined convection and radiation loss. It is evident, therefore, that the nozzle convection is somewhat overestimated by the simple theory presented in Reference 71.

## Radiation Losses Upstream

The treatment of this case is exactly the same as that of the nozzle radiation and the results shown in Figures 48 and 49 apply equally well to the upstream boundary. However, at the present time, knowledge of acoustic behavior of turbomachinery blade rows is nonexistent, and, therefore, estimates of the decrement for this particular loss mechanism are not possible. It is unlikely, however, that this loss would be as great as the loss through the propulsion nozzle because of the relatively large area blockage presented by turbomachinery blade rows.

## EVALUATION OF THE IMPORTANCE OF THE VARIOUS LOSSES

Having made estimates of the order of magnitude of the various losses, the next step is to reject from further consideration those losses which are

# Contrails

unimportant relative to others. A comparison of the estimates of the losses is made in the following table.

<u>Loss Mechanism</u>	<u>Decrements</u>	<u>Comments</u>
1. Viscous - Bulk	$\sim 10^{-4}$	} Calculated from fundamental acoustic theory.
2. Heat Conduction - Bulk	$\sim 0.25 \times 10^{-4}$	
3. Relaxation - Bulk	$\sim 0.06$	Could be considerably less than this value due to the presence of water vapor.
4. Fuel Spray Damping	$0.34 \times 10^{-2}$	Based on a droplet size of 100 microns. Decrement varies inversely with square of drop size.
5. Carbon Particle Damping	0.016	Assumes all carbon in products is "free".
6. Viscous - Wall	$0.37 \times 10^{-2}$	Calculated for first transverse mode.
	0.08	Measured (Ref 64) for first transverse mode.
	0.13	Measured (Ref 64) for first longitudinal mode.
7. Heat Conduction - Wall	$0.12 \times 10^{-2}$	Calculated transverse mode of oscillation.
8. Radiation to Liners	0.4	Calculated at the characteristic frequency of the liner. Strong function of amplitude, and velocity through and past liner.
9. Nozzle Convection	1	Fundamental longitudinal mode - increases with duct Mach number.
10. Nozzle Radiation	$\sim 1$	A function of the nozzle characteristics and frequency of oscillation.
11. Radiation Upstream	Probably $\ll 1$	No data available and difficult to assess theoretically.

# *Contrails*

The foregoing comparison indicates that nozzle convection and nozzle radiation are the mechanisms which provide the most significant acoustic energy loss per cycle. For a predominantly transverse mode of oscillation when the nozzle losses are a minimum (but still significant), the damping from acoustic liners is a maximum and provides a major contribution to the over-all damping. Which of these three mechanisms is the predominant one in a particular case will depend upon many factors including the mode and frequency of oscillation, geometry of the chamber, design of the nozzle and of the acoustic liner (if any) and the temperature, pressure, and velocity of the gases in the chamber. Thus, with the exceptions of those losses just discussed and the possible exceptions of the viscous wall losses (according to the experimental measurements of Ref 64) and the upstream radiation losses, the remaining losses can be disregarded in the subsequent instability model formulation.

# *Contrails*

## Appendix D

### LOSS DECREMENTS

#### RADIATION LOSSES TO THE WALLS

The wall loss is derived, initially, as the fraction of the total energy of the oscillation which is lost to the walls per cycle of oscillation. This fraction may be written as:

$$E_w = \frac{\text{energy absorbed at walls per second}}{\text{total energy of vibration through chamber volume} \times \text{frequency}}$$

it is related to the decrement of the oscillation,  $\delta$ , by:

$$E_w = 1 - e^{-2\delta}$$

or

$$\delta = \frac{1}{2} \ln \left( \frac{1}{1 - E_w} \right)$$

and for  $\delta \ll 1$ ,

$$\delta \approx \frac{1}{2} E_w$$

#### ENERGY ABSORBED AT THE WALLS

Acoustical energy crossing a boundary per unit time and area is

$$\dot{E}'' = p u_n'$$

where  $p = p_0 + p'$   
 $u_n'$  is normal velocity component

Because the wall, in general, will not be rigid, a phase difference exists between the pressure and velocity perturbations. Expressing this phase effect by writing

$$p' = F_p(r, \phi, z, n, z, \delta') e^{i\omega t}$$

and

$$u_n' = F_u(r, \phi, z, n, z, \delta') e^{i(\omega t + \xi)}$$

Then

$$\dot{E}'' = [p_0 + F_p \cos(\omega t)] [F_u \cos(\omega t + \xi)] \quad (D-1)$$

# Contrails

The time-average value of  $\dot{E}''$  is given by

$$\bar{\dot{E}}'' = \frac{\omega}{2\pi} \int_0^{2\pi/\omega} \dot{E}'' dt$$

which in view of Equation D-1 is

$$\bar{\dot{E}}'' = \frac{1}{2} F_p F_u \cos \xi \quad (D-2)$$

Introducing an admittance coefficient  $A_w = \kappa + i\sigma_w$  where

$$A_w = \frac{u'_w}{p'} = \frac{F_u e^{i\xi}}{F_p}$$

then

$$\kappa_w = \frac{F_u}{F_p} \cos \xi ; \quad \sigma_w = \frac{F_u}{F_p} \sin \xi \quad (D-3)$$

Equations D-2 and D-3 give:

$$\bar{\dot{E}}'' = \frac{\kappa_w}{2} F_p^2$$

where  $\kappa_w$  is termed the conductance of the wall. Therefore, the total rate of energy absorbed at the wall is:

$$\bar{\dot{E}} = \frac{1}{2} \int_S \kappa_w F_p^2 dS$$

If the walls considered are those of a cylinder and  $\kappa_w$  is uniform, then

$$\dot{E} = \frac{\kappa_w a}{2} \iint_{r=a} (F_p^2) d\phi dz \quad (D-4)$$

## TOTAL ENERGY OF VIBRATION IN CHAMBER

The total acoustic energy of a standing wave in an enclosure is given by (Ref 58):

$$E_t = \frac{g_0}{2\rho_0 c_0^2} \int_V \left[ \frac{\rho_0^2 c_0^2 (\dot{u}')^2}{g_0^2} + (p')^2 \right] dV$$

# Contrails

The integrand in the preceding relation consists of a kinetic energy term and a potential energy term. Each of these energy terms is a function of time (as well as position) but the sum of the terms must be independent of time (assuming negligible losses in the volume and no energy addition). The pressure fluctuation has the form

$$p' = F_p e^{-i\omega t}$$

where  $F_p$  is the maximum value of  $p'$ . When  $t$  is a maximum,  $(\rho_0^2 c_0^2 / g_0^2) (\underline{u}')^2$  is zero. Evaluating the energy integral at this period of time, that is when  $\underline{u}'$  is zero and  $p'$  is a maximum, then

$$E_t = \frac{g_0}{2\rho_0 c_0^2} \int_V F_p^2 dV$$

## WALL-LOSS DECUREMENT

The energy loss fraction at the wall,  $E_w$  is given by:

$$E_w = \frac{\bar{E}}{E_t}$$

Substitution of the expressions derived for  $\bar{E}$  and  $E_t$  gives:

$$E_w = \frac{\frac{\kappa_w a}{2} \iint (F_p)_{r=a}^2 d\phi dz}{\frac{g_0}{2\rho_0 c_0^2} \int_V F_p^2 dV}$$

For the case of a circular cylinder, the pressure amplitude function,  $F_p$ , can be written as:

$$F_p = f_1(\phi) f_2(z) J_m(\alpha r)$$

# Contrails

therefore,

$$E_w = \frac{\rho_0 c_0^2 K_w}{g_0 t} \left[ \frac{a J_m^2(\alpha a)}{\int_0^a J_m^2(\alpha r) r dr} \right]$$

$$E_w = \frac{\rho_0 c_0^2 K_w a J_m^2(\alpha a)}{f g_0 \frac{a^2}{2} \left[ 1 - \left( \frac{m}{\alpha a} \right)^2 \right] J_m^2(\alpha a)}$$

$$E_w = \frac{2 \rho_0 c_0^2 K_w}{f a g_0 \left[ 1 - \left( \frac{m}{\alpha a} \right)^2 \right]}$$

The frequency of oscillation is given by:

$$f = \frac{c_0}{2\pi} (\alpha^2 + n^2)^{1/2}$$

Therefore,

$$E_w = \frac{4\pi \rho_0 c_0 K_w}{a g_0 \left[ 1 - \left( \frac{m}{\alpha a} \right)^2 \right] (\alpha^2 + n^2)^{1/2}}$$

In terms of the dimensionless quantities,  $K_w' = K_w \rho_0 c_0 / g_0$ ,  $\nu = nL/\pi$ , and  $\beta = \alpha a / \pi$ ,  $E_w$  becomes:

$$E_w = \frac{4 K_w'}{\left[ 1 - \left( \frac{m}{\pi \beta} \right)^2 \right] \left[ \beta^2 + \left( \frac{\nu}{L} \right)^2 \right]^{1/2}}$$

The decrement  $\delta_w$  is related to the above quantity by:

$$\delta_w = \frac{1}{2} \ln \left( \frac{1}{1 - E_w} \right)$$

## RADIATION LOSSES THROUGH THE NOZZLE

Following a similar procedure to that in the previous section, the



# Contrails

fraction of the total energy of the oscillation which is radiated through the nozzle per cycle of oscillation is given by:

$$E_N = \frac{\rho_0 c_0^2 K_N \iint (F_p^2)_{z=L} r d\phi dr}{fg_0 \int_V F_p^2 dV}$$

The form of the pressure amplitude function,  $F_p$ , depends upon, among other things, the end boundary conditions. For simplicity the case of a closed upstream boundary will be considered which leads to the following form for  $F_p$ :

$$F_p = f_1(\phi) f_2(r) \cos n z$$

The value of  $n$  depends upon the nozzle boundary condition. Substitution of this expression for  $F_p$  into the relation for  $E_N$  yields:

$$E_N = \frac{\rho_0 K_N c_0^2}{fg_0} \times \frac{\cos nL}{\int_0^L \cos n z dz}$$

$$E_N = \frac{n \rho_0 c_0^2 K_N \cot(nL)}{fg_0}$$

Introducing into the above expression the dimensionless quantities  $\nu$ ,  $\beta$ , and  $K'_N$  and also the relation for the frequency, it becomes:

$$E_N = \frac{\pi \nu a K'_N \cot(\nu \pi)}{L [\beta^2 + (\frac{\nu a}{L})^2]^{1/2}}$$

The decrement associated with the nozzle radiation loss is given by:

$$\delta_N = \frac{1}{2} \ln \left( \frac{1}{1 - E_N} \right)$$

# *Contrails*

## Appendix E

### DOWNSTREAM BOUNDARY REPRESENTED BY A COMPLEX ADMITTANCE

A pure longitudinal mode of oscillation is considered. The effects on the perturbed pressure distribution of a through-flow velocity are neglected (alternatively, the case of zero through-flow velocity is considered).

Within the above limitations, the perturbed pressure can be represented by the following expression:

$$p' = [C e^{i(\omega+i\lambda)z/c_0} + D e^{-i(\omega+i\lambda)z/c_0}] e^{i(\omega+i\lambda)t} \quad (E-1)$$

where  $C$  and  $D$  are constants,  $(\omega+i\lambda)$  is the complex frequency,  $\lambda$  represents damping, and  $\omega$  is the angular frequency. For simple-harmonic oscillations,

$$\frac{\partial u'_z}{\partial t} = i(\omega+i\lambda)u'_z \quad (E-2)$$

where  $u'_z$  is the longitudinal component of velocity. From momentum considerations in the axial direction:

$$\frac{\partial u'_z}{\partial t} = -\frac{g_0}{\rho_0} \frac{\partial p'}{\partial z} \quad (E-3)$$

From Equations E-1, E-2, and E-3:

$$u'_z = -\frac{i(\omega+i\lambda)g_0}{\rho_0 c_0 i(\omega+i\lambda)} [C e^{i(\omega+i\lambda)z/c_0} - D e^{-i(\omega+i\lambda)z/c_0}] e^{i(\omega+i\lambda)t}$$

For a closed upstream boundary,  $u'_z = 0$  when  $z=0$  therefore  $C=D$  and:

$$u'_z = -\frac{2Cg_0}{\rho_0 c_0} \sinh [(\omega+i\lambda)z/c_0] e^{i(\omega+i\lambda)t}$$

also

$$p' = 2C \cosh [(\omega+i\lambda)z/c_0] e^{i(\omega+i\lambda)t}$$

The admittance coefficient for the downstream boundary is defined by:

$$A = \kappa + i\sigma = \left[ \frac{u'_z}{p'} \frac{\rho_0 c_0}{g_0} \right]_{z=L} = -\tanh [(\omega+i\lambda)\frac{L}{c_0}]$$

# Contrails

Thus, the specification of the complex admittance is sufficient to determine  $\omega$  and  $\lambda$ . Separating this equation into real and imaginary parts yields:

$$\kappa_{\omega} = \frac{\tanh\left(\frac{\lambda L}{c_0}\right) \left[1 + \tan^2\left(\frac{\omega L}{c_0}\right)\right]}{1 + \tan^2\left(\frac{\omega L}{c_0}\right) \tanh^2\left(\frac{\lambda L}{c_0}\right)}$$

and

$$\sigma = \frac{\tan\left(\frac{\omega L}{c_0}\right) \left[\tanh^2\left(\frac{\lambda L}{c_0}\right) - 1\right]}{1 + \tan^2\left(\frac{\omega L}{c_0}\right) \tanh^2\left(\frac{\lambda L}{c_0}\right)}$$

The above equations have been solved graphically to determine  $\omega L/c_0$  and  $\lambda L/c_0$  for given values of  $\kappa$  and  $\sigma$ . From these results, the decrement,  $\delta$ , can be calculated from  $\delta = 2\pi/\omega$  and the longitudinal wave number,  $\nu$ , is given by  $\nu = \omega L/\pi c_0$ .

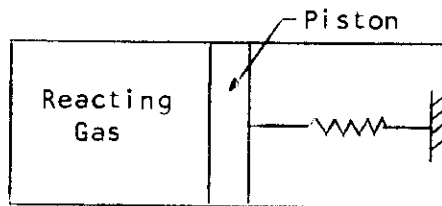
The results from calculations of  $\delta$  and  $\nu$  are shown in Figures 48 and 49 for constant  $\kappa$  and constant  $\sigma$ , respectively. A value of  $10^{-3}$  was assigned to  $L/c_0$  in the calculation of  $\nu$ .

## Appendix F

### ASSESSMENT OF DRIVING MECHANISMS

#### ELEMENTARY CONSIDERATIONS

In order to demonstrate simply the manner in which oscillations can be driven by a combustion process, consideration is given here to the elementary situation of a reacting gas enclosed in a cylinder by a spring-mounted piston at one end. This is indicated schematically below.



It will be assumed that the time period of the piston motion is sufficiently less than the transit time of a sound wave through the gas such that the gas properties may be considered functions of time only. This situation can be related (crudely) to the actual situation in a burner by visualizing the gas enclosed by a piston as a small volume (of dimensions substantially less than an acoustical wavelength) of gas in the actual burner.

The equations governing the motion of the piston and the state of the gas are:

$$M\ddot{x} + Kx = p'A \quad (F-1)$$

$$Q - pA\dot{x} = mC_r\dot{T} \quad (F-2)$$

$$pV = mKT \quad (F-3)$$

$$V = V_0 + Ax \quad (F-4)$$

where  $M$  = mass of piston  
 $K$  = spring constant  
 $x$  = displacement of piston from equilibrium position  
 $p$  =  $p - p_0$ , where  $p$  is the instantaneous pressure and  $p_0$  is the pressure in absence of piston motion  
 $V$  = gas volume  
 $A$  = piston cross-sectional area

# Contrails

$m$  = mass of gas enclosed by piston

$\dot{Q}$  = total energy release rate in gas, assumed to vanish in absence of piston motion.

For small departures from the equilibrium position, the preceding equations may be linearized and damped oscillatory solutions of the form  $p' = \tilde{p} e^{ik't}$ , etc., may be sought in the usual way. With the assumption that the fluctuating energy release rate can be expressed in terms of the pressure as

$$\tilde{Q} = N \tilde{p} \quad (\text{F-5})$$

where  $N$  may be complex, the following characteristic equation for the (complex) frequency  $k$  can be obtained straightforwardly

$$k^2 - \frac{k}{M} - \frac{\gamma p_0 A^2}{M V_0} = \frac{\gamma - 1}{i k V_0} \left(1 - \frac{k}{k^2 M}\right) N \quad (\text{F-6})$$

and the piston motion is related to pressure by

$$\tilde{x} = -\frac{V_0}{\gamma p_0 A} p + \frac{\gamma - 1}{i k \gamma p_0 A} V_0 N \tilde{p} = -\frac{V_0}{\gamma p_0 A} \tilde{p} + \frac{\gamma - 1}{i k \gamma p_0 A} \tilde{Q} \quad (\text{F-7})$$

Assuming that the term on the right side of Equation F-6 is small (which is consistent with the view adopted throughout this report that the energy supplied to an oscillation by the combustion process is small compared to the energy in the oscillation), a first-order perturbation solution can readily be obtained by defining

$$\tilde{p} = \tilde{p}_0 + \tilde{p}_1$$

$$k = k_0 + k_1$$

where  $\tilde{p}_1$  and  $k_1$  are assumed to be first-order quantities. The resulting solution of Equation F-6 is

$$k_0^2 = \omega_0^2 = \frac{k}{M} + \frac{\gamma p_0 A^2}{M V_0} \quad (\text{F-8})$$

$$k_1 - i \lambda_1 = -i \frac{(\gamma - 1)}{2 V_0} N \left[ \frac{\gamma p_0 A^2 / k V_0}{1 + (\gamma p_0 A^2 / k V_0)} \right] \quad (\text{F-9})$$

Since, to first order, the solution for pressure is

$$p' = \tilde{p}_0 e^{-(k_0 + k_1)t} = \tilde{p}_0 e^{-\lambda_1 t} e^{i \omega_0 t} \quad (\text{F-10})$$

it is obvious from Equation F-9 that if  $N$  has a positive real part the oscillation amplitude will increase without limit. Alternatively, if

Equation F-5 is rewritten as

$$\tilde{Q} = |N| e^{i\phi} \tilde{p} \quad (F-11)$$

where  $\phi$  is the phase between pressure and energy release fluctuations, then Equations F-9 and F-10 indicate that for  $-\pi/2 < \phi < \pi/2$  the oscillation will be driven by the combustion process, while if  $\pi/2 < \phi < 3\pi/2$  the oscillation will be damped by the combustion process. This merely demonstrates the Rayleigh principle to the effect that the driving is maximum when the fluctuating energy release is in phase with the pressure.

The solution for the piston velocity is obtained readily from Equation F-7 as

$$\dot{x} = ik\tilde{x} = -\frac{ckV_0}{\gamma p_0 A} \tilde{p} + \frac{\gamma-1}{\gamma p_0 A} \tilde{Q} \quad (F-12)$$

As can be expected, maximum driving occurs when the piston velocity and the pressure have the maximum in-phase component.

In order to assess the relative importance of the various driving mechanisms, the concept of the ratio of energy added by the combustion process per oscillation cycle to the energy contained in the acoustic oscillation will be used; this is completely analogous to the procedure used in the previous assessment of loss mechanisms. The simple example considered here can be used to obtain a sufficiently accurate estimate of this quantity, as follows. The gas energy associated with the oscillation (again neglecting the contribution of the combustion process) is merely the difference between the maximum kinetic energy of the piston ( $\frac{1}{2} M |\dot{\tilde{x}}|^2 = \frac{1}{2} k^2 M |\tilde{x}|^2$ ) and the maximum potential energy of the spring ( $\frac{1}{2} K |\tilde{x}|^2$ ). Denoting this difference by  $E_a$ , then

$$E_a = \frac{1}{2} (k^2 M - K) |\tilde{x}|^2$$

and from Equations F-6 and F-7 (neglecting the last terms in both)

$$E_a = \frac{1}{2} \left( \frac{V_0}{\gamma p_0} \right) |\tilde{p}|^2 \quad (F-13)$$

This is of course the analog of the acoustic energy.

The energy added by the combustion process per oscillation cycle is

$$E_c = \int_0^T c' A \dot{x} dt$$

where  $T = 2\pi/\omega_0 = 1/f$ . In terms of the complex amplitudes, taking  $\tilde{p}$  as real, this becomes

$$E_c = \left( \frac{\pi}{\omega_0} \right) \left( \frac{\gamma-1}{\gamma p_0} \right) |\tilde{p}| R_c(\tilde{Q})$$

# Contrails

or, using Equation F-11...

$$E_c = \left(\frac{\pi}{\omega_0}\right) \left(\frac{\gamma-1}{\gamma p_0}\right) |N| \cos \phi |\tilde{p}|^2 \quad (\text{F-14})$$

Accordingly, the decrement  $\delta$  associated with the combustion process is

$$2\delta = \frac{E_c}{E_a} = \frac{2(\gamma-1)}{\gamma V_0} |N| \cos \phi \quad (\text{F-15})$$

Although Equation F-15 is quite adequate for the simple situation considered here, the actual burner process is better represented by referencing the fluctuating energy release to the steady-state value; thus, in place of Equation F-11

$$\frac{\tilde{Q}}{Q_0} = |N| e^{i\phi} \frac{\tilde{p}}{p_0} \quad (\text{F-16})$$

and hence Equation F-15 becomes

$$\delta = \frac{(\gamma-1)}{p_0 f} \left(\frac{Q_0}{V_0}\right) |N| \cos \phi \quad (\text{F-17})$$

This relation will be used to assess the relative importance of the various driving mechanisms.

It is worth noting even at this point that low pressures, low frequencies (large sizes) and high volumetric energy release rates all contribute to relatively greater driving.

## MODEL OF DRIVING PROCESSES

### THE ENERGY RELEASE RATE

In order to make an assessment of any driving mechanism it is necessary to define the quantities  $N$  and  $\phi$  appearing in Equation F-16 more precisely; that is, a relationship is required between fluctuations in energy release rate and pressure in terms of readily identifiable physical conditions in the burner. Since it is quite obvious from the previous discussion of the literature that the incorporation of a precise analysis of all possibly important driving mechanisms into a combustion instability analysis is well beyond the state of the art, rather drastic simplifications are required. Accordingly, the purpose of this section is to present the development of a simple model of the combustion process which will hopefully both contain the essential features of the actual combustion process and be capable of physical interpretation.



# Contrails

The central basis for the following development is that the energy release rate per unit mass for a given fluid element can be expressed phenomenologically as (e.g., for the case of chemical processes see Ref 72)

$$\left(\frac{\dot{w}_c}{\bar{S}}\right) = \dot{w}_p = \frac{\chi}{\tau}$$

where  $\chi$  is some measure of the departure of the mixture composition from its final equilibrium state, and  $\tau^{-1}$  is a measure of the rate of the process (and is a function of the state of the mixture). It seems at least plausible to assume that  $\chi$  is proportional the amount of fuel remaining to be burned; hence,

$$\chi = E - \int_0^t \dot{w}_p dt$$

where  $E$  is the heat of combustion per unit mass of the initially unreacted mixture and  $t=0=0$  is the time at which the particle enters the reaction zone. Equations F-18 and F-19 can be solved explicitly for  $\dot{w}_p$  to obtain

$$\dot{w}_p = \frac{E}{\tau} e^{-\int_0^t \frac{dt}{\tau}} \quad (\text{F-20})$$

Equation F-20 satisfies the desirable energy conservation requirement that  $\int_0^\infty \dot{w}_p dt = E$ , and it represents the basic model of the combustion process employed in this report.

It is further assumed that the steady combustion process can be characterized by a single inverse rate (i.e., a characteristic time)  $\bar{\tau}$  which is however sensitive to fluctuations in thermodynamic properties induced by oscillations. Thus  $\tau$  can be written as

$$\tau = \bar{\tau} + \tau'$$

where it is assumed that  $\tau'/\bar{\tau} \ll 1$ . Denoting unperturbed quantities by an overbar and fluctuating quantities by a prime, Equation F-20 can be written as

$$\dot{w}_p' + \bar{\dot{w}}_p = \frac{E}{\bar{\tau}(1 + \frac{\tau'}{\bar{\tau}})} e^{\int_0^t \frac{dt}{\bar{\tau}(1 + \frac{\tau'}{\bar{\tau}})}} \quad (\text{F-21})$$

while the unperturbed rate is

$$\bar{\dot{w}}_p = \frac{E}{\bar{\tau}} e^{-t/\bar{\tau}} \quad (\text{F-22})$$

# Contrails

Neglecting terms higher than the first order in  $\tau'/\bar{\tau}$ , Equations F-21 and F-22 can be combined to yield

$$\dot{\omega}'_p = \frac{E}{\bar{\tau}} e^{-t/\bar{\tau}} \left[ -\frac{\tau'}{\bar{\tau}} + \int_0^t \frac{\tau'}{\bar{\tau}} \frac{dt}{\bar{\tau}} \right] \quad (F-23)$$

or alternatively

$$\dot{\omega}'_p = \bar{\omega}'_p \left[ -\frac{\tau'}{\bar{\tau}} + \int_0^t \frac{\tau'}{\bar{\tau}} \frac{dt}{\bar{\tau}} \right] \quad (F-24)$$

It is pointed out that for a time variation of  $\tau' \sim e^{i\omega t}$ , the approximation involved in obtaining the integral term in Equations F-23 and F-24 is accurate to first order in  $\tau'/\omega\bar{\tau}^2$ .

The form of the unperturbed rate given by Equation F-22 could be improved by eliminating the feature that the maximum rate occurs at the beginning of the reaction period; this could be accomplished by either incorporating an "ignition delay" time during which the rate vanishes or by assuming a universal time dependence for the unperturbed characteristic time  $\bar{\tau}$  in which the initial value of  $\bar{\tau}$  is somewhat greater than the final value. With regard to the latter possibility, it is worth noting that Equation F-24 is also valid if  $\bar{\tau}$  is a function of time, provided that  $\bar{\omega}'_p$  is interpreted as

$$\bar{\omega}'_p = \frac{E}{\bar{\tau}} e^{-\int_0^t \frac{dt}{\bar{\tau}}}$$

For the purposes of the present report, however, the incorporation of either an "ignition delay" time or a variable characteristic time seems premature and will not be considered further.

Equation F-23 is the appropriate expression for the perturbed energy release rate (per unit mass) for a fluid element of fixed mass. For the purposes of subsequent analysis, the corresponding Eulerian form applicable to a point fixed in space is required. To accomplish this transformation, it is assumed here that all particles have an unperturbed (and constant) velocity  $\bar{u}$  only in an axial ( $z$ ) direction; the relationship between the axial distance  $z$  measured from the beginning of the reaction zone and the particle time is then

$$dz = (\bar{u} + u') dt$$

or, to first order in  $u'/\bar{u}$

$$t = \frac{z}{\bar{u}} - \int_0^z \frac{u'}{\bar{u}} \frac{dz}{\bar{u}} \quad (F-25)$$

# Contrails

It is important to note that the implicit assumption of  $u'/a \ll 1$  is considerably more restrictive than  $\tau'/\bar{\tau} \ll 1$ , since the latter can be expected to be of the same order as the acoustic requirement of  $u'/c_0 \ll 1$  where  $c_0$  is the speed of sound. Combining Equations F-23 and F-25 yields, for a fixed spatial location,

$$\dot{w}'(r, \phi, z, t) = \frac{\bar{E}}{\bar{\tau}} e^{-\frac{z}{\bar{a}\bar{\tau}}} \left[ -\frac{\tau'}{\bar{\tau}}(r, \phi, z, t) + \int_0^z \frac{\tau'}{\bar{\tau}}(r, \phi, \xi, t - \frac{z}{\bar{a}} + \frac{\xi}{\bar{a}}) \frac{d\xi}{\bar{a}\bar{\tau}} + \int_0^z \frac{u'}{\bar{a}}(r, \phi, \xi, t - \frac{z}{\bar{a}} + \frac{\xi}{\bar{a}}) \frac{d\xi}{\bar{a}\bar{\tau}} \right] \quad (\text{F-26})$$

where the change in the time variable within the integrals is dictated by the fact that the integrations are made following the motion of a fluid particle.

As will be seen subsequently, it will be convenient to determine the perturbed energy release rate per unit volume, or per unit average mass. Denoting the energy release rate per unit volume by  $w'_c$ , then

$$w'_c = \rho \dot{w}'$$

so that, to first order

$$\bar{w}_c + w'_c = \rho_0 \bar{w} + \rho_0 \dot{w}' + \bar{w} \rho'$$

or

$$w'_c = \rho_0 \dot{w}' + \bar{w} \rho'$$

which from Equation F-26 yields

$$w'_c = \rho_0 \frac{\bar{E}}{\bar{\tau}} e^{-\frac{z}{\bar{a}\bar{\tau}}} \left[ -\frac{\tau'}{\bar{\tau}} + \int_0^z \frac{\tau'}{\bar{\tau}} \frac{d\xi}{\bar{a}\bar{\tau}} + \int_0^z \frac{u'}{\bar{a}} \frac{d\xi}{\bar{a}\bar{\tau}} + \frac{\rho'}{\rho_0} \right] \quad (\text{F-27})$$

and the energy release rate per unit average mass is  $w'_c/\rho_0$ . Finally, it can be expected that in general fluctuations in  $\bar{E}$  will exist due to variations in fuel/air ratio at the beginning of the reaction zone; incorporation of these fluctuations into Equation F-27 yields the most general form of the perturbed energy release rate considered here:

$$w'_c = \rho_0 \frac{\bar{E}}{\bar{\tau}} e^{-\frac{z}{\bar{a}\bar{\tau}}} \left[ -\frac{\tau'}{\bar{\tau}} + \int_0^z \frac{\tau'}{\bar{\tau}} \frac{d\xi}{\bar{a}\bar{\tau}} + \int_0^z \frac{u'}{\bar{a}} \frac{d\xi}{\bar{a}\bar{\tau}} + \frac{\rho'}{\rho_0} + \frac{\bar{E}'}{\bar{E}} \left( z = \bar{a} \bar{\tau} \left( t - \frac{z}{\bar{a}} \right) \right) \right] \quad (\text{F-28})$$

It would be presumptuous to suppose that Equation F-28 is an accurate representation of the energy release process; it is plausible, however, that the essential qualitative features of the process are at least crudely represented. The primary virtue of this form of the energy release rate as

# Contrails

opposed to other forms previously advanced in the literature (e.g., see Refs 1 and 2) is that the quantities  $\bar{E}$  and  $\bar{\tau}$  are readily capable of physical interpretation.

As a final remark it is worth noting that a somewhat different model for the driving process can be formed by interpreting the fluctuation in characteristic time for a fluid element as a quantity which is fixed solely by the conditions encountered when the fluid element enters the reaction zone. Thus, the subsequent behavior of the combustion process (following the particle) is insensitive to property fluctuations. In this case, the appropriate form of Equation F-28 becomes

$$\omega_c' = \rho_0 \frac{\bar{E}}{\bar{\tau}} e^{-\frac{z}{\bar{u}\bar{\tau}}} \left[ -\frac{\tau'}{\bar{\tau}}(z=0, t-\frac{z}{\bar{u}}) + \left(\frac{z}{\bar{u}\bar{\tau}}\right) \frac{\tau'}{\bar{\tau}}(z=0, t-\frac{z}{\bar{u}}) + \int_0^z \frac{u'}{\bar{u}} \frac{d\bar{\tau}}{\bar{u}\bar{\tau}} + \frac{\rho'}{\rho_0} + \frac{E'}{\bar{E}}(z=0, t-\frac{z}{\bar{u}}) \right] \quad (\text{F-28a})$$

It would seem that the assumption that the fluctuation in characteristic time is insensitive to local conditions in the reaction zone is less desirable than the assumption underlying Equation F-28; the interpretation of the characteristic time fluctuation is somewhat easier in the former case, however.

## SOME TYPICAL FORMS OF THE ENERGY RELEASE RATE

The expression to be employed here for the perturbed energy release rate (Equation F-28) depends not only on the dependence of the characteristic time upon thermodynamic variables (e.g.,  $\tau'(p')$ ); but on the type of acoustic mode in the burner as well. Since Equation F-28 is rather difficult to interpret in the form presented previously, it is instructive to consider its form for some simple acoustic modes.

Consider first the case of a simple longitudinal mode for which, in the acoustic approximation, the velocity and density fluctuations are related to the pressure fluctuations by

$$\frac{\tilde{u}}{\bar{u}} = i \frac{1}{\gamma M} \left[ \left( \frac{\lambda}{2\pi} \right) \frac{\partial(\tilde{p}/p_0)}{\partial z} \right] \quad (\text{F-29})$$

$$\frac{\tilde{\rho}}{\rho_0} = \frac{1}{\gamma} \frac{\tilde{p}}{p_0} \quad (\text{F-30})$$

where  $\lambda$  is the acoustical wavelength of the longitudinal mode. It is of interest to examine the extremely simple case where  $\tau' = E' = 0$ ; that is, both the characteristic time and the fuel/air ratio are insensitive to

# Contrails

fluctuations in thermodynamic properties. Taking  $\omega_c' = \tilde{\omega}_c e^{i\omega t}$ , substitution of Equations F-29 and F-30 into Equation F-28 yields

$$\tilde{\omega}_c = \rho_0 \frac{\bar{E}}{\bar{c}} e^{-\frac{z}{\bar{u}\bar{c}}} \left\{ \int_0^z \frac{1}{\delta M} \left[ \left( \frac{\lambda}{2\pi} \right) \frac{\partial(\bar{p}/\rho_0)}{\partial z} \right] e^{-i\omega \frac{z}{\bar{u}} + i\omega \frac{z}{\bar{u}}} \frac{d\bar{p}}{\bar{u}\bar{c}} + \frac{1}{\delta} \frac{\bar{p}}{\rho_0} \right\} \quad (\text{F-31})$$

If it is further assumed that the wavelength  $\lambda$  is much larger than the length of the reaction zone ( $\bar{u}\bar{c}$ ), it is permissible to remove the term in brackets from the integral, to obtain

$$\tilde{\omega}_c = \rho_0 \frac{\bar{E}}{\bar{c}} e^{-\frac{z}{\bar{u}\bar{c}}} \left\{ \frac{1}{\delta M} \left[ \left( \frac{\lambda}{2\pi} \right) \frac{\partial(\bar{p}/\rho_0)}{\partial z} \right]_{z=0} \frac{1}{\omega \bar{c}} \left[ -e^{-i\omega \frac{z}{\bar{u}}} \right] + \frac{1}{\delta} \frac{\bar{p}}{\rho_0} \right\} \quad (\text{F-32})$$

The total amount of driving provided to a longitudinal mode is of course the integral over the total reaction zone of that portion  $\omega_c'$  which is in phase with the pressure; subject again to the assumption that  $\lambda \gg \bar{u}\bar{c}$ , then

$$\int_0^{\infty} \text{Re}(\tilde{\omega}_c) dz = \rho_0 \bar{E} \bar{u} \left\{ \left[ \left( \frac{\lambda}{2\pi} \right) \frac{\partial(\bar{p}/\rho_0)}{\partial z} \right]_{z=0} \frac{1}{\delta M} \frac{\omega \bar{c}}{1+(\omega \bar{c})^2} + \frac{1}{\delta} \left( \frac{\bar{p}}{\rho_0} \right)_{z=0} \right\} \quad (\text{F-33})$$

so that in this case the total fractional driving can be written as

$$D = \frac{\int_0^{\infty} \text{Re}(\tilde{\omega}_c) dz}{\rho_0 \bar{E} \bar{u}} = \left\{ \left[ \left( \frac{\lambda}{2\pi} \right) \frac{1}{\bar{p}/\rho_0} \frac{\partial(\bar{p}/\rho_0)}{\partial z} \right]_{z=0} \frac{1}{\delta M} \frac{\omega \bar{c}}{1+(\omega \bar{c})^2} + \frac{1}{\delta} \right\} \left( \frac{\bar{p}}{\rho_0} \right)_{z=0} \quad (\text{F-34})$$

The term in braces in Equation F-34 is equivalent to the term  $|N| \cos \phi$  appearing in Equation F-17 times the ratio  $|\bar{p}|/(\bar{p})_{z=0}$ .

Several features of Equation F-34 deserve mention. The maximum driving occurs at  $\omega \bar{c} = 1$  but does not exhibit a very sharp frequency response which is in accord with experimental findings. It is also noted that driving can be obtained even in the absence of any sensitivity of the characteristic time of the energy release process to pressure fluctuations, and is attributable solely to purely fluid dynamic effects. For the typical spatial variation of a longitudinal mode of  $\bar{p}/\rho_0 \sim \sin(2\pi z/\lambda + \beta)$ , maximum driving occurs when the reaction zone is located midway between a pressure node and a velocity node. A typical maximum magnitude for  $|N| \cos \phi$  (for  $M = 0.3$ ,  $\gamma = 1.4$ ,  $\omega \bar{c} = 1$ , and  $\beta = \pi/4$ ) is approximately 1.1. Referring to Equation F-17 for typical burner conditions of  $P_0 = 2000$  lbf per ft<sup>2</sup>,  $f = 500$  cps, and  $Q/V_0 = 10^6$  ft-lbf per ft<sup>3</sup>, then  $\delta = 0.44$  which, from comparison with the previous corresponding values for losses (see Appendix C), represents

# Contrails

quite a substantial amount of driving. Finally, it is to be noted that the assumption employed that  $\lambda \gg \bar{\tau}$  is equivalent to  $\omega \bar{\tau} \ll 2\pi/M$ , and hence the present results can be expected to be valid for  $\omega \bar{\tau} \lesssim 2$ .

It is of some interest to attempt to fit this result (Equation F-34) to the  $n-\tau_c$  model proposed by Crocco. In the latter, the term in braces in Equation F-34 for the case just cited is represented by

$$|N| \cos \phi = \frac{\sqrt{2}}{2} n (1 - \cos \omega \tau_c) \quad (\text{F-35})$$

If the results of the two expressions are matched such that the maximum values are equal when  $\omega \bar{\tau} = 1$  and  $\omega \tau_c = \pi$ , the following comparison is obtained:

$\omega \bar{\tau}$	$ N  \cos \phi$ (Eq F-34)	$ N  \cos \phi$ (Eq F-35)
0	0	0
0.3	0.833	0.227
0.6	1.030	0.719
0.8	1.085	0.994
1.0	1.100	1.100
1.2	1.090	0.994
1.4	1.068	0.719
2	0.981	0

It is quite obvious that the  $n-\tau_c$  representation would yield only a crude approximation in this case. More importantly, perhaps, the  $n-\tau_c$  representation would of necessity yield values of  $n$  and  $\tau_c$  which depend upon the physical parameters of the problem (e.g.,  $M$ ,  $\bar{\tau}$ ) in an unknown way and these values would further depend upon the position of the reaction zone relative to the pressure and velocity modes. Hence, it is virtually impossible to attach any physical significance to the parameters  $n$  and  $\tau_c$ .

Turning attention to the case of a simple tangential mode, where  $\omega' = 0$  and  $P' \neq 0(z)$ , consider the case where the characteristic time fluctuation is given by  $\tau'/\bar{\tau} = \hat{\tau}(r, \phi) e^{i\omega t}$  (for a purely pressure-sensitive time of the form  $\tau \sim \bar{p}^n$ ,  $\hat{\tau} = -n\bar{p}/P_c$ ). Equation F-28 becomes, assuming  $E' = 0$

$$\tilde{\omega}_c = \int_0^{\bar{\tau}} \frac{\bar{E}}{\bar{\tau}} e^{-\frac{z}{\bar{\tau}}} \left\{ -\hat{\tau} + \frac{\hat{\tau}}{i\omega \bar{\tau}} [1 - e^{-i\omega \frac{z}{\bar{\tau}}}] + \frac{1}{\delta} \left( \frac{\hat{P}}{P_c} \right) \right\} \quad (\text{F-36})$$

Integration of  $\text{Re}(\tilde{\omega}_c)$  over  $z$  yields the total driving per unit cross-sectional area:

# Contrails

$$D = -\tilde{\tau} \frac{\omega^2 \tilde{\tau}^2}{1 + (\omega \tilde{\tau})^2} + \frac{1}{\gamma} \left( \frac{\tilde{p}}{p_0} \right) \quad (\text{F-37})$$

where it has been assumed that  $\tilde{\tau}$  is real.

In this case, maximum driving occurs as  $\omega \tilde{\tau} \rightarrow \infty$ , although  $\omega \tilde{\tau} \geq 2$  closely approximates the maximum for practical purposes. This result indicates that to attain appreciable driving, it is necessary only that the characteristic time of the energy release process be sufficiently greater than the oscillation period of the acoustic mode. This observation must be tempered by the fact that as  $\omega \tilde{\tau} \rightarrow \infty$ ,  $|\tilde{\tau}| \rightarrow 0$ . As was the case with the longitudinal mode, the frequency response of the driving is quite flat. It is also apparent that an  $\omega - \tilde{\tau}_c$  representation of this driving would not be very satisfactory.

As an aside, the expression for  $D$  which results from the use of the model of a constant characteristic time fluctuation for any particle (Equation F-28a) is

$$D = -\tilde{\tau} \frac{2(\omega \tilde{\tau})^2}{[1 + (\omega \tilde{\tau})^2]^2} + \frac{1}{\gamma} \frac{\tilde{p}}{p_0}$$

This yields a somewhat different response in that maximum driving is obtained at  $\omega \tilde{\tau} = 1$ . As mentioned previously, however, it is felt that this model is somewhat inferior to that corresponding to Equation F-28.

## CRITERIA FOR ASSESSMENT OF DRIVING MECHANISMS

The preceding development enables some approximate quantitative criteria for the assessment of driving mechanisms to be specified. From Equations F-28, F-34, and F-39 these criteria obviously involve the relationship between the oscillation frequency and the unperturbed characteristic time of the energy release process (i.e.,  $\omega \tilde{\tau}$ ), the sensitivity of the energy release process to fluctuations in thermodynamic variables ( $\tau'/\tilde{\tau}$ ), and any oscillation induced variations in fuel/air ratio entering the reaction zone. The previous considerations indicate that to achieve substantial driving, it is required that  $\omega \tilde{\tau} \sim 1$  (say  $0.3 < \omega \tilde{\tau} < 3$ ). In the presence of a substantial longitudinal component in the acoustic mode, this requirement is sufficient to produce substantial driving, as indicated earlier. In the absence of a longitudinal component, it is also necessary that the sensitivity of the characteristic time to the fluctuations in thermodynamic properties be sufficiently high. If, for example, it is assumed that  $\tau'/\tilde{\tau} = -n p'/p_0$ , then Equation F-34 indicates that  $n \sim 1$  to obtain a substantial driving contribution. Fluctuations in  $E'$ , from Equation F-28, should also be such that  $E'/E \sim p'/p_0$  to obtain substantial driving. These criteria will be employed in the following section to aid in the evaluation of driving mechanisms.

## PHYSICAL MECHANISMS

The basic physical mechanisms which control the energy release rate in burners are:

1. Fuel vaporization.
2. Chemical kinetics.
3. Transport processes between fuel vapor and air.

In the following sections, estimates of typical characteristic times for these processes are made in order that their relative importance as driving mechanisms can be evaluated. In this evaluation, both the characteristic time of the steady-state combustion process and the response of this time to property fluctuations are of interest.

## FUEL VAPORIZATION

The characteristic time of the fuel vaporization process can be estimated from the consideration of the vaporization of a single droplet. The over-all process is of course controlled largely by heat transfer to the droplet and mass transfer from the droplet which are in turn influenced by the dynamics of the droplet relative to the gas.

The characteristic time of the vaporization process can be estimated from consideration of a single droplet; the lifetime of a fuel droplet in a gas stream in which combustion is occurring can be approximated by (Refs 73 and 74):

$$\tau_{100} = \frac{d_0^2}{\lambda} \quad (F-38)$$

where  $d_0$  = initial droplet diameter  
 $\lambda = (4k_g/\rho_F C_p) \ln(1+B) [2 + 0.6 Re_d^{0.5} Pr_f^{0.38}]$   
 $k_g$  = thermal conductivity of combustion products  
 $\rho_F$  = density of liquid fuel  
 $Re_d$  = droplet Reynolds number =  $(\rho_o u_{rel} d / \mu)$   
 $Pr_f$  = fuel Prandtl number

$$B = \frac{(\Delta H / z_{st}) + C_p (T_j - T_s)}{Q}$$

$\Delta H$  = heat of combustion of fuel  
 $z_{st}$  = stoichiometric fuel-air ratio  
 $T_j$  = local temperature of combustion products  
 $T_s$  = surface temperature of droplet  
 $Q$  = heat required to vaporize fuel-- sensible heat and latent heat.

Taking heptane as representative of an aircraft fuel (see Ref 75 for the properties of heptane), Equation F-38 yields the following droplet lifetimes for a 50 micron drop:



# Contrails

$T$ (deg R)	$\lambda$ ( $\mu^2/sec$ )	$t_{100}$ (sec)	$f$ at $\omega \bar{t} = 1$ (cps)
2000	$2.62 \times 10^6$	$.95 \times 10^{-3}$	249
3000	$3.82 \times 10^6$	$.66 \times 10^{-3}$	361
4000	$4.22 \times 10^6$	$.59 \times 10^{-3}$	405

where it has been assumed that the term involving Reynolds number in Equation F-38 is approximately equal to 2. The last column in the above table indicates the frequency at which  $\omega \bar{t} = 1$ , and hence the frequency at which driving is the most effective, where  $\bar{t} \approx (2/3)t_{100}$  in accord with the definition of  $\bar{t}$ . The most important variable affecting vaporization is the droplet diameter; the frequencies at which  $\omega \bar{t} = 1$  are lower than those shown above by a factor of four for a 100-micron drop and higher by a factor of 4 for a 25 micron drop. It can therefore be concluded that droplet vaporization can be an important driving mechanism in a frequency range of (roughly) 100 cps to 2000 cps.

The fluctuations of the characteristic time in response to oscillations in thermodynamic properties appear to be controlled largely by the last term in Equation F-38. The magnitude of this term is in turn controlled largely by the relative velocity between the droplet and the gas. A characteristic time for the dynamic response of the droplet is the time required for a droplet initially at rest in a gas stream to attain 2/3 of the velocity of the stream. Elementary particle dynamics yield

$$t = \frac{8 \rho_l d}{9 \rho_g C_D u_{rel,f}}$$

where  $\rho_l$  = liquid density  
 $d$  = droplet diameter  
 $\rho_g$  = gas density  
 $C_D$  = drag coefficient of particle  
 $u_{rel,f}$  = relative velocity of droplet at time  $t$

For  $u_{rel,f} = 150$  ft per sec,  $\rho_l = 45$  lbm per cu ft, and  $C_D = 2$ , the following times (in milliseconds) result:

	$d = 25 \mu$	$d = 50 \mu$	$d = 100 \mu$
$\rho_g = 5 \times 10^{-3}$ lbm per ft <sup>3</sup>	1.1	2.2	4.4
$\rho_g = 9 \times 10^{-2}$ lbm per ft <sup>3</sup>	.062	.12	.25

The two density levels represent the extreme limits to be expected in aircraft burners. It is quite apparent that at the lower density levels the droplet dynamic response is relatively slow and hence that variations in the last term in Equation F-38 due to fluctuations will become appreciable.

# Contrails

At high density levels, the droplet dynamic response will be rapid and the contribution of the last term in Equation F-38 will be relatively less. The latter situation would correspond generally to conditions encountered in liquid rockets, while the former is more representative of aircraft burners.

From the preceding considerations, it seems reasonable to represent the characteristic time of the vaporization process as

$$\tau^{-1} = 1 + a p^n \quad (\text{F-39})$$

where  $n \lesssim 1/2$  (if the droplet dynamic response is slow, then  $n = 1/2$ , but as  $p$  increases the dynamic response becomes more rapid; Refs 32, 33, and 75 indicate that  $n = 1/3$  for conditions typical of liquid rockets). The parameter  $a$  will in general depend upon the oscillation amplitude. The effects of velocity fluctuations have been omitted from Equation F-39, since the effect on driving is relatively small; i.e., increases in vaporization rate due to a velocity fluctuation occur twice per oscillation cycle and hence tend to cancel (see Ref 32). From Equation F-39, the fluctuation in  $\tau$  can be obtained:

$$\frac{\tau'}{\tau} = -\frac{n a_0 p_0^n}{1 + a_0 p_0^n} \left( \frac{p'}{p_0} \right) - \frac{a' p_0^n}{1 + a_0 p_0^n} \quad (\text{F-40})$$

where  $a'$  is the fluctuation in  $a$ . If  $a_0 p_0^n \gg 1$  and  $a'/a_0 \ll 1$  then

$$\frac{\tau'}{\tau} \cong -n \left( \frac{p'}{p_0} \right) \quad (\text{F-41})$$

where  $n \lesssim 1/2$ . For a pure tangential mode, Equations F-41, F-37, and F-17 yield for  $\omega \tau = 1$

$$\delta = 0.386$$

for the representative case of  $p_0 = 2000$  lbf per sq ft,  $f = 500$  cps, and  $Q/V_0 = 10^6$  ft-lbf/ft<sup>3</sup>. This is quite a substantial amount of driving. Equation F-41 will of course be unsatisfactory when  $\omega \tau \gg 1$ .

To conclude this discussion of the vaporization process, some remarks on nonlinearity are in order. As indicated earlier, the chief nonlinearity is expected in the parameter  $\hat{a}$ , through its dependence on the relative velocity between droplet and gas. The level of the relative velocity can be expected to increase with the disturbance amplitude; i.e.,  $\hat{a}/a_0 \sim |p'/p_0|^m$  where  $m \lesssim 1/2$ . In this case, Equation F-41 becomes

$$\frac{\tau'}{\tau} \cong -n \left( 1 + \kappa \left| \frac{p'}{p_0} \right|_{\text{max}}^m \right) \left( \frac{p'}{p_0} \right) \quad (\text{F-42})$$

Accordingly, the maximum variation of driving is an increase as the square root of the disturbance amplitude. This nonlinear mechanism can be expected to be most pronounced for spinning transverse modes in which the pressure fluctuations and tangential velocity fluctuations are in phase.

# Contrails

## CHEMICAL KINETICS

The characteristic time of the chemical process of combustion of fuel and air can be estimated from empirical data obtained from shock tube experiments with premixed hydrocarbon-air mixtures. The data which seems most applicable is that of Reference 76, obtained for mixtures of propane, oxygen, and argon. This data, when applied to heptane-air mixtures by assuming that the reaction time of a heptane-air mixture is equal to that of a propane-air mixture provided that the mass fraction of hydrocarbon is equal in both cases, yields the following correlation for reaction time:

$$\tau = \frac{0.1887 \times 10^{-13} R' T_f}{P^{3/8} X_R^{0.2}} \times \frac{\phi^{0.2} (5+\phi)}{\sqrt{5}} \times \exp \frac{31.29}{RT_f} \quad (F-43)$$

for  $T_f > 2250$  deg R and

$$\tau = \frac{0.6335 \times 10^{-11} R' T_f}{P^{3/8} X_R^{0.2}} \times \frac{\phi^{0.2} (5+\phi)}{\sqrt{5}} \times \exp \frac{17.01}{RT_f} \quad (F-44)$$

for  $T_f < 2250$  deg R,

where  $\phi$  = equivalence ratio  
 $T_f$  = temperature before combustion, deg K  
 $P$  = pressure in atmospheres  
 $X_R$  = mole fraction of reactants  
 $R'$  = 82.06 atm-cm<sup>3</sup>/mole-deg K  
 $R$  = 1.986 cal/mole-deg K.

This reaction time is the time required (at  $T_f$ ) to attain essentially complete combustion; as is the case with most hydrocarbons this time is composed of an "ignition delay" time and a heat release time-- these will not be separately identified here. Equations F-43 and F-44 yield the following characteristic times (in milliseconds):

$T$ (deg R)	$P = 5$ psia $\phi = 0.2$	$P = 30$ psia $\phi = 0.2$	$P = 5$ psia $\phi = 1.0$	$P = 30$ psia $\phi = 1.0$
1250	276			
1750	11.4			
2250	1.9	0.98	3.0	1.55
2750	0.23	0.12	0.37	0.19
3350	0.058	0.029	0.092	0.047
3750	0.021	0.011	0.033	0.017

Considering the nature of the gas dynamic process in aircraft burners,

wherein the incoming air is at relatively low temperatures and must therefore be heated appreciably by transport processes (e.g., turbulent mixing) involving the combustion products before a reaction can take place, it is extremely unlikely that chemical kinetics has a significant role in driving combustion instability. This is due to the fact that the heating rate of the fuel-air mixture will be sufficiently rapid such that the reaction will not take place until a relatively high temperature has been reached. Accordingly, expressions for fluctuations in characteristic time and the resultant nonlinear aspects will not be discussed here, although they may be developed straightforwardly from Equations F-43 and F-44.

## TRANSPORT PROCESSES

The transport processes which occur in aircraft burners are governed by properties of the highly turbulent flow in the burner, and hence quantitative estimates of the characteristic times involved in the processes are exceedingly difficult to make. The treatment here is accordingly very crude.

The view adopted here is that the basic transport process involving turbulent flow can be represented by the entrainment of macroscopic volumes of cold fuel-air mixture into the flow of combustion products and the subsequent heating of the gas in these volumes by essentially laminar means to a temperature at which combustion takes place virtually instantaneously. From consideration of the laminar heating of a spherical volume, the characteristic time for the process is

$$\tau = \frac{\rho c_p r_c^2}{k} \quad (F-45)$$

where  $r_c$  is the radius of the sphere, Equation F-45 yields the following characteristic times (in milliseconds):

	<u><math>r_c = 100\mu</math></u>	<u><math>r_c = 1000\mu</math></u>
$\rho = 5 \times 10^{-3}$ lbm per ft <sup>3</sup>	6.4 x 10 <sup>-3</sup>	0.64
$\rho = 9 \times 10^{-2}$ lbm per ft <sup>3</sup>	0.12	12

It is apparent that the critical parameter in this model is the effective radius,  $r_c$ , of the macroscopic volumes. Unfortunately, time limitations have prevented the development of appropriate estimates of these effective radii in terms of the other physical parameters of the combustion region. It is well known, however, that the energy release in turbulent flames in premixed fuel/air mixtures is controlled by the turbulent mixing process (e.g., see Refs 77 and 78), and that characteristic times for the process are in the vicinity of 1 millisecond at least at some conditions of practical interest. It can therefore be concluded that the turbulent mixing process is a possible mechanism in driving combustion instabilities, particularly in the lower frequency range.

# Contrails

The problem of estimating the response of the turbulent mixing process to property fluctuations in any quantitative way is beyond the scope of the present study. Qualitatively, it appears that the process should be particularly sensitive to velocity fluctuations and rather insensitive to pressure fluctuations, from consideration of the effects of these fluctuations on the "typical volume" size. Thus, a dependence of  $\tau \sim 1 + a(u')^n$  can be expected, where the value of the exponent can probably be accurately deduced only from experiment. Such a dependence would indicate a greater susceptibility for spinning transverse modes.

# *Contrails*

## Appendix G

### DEVELOPMENT OF THE INSTABILITY MODEL

#### GOVERNING EQUATIONS

The following development parallels that presented by Culick in References 1 and 39.

The equations governing the flow in a burner are the usual conservation laws of mass, momentum, and energy supplemented by caloric and thermal equations of state. These can be written as:

$$\frac{\partial \rho}{\partial t} + \nabla \cdot (\rho \underline{u}) = 0 \quad (G-1)$$

$$\rho \frac{\partial \underline{u}}{\partial t} + \rho (\underline{u} \cdot \nabla) \underline{u} + \nabla p = 0 \quad (G-2)$$

$$\rho \frac{\partial e}{\partial t} + \rho (\underline{u} \cdot \nabla) e + p (\nabla \cdot \underline{u}) = \omega_c \quad (G-3)$$

$$e = \frac{1}{\gamma - 1} \frac{p}{\rho} \quad (G-4)$$

$$p = \rho R T \quad (G-5)$$

It is assumed throughout that the variations in  $\gamma$  and  $R$  are negligible in the burner.

Following the usual acoustical procedure, the flow is assumed to be composed of a steady mean flow and an oscillatory flow; hence  $p = p_0 + \tilde{p}$ ,  $\underline{u} = \underline{u}_0 + \tilde{\underline{u}}$ , etc., where  $p_0$ ,  $\underline{u}_0$ , etc. are the mean flow properties and  $\tilde{p}$ ,  $\tilde{\underline{u}}$  are associated with the oscillatory flow. Introducing these definitions into Equations G-1 to G-5 and assuming that second order terms (e.g.,  $\tilde{p}^2$ ) are negligible, the following equations governing the oscillatory flow are obtained:

$$\frac{\partial \tilde{p}}{\partial t} + \nabla \cdot (\rho \underline{u}_0) + \nabla \cdot (\rho_0 \tilde{\underline{u}}) = 0 \quad (G-6)$$

# Contrails

$$\frac{\partial \tilde{u}}{\partial t} + (\tilde{u} \cdot \nabla) u_0 + (u_0 \cdot \nabla) \tilde{u} + \frac{\tilde{p}}{\rho_0} (\underline{u}_0 \cdot \nabla) u_0 + \frac{1}{\rho_0} \nabla \tilde{p} = 0 \quad (G-7)$$

$$\frac{\partial \tilde{e}}{\partial t} + (u_0 \cdot \nabla) \tilde{e} + (\tilde{u} \cdot \nabla) e_0 + \frac{\tilde{p}}{\rho_0} (\underline{u}_0 \cdot \nabla) e_0 + \frac{\tilde{p}}{\rho_0} (\nabla \cdot u_0) + \frac{p_0}{\rho_0} (\nabla \cdot \tilde{u}) = \frac{\tilde{w}}{\rho_0} \quad (G-8)$$

$$\frac{\tilde{p}}{p_0} = \frac{\tilde{p}}{p_0} + \frac{\tilde{T}}{T_0} \quad (G-9)$$

$$\frac{\tilde{e}}{e_0} = \frac{\tilde{T}}{T_0} \quad (G-10)$$

Since only harmonic solutions are of interest, solutions of the form  $\tilde{p} = \eta \bar{p}_0 e^{ikt}$ ,  $\tilde{u} = \underline{u}' e^{ikt}$ , etc., are sought. Here,  $k = \omega + i\lambda$  where  $\omega$  is the oscillation frequency and  $\lambda$  is the damping constant; the oscillation amplitudes  $\eta$ ,  $\underline{u}'$ , etc., are in general complex. For the moment,  $\bar{p}$  is taken as a constant reference pressure. Introducing these relations into Equations G-6 through G-10, eliminating  $\tilde{T}$ ,  $\tilde{e}$ , and  $\tilde{p}$ , and making use of the fact that  $\nabla \cdot (\rho_0 u_0) = 0$  yields:

$$ik \underline{u}' + \frac{c_0^2}{\gamma} \nabla \eta = -(\underline{u}' \cdot \nabla) u_0 - (u_0 \cdot \nabla) \underline{u}' \quad (G-11)$$

$$ik \eta p_0 + \gamma p_0 (\nabla \cdot \underline{u}') = (\gamma - 1) \omega^2 \eta - \gamma \eta p_0 (\nabla \cdot u_0) - (u_0 \cdot \nabla) \eta p_0 - \underline{u}' \cdot \nabla p_0 \quad (G-12)$$

where  $c_0^2 = \gamma \bar{p} / \rho_0$ . It is now further assumed that the Mach number is sufficiently small so that terms of second order can be neglected; this permits the last term in each of the two preceding equations to be neglected, and also permits the approximation that  $p_0$  is a constant. Setting  $\bar{p} = p_0$ , rewriting Equation G-11, and combining Equations G-11 and G-12 yields:

$$\underline{u}' = -\frac{c_0^2}{ik\gamma} \nabla \eta - \frac{1}{ik} [(\underline{u}' \cdot \nabla) u_0 + (u_0 \cdot \nabla) \underline{u}'] \quad (G-13)$$



# Contrails

$$\begin{aligned} \nabla \cdot c_0^2 \nabla \eta + k^2 \eta &= -\frac{ik}{\rho_0} (\gamma-1) \omega_c' + ik \gamma \eta (\nabla \cdot \underline{u}_0) \\ &+ ik (\underline{u}_0 \cdot \nabla) \eta - \gamma \nabla \cdot [(\underline{u}' \cdot \nabla) \underline{u}_0 + (\underline{u}_0 \cdot \nabla) \underline{u}'] \end{aligned} \quad (G-14)$$

Consistent with the assumption of small Mach number, it is permissible to replace  $\underline{u}'$  as it appears on the right side of the above equations by the acoustic approximation  $\underline{u}' = -c_0^2 \nabla \eta / ik \gamma$  :

$$\underline{u}' = -\frac{c_0^2}{ik \gamma} \nabla \eta - \frac{c_0^2}{k^2 \gamma^2} [(\nabla \eta \cdot \nabla) \underline{u}_0 + (\underline{u}_0 \cdot \nabla) c_0^2 \nabla \eta] \quad (G-15)$$

$$\begin{aligned} \nabla \cdot c_0^2 \nabla \eta + k^2 \eta &= -\frac{ik}{\rho_0} (\gamma-1) \omega_c' + ik \gamma \eta (\nabla \cdot \underline{u}_0) + ik (\underline{u}_0 \cdot \nabla) \eta \\ &+ \frac{1}{ik} \left\{ \nabla \cdot [c_0^2 (\nabla \eta \cdot \nabla) \underline{u}_0 + (\underline{u}_0 \cdot \nabla) c_0^2 \nabla \eta] \right\} \end{aligned} \quad (G-16)$$

The first two terms in each of these equations represent the usual acoustics problem in the absence of mean flow and combustion. The view adopted here is that the effects of mean flow and combustion on the oscillatory behavior are small in the sense that the other terms in these equations are small compared to the purely acoustic terms.

Finally, it is assumed that  $\underline{u}_0$ ,  $\rho_0$ , and  $c_0$  are functions of  $z$  only (a cylindrical coordinate system  $r, \phi, z$  is employed throughout) and hence that the direction of  $\underline{u}_0$  is axial; then for a burner in which the effect of combustion on the mean flow can be represented by discontinuities in  $\underline{u}_0$  and  $c_0$  (but that  $\omega_c'$  and  $\eta$  are continuous), at a location  $z_l$ , Equations G-15 and G-16 can be rearranged and written formally as:

$$\begin{aligned} \underline{u}' &= \frac{c_0^2}{ik \gamma} \nabla \eta - \frac{c_0^2}{k^2 \gamma^2} [(\nabla \eta \cdot \nabla) \underline{u}_0 + \underline{u}_0 \cdot \frac{\partial}{\partial z} (c_0^2 \nabla \eta)] \\ &- \frac{1}{\gamma k^2} \Delta (c_0^2 \frac{\partial \eta}{\partial z} \underline{u}_0) \delta(z_l) \end{aligned} \quad (G-17)$$

$$\begin{aligned} \nabla \cdot c_0^2 \nabla \eta + k^2 \eta &= -\frac{ik}{\rho_0} (\gamma-1) \omega_c' + ik (z \underline{u}_0 - \frac{c_0^2}{k^2} \frac{d^2 \underline{u}_0}{dz^2}) \frac{\partial \eta}{\partial z} \\ &+ ik (\gamma \eta - \frac{z c_0^2}{k^2} \frac{\partial^2 \eta}{\partial z^2}) \frac{d \underline{u}_0}{dz} \\ &+ ik \gamma \eta \Delta (\underline{u}_0) \delta(z_l) + \Delta \left[ \frac{z}{\partial z} (\frac{\gamma c_0^2}{ik} \frac{\partial \eta}{\partial z}) \right] \delta(z_l) \end{aligned} \quad (G-18)$$

# Contrails

where  $\delta(z_f)$  is the Dirac delta function and  $\Delta(u_o)$  is the magnitude of the discontinuity in  $u_o$  across the flame front (i.e.,  $\Delta(u_o) \equiv u_{o+} - u_{o-}$  where  $u_{o+}$  is the value of  $u_o$  immediately downstream of the discontinuity and  $u_{o-}$  is the value of  $u_o$  immediately upstream of the discontinuity). Equation G-18 is the main governing equation of the instability model developed here; for convenience, it is abbreviated by defining the function  $h$  such that

$$\nabla \cdot c_o^2 \nabla \eta + k^2 \eta = h \quad (G-19)$$

## BOUNDARY CONDITIONS

At all exterior boundaries of the burner, the appropriate boundary conditions are written in terms of the complex acoustical admittance defined by

$$\frac{u_n'}{p'} = A$$

where  $u_n'$  is the velocity normal to the bounding surface defined positive in the outward direction. Substitution of Equation G-17 into this definition yields the appropriate form of the boundary conditions as follows. For the downstream end (the inlet to the nozzle)

$$\frac{1}{\eta} \frac{\partial \eta}{\partial z} = -ik \left[ \rho_o A_L + \frac{u_o}{k^2 \eta} \frac{\partial^2 \eta}{\partial z^2} \right] \quad (G-20)$$

For the upstream end

$$\frac{1}{\eta} \frac{\partial \eta}{\partial z} = ik \left[ \rho_o A_o - \frac{u_o}{k^2 \eta} \frac{\partial^2 \eta}{\partial z^2} \right] \quad (G-21)$$

For the outer radius

$$\frac{1}{\eta} \frac{\partial \eta}{\partial z} = -ik \rho_o A_R \quad (G-22)$$

For the inner radius (if one is present)

$$\frac{1}{\eta} \frac{\partial \eta}{\partial z} = ik \rho_o A_I \quad (G-23)$$

In Equations G-20 through G-23 it has been assumed that  $du_o/dz = 0$  at the axial boundaries and that the convective term which should appear in Equation G-23 (of the form  $u_o \partial u_r' / \partial z$ ) is negligible. In addition to the conditions at the boundaries, the conditions at the discontinuity

# Contrails

representing the flame front are:

$$\eta_- = \eta_+ \quad (G-24)$$

$$\left(c_0^2 \frac{\partial \eta}{\partial z}\right)_- = \left(c_0^2 \frac{\partial \eta}{\partial z}\right)_+ \quad (G-25)$$

where the subscripts + and - refer to the upstream and downstream sides of the discontinuity, respectively.

The last two conditions deserve comment in two respects. First, strictly speaking these conditions apply only to the case without mean flow (i.e.,  $u_0=0$ ). Consistent with the view adopted previously that the convective effect may be treated as a perturbation of the usual acoustical problem, the convective terms may be neglected. This assumption will be further supported by the subsequent solutions obtained in which the only solution for  $\eta$  which is of practical importance is shown to be that in the absence of internal convective effects. Second, in an actual burner the physical structure of the flame stabilization devices (which serve to anchor the flame front, or "discontinuity" as idealized here) will supply some additional impedance. The easiest way in which such an impedance could be incorporated into the formal development presented here would be to treat the regions upstream and downstream of the flame front separately, where conditions at the flame front would be represented by an appropriate admittance  $A_f$  in Equation G-21 or G-20. The admittance would then be a function of the structure of the flameholder, the geometry and mean flow conditions of both sides of the burner, and the acoustic mode being treated. While such a procedure can be implemented in a straightforward way, it is felt to be premature at this time due to both the uncertainty in determining the appropriate admittance and the likelihood that in a typical low-pressure loss burner, Equations G-24 and G-25 are satisfactory approximations.

Finally, for convenience, equivalent acoustical admittances,  $\bar{A}$ , are defined in Equations G-20 through G-23 such that these equations can be rewritten as, respectively:

$$\left(\frac{1}{\eta} \frac{\partial \eta}{\partial z}\right)_{z=L} = \bar{A}_L \quad (G-26)$$

$$\left(\frac{1}{\eta} \frac{\partial \eta}{\partial z}\right)_{z=0} = \bar{A}_0 \quad (G-27)$$

$$\left(\frac{1}{\eta} \frac{\partial \eta}{\partial z}\right)_{r=R} = \bar{A}_R \quad (G-28)$$

$$\left(\frac{1}{\eta} \frac{\partial \eta}{\partial z}\right)_{r=r_i} = \bar{A}_I \quad (G-29)$$

The complete mathematical formulation of the instability model is therefore given by Equation G-19, with boundary conditions given by Equations G-26 through G-29, and where the conditions given by Equations G-24 and G-25 must be satisfied at the flame front.

### SOLUTIONS OF THE MODEL EQUATIONS

Two approximate solutions of the model equations are presented here. The first, and more accurate one, parallels the Green's function solution developed by Culick (Ref 1); the only additional feature is the treatment of the flame-front discontinuity. This solution is termed the "iterative" solution. The second solution is a perturbation solution developed by standard methods and has the advantages of portraying the contributions of the various gain and loss mechanisms explicitly and of being somewhat more amenable to hand calculations. This solution is termed the "perturbation solution".

#### ITERATIVE SOLUTION

In a way completely analogous to that fully developed by Culick in References 1 and 39, a first approximation to the solution of the model equations for the complex frequency  $K$  is given by

$$K_n^2 = k_{n,0}^2 + \int_0^L \int_0^{2\pi} \int_{r_i}^R h(\eta_{n,0}) \eta_{n,0} r dr d\phi dz \quad (G-30)$$

where  $K_n$  is the frequency of the mode ( $n$ ) being considered, and  $k_{n,0}$ ,  $\eta_{n,0}$  are solutions for the  $n^{\text{th}}$  mode of the homogeneous problem represented by Equation G-19 with  $K=0$  and Equations G-24 through G-29. The modes defined by  $k_{n,0}$  and  $\eta_{n,0}$  are the so-called natural modes; i.e., the resonant acoustical modes of the chamber in the absence of effects due to mean flow and fluctuating energy release. These modes are normalized such that  $\int_V (\eta_{n,0})^2 dV = 1$ . The practical solutions sought are the stability characteristics of individual modes; hence only one mode is treated at a time. Accordingly, the values of  $k_{n,0}$  and  $\eta_{n,0}$  for any mode of interest can be obtained by the methods presented in Appendix B.

A particular feature worthy of special mention of the development of the preceding solution is the treatment of boundary conditions of the form of Equations G-26 and G-27, where  $\bar{A}$  is defined in accordance with Equations G-20 and G-21. In principle, such boundary conditions, which involve the term  $\partial^2 \eta / \partial z^2$ , render invalid the usual orthogonality properties

utilized in constructing Green's function solutions. This difficulty is overcome by treating the  $\bar{A}$ 's as constants for the particular mode considered; this is accomplished by means of the approximation

$$\frac{1}{\bar{n}} \frac{\partial^2 \bar{n}}{\partial z^2} \approx \frac{1}{\bar{n}_{n,0}} \frac{\partial^2 \bar{n}_{n,0}}{\partial z^2}$$

used appropriately in the expressions for  $\bar{A}$ .

## PERTURBATION SOLUTION

This solution is obtained by making use of the general theorem that the problem defined by Equation G-19 and the inhomogeneous boundary conditions (Equations G-26 through G-29) can be converted to an equivalent problem with homogeneous boundary conditions. Accordingly, it can be shown that the problem expressed by Equations G-19 and G-26 through G-29 is formally equivalent to either (for example) of the following problems (see Ref 79).

$$\begin{aligned} \nabla \cdot c_0^2 \nabla \tilde{\eta} + k^2 \tilde{\eta} = h - \left( c_0^2 \frac{\partial \bar{n}}{\partial r} \right)_{r=R} R \frac{\delta(r-R)}{r} + \left( c_0^2 \frac{\partial \bar{n}}{\partial r} \right)_{r=r_i} r_i \frac{\delta(r-r_i)}{r} \\ + \left( c_0^2 \frac{\partial \bar{n}}{\partial z} \right)_{z=0} \delta(z) - \left( c_0^2 \frac{\partial \bar{n}}{\partial z} \right)_{z=L} \delta(z-L) \end{aligned} \quad (G-31)$$

with the boundary conditions

$$\left( \frac{\partial \tilde{\eta}}{\partial z} \right)_{z=L} = \left( \frac{\partial \tilde{\eta}}{\partial z} \right)_{z=0} = \left( \frac{\partial \tilde{\eta}}{\partial r} \right)_{r=R} = \left( \frac{\partial \tilde{\eta}}{\partial r} \right)_{r=r_i} = 0 \quad (G-32)$$

Or, alternatively

$$\begin{aligned} \nabla \cdot c_0^2 \nabla \tilde{\eta} + k^2 \tilde{\eta} = h - \left( c_0^2 \frac{\partial \bar{n}}{\partial r} \right)_{r=R} R \frac{\delta(r-R)}{r} + \left( c_0^2 \frac{\partial \bar{n}}{\partial r} \right)_{r=r_i} r_i \frac{\delta(r-r_i)}{r} \\ + \left( c_0^2 \bar{n} \right)_{z=0} \delta'(z) - \left( c_0^2 \bar{n} \right)_{z=L} \delta'(z-L) \end{aligned} \quad (G-33)$$

with the boundary conditions

$$\left( \tilde{\eta} \right)_{z=0} = \left( \tilde{\eta} \right)_{z=L} = 0 \quad (G-34)$$

# Contrails

$$\left(\frac{\partial \tilde{\eta}}{\partial r}\right)_{r=R} = \left(\frac{\partial \tilde{\eta}}{\partial r}\right)_{r=r_i} = 0 \quad (G-35)$$

In the preceding equations,  $\delta$  and  $\delta'$  are respectively the Dirac delta function and its derivative. In both Equations G-31 and G-33  $\tilde{\eta}$  may be interpreted as a function with the property:

$$\tilde{\eta} = \eta ; \quad 0 < z < L, \quad r_i < r < R, \quad 0 < \phi < 2\pi$$

The differences in Equations G-31 and G-33 result from the different types of boundary conditions which  $\tilde{\eta}$  is constructed to satisfy as indicated by Equations G-32, G-34, and G-35. Obviously, other forms of the basic differential equation are possible for other combinations of the boundary conditions  $\tilde{\eta} = 0$  and  $\partial \tilde{\eta} / \partial n = 0$ .

A first approximation to the solution for the complex frequency  $k$  can be obtained by the use of conventional perturbation theory (see Ref 80). The basis for the approximation rests with the assumption that the right-hand side of Equation G-31 (or Equation G-33) is small compared with the terms on the left-hand side. Thus, the first-order perturbation solution for Equation G-31 would be expected to be a reasonable approximation if the actual boundary conditions (Equations G-26 through G-29) did not depart substantially from "closed-end" conditions (note Equation G-32). Similarly, the first-order perturbation solution for Equation G-33 would be expected to be a reasonable approximation if the actual boundary conditions did not depart substantially from "closed-end" conditions at the radial boundaries and "open-end" conditions at the axial boundaries.

To illustrate the perturbation solution, the first-order approximation for  $k$  for Equation G-31 is written here; forms suitable for other boundary conditions can be obtained in a straightforward manner.

$$\begin{aligned} k_n^2 = k_{n,1}^2 &+ \int_0^L \int_0^{2\pi} \int_{r_i}^R h(\tilde{\eta}_{n,1}) \tilde{\eta}_{n,1} r dr d\phi dz \\ &- \int_0^L \int_0^{2\pi} R (c_0^2 \tilde{\eta}_{n,1}^2)_{r=R} \bar{A}_R d\phi dz \\ &+ \int_0^L \int_0^{2\pi} r_i (c_0^2 \tilde{\eta}_{n,1}^2)_{r=r_i} \bar{A}_I d\phi dz \\ &+ \int_0^{2\pi} \int_{r_i}^R (c_0^2 \tilde{\eta}_{n,1}^2)_{z=0} \bar{A}_0 r dr d\phi \\ &- \int_0^{2\pi} \int_{r_i}^R (c_0^2 \tilde{\eta}_{n,1}^2)_{z=L} \bar{A}_L r dr d\phi \end{aligned} \quad (G-36)$$

# Contrails

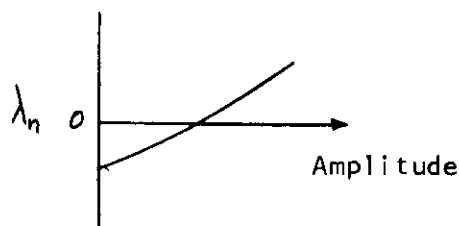
Here  $k_n$  is the complex frequency of the mode ( $n$ ) being considered, and  $k_{n,i}$ ,  $\tilde{\eta}_{n,i}$  are solutions for the  $n^{\text{th}}$  mode of the homogeneous problem represented by Equation G-31 with the right-hand side taken to be zero and the boundary conditions given by Equation G-32. The modes defined by  $k_{n,i}$  and  $\tilde{\eta}_{n,i}$  are the resonant acoustical modes of a chamber in which no acoustical losses occur at the boundaries. These modes are normalized such that  $\int_V (\tilde{\eta}_{n,i})^2 dV = 1$ . Evaluation of these modes can be made by the methods presented in Appendix B.

## NATURE OF SOLUTION

Equations G-30 and G-36 represent alternative solutions to the model formulated here. Since  $k_n = \omega_n + i\lambda_n$ , either equation in actuality yields two equations corresponding to real and imaginary parts; in physical terms, the real part is a solution for the angular frequency of oscillation and the imaginary part is a solution for the damping constant  $\lambda$ . The latter quantity is crucial to the stability problem; steady oscillations are the solutions of most interest, and these are defined by  $\lambda = 0$  (or  $\text{Im}(k_n) = 0$ ).

The contributions of the various loss and gain mechanisms to the stability problem are readily identified in the perturbation solution (Equation G-36). The first integral contains the contributions of fluctuating energy release and gross convective effects; the second and third integrals are associated with the losses at the radial boundaries (usually acoustical liners of some sort); and the fourth and fifth integrals are associated with the losses (or gains) due to acoustical radiation at either end of the chamber. The contribution of these various mechanisms are not identified so explicitly in the iterative solution (Equation G-30), since the contributions at the bounding surfaces (except for gross convection) are contained implicitly in the solutions for the natural modes defined by  $k_{n,0}$  and  $\tilde{\eta}_{n,0}$ .

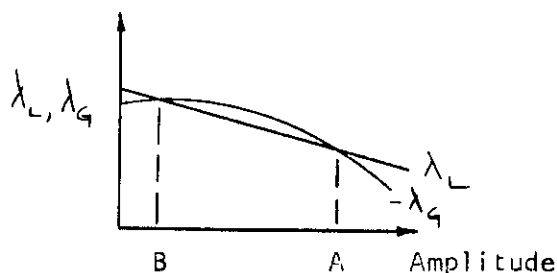
Although both Equations G-30 and G-36 are first-order approximations to a linearized equation it is still possible to include the nonlinear effects associated with the amplitude, frequency, and mode shape dependencies of the quantities  $h$ ,  $A_0$ ,  $\bar{A}_L$ ,  $\bar{A}_R$  and  $\bar{A}_T$ . For example, it can be anticipated that these quantities vary with oscillation amplitude in a known way. Then, for a number given amplitudes  $\lambda_n$  can be evaluated from either equation, and the results plotted as a function of amplitude:



# Contrails

The amplitude at which  $\lambda_n = 0$  and for which  $\lambda_n < 0$  at lesser amplitudes and  $\lambda_n > 0$  at greater amplitudes then represents the steady-state oscillation amplitude.

It is somewhat more instructive to separate  $\lambda_n$  into loss and gain components, denoted by  $\lambda_L$  and  $\lambda_G$ , respectively (where, by definition,  $\lambda_L > 0$  and  $\lambda_G < 0$ ). In the usual case, contributions to  $\lambda_G$  will come from only the combustion term in Equation G-30 or G-36 while the remainder of the terms contribute to  $\lambda_L$ . These contributions can then be computed separately as a function of amplitude, mode shape, etc., and the burner stability properties evaluated. For example, a particular case of interest would be of the following form:



Such a situation would be nonlinearly unstable in that for disturbances with an amplitude less than B no oscillation would occur, while for disturbances greater than an amplitude B a steady-state oscillation of amplitude A would result. Obviously, many other possible forms of solution exist.

Finally, by way of summary, it should be noted that eight parameters are required for the model. These are the four equivalent impedances  $\bar{A}_0$ ,  $\bar{A}_L$ ,  $\bar{A}_R$ ,  $\bar{A}_T$ , and the four parameters defined in Appendix F which characterize the combustion process ( $\bar{\tau}$ ,  $\bar{E}$ ,  $\tau'$ ,  $E'$ ); the latter parameters are contained in the unsteady combustion term in the function  $h$  defined by Equations G-18 and G-19. The dependencies of these parameters on amplitude, frequency, and mode shape are required. In the most general case, a ninth parameter,  $A_c$ , (the equivalent admittance presented by the interface between the cold upstream region and the combustion zone) would also be required.

## FORM OF PERTURBATION SOLUTION FOR ILLUSTRATIVE EXAMPLE

In Appendix H, an illustrative example of the application of the model developed here is presented utilizing the perturbation solution. The particular burner considered is cylindrical in shape, and the axial boundary conditions are such that the upstream end is every nearly a "closed-end" condition and the downstream end is very nearly an "open-end" condition. The appropriate form of the perturbation solution can be developed straightforwardly, and is written here for reference purposes:



# Contrails

$$\begin{aligned}
 K_n^2 &= K_{n,1}^2 + \int_0^L \int_0^{2\pi} \int_0^R h(\tilde{\eta}_{n,1}) \tilde{\eta}_{n,1} r dr d\phi dz \\
 &\quad - \int_0^L \int_0^{2\pi} R (c_0^2 \tilde{\eta}_{n,1}^2)_{r=R} \bar{A}_R d\phi dz \\
 &\quad + \int_0^{2\pi} \int_0^R (c_0^2 \tilde{\eta}_{n,1}^2)_{z=0} \bar{A}_0 r dr d\phi \\
 &\quad - \int_0^{2\pi} \int_0^R \left[ c_0^2 \left( \frac{\partial \tilde{\eta}_{n,1}}{\partial z} \right)^2 \right]_{z=L} (1/\bar{A}_L) r dr d\phi
 \end{aligned} \tag{G-37}$$

The boundary conditions satisfied by  $\tilde{\eta}_{n,1}$  are accordingly

$$(\tilde{\eta}_{n,1})_{z=L} = 0 \tag{G-38}$$

$$\left( \frac{\partial \tilde{\eta}_{n,1}}{\partial z} \right)_{z=0} = \left( \frac{\partial \tilde{\eta}_{n,1}}{\partial r} \right)_{r=R} = 0 \tag{G-39}$$

# *Contrails*

## Appendix H

### ILLUSTRATIVE APPLICATION OF THE INSTABILITY MODEL

#### INTRODUCTION

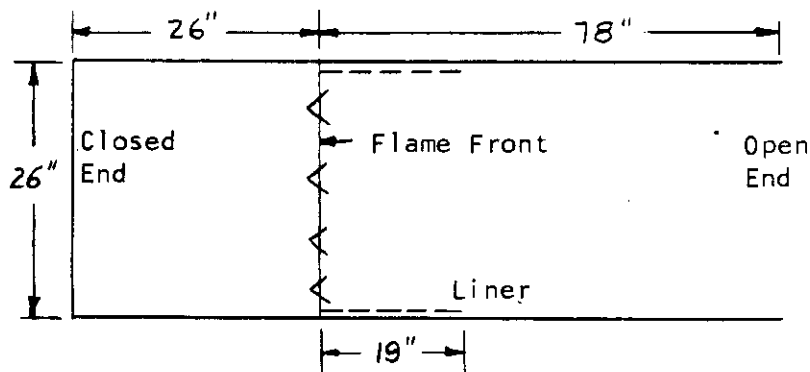
In Appendix G, an analytical model was presented for the unstable operation of a combustion chamber. It is the purpose of the present appendix to demonstrate the application of this model to a particular case of an unstable NACA 26-inch experimental afterburner (Ref 9).

The basis for the selection of this burner to demonstrate the model consisted of the following factors:

1. The geometry of the burner is a simple constant area duct of circular cross section.
2. Experimental data are available (Ref 9) from tests carried out under conditions of unstable (screech) combustion.
3. The suppression of the instability was achieved by means of an acoustic liner, a complete description of which is included in Reference 9.

This last factor is an important one because it provides the analysis with an energy loss term which, depending upon its inclusion or exclusion, should render the combustor stable or unstable.

For the purpose of the analysis, the geometry of the NASA duct burner has been idealized to the configuration shown in the following sketch:



The idealized boundary conditions adopted are a closed-end upstream boundary located approximately at the fuel spray bars, an approximate "open-end" downstream boundary and rigid chamber walls with a short section of acoustic liner located immediately downstream of the flame stabilizers. The perturbation solution to the model will be used here, and for this situation the appropriate form of the solution is given by Equation G-37 in Appendix G. Acoustical admittances have been calculated for the open end condition and for the acoustic

# Contrails

liner ( $A_L$  and  $A_R$ , respectively); for the closed end and rigid walls, the admittance coefficients ( $A_0$  and  $A_L$ , respectively) are zero. For the acoustic analysis and energy loss calculations, the temperature distribution along the combustor has been approximated by a step change occurring at the flame stabilizers; for the energy gain associated with the driving mechanism, an exponential rise in temperature is assumed.

The NASA duct burner was tested under many varied conditions; one particular set of conditions has been arbitrarily chosen for the present analysis, as follows:

Inlet Total Temperature,  $T_{01} = 1710$  deg R

Inlet Mach Number,  $M_1 = 0.22$

Inlet Total Pressure,  $P_{01} = 8.86$  psi abs

Airflow Rate = 20.5 lbm per sec

Fuel/Air Ratio = 0.0577

From the above values, the following conditions downstream of the flame front may be deduced (assuming a combustion efficiency of 90 per cent):

Total Temperature,  $T_{02} = 4270$  deg R

Mach Number,  $M_2 = 0.39$

Mean Air Velocity,  $U_2 = 1190$  ft per sec

Sonic Velocity,  $C_{02} = 3060$  ft per sec

The observed frequency of oscillation of the burner when tested under the above conditions was approximately 700 cycles per second, corresponding to the first transverse mode. Measurements of the pressure amplitude during screech were found, typically, to have a maximum value of 0.34 times the mean static pressure which in this case is approximately 2.7 psi.

In the following section, the pure acoustic frequency and mode shape will be estimated using procedures described in Appendix B. This will be followed by sections in which the energy loss and gain terms in Equation G-37 are evaluated and then examined in the light of the experimental evidence.

## ACOUSTIC MODE SHAPE

The purpose of this section is to estimate the longitudinal variation of acoustic pressure corresponding to the unperturbed mode  $\tilde{\chi}_{n,1}$  in Equation G-37; this mode satisfies the boundary conditions given by Equations G-38 and G-39. The pressure variation or mode shape in the transverse plane is assumed to be that of the first transverse mode of oscillation and neglects

# Contrails

any effects on the mode shape from the acoustic liner. Following the procedure presented in Appendix B, the variation of acoustic pressure, throughout the chamber volume may be expressed in the following manner:

$$P_{n,1}' = -1.01 P_A \cos \phi J_1(\alpha r) \cos \frac{\nu_2 \pi z}{L} e^{i k_{n,1} t}$$

for the region upstream of the flame front and

$$P_{n,1}' = P_A \cos \phi J_1(\alpha r) \left[ \cos \frac{\nu_2 \pi z}{L - z_f} - \cot \frac{\nu_2 \pi L}{L - z_f} \sin \frac{\nu_2 \pi z}{L - z_f} \right] e^{i k_{n,1} t}$$

for the region downstream of the flame front where the longitudinal mode numbers have been estimated for the conditions to be  $\nu_1 = 1.71$  and  $\nu_2 = 1.80$ ,  $P_A$  is the pressure amplitude, and  $\alpha$  has the value  $0.586\pi/R$  for the first transverse mode of a circular cylinder; the subscript  $n$  indicates that the pressure distribution is that of the normal mode.

The frequency of the natural mode is purely real and is given by

$$k_{n,1} = \omega_{n,1} = C_0 \pi \sqrt{\left(\frac{\nu_1}{R}\right)^2 + \left(\frac{\nu_2}{L}\right)^2}$$

Thus,

$$k_{n,1} = (1950)(\pi) \sqrt{\left(\frac{0.586 \times 12}{13}\right)^2 + \left(\frac{1.71}{26} \times 12\right)^2} = 5860$$

The corresponding frequency of the normal mode,  $f_{n,1} = \omega_{n,1}/2\pi$  is:

$$f_n = 930 \text{ cps}$$

This value is somewhat higher than the observed frequency of oscillation of 700 cps; some difference, however, is to be expected because of the idealized boundary conditions. A more accurate prediction would be given if the duct geometry were given in Reference 9 in sufficient detail to permit more accurate assessment of the upstream and downstream boundary conditions. Some error is also attributable to the representation of the heat release region as a discontinuity.

## NORMALIZATION OF THE ACOUSTIC PRESSURE

The dimensionless acoustic pressure,  $\tilde{p}_{n,1}$ , employed in Equation G-37 is normalized such that

$$\int \tilde{p}_{n,1}^2 dV = 1$$

# Contrails

Introducing a normalizing factor,  $N$ , where  $\bar{\eta}_{n,i} = N\eta = N \frac{P'}{P_0}$ , then for the conditions considered:

$$\left(\frac{P_A}{P_0} N\right)^2 \int_0^R \int_0^{2\pi} \cos^2 \phi J_1^2(\alpha r) r dr d\phi \left\{ \int_0^{z_L} \cos^2\left(\frac{1.71\pi z}{z_L}\right) dz + \int_{z_L}^L \left[ \cos\left(\frac{1.8\pi z}{L-z_L}\right) - 0.325 \sin\left(\frac{1.8\pi z}{L-z_L}\right) \right]^2 dz \right\} = 1$$

Therefore,  $\left(N \frac{P_A}{P_0}\right) = 0.684$  and the normalized pressures become

$$\left(\tilde{\eta}_{n,i}\right)_{z < z_L} = -0.691 \cos \phi J_1(\alpha r) \cos\left(\frac{1.71\pi z}{z_L}\right)$$

and

$$\left(\tilde{\eta}_{n,i}\right)_{z > z_L} = +0.684 \cos \phi J_1(\alpha r) \left[ \cos\left(\frac{1.8\pi z}{L-z_L}\right) - 0.325 \sin\left(\frac{1.8\pi z}{L-z_L}\right) \right]$$

## EVALUATION OF LOSS TERMS

The acoustic energy losses which are represented by terms in Equation G-37 include:

1. Net convection loss.
2. Radiation loss upstream.
3. Radiation loss downstream.
4. Radiation loss to the walls.

The net convection loss is the difference between the acoustic energy which is convected out of the downstream end of the combustor and the acoustic energy carried into the upstream end of the combustor by convection. If it is assumed that all of the acoustic energy is generated within the combustion chamber (that is, the upstream conditions provide no acoustic energy source), then the energy which is convected into the upstream end of the chamber must be supplied by radiation out of the chamber in the upstream direction. To simplify the problem, it is further assumed that all of the energy radiated in the upstream direction is eventually convected back into the chamber. This simplification eliminates the need to evaluate the upstream radiation term and that part of the net convective loss term which accounts for convection into the chamber; it is also necessary in the present case, since the upstream boundary condition cannot be defined precisely from the information presented in Reference 9.

## CONVECTION LOSS TERM

Loss or gain of acoustic energy from the combustor arises as a result of the acoustic energy level of the gases as they leave or enter the chamber. This convection of energy is represented by part of the first integral term of Equation G-37, as described in Appendix G. However, in the particular case considered here, it is unnecessary to evaluate the integral because:

1. The convection into the upstream end of the combustor has been assumed equal to the radiation out of the chamber in the upstream direction; neither of these terms are therefore evaluated.
2. The convection out of the downstream end of the combustor, which is essentially the product of the square of the acoustic pressure and the mean flow velocity, is zero as a result of the idealized downstream boundary in the acoustic analysis (that is,  $(\tilde{\eta}_{n,1})_{z=L} = 0$ ). It should be noted that this portion of the convective contribution would not vanish if the iterative solution (Equation G-30) were employed since the natural modes do not satisfy the condition  $\tilde{\eta}_{n,0} = 0$ .

## RADIATION LOSS DOWNSTREAM

The term in Equation G-37 which represents the energy loss by radiation from an open-end downstream boundary is:

$$- \int_0^{2\pi} \int_0^R \left[ c_0^2 \left( \frac{\partial \tilde{\eta}_{n,1}}{\partial z} \right)^2 \right]_{z=L} \frac{1}{\bar{A}_L} r d\phi dr$$

where the quantity  $\bar{A}_L$  is given by the downstream boundary condition, Equation G-20, which is

$$\bar{A}_L = \left( \frac{1}{\eta} \frac{\partial \eta}{\partial z} \right)_{z=L} = -ik_{n,1} \left( \rho_0 A_L + \frac{u_z z^2 \pi^2}{k_{n,1}^2 (L-z_2)^2} \right)$$

$A_L$  is the complex admittance coefficient of the downstream boundary and has been estimated for an open-ended tube, from theoretical results given in Reference 58, as:

$$\rho_0 c_0 A_L = K_L + i\sigma = 0.74 - 0.6i$$

The integral can then be evaluated, with the result being  $(-0.069 + 0.076i) c_0^2$  which represents the contributions to the real and imaginary parts of the square of the complex frequency due to the radiation at the downstream boundary.

# Contrails

## RADIATION LOSS TO THE WALLS

In the idealized model of the combustion chamber, the chamber walls were assumed to be rigid. Radiation losses to the walls, therefore, occur only in the presence of the acoustic liner. The term in Equation G-37 which accounts for the wall losses is:

$$- \int_0^{2\pi} \int_0^L R [C_0^2 \tilde{n}_{n,1}^2]_{r=R} \bar{A}_R d\phi dz$$

where  $\bar{A}_R$  can be written as

$$\bar{A}_R = -\frac{ik_{n,1}}{C_0} (K_w + i\sigma_w)$$

$K_w$  and  $\sigma_w$  are the real and imaginary parts of the liner admittance coefficient. The integral can be evaluated explicitly to yield  $(-1.44 \times (\sigma_w - iK_w) C_0^2)$ .

The complex admittance coefficient of the liner for the observed frequency of oscillation can be estimated as follows. Details of the liner employed in the burner are:

Location - Immediately Downstream of Flameholder

Length - 19 inches

Thickness,  $t$  - 0.0625 inches

Backing Distance,  $l$  - 0.75 inches

Hole Diameter,  $d$  - 0.1875 inches

Hole Spacing - 0.5 inches

Assumed Temperature at the Liner - 1700 deg R

From the above data, the following relevant quantities may be deduced:

Liner Open Area Ratio,  $\alpha = 0.11$

Effective Acoustic Length,  $l_{eff} = t + 0.8501 \times (1 - 0.7\sqrt{\alpha}) = 0.184$  inches

Sonic Velocity of Gas at 1700 deg R = 2000 ft per sec

Gas Viscosity = 0.097 lb per ft hr

Gas Density = 0.0136 lbm per cu ft



# Contraails

The resonant frequency of the acoustic liner is given by the following relation:

$$f_0 = \frac{c}{2\pi} \sqrt{\frac{\alpha}{l l_{\text{eff}}}} = 3400 \text{ cps}$$

This estimate of the resonant frequency of the liner indicates that it was not well tuned for the mode of interest in this example, since, for maximum damping of an oscillation, the resonant frequency of the liner should be close to the frequency of oscillation. For the present combustor, the most predominant frequencies observed were around 700 cps and 1500 cps. Nevertheless, the liner did prove to be effective in suppressing the oscillations.

Formulae were presented in Appendix B for the complex impedance coefficient of an acoustic liner  $\mathcal{Z} = \theta + i\chi$ . The real and imaginary parts of the admittance coefficient are related to the above quantities by

$$\kappa + i\sigma = \frac{1}{\mathcal{Z}} = \frac{1}{\theta + i\chi}$$

or, alternatively:

$$\kappa = \frac{\theta}{\theta^2 + \chi^2}$$

$$\sigma = -\frac{\chi}{\theta^2 + \chi^2}$$

The reactance ratio,  $\chi$ , is given by the equation:

$$\chi = 2\pi f_0 \frac{l_{\text{eff}}}{c\alpha} \left( \frac{f}{f_0} - \frac{f_0}{f} \right) = -6.78$$

The resistance ratio,  $\theta$ , is given by:

$$\theta = \frac{4\sqrt{\pi\mu g f}}{\alpha \rho c} \left( 1 + \frac{t}{d} + \frac{\Delta_{nl}}{d} \right)$$

where

$\Delta_{nl}/d$  is the nonlinear term and is approximately equal to  $1.62 p_i$

$p_i$  is the RMS pressure amplitude of the oscillation in lb per ft<sup>2</sup>.

Insertion of the known quantities into the above expression for  $\theta$  gives:

$$\theta = 0.061(0.825 + p_i)$$

The table on the following page presents values of the real and imaginary parts of the wall loss integral  $(-1.44 (\sigma_w - i\kappa_w) C_{02}^2)$  for a range of values of the pressure amplitude,  $p_i$ .

# Contrails

$P_i$ (lb $\bar{f}/ft^2$ )	$\theta$	$\kappa$	$\sigma$	$\text{Im}(k^2)/C_0^2$	$\text{Re}(k^2)/C_0^2$
0	0.0503	0.0011	0.1475	0.0016	0.212
1	0.110	0.0024	0.1475	0.0035	0.212
4	0.2940	0.0064	0.1470	0.0092	0.212
10	0.6600	0.0142	0.1460	0.0204	0.210
40	2.4900	0.0476	0.1300	0.0685	0.187
100	6.1400	0.0733	0.0810	0.1055	0.117
400	24.4	0.0380	0.0106	0.0547	0.0153
1000	61.0	0.0162	0.0018	0.0233	0.0026

## SUMMARY OF LOSS TERMS

The contributions from the acoustic losses to the imaginary part of the complex frequency (Equation G-37) are provided by two sources, namely, radiation from the downstream boundary and radiation to the acoustic liner. The downstream radiation term has a constant value of  $0.076 C_0^2$  whereas the liner term is a function of the amplitude of the oscillation. Figure 2 shows the contributions from these two terms plotted against the pressure amplitude (where  $\lambda_L^2 \equiv \text{Im}(k^2)$  due to losses). It should be noted that the losses initially increase with amplitude but then pass through a maximum and decrease eventually to the value given by the downstream radiation.

## EVALUATION OF ACOUSTIC DRIVING

In Appendix G it was shown that the gain or attenuation of an acoustic oscillation can be expressed in terms of the imaginary part of complex frequency for the oscillation. In this section, the contribution of the driving mechanisms to the imaginary part of the frequency are calculated for the NACA 26-inch burner (Ref 9).

The term requiring evaluation is, from Equations G-37, G-19, and G-18 of Appendix G

$$k_G^2 = - \frac{ik_{n,1}}{P_0} (\gamma-1) \int_V \omega_{\epsilon}' \tilde{\eta}_{n,1} dV \quad (H-1)$$

which serves to define  $k_G^2$  and where  $\omega_{\epsilon}'$  is given by Equation F-28 in Appendix F. There is insufficient information provided in Reference 9 to enable the role of each driving mechanism to be evaluated. Therefore, in Equation F-28, it was assumed that

# Contrails

$$\frac{r'}{r} = \eta \left( \frac{p'}{p_0} \right)$$

$$\frac{E'}{E} = 0$$

(H-2)

and Equation H-1 was evaluated for three values of  $\eta$  (-0.5, -1.0, -2.0) and three values of  $\bar{u}\bar{r}$  (0.1, 1.0, 3.0 ft) for the oscillatory mode and mean operating conditions described in the previous section. The resulting values of  $\text{Im}(k_4^2)$  are shown in Figure 52, from which it can be seen that the  $\text{Im}(k_4^2)$  is significantly dependent upon  $\eta$  and  $\bar{u}\bar{r}$ . The values of  $\text{Im}(k_4^2)$  when  $\eta = 0$  are the contribution to the gain due to the last two terms in Equation F-27. It may be concluded that as the energy release zone becomes small (i.e.,  $\bar{u}\bar{r} \rightarrow 0$ ), a major contribution to the driving is due to the axial velocity fluctuations which are associated with the axial mode component of the acoustic oscillation. For larger values of  $\bar{u}\bar{r}$ , (0(1)), the pressure sensitive gains become dominant. For the example burner, it is expected that  $\bar{u}\bar{r} \sim 3$  feet, but unfortunately  $\eta$  is not known, except that it should be of order -0.5 (see Appendix F). It may, therefore, be concluded that the  $\text{Im}(k_4^2)$  due to driving mechanisms is  $\approx 0.1 C_{O_2}^2$ .

Comparing the above value of  $\text{Im}(k_4^2)$  due to driving with the contribution from the loss mechanisms it may be concluded that (see Fig 2, where  $\lambda_4^2 \equiv \text{Im}(k_4^2)$ ):

1. The driving and loss terms are of the same order of magnitude.
2. At low amplitudes of pressure oscillation, driving exceeds losses.
3. At pressure amplitudes of one hundredth of the mean pressure level the losses exceed the gains with the acoustic liner present.

The uncertainties in both the driving and loss terms do not permit accurate prediction of the stability boundaries, and amplitudes of steady oscillation, at this time. However, it can be concluded that the example burner will be unstable at low amplitudes, with or without the acoustic liner, and close to stable operation at amplitudes of approximately one hundredth of the mean pressure level with the liner present. This is qualitatively in accord with the experimental observations.

The driving analysis, which is a linearized analysis, indicates a trend towards unstable operation at amplitudes greater than one tenth of the mean pressure level. However, in practice it is observed that at

# Contrails

large amplitudes burners operate in a stable manner, due to nonlinear effects in both the driving and dissipative mechanisms. One such effect in the driving terms may be evaluated by retaining a higher order term in Equation H-2, where it may be shown that

$$\frac{\zeta'}{\zeta} = \eta \left( \frac{p'}{p_0} \right) \left[ 1 + \frac{\eta-1}{2} \left( \frac{p'}{p_0} \right) \right] \equiv N \eta \frac{p'}{p_0} \quad (H-3)$$

At constant values of  $\eta$ ,  $N'$  decreases with increasing amplitudes as shown in the following table:

	<u><math>p'/p_0 = 0.1</math></u>	<u><math>p'/p_0 = 0.25</math></u>	<u><math>p'/p_0 = 0.4</math></u>
$\eta = -0.1$	0.945	0.875	0.8
$\eta = -0.5$	0.925	0.813	0.7
$\eta = -1.0$	0.90	0.750	0.6
$\eta = -2.0$	0.85	0.625	0.4

Referring to Figure 52, it can be observed that  $\text{Im}(k_0^2)$  decreases as the exponent in the  $\zeta' - p'$  relationship decreases. Therefore, nonlinear effects reduce the gain from the driving mechanisms at large amplitudes of oscillation.

## Appendix I

### DISCUSSION OF TEST PLAN

#### INTRODUCTION

It is emphasized at the outset that the test plan formulated here is intended primarily for the purpose of verifying the analytical model; this allows some freedom in the selection of experimental apparatus and test techniques which would not otherwise be available if the test plan were to be directed solely toward operational hardware.

The plan consists basically of the following tests to be conducted on a model burner:

1. The determination of the acoustical losses associated with the nozzle and the upstream boundary of the burner under cold flow conditions. This can be accomplished by observing the decay rate of resonant oscillations induced by an appropriate oscillator. The amplitude dependence of these losses is of particular interest.
2. The determination of the acoustical losses associated with a liner, under cold flow conditions. This can be accomplished by adding different lengths of liner to the basic burner configuration and observing the decay rate of oscillations as in 1 above.
3. The determination of oscillation amplitudes as a function of fuel-air ratio and mean static pressure level in the burner, with combustion. This is a straightforward procedure provided that instability can be induced in the burner. It is anticipated that appropriate modifications of the fuel injection system will be necessary to induce instability. Data should be obtained for various lengths of liner in the burner.
4. The determination of oscillation amplitudes as a function of fuel-air ratio and mean static pressure level in the burner, with combustion and when subjected to external oscillatory disturbances of appreciable magnitude. Emphasis here should be placed upon investigating operating conditions which yield stable performance in the absence of external disturbances.
5. A repeat of step 4, but with various inlet flow distortion patterns imposed upon the burner rather than external oscillatory disturbances.

The following sections are devoted to a discussion of the test rig requirements, the nature of the tests, and the required data reduction techniques necessary for the successful execution of such a test plan.

# Contrails

For the purpose of illustrating the use of the data in assessing the analytical model, the perturbation form of the solution (Equation G-36) will be used here. Specifically, the form of Equation G-36 applicable to a cylindrical burner will be employed; hence the complex frequency is given by

$$\begin{aligned}
 k_n^2 = k_{n,1}^2 &+ \int_0^L \int_0^{2\pi} \int_0^R h(\tilde{\eta}_{n,1}) r dr d\phi dz \\
 &- \int_0^L \int_0^{2\pi} R (c_0^2 \tilde{\eta}_{n,1}^2)_{r=R} \bar{A}_R d\phi dz \\
 &+ \int_0^{2\pi} \int_0^R (c_0^2 \tilde{\eta}_{n,1}^2)_{z=0} \bar{A}_0 r dr d\phi \\
 &- \int_0^{2\pi} \int_0^R (c_0^2 \tilde{\eta}_{n,1}^2)_{z=L} \bar{A}_L r dr d\phi
 \end{aligned} \tag{I-1}$$

In terms of this equation, then, the purpose of the test plan is to determine the equivalent acoustical admittances  $\bar{A}_R$ ,  $\bar{A}_0$ , and  $\bar{A}_L$  (associated with the liner, upstream boundary, and nozzle, respectively) as a function of oscillation amplitude and frequency; to determine, for a single geometrical configuration, the parameters of the driving mechanisms ( $\bar{\tau}$ ,  $\bar{\tau}'$ ,  $\bar{E}$ ,  $\bar{E}'$ ) incorporated into the function  $h$  as a function of oscillation amplitude and frequency; and to apply the model with the parameters so determined to other geometrical configurations.

The choice of the use of the perturbation solution rather than the iterative solution (e.g., Equation G-30) is primarily a matter of convenience in that the contributions of the boundary losses are displayed explicitly in Equation I-1; in principle, either solution can be used.

## TEST RIG REQUIREMENTS

### ENERGY CONSIDERATIONS

A primary consideration is the amount of acoustical power required to maintain oscillations of an appreciable amplitude during the cold-flow tests. The amount of power required can be estimated from the fact that the maximum fractional acoustical energy loss per cycle of oscillation can be expected to be approximately unity (see Appendix C). The acoustical energy in a cylindrical volume is given approximately by

# Contrails

$$E \approx \frac{1}{4\rho_0 c_0^2} (P')^2 V$$

If an L/D ratio of three is assumed, then

$$E \approx \frac{3\pi}{16\gamma} \left(\frac{P'}{\rho_0}\right)^2 \rho_0 D^3$$

The oscillation frequency of the first transverse mode is

$$f = 0.586 c_0 / D \quad (1-2)$$

so that the acoustical power required to maintain an oscillation

$$P = Ef \approx \frac{3\pi}{16} (0.586) c_0 \rho_0 D^2 \left(\frac{P'}{\rho_0}\right)^2 \quad (1-3)$$

For  $\rho_0 = 15$  psia,  $T = 2600$  deg R, and  $(P'/\rho_0) = 0.2$  Equations 1-2 and 1-3 yield the following results for oscillation frequency and acoustic power required as a function of burner diameter:

$\frac{D}{\text{(ft)}}$	$\frac{f}{\text{(cps)}}$	$\frac{P}{\text{(hp)}}$
0.5	2930	23.7
1.0	1465	95
2.0	732	380

These numbers indicate the obvious desirability of confining tests to rather small burners.

## BURNER CONFIGURATION AND AUXILIARY EQUIPMENT REQUIREMENTS

The requirements for the burner configuration are basically quite simple. A cylindrical burner is required, and provisions should be made for enabling either end to be acoustically closed during cold flow tests. For the cold flow tests, it would in fact be desirable to use a smaller scale version of the burner than that used for tests with combustion; this would have the advantages of requiring less acoustical power for driving and providing resonant frequencies for cold flow in the same range as those for hot flow in the larger burner (since  $f \sim \sqrt{T}$ ), while not sacrificing the accuracy of the measurements (since the cold flow losses can be easily scaled).

In addition to the burner, two acoustic liners varying only in length should be provided. The hole size, spacing, and backing cavity should be selected to yield a resonant liner frequency in the same range as the

expected oscillation frequency, although this is not absolutely necessary.

A conventional converging nozzle should also be provided, as well as the means for acoustically closing either end of the burner while maintaining a through flow velocity during cold-flow tests. This can probably best be accomplished by means of perforated diaphragms.

The major item of auxiliary equipment required is the acoustic oscillator. The requirements for such an oscillator are that it be capable of supplying the power required by the burner size, that it be capable of a variable frequency output, and that it can be used to excite various transverse modes efficiently. At lower power levels, conventional oscillators or bi-stable jets would appear to be satisfactory. At higher power levels, it seems inevitable that the energy of the flow entering the burner will have to be employed as the source of acoustical power; a rotating disk configuration upstream of the burner offers some promise in this regard.

## INSTRUMENTATION

The instrumentation required for the measurement of mean flow quantities (pressures, temperatures, velocities, flow, etc) is quite standard. In addition, static pressure transducers, with a response appropriate to the frequency range being considered, will be required at various axial and circumferential locations; their purpose is of course to identify the mode shape, as well as to measure oscillation frequency. Hence, it will be necessary to sense the relative phase differences between the various transducers. Finally, some method of detecting unsteady velocity distributions within the burner is desirable. The basic purpose of such measurements would be to obtain semi-quantitative information on the mode shape in the radial direction; hence, the measurements need not be quantitatively precise.

## TEST PROCEDURES AND DATA REDUCTION

### COLD FLOW TESTS WITHOUT LINERS

#### Test Procedure

For any selected instability mode, the test procedure will consist of exciting the mode with an oscillator, tuning the oscillator to obtain maximum oscillation amplitude, observing the frequency and mode shape, turning off the oscillator, and observing the rate of decay of the oscillation as a function of time.

This procedure should be conducted for the following configurations:

1. Burner with downstream end (acoustically) closed, for several (i.e., at least three) oscillation amplitudes and mean flow velocities.



# Contrails

2. Burner and nozzle with upstream end (acoustically) closed, for several oscillation amplitudes and mean flow velocities.
3. Burner and nozzle with upstream end open, for several oscillation amplitudes and mean flow velocities.

## Data Reduction

The results of the preceding tests can be used to obtain the acoustical admittances of the nozzle and upstream end of the burner ( $A_L$  and  $A_o$  which appear in  $\bar{A}_L$  and  $\bar{A}_o$  in Equation 1-1) as a function of oscillation amplitude and mean flow velocity as follows.

In the first series of tests,  $A_L \approx 0$ , and hence Equation 1-1 yields two equations of the following functional form:

$$\omega^2 = f_1 [A_o(p_i', u_o), u_o] \quad (1-4)$$

$$\lambda^2 = f_2 [A_o(p_i', u_o), u_o] \quad (1-5)$$

where  $p_i'$  is the oscillation amplitude and it is to be noted that  $A_o$  is in general complex. For any given mean flow velocity ( $u_o$ ) and oscillation amplitude,  $\omega$  is known from the observed frequency and  $\lambda$  can be deduced from the rate of decay of the oscillation; hence Equations 1-4 and 1-5 can be solved simultaneously for the two components of  $A_o(p_i', u_o)$ .

In the second series of tests,  $A_o \approx 0$ , and Equation 1-1 yields

$$\omega^2 = f_1 [A_L(p_i', u_o), u_o] \quad (1-6)$$

$$\lambda^2 = f_2 [A_L(p_i', u_o), u_o] \quad (1-7)$$

Hence, Equation 1-6 and 1-7 can be solved simultaneously for the two components of  $A_L(p_i', u_o)$ .

The third series of tests is in actuality redundant, but serve the useful purpose of confirming the results of the previous tests. That is, Equation 1-1 yields

$$\omega^2 = f_1 [A_o(p_i', u_o), A_L(p_i', u_o), u_o]$$

$$\lambda^2 = f_2 [A_o(p_i', u_o), A_L(p_i', u_o), u_o]$$

which can be used to check the consistency of the results, since  $A_L$  and  $A_o$  are now presumably known.

# Contrails

## COLD FLOW TESTS WITH LINERS

### Test Procedure

The test procedure in this series of tests will be identical to that of the previous tests; the only difference will be the presence of the liner.

Tests will be conducted for at least two different liner lengths, for several oscillation amplitudes and mean flow velocities. The tests need be conducted only for the burner and nozzle, with the upstream end open.

### Data Reduction

The results of these tests can be used to obtain the acoustical admittance ( $A_R$ , which appears in  $\bar{A}_R$  in Equation 1-1) as a function of oscillation amplitude and mean flow velocity as follows.

In the configuration of these tests, Equation 1-1 yields two equations of the following functional form:

$$\omega^2 = f_1 [A_o(p'_i, u_o), A_L(p'_i, u_o), A_R(p'_i, u_o), u_o] \quad (1-8)$$

$$\lambda^2 = f_2 [A_o(p'_i, u_o), A_L(p'_i, u_o), A_R(p'_i, u_o), u_o] \quad (1-9)$$

Since  $A_o(p'_i, u_o)$  and  $A_L(p'_i, u_o)$  are known from the results of the tests without the liners, Equations 1-8 and 1-9 may be solved simultaneously for the two components of  $A_R(p'_i, u_o)$ . This can be accomplished for both lengths of liner, where the results of one may be used to check the consistency of the other.

## COMBUSTION TESTS WITH UNIFORM FLOW

### Test Procedure

The test procedure here consists of establishing the frequency, mode shape, and oscillation amplitude of any instability found in the three burner configurations (i.e., without liner, and with two different lengths of liner) as a function of static pressure level, fuel-air ratio, mean flow velocity, and, possibly, inlet temperature.

### Data Reduction

The results of these tests for a single geometrical configuration can be used to deduce two parameters of the driving mechanisms as follows. If it is assumed that the driving mechanisms can be characterized by the two

# Contrails

parameters  $\eta$  and  $\bar{a}$  (see Appendix F) then Equation 1-1 will yield the following two functional relations:

$$\omega^2 = f_1[\eta(p_i', u_o, \text{etc}), \bar{a}(p_i', u_o, \text{etc}), A_o, A_L, A_R, u_o] \quad (1-10)$$

$$0 = f_2[\eta, \bar{a}, A_o, A_L, A_R, u_o] \quad (1-11)$$

where the second equation is a result of the fact that for steady oscillations,  $\lambda = 0$ . Since  $A_o$ ,  $A_L$ , and  $A_R$  are known from the results of previous tests, then Equations 1-10 and 1-11 can be solved for  $\eta$  and  $\bar{a}$  for any given set of experimental conditions.

The results of the tests for the other burner configurations (i.e., excluding the configuration for which  $\eta$  and  $\bar{a}$  were determined) can then be used to assess the adequacy of the model. That is, Equations 1-10 and 1-11 can be used to predict  $p_i'$  as a function of mean flow conditions (e.g., fuel-air ratio) since  $\eta(p_i')$ ,  $\bar{a}(p_i')$ ,  $A_o$ ,  $A_L$ , and  $A_R$  will be known.

## COMBUSTION TESTS WITH TRANSIENT DISTURBANCES

### Test Procedure

The test procedure for these tests is quite obvious. The only point worthy of special mention is that care must be exercised in identifying the magnitude of initial disturbance; this can be accomplished from the amplitude and frequency indicated by the static pressure transducers.

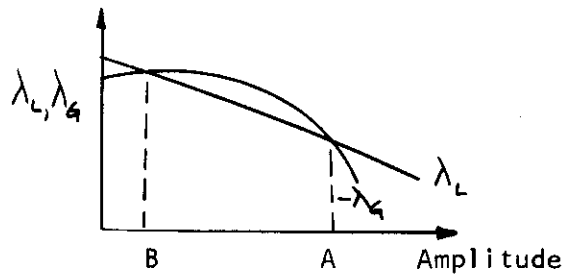
### Data Reduction

The data obtained from these tests can be used for further assessment of the model, as follows. Equation 1-11 can be written symbolically as

$$\lambda_L + \lambda_G = 0 \quad (1-12)$$

where  $\lambda_L$  denotes the contribution of all of the acoustic loss terms, and  $\lambda_G$  denotes the contribution of the acoustic gain terms. Since the previous tests have yielded all of the parameters which determine  $\lambda_L$  and  $\lambda_G$  as a function of oscillation amplitude and mean flow conditions, then for any set of mean flow conditions, curves of  $\lambda_L$  and  $\lambda_G$  versus oscillation amplitude can be constructed. In particular, for any transient-disturbance test which indicates unstable behavior of a burner which is stable to small amplitude disturbances, such curves can be constructed. If they are to correctly reflect the experimental results, then they must be of the following form:

# Contrails



Thus, the model should be capable of predicting this type of behavior.

## COMBUSTION TESTS WITH NONUNIFORM INLET FLOW

These tests are self-explanatory, and require no further discussion here.

## REFERENCES

1. Culick, F. E. C., "Stability of High-Frequency Pressure Oscillations in Rocket Combustion Chambers", AIAA Journal, vol. 1, no. 5, May, 1963, p. 1097.
2. Crocco, L. and Cheng, S.-I., Theory of Combustion Instability in Liquid Propellant Rocket Motors, The Advisory Group for Aeronautical Research and Development, North Atlantic Treaty Organization, 1956.
3. Priem, R. J. and Guentert, D. C., Combustion Instability Limits Determined by a Nonlinear Theory and a One-Dimensional Model (NASA TN D-1409), National Aeronautics and Space Administration, Washington, D. C., October, 1962.
4. Sirignano, W. A. and Crocco, L., "A Shock Wave Model of Unstable Rocket Combustors", AIAA Journal, vol. 2, no. 2, 1964, p. 1285.
5. Crocco, L., "Theoretical Studies on Liquid-Propellant Rocket Instability", Tenth Symposium (International) on Combustion, The Combustion Institute, 1965, p. 1101.
6. Priem, R. J., Influence of Combustion Process on Stability (NASA TN D-2957), National Aeronautics and Space Administration, Washington, D. C., August, 1965.
7. Hart, R. W. and McClure, F. T., "Theory of Acoustic Instability in Solid Propellant Rocket Combustion", Tenth Symposium (International) on Combustion, The Combustion Institute, 1965, p. 1047.
8. Clapp, C. J., Full Scale Turbofan Duct Burner Test Program (NASA CR 54637), National Aeronautics and Space Administration, Cleveland, Ohio, March 18, 1968.
9. Harp, J. L., et al, Investigation of Combustion Screech and a Method of Its Control (NACA RM E53L24b), National Advisory Committee for Aeronautics, Washington, D. C., March, 1954.
10. Takeno, T., Experimental Studies on Driving Mechanism of the High Frequency Combustion Oscillation in a Premixed Gas Rocket, Institute of Space and Aeronautical Science Report No. 420, University of Tokyo, January, 1968.
11. Trout, A. M., et al, Investigation of Afterburner Combustion Screech and Methods of Its Control at High Combustor (NACA RM E55K25), National Advisory Committee for Aeronautics, Washington, D. C., May 14, 1956.
12. A Summary of Preliminary Investigations Into the Characteristics of Combustion Screech in Ducted Burners (NACA Report No. 1384), Lewis Laboratory Staff, National Advisory Committee for Aeronautics, Washington, D. C., 1958.

# Contrails

13. King, Charles, R., Experimental Investigation of Effects of Combustion - Chamber Length and Inlet Total Temperature, Total Pressure, and Velocity on Afterburner Performance (NACA RM E57C07), National Advisory Committee for Aeronautics, Washington, D. C., June 3, 1957.
14. Bragdon, Thomas A., et al, Interim Report on Experimental Investigation of High Frequency Oscillations in Ramjet Combustion Chambers (METEOR Report No. UAC-53), United Aircraft Corporation, Research Department, October, 1951.
15. "The Interrelation of High Frequency Pressure Oscillations and the Combustion Process in Air-Breathing Engines", Fourth Symposium on Combustion Instability in Liquid Propellant Rocket Motors (AD 426 912), Defense Documentation Center for Scientific and Technical Information, Alexandria, Va., 1967.
16. Rogers, D. E. and Marble, F. E., "A Mechanism for High-Frequency Oscillation in Ramjet Combustors and Afterburners", Jet Propulsion, Guggenheim Jet Propulsion Center, California Institute of Technology, June, 1956.
17. Basic Considerations in the Combustion of Hydrocarbon Fuels with Air, Propulsion Chemistry Division, Lewis Flight Propulsion Laboratory (NACA 1300), National Advisory Committee for Aeronautics, 1957.
18. Newton, R. T. and Truman, J. C., An Approach to the Problem of Screech in Ducted Burners, General Electric Company, General Engineering Laboratory, Schenectady, N. Y., March, 1954.
19. Berman, K. and Cheney, S. H., "Combustion Studies in Rocket Motors", J. American Rocket Soc., vol. 23, 1953, p. 89.
20. Ellis, H., et al, "Experimental Investigation of Combustion Instability in Rocket Motors", Fourth Symposium on Combustion, Williams and Wilkins Co., Baltimore, Md., 1953, p. 880.
21. Reardon, F. H., Combustion Instability of Liquid Propellant Rocket Motors (AD 259 357), Department of Aeronautical Engineering, Princeton University, Princeton, N. J., June, 1961.
22. Hammer, S. S. and Agosta, V. D., "Longitudinal Wave Propagation in Liquid Propellant Rocket Motors", ARS Journal, vol. 32, no. 3, March, 1962, pp. 366-376.
23. Crocco, L., Grey, J., and Harrje, D. T., "Theory of Liquid Propellant Combustion Instability and Its Experimental Verification", ARS Journal, vol. 30, no. 2, February, 1960, p. 159.
24. Ross, C. C. and Datner, P. P., Combustion Instability in Liquid Propellant Rocket Motors--A Survey, AGARD, NATO, December, 1953.
25. Bailey, C. R., An Investigation of the Use of Acoustic Energy Absorbers to Damp LOX/RP-1 Combustion Oscillations (NASA TN D-4210), National

# Contrails

- Aeronautics and Space Administration, Washington, D. C., November, 1967.
26. Combs, L. P., et al, Combustion Stability Rating Techniques (AFRPL-TR-66-229), Rocketdyne, A Division of North American Aviation, Inc., Canoga Park, Cal., September, 1966.
  27. Crocco, L., Grey, J., and Harrje, D. T., "Theory of Liquid Propellant Rocket Combustion Instability and Its Experimental Verification", ARS Journal, vol. 30, no. 2, February, 1960.
  28. Crocco, L., Harrje, D. T., and Reardon, F. H., "Transverse Combustion Instability in Liquid Propellant Rocket Motors", ARS Journal, vol. 32, no. 3, March, 1962, pp. 366-376.
  29. Propellant Sprays in Liquid Rocket Engines (AD 637 236), Dynamic Science Division, Monrovia, Cal., June, 1966.
  30. Beltran, M. R., et al, Analysis of Liquid Rocket Engine Combustion Instability (TN Report No. AFRPL-TR-65-254, AD 482 021), Dynamic Science Corporation, Monrovia, Cal., January, 1966, pp. 1-150.
  31. Zinn, B. T., "A Theoretical Study of Nonlinear Combustion Instability in Liquid Propellant Rocket Engines", Third Combustion Conference (AD 807 276), Georgia Institute of Technology, Atlanta, Ga., vol. 1, February, 1967, pp. 441-452.
  32. Heidmann, Marcus F. and Wieber, Paul R., Analysis of Frequency Response Characteristics of Propellant Vaporization (NASA TN D-3749), National Aeronautics and Space Administration, Washington, D. C., December, 1966.
  33. Heidmann, Marcus F. and Wieber, Paul R., Analysis of n-Heptane Vaporization in Unstable Combustor with Traveling Transverse Oscillations (NASA TN D-3424), National Aeronautics and Space Administration, Washington, D. C., May, 1966.
  34. Dykema, O. W., An Engineering Approach to Combustion Instability (AD 475 934), Aerospace Corporation, El Segundo, Cal., November, 1965.
  35. Tobey, Aubrey C., Combustion Instability Studies (AD 449 764), 1964 Spring Meeting, Western States Section, The Combustion Institute, Stanford University, Stanford, Cal., April, 1964.
  36. Sirignano, W. A., A Theoretical Study of Non-Linear Combustion Instability: Longitudinal Mode, Guggenheim Laboratories for the Aerospace Propulsion Sciences, Princeton University, Princeton, N. J., March, 1964.
  37. Priem, Richard J., "Tutorial Seminar Paper on 'L and J Combustion Model' ", Second Combustion Conference (AD 484 561), National Aeronautics and Space Administration, Cleveland, Ohio, vol. 1, May, 1966, pp. 139-146.

# Contrails

38. Tsien, H. S., "The Transfer Functions of Rocket Nozzles", ARS Journal, May-June, 1952.
39. Culick, Fred E. C., Stability of High Frequency Pressure Oscillations in Gas and Liquid Rocket Combustion Chambers (Technical Report 480), Massachusetts Institute of Technology Aerophysics Laboratory, June, 1961.
40. Crocco, L., Harrje, D. T., and Sirignano, W. A., "Nonlinear Aspects of Combustion Instability in Liquid Propellant Rocket Motors", Second Combustion Conference (AD 484 561), Princeton University, Princeton, N. J., vol. 1, May, 1966, pp. 63-106.
41. Sirignano, W. A., Crocco, L., and Harrje, D. T., "Acoustic Liner Studies", Third Combustion Conference (AD 807 276), Princeton University, Princeton, N. J., vol. 1, February, 1967, pp. 581-586.
42. Garrison, G., "The Application of Absorbing Liners for the Suppression of Rocket Combustion Instability", Third Combustion Conference (AD 807 276), Jet Propulsion Laboratory, Pasadena, Cal., vol. 1, February, 1967, pp. 553-554.
43. McClure, F. T., Hart, R. W., and Bird, J. F., "Acoustic Resonance in Solid Propellant Rockets", J. Applied Physics, vol. 31, May, 1960, pp. 884-896.
44. Bird, J. F., McClure, F. T., and Hart, R. N., "Acoustic Instability in the Transverse Modes of Solid Propellant Rockets", 12th International Astronautical Congress, Academic Press, 1963, pp. 459-473.
45. McClure, F. T., Hart, R. W., and Bird, J. F., "Solid Propellant Rockets as Acoustic Oscillators", Progress in Astronautics and Rocketry, Volume 1, Solid Propellant Research (M. Summerfield, Editor), Academic Press, 1960, pp. 423-451.
46. Hart, R. W. and Bird, J. F., "Scaling Problems Associated with Unstable Burning in Solid Propellant Rockets", Ninth Symposium (International) on Combustion, The Combustion Institute, 1963, pp. 993-1004.
47. Cantrell, R. H. and Hart, R. W., "Interaction between Sound and Flow in Acoustic Cavities: Mass, Momentum, and Energy Considerations", J. Acoustical Society of America, vol. 36, 1964, pp. 697-706.
48. Hart, R. W. and McClure, F. T., "Combustion Instability: Acoustic Interaction with a Burning Propellant Surface", J. Chemical Physics, vol. 30, June, 1959, pp. 1501-1514.
49. Bird, J. F., et al, "Effect of Solid Propellant Compressibility on Combustion Instability", J. Chemical Physics, vol. 32, May, 1960.
50. Porrinelli, L. A., One-Dimensional Nonlinear Model for Determining Combustion Instability in Solid Propellant Rocket Motors, (NASA



# Contrails

- TN D-3410), National Aeronautics and Space Administration, April, 1966.
51. Price, E. W., "Experimental Solid Rocket Combustion Instability", Tenth Symposium (International) on Combustion, The Combustion Institute, 1955, pp. 1067-1080.
  52. Zucrow, M. J. and Osborn, J. R., "An Experimental Study of H-F Combustion Pressure Oscillations in a Gaseous Air-Propellant Rocket Motor", 4th Symposium on Combustion Instability in Liquid Propellant Rocket Motors, December, 1957.
  53. Zucrow, M. J., Osborn, J. R., and Bonnell, J. M., Summary of Experimental Investigations of Combustion Pressure Oscillations in Gaseous Propellant Rocket Motors (Report No. F-32-2), Jet Propulsion Center, Purdue University, Lafayette, Ind., June, 1963.
  54. Zucrow, M. J., Osborn, J. R., and Bonnell, J. M., High Frequency Combustion Pressure Oscillations in Motors Burning Gaseous Propellants (Report No. TM-65-5), Jet Propulsion Center, Purdue University, Lafayette, Ind., August, 1965.
  55. Zucrow, M. J., et al, Limiting Conditions for the Onset of Combustion Pressure Oscillations (Transverse Mode) in Gaseous Propellant Rocket Motors (AIAA Paper 64-370), 1st Annual AIAA Meeting, Washington, D. C., June, 1964.
  56. Bowman, C. T., Experimental Investigation of H-Frequency Longitudinal Combustion Instability in Gaseous Propellant Rocket Motors (Technical Report 784), Department of Aerospace and Mechanical Sciences, Princeton University, Princeton, N. J., January, 1967.
  57. Bowman, C. T., Glassman, I., and Crocco, L., "Combustion Instability in Gas Rockets", AIAA Journal, vol. 3, no. 10, October, 1965, p. 1981.
  58. Morse, P. M., Vibration and Sound, McGraw Hill, Second Edition, 1948.
  59. Kinsler, L. E. and Frey, A. R., Fundamentals of Acoustics, John Wiley and Sons, Inc., New York, Second Edition, 1962.
  60. Lambe, C. G. and Tranter, C. J., Differential Equations for Engineers and Scientists, English University Press, 1961.
  61. Stollery, J. L., Smith, J. E., and Park, C., The Effects of Vibrational Relaxation on Hypersonic Nozzle Flows (Report No. 111a), Department of Aeronautics, Imperial College, University of London, England, 1962.
  62. Lukasik, S. J. and Young, J. E., "Vibrational Relaxation Times in Nitrogen", J. Chemical Physics, Acoustics Laboratory, Massachusetts Institute of Technology, Cambridge, Mass., vol. 27, no. 5, November, 1957, pp. 1149-1155.

# Contrails

63. Temkin, S., Attenuation and Dispersion of Sound by Particulate Relaxation Processes (Contract No. nonr 562(37)), Department of the Navy, Office of Naval Research, February, 1966.
64. Wieber, R. W. and McClure, F. T., "Theory of Acoustic Instability in Solid-Propellant Rocket Combustion", Tenth Symposium (International) on Combustion, The University of Cambridge, Cambridge, England, 1965, pp. 1047-1065.
65. A Study of the Suppression of Combustion Oscillations with Mechanical Damping Devices (Report No. PWA FR-2596), Pratt & Whitney Aircraft, Florida Research and Development Center, 1967.
66. Utvik, D. H., et al, "Evaluation of Absorption Liners for Suppression of Combustion Instability in Rocket Engines", AIAA Propulsion Joint Specialist Conference (AIAA Paper No. 65-585), American Institute of Aeronautics and Astronautics, New York, June, 1965.
67. Blackman, A. W., "Effect of Nonlinear Losses on the Design of Absorbers for Combustion Instabilities", ARS Journal, American Rocket Society, New York, vol. 30, no. 11, November, 1960, pp. 1022-1028.
68. McAuliffe, C. E., The Influence of High Speed Air Flow on the Behavior of Acoustical Elements, M. Sc. Thesis, Massachusetts Institute of Technology, Cambridge, Mass., 1950.
69. Buffum, F. G., et al, Acoustic Losses of a Subscale, Cold-Flow Rocket Motor for Various "J" Values (NAVWEPS Report No. 8971), U. S. Naval Ordnance Test Station, China Lake, California, February, 1966.
70. Combustion of Solid Propellants and Low Frequency Combustion Instability (NOTS TP 4244), U. S. Naval Ordnance Test Station, China Lake, California, June, 1967.
71. Whitehead, D. S., "The Vibration of Air in a Duct with a Subsonic Mean Flow", The Aeronautical Quarterly, University Engineering Laboratory, Cambridge, England, 1961, p. 34.
72. Vincenti, W. G., Lectures on Physical Gas Dynamics, Stanford University, Stanford, California, 1961.
73. Spalding, D. B., Some Fundamentals of Combustion, Butterworths Scientific Publications, London, England, 1955.
74. Spalding, D. B., "Combustion of a Single Droplet and of a Fuel Spray", Selected Combustion Problems (AGARD), Butterworths Scientific Publications, London, England, 1954.
75. Priem, R. J. and Heidmann, M. F., Propellant Vaporization as a Design Criterion for Rocket Engine Combustion Chambers (NASA TR R-67), National Aeronautics and Space Administration, 1960.

# Contrails

76. Myers, B. F. and Bartle, E. R., Reaction and Ignition Delay Times in the Oxidation of Propane, AIAA Preprint 68-633, June, 1968.
77. Zukoski, E. E. and Wright, F. H., "Flame Spreading from Bluff-Body Flameholders", Eighth Symposium (International) on Combustion, Williams and Williams, Baltimore, Md., 1962, pp. 933-943.
78. Howe, N. M. Jr., Shipman, C. W., and Vranos, A., "Turbulent Mass Transfer and Rates of Combustion in Confined Turbulent Flames", Ninth Symposium (International) on Combustion, Academic Press, New York, 1963, pp. 36-47.
79. Friedman, B., Principles and Techniques of Applied Mathematics, John Wiley and Sons, Inc., New York, 1956, pp. 153-156, 227-229.
80. Courant, R. and Hilbert, D., Methods of Mathematical Physics, Interscience Publishers, Inc., New York, vol. 1, 1953, pp. 343-350.

# *Contrails*

## DOCUMENT CONTROL DATA - R &amp; D

(Security classification of title, body of abstract and indexing annotation must be entered when the overall report is classified)

1. ORIGINATING ACTIVITY (Corporate author)		2a. REPORT SECURITY CLASSIFICATION	
Northern Research and Engineering Corporation (NREC)		UNCLASSIFIED	
		2b. GROUP	
3. REPORT TITLE			
PROPULSION SYSTEM FLOW STABILITY PROGRAM (DYNAMIC) PART XII. UNSTEADY COMBUSTION IN DUCT BURNERS AND AFTERBURNERS			
4. DESCRIPTIVE NOTES (Type of report and inclusive dates)			
Phase I Final Technical Report			
5. AUTHOR(S) (First name, middle initial, last name)			
D. M. Dix, P. L. Duffield and J. E. Smith (NREC)			
6. REPORT DATE		7a. TOTAL NO. OF PAGES	7b. NO. OF REFS
December 1968		1 - xiv plus 229	80
8a. CONTRACT OR GRANT NO.		9a. ORIGINATOR'S REPORT NUMBER(S)	
F33615-67-C-1848		EDR 5908, Part XII	
b. PROJECT NO.			
c.		9b. OTHER REPORT NO(S) (Any other numbers that may be assigned this report)	
d.		AFAPL-TR-68-142, Part XII	
10. DISTRIBUTION STATEMENT			
This document is subject to special export controls and each transmittal to foreign governments or foreign nationals may be made only with prior approval of the Air Force Aero Propulsion Laboratory (APLA), Air Force Systems Command, Wright-Patterson Air Force Base, Ohio.			
11. SUPPLEMENTARY NOTE:		12. SPONSORING MILITARY ACTIVITY	
The dist. limitation was changed to U2 on 4/12/72		Air Force Aero Propulsion Laboratory Air Force Systems Command Wright-Patterson Air Force Base, Ohio 45433	
13. ABSTRACT			
<p>An analytical model of combustion instability in afterburners and duct burners has been formulated which incorporates in a readily identifiable way the significant loss and gain processes associated with oscillatory combustion. The dominant loss mechanisms, as revealed by a literature survey and subsequent assessment, are those due to convection and radiation from the nozzle and absorption by acoustic liners. The gain mechanisms have been incorporated in a general way which permits physical interpretation; those mechanisms considered to be of most importance in aircraft burners are those associated with fuel vaporization and turbulent transport processes. The analytical model is also capable of treating approximately the significant non-linear aspects of combustion instability associated with the dependencies of the major losses and gains on oscillation amplitude. The total mathematical requirements to obtain numerical results are the solution of transcendental algebraic equations and the evaluation of definite integrals. An application of the model to a known experimental situation yielded results which were qualitatively correct and quantitatively of the correct order of magnitude. Finally, a test plan has been formulated to enable the adequacy of the analytical model to be further assessed.</p>			

14. KEY WORDS	LINK A		LINK B		LINK C	
	ROLE	WT	ROLE	WT	ROLE	W
Combustion instability  Afterburners  Duct burners  Gain and loss processes in oscillatory combustion						